Tor Nordam

Scattering of light from weakly rough surfaces

Thesis for the degree of Philosophiae Doctor

Trondheim, February 2013

Norwegian University of Science and Technology
Faculty of Natural Sciences and Technology
Department of Physics

NTNU – Trondheim
Norwegian University of
Science and Technology

Abstract

A formalism is introduced for the non-perturbative, purely numerical, solution of the reduced Rayleigh equation for the scattering of light from two-dimensional penetrable rough surfaces. In the papers included in this thesis, we apply this formalism to study the scattering of p- or s-polarised light from two-dimensional dielectric or metallic randomly rough surfaces, or from two-dimensional randomly rough thin dielectric films on metallic substrates, by calculating the full angular distribution of the co- and cross-polarised intensity of the scattered light.

We present calculations of the mean differential reflection coefficient for glass and silver surfaces characterised by (isotropic or anisotropic) Gaussian and cylindrical power spectra, and find a good match with experimental results, as well as results obtained from another numerical method. We also present a numerical calculation of the Mueller matrix for scattering from rough surfaces, based on the same method.

We investigate the optical phenomena of enhanced backscattering, enhanced forward scattering and satellite peaks. Enhanced backscattering is a well known phenomenon, and is used as one among several indicators of correct results. The phenomenon of enhanced forward scattering has not previously been investigated in two-dimensional systems. We demonstrate its presence, and provide an explanation for why it is qualitatively different from the same phenomenon in one dimension. Regarding satellite peaks, there has been a dispute in the literature, where one group found they should be present in scattering from a thin dielectric film on a metallic substrate, while another group found they should not. We have demonstrated their presence, and shown how the one-dimensional phenomenon of satellite peaks become "satellite rings" in the two-dimensional case.

The proposed method is found, within the validity of the Rayleigh hypothesis, to give reliable results. For a non-absorbing metal surface the conservation of energy was explicitly checked, and found to be satisfied to within 0.03%, or better, for the parameters assumed. This testifies to

the accuracy of the approach and a satisfactory discretisation. We also perform a numerical investigation of the range of validity of the reduced Rayleigh equation for scattering from two-dimensionally rough silver and perfectly conducting surfaces.

The advantage of using a numerical solution of the reduced Rayleigh equation, rather than a rigorous numerical method such as the surface integral method, lies in the required computational resources. The main limitation of these methods for considering two-dimensionally rough surfaces are their memory requirements. To calculate the scattering amplitude for a typical system studied in this thesis, by the reduced Rayleigh equation, requires 12 GB of memory. To solve a similarly sized system with a rigorous method requires one or two orders of magnitude more. The limitation of the reduced Rayleigh equation is that it can only be applied to weakly rough surfaces, due to the assumption of the Rayleigh hypothesis.

Preface

This thesis is submitted as part of the requirements for the degree of Philosiphiae Doctor at the Norwegian University of Science and Technology (NTNU), in Trondheim, Norway. The work on this thesis began in December 2008, and was concluded in December 2012. My supervisor has been Professor Ingve Simonsen, at the Department of Physics, NTNU, and my secondary supervisor was Associate Professor Turid Worren Reenaas, also at the Department of Physics, NTNU. This work has mainly been carried out at NTNU, but with several visits to the University of Edinburgh. The first part of the thesis serves as an introduction to the work done, while the last part consists of the papers published and submitted for publication as a result of this work.

I would like to thank Professor Ingve Simonsen, who took me on as a PhD student even though I had never compiled a program in my life. He has taught me a lot about science and computational work in general, and rough surface scattering in particular.

My secondary supervisor, Associate Professor Turid Worren Reenaas, tried in vain to keep my work related to photovoltaics. It is not her fault it turned out otherwise. Still, I think it is good for me to be reminded of the existence of the "real world" and its practical applications, and I still hope to use the simulation code developed during my work with this thesis to study the effect of rough surfaces on photovoltaic cells.

Most of the work contained in this thesis has been carried out in collaboration with Paul Anton Letnes, without whom it would only have been half as thick. He has proved to be excellent company during the more than three years we shared an office, and has also taught me to appreciate the command line in a way I never could before.

Professor Alexei Maradudin, at the University of California at Irvine, has also been a collaborator on several of the papers in this thesis. I have only met him once, but he immediately struck me as a thoroughly likable fellow. I am glad I took the trip to California to see him.

Knut Gjerden also deserves thanks for being a good friend and excellent company on our trips abroad, as well as for the stapler[1]. It has been very handy.

Furthermore, I would like to thank my other colleagues in the optics corridor, Jérôme Maria, Lars Martin Aas, Pål Gunnar Ellingsen, Ingar Stian Nerbø, Daniel Skåre, Professor Morten Kildemo and Professor Mikael Lindgren, as well as Åsmund Monsen and Håvard Granlund. They have made my days fun and interesting.

I would also like to thank Jamie Cole at the School of Physics at the University of Edinburgh, who accepted me as a visitor for no better reason than that I wanted to stay in Edinburgh for a while. It is always a pleasure to talk with Jamie, both on physics and other subjects. I am also grateful to my other friends at the School of Physics, Paul Lane, Greg Isted, Tom Underwood, Andrew Jones and Terri Amos. They made me feel very welcome during the autumn of 2009, which I spent in Edinburgh, and at the many shorter visits since. I also thank Colin Thomson, Technical Services Manager at the School of Physics, for being very helpful in providing a key and an office at the JCMB.

My gratitude also goes out to Jan Christian Meyer, at the NTNU HPC Group, for providing excellent support, as well as going way outside any reasonable requirements of his job in providing long and detailed answers to questions such as "Why does the machine crash instead of terminate the program when you ask for more memory than what's available?"[2]

Some of the work in this thesis has been carried out with support from the HPC-Europa2 project. Under this project, Paul Anton and I got funding for two stays of five weeks each at the EPCC at the University of Edinburgh, as well as time on HECToR, one of the most powerful computers in Europe. I would like to thank Catherine Inglis who made all the arrangements and made our visits run smoothly, and Fiona Reid and Chris Johnson, who provided excellent technical help and support.

---

[1] And the staples.

[2] The short answer: because you have to do a system call to tell how much memory is available, and as the system clock only ticks at 1 kHz, it would be unreasonably slow to do a system call every time you wanted to create a variable. Thus, you are granted however much memory you want from the enormous 64-bit address space, the machine starts swapping, and even though it doesn't actually crash, everything is so slow it might as well have.

List of papers

Paper 1

T. A. Leskova, P. A. Letnes, A. A. Maradudin, T. Nordam, and I. Simonsen, "The scattering of light from two-dimensional randomly rough surfaces," *Proc. SPIE*, vol. 8172, p. 817209, 2011

The paper is an overview of several techniques for studying rough surface scattering. My contributions are to the parts of the paper discussing the reduced Rayleigh equation. I co-developed the simulation code used to solve the two-dimensional reduced Rayleigh equation, and I performed some of the simulations. P.A. Letnes had a similar role to mine, while T.A. Leskova, A.A. Maradudin and I. Simonsen contributed the rest of the paper, and prepared the manuscript for publication.

Paper 2

T. Nordam, P. Letnes, I. Simonsen, and A. Maradudin, "Satellite peaks in the scattering of light from the two-dimensional randomly rough surface of a dielectric film on a planar metal surface," *Opt. Express*, vol. 20, no. 10, p. 11336, 2012

The paper is a study of the satellite peaks phenomenon for a two-dimensionally rough dielectric film on a smooth silver substrate. I co-developed the simulation code used to obtain the numerical results, ran some of the simulations and participated in plotting the results. P.A. Letnes had a similar role to mine. The first draft of the paper was prepared by A.A. Maradudin, while all authors contributed to the editing and final preparation of the manuscript.

Paper 3

P. A. Letnes, A. A. Maradudin, T. Nordam, and I. Simonsen, "Calculation of the Mueller matrix for scattering of light from two-dimensional rough surfaces," *Phys. Rev. A*, vol. 86, p. 031803, 2012

The paper presents a calculation of the Mueller Matrix for scattering from a two-dimensionally rough surface, based on solving the reduced Rayleigh equation for reflection. I co-developed the simulation code used to obtain the numerical results, ran some of the simulations and participated in plotting the results. P.A. Letnes had a similar role to mine. The first draft of the paper was prepared by A.A. Maradudin, while all authors contributed to the editing and final preparation of the manuscript.

Paper 4

T. Nordam, P. A. Letnes, and I. Simonsen, "Numerical simulations of scattering of light from two-dimensional surfaces using the reduced Rayleigh equation," *arXiv:1204.4984 (submitted to Optics Express)*, 2013

The paper presents details of the implementation of a framework for numerical solution of the reduced Rayleigh equation for reflection from a two-dimensionally rough surface, as well as some results obtained by this code, with comparisons to experiments and another numerical method. I co-developed the simulation code with P.A. Letnes, and performed some of the simulations. I wrote the first draft of the paper, and plotted the comparison with experiments. All authors contributed to the editing and final preparation of the manuscript.

Paper 5

T. Nordam, P. A. Letnes, and I. Simonsen, "Validity of the Rayleigh hypothesis for two-dimensional randomly rough metal surfaces," *Accepted for publication in Proceedings of CCP2012*, 2012

The paper presents a numerical investigation into the range of validity of the reduced Rayleigh equation. I co-developed the simulation code with

P.A. Letnes, performed all of the simulations and presentation of results, and wrote most of the paper. Some parts of the paper was written by I. Simonsen. All authors contributed to the editing and final preparation of the manuscript.

Paper 6

P. A. Letnes, T. Nordam, and I. Simonsen, "Coherent effects in the scattering of light from two-dimensional rough metal surfaces," *Submitted to Journal of the Optical Society of America A*, 2013

The paper presents a numerical study of the enhanced forward scattering phenomenon, which occurs for rough surfaces with particular statistical properties. I co-developed the simulation code used to obtain the numerical results with P.A. Letnes, ran some of the simulations and participated in plotting the results. I wrote the paper in collaboration with P.A. Letnes. I. Simonsen provided theoretical insight, and was involved in the editing and final preparation of the manuscript.

Contents

Contents

1. Introduction - a brief history of light

"
Amicus Plato – amicus Aristoteles – magis amica veritas.

— Isaac Newton

Light is a physical phenomenon that has always fascinated natural philosophers, even in the ancient world. While various other philosophers had a range of generally uninformed opinions, the empirical study of light can be said to have started with Euclid, who lived around 300 BC, and his work *Optics*. Without speculating too much on the physical nature of light, he introduced a geometrical description of vision, stating that the visual cone extends from the eye in straight lines. Note that this is not the same as saying light itself comes from the eye. He did in fact express some doubts about this idea, proposed by Empedocles (490 BC–430 BC), as it would require light to move infinitely fast, since we can immediately see distant objects when opening our eyes.

Many others have contributed to the theory of light. For example, Snell's law, named after Willebrord Snellius (1580–1626), which describes how light is deflected when moving from one medium to another, was in fact described by Ibn Sahl (ca 940–1000) in his treatise *On burning mirrors and lenses*. Isaac Newton (1642–1727) experimented with prisms and lenses. He realised that the problem known as chromatic aberration, i.e., that a lens does not focus all colours at the same spot, is caused by the lens acting like a prism in splitting the colours. To circumvent the problem, he invented the reflecting telescope now known as the Newtonian telescope, using a curved mirror to focus light instead of a lens.

An increasingly better description of the behaviour of light was made available in the centuries leading up to the 1700s. However, fundamental questions about the nature of light remained unanswered. What light

1

really is, why it behaves as it does, and even how fast it moves where still unknown in the early 1600s. Around 1670, however, a tentative answer to the question of the speed of light was found, marking the discovery of the first fundamental constant of Nature (beating Newton's gravitational constant by about 15 years), and laying the groundwork for Einstein's theory of relativity.

1.1. The speed of light

There has always been a consensus that whatever light is, it does not move slowly. It has been claimed that it does not move at all, it just is, that it moves infinitely fast (which is perhaps the same thing as not moving) and to simply move too fast to be measured. The first to make a reasonably accurate quantitative measurement of the speed of light was the Danish astronomer Ole Rømer (1644–1710). Around 1670 he noticed that the times for eclipses of the moons of Jupiter varied with the Earth's position around the Sun, and calculated that light takes 22 minutes to travel the diametre of the orbit of the Earth. He did not actually calculate the speed of light himself, but others did based on his measurements, and found a value for the speed of light of about 222,000 kilometres per second. A century later, Jean Baptiste Joseph Delambre repeated the calculation, with the more accurate observations then available, and found that light takes 8 minutes and 12 seconds to travel from the Sun to the Earth. This is very close to the modern value of 8 minutes 19 seconds.

Incidentally, Rømer can also be said to have discovered the Doppler effect, which is the shift of frequency in a phenomenon that is observed when the sender or the receiver (or both) is moving along the line between them. What he observed was that the frequency with which the moon eclipsed Jupiter seemed to change with the position of the Earth. The explanation is that as the Earth moves towards Jupiter, the light from the moon has to travel a shorter distance each time, and each consecutive eclipse appears to happen a little earlier than expected, with the opposite being true when the Earth moves away from Jupiter.

The first terrestrial measurements of the speed of light happened around 180 years later. The main problem with so-called time of flight measurements is of course that light moves very fast, which means that measuring

its speed with accuracy amounts to measuring exceedingly short intervals of time. While today, we have clocks accurate enough to be able to send light a few metres in the lab and measure the time it takes to travel this distance with an accuracy of a few percent, this was not possible in the 17th century.

The trick used to measure time of flight accurately was to use a spinning wheel with notches along the edge. Knowing the angular frequency of the wheel's rotation, one could calculate the time between consecutive notches. Starting out with the wheel stationary, light was sent through one notch, onto a mirror some distance away, and back through the same notch to the observer. Setting the wheel in motion at increasingly higher speed, you would eventually get the situation where light passed through one notch, hit the mirror, and on its way back hit the wheel between two notches. Increasing the speed further, light might be able to pass through the next notch on the return journey. When the distance to the mirror, as well as the rotational speed of the wheel, was known, it was then possible to calculate the speed of light with impressive accuracy.

This apparatus was designed by Hippolyte Fizeau (1819–1896) and Léon Foucault (1819–1868), who used it separately to measure the speed of light. Fizeau, using a mirror located 8 kilometres away, measured a speed of 315,000 kilometres per second, a result he published in 1849. Foucault, using a modified version of the apparatus with a rotating mirror deflecting the beam in place of the notched wheel, obtained in 1862 a value of 298,000 kilometres per second, very close to the current value of 299,792.458 kilometres per second.

Interestingly, the current value of the speed of light is in fact exact. The reason for this is that the metre since 1983 has been defined as the distance light travels through vacuum in 1/299792458 seconds, a way of defining distance that was in fact suggested by Fizeau in 1864. This, in a sense, makes the speed of light a defined, rather than measured, quantity.

1.2. Wave or particle?

For a long time, the corpuscular theory of light advocated by Newton, i.e., that light consists of small particles, dominated. However, in the early 1800s, Thomas Young (1773–1829) performed the famous double

slit experiment, and demonstrated that light can display interference phenomena, just like water waves. The experiment consisted of sending light through two parallel, narrow slits, and allowing it to shine onto a screen some distance away. This was observed to produce an interference pattern of bright and dark bands.

If light consisted of classical particles, i.e., tiny, hard spheres, no such pattern would be observed. When adding the intensity of two classical particle beams, one simply adds the number of particles in each beam. Waves, on the other hand, have a phase, and when two waves are out of phase they interfere destructively, so the resultant intensity can reach zero.

After Young's double slit experiment had established that light exhibits wave-like properties, this was the dominant view for around 100 years. This view was of course reinforced by James Clerk Maxwell (1831–1879), who in the 1860s provided the mathematical description of light as electromagnetic waves. However, around the turn of the century, quantum theory was starting to emerge, and it became clear that the wave theory of light was insufficient to explain all observations.

Einstein, who had started playing with the idea of light particles in his thought experiments, in 1905 provided a correct theory for the photoelectric effect, the effect that electrons can be ejected from a metal when light is shone upon it, by describing light as small particles with a certain amount of energy. His theory for the photoelectric effect says that an electron can only be emitted if it is hit by a particle of light, called a photon, with at least enough energy to overcome the binding energy of the material. This explained the observation that only light of certain wavelengths could eject electrons. If using light of too long wavelengths, increasing the intensity of the light still didn't lead to electrons being ejected. If the light had short enough wavelengths, however, increasing the intensity would increase the number of electrons ejected. Thus Einstein concluded that light consisted of small particles, whose energy was determined by the wavelength of the light, with shorter wavelengths corresponding to higher energies, and that intensity was proportional to the number of particles. It was in fact for the theory of the photoelectric effect, and not for the more famous theory of relativity, that Einstein got the 1921 Nobel Prize in physics.

In the early 1900s, one was thus in the seemingly paradoxical situation

that light behaves as both a wave and a particle. It is fairly common, at least in high school physics books, to interpret this to mean that light actually *is* both a wave and a particle, whereas the obvious interpretation seems to be that it is neither. Rather, it is something new altogether which exhibits both wave-like and particle-like properties, depending on the experiment. During the 1920s and 1930s, when quantum mechanics was developed, it eventually became clear that this wave-particle duality is indeed the normal order of things, and that particles can also exhibit wave-like properties like interference. The quantum nature of light and matter is however outside the scope of this thesis. From here on, we will treat light as classical electric and magnetic fields, the theory of which will be introduced in the next chapter.

2. Basic theory

> “
> We can scarcely avoid the inference that light consists in the transverse undulations of the same medium which is the cause of electric and magnetic phenomena.
>
> — James Clerk Maxwell

2.1. Electricity

Both electric and magnetic phenomena have been known since ancient times. For example, the ancient Greeks knew and described how a piece of amber[1], when rubbed with a piece of fur, could attract light objects like hair. This phenomenon is today known as static electricity, caused by charge building up on the piece of amber.

Eventually, it was realised that electric charge could flow like a current between objects of different charge. Benjamin Franklin described electricity as a fluid which naturally occurs in all things, and said that objects which are deficient in this fluid are negatively charged, whereas objects with excess fluid are positively charged. Franklin was also responsible for the convention of the electron being negatively charged, by arbitrarily calling the kind of electric charge that builds up on a piece of resin rubbed with fur negative. This was more than one hundred years before the discovery of the electron, and had the unintended effect that the current in a wire, which is conventionally defined as the movement of positive charge, flows in the opposite direction of the movement of the charge carriers, which are the electrons.

---

[1] In fact, the word *electron* comes from the Greek word for amber.

2.1.1. Coulomb's law

Coulomb's law, first formulated by Charles Augustin de Coulomb in 1785, describes the electric force between two charged objects. Using a torsion pendulum to perform accurate measurements, he discovered that the force is proportional to the product of the charges on the objects, as well as inversely proportional to the square of the distance between the objects:

$$\mathbf{F}_e = \hat{\mathbf{r}} k_e \frac{q_1 q_2}{r^2}. \tag{2.1}$$

Here, k_e is a proportionality constant, sometimes known as Coulomb's constant, q_1 and q_2 are the charges of the objects, r is the centre to centre distance between them, and $\hat{\mathbf{r}}$ is the unit vector pointing from the centre of one object, directly away from the other. Thus, we see that if q_1 and q_2 have the same sign, the force is repulsive, whereas if they have opposite signs, the force is attractive.

Coulomb's law is also frequently written in the form

$$\mathbf{F}_e = \hat{\mathbf{r}} \frac{1}{4\pi\varepsilon_0} \frac{q_1 q_2}{r^2}, \tag{2.2}$$

i.e., with k_e replaced by $1/4\pi\varepsilon_0$, where $\varepsilon_0 \approx 8.85 \cdot 10^{-12}$ F/m is known as the vacuum permittivity. As we will see later in this chapter, the vacuum permittivity is a property of the vacuum which also shows up in the expression for the speed of light. However, this was not discovered until about 80 years later, by Maxwell.

2.1.2. Gauss law

Michael Faraday (1791–1867) introduced the concept of the electric field, which is often a more convenient tool than working directly with Coulomb's law and forces between pairs of particles. When a particle with charge q, is placed in an electric field $\mathbf{E}$, the electric force on the particle is given by

$$\mathbf{F}_e = q\mathbf{E}. \tag{2.3}$$

Thus, we can trivially derive the expression for the electric field due to a charged particle by combining Eqs. (2.2) and (2.3). A more general formula for the electric field due to the presence of charge is Gauss' law. It

was formulated by Carl Friedrich Gauss (1777–1855) in 1835, and published 12 years after his death, and reads

$$\oint_{\mathcal{S}} \mathbf{E} \cdot \mathrm{d}\mathbf{a} = \frac{Q}{\varepsilon_0}. \tag{2.4}$$

Here, the integral is to be taken over a closed surface $\mathcal{S}$, and Q is the charge enclosed by the surface. Gauss' law says that the flux of the electric field through a surface is directly proportional to the amount of charge enclosed by the surface. Gauss' law is always true, which makes it more general than Coulomb's law, which strictly speaking only holds for stationary point charges, but Gauss' law alone does not give the expression for the force between two charged particles. With the extra assumption that the field is spherically symmetric, however, Gauss' law can be used to obtain the electric field from a point charge, and thus to derive Coulomb's law.

2.2. Magnetism

Similarly to electric forces, magnetic forces have been known for a long time. The naturally occurring magnetic mineral *lodestone*, and its ability to attract iron, was described by Thales of Miletus around 600 BC. Magnetic forces have also been used in navigation for at least a thousand years, in the form of the compass. A needle, magnetised by rubbing it with a piece of magnetic material, and suspendend so it can rotate freely in the plane, will always point north-south.

2.2.1. The Biot-Savart law

In 1820, Hans Christian Ørsted (1777–1851) discovered that a current through a wire could deflect a compass needle, thus discovering the first connection between electric and magnetic phenomena. He found that a steady current in a wire would set up a circular magnetic field around the wire. In the same year, Jean-Baptiste Biot (1774–1862) and Félix Savart (1791–1841) performed a series of experiments and worked out a general formula for the magnetic field, $\mathbf{B}$, due to a steady current in a thin wire:

$$\mathbf{B} = \frac{\mu_0}{4\pi} I \int \frac{\mathrm{d}\mathbf{l} \times \hat{\mathbf{r}}}{r^2}. \tag{2.5}$$

Here, $\mu_0 = 4\pi \cdot 10^{-7}$ H/m is the vacuum permeability, which is a property of the vacuum that will be seen to enter in the expression for the speed of light, along with the vacuum permittivity. The current in the wire is given by I, $\mathrm{d}\mathbf{l}$ points in the direction of the current, and r is the distance from the wire element to the point where the field is to be calculated. This law is now known as the Biot-Savart law.

2.2.2. Ampère's law

Ampère's law, discovered by André-Marie Ampère (1775–1836) in 1826, relates the integrated magnetic field around the boundary of a surface to the total current passing through the surface:

$$\oint_{\mathcal{L}} \mathbf{B} \cdot \mathrm{d}\mathbf{l} = \mu_0 I. \tag{2.6}$$

Here, the integral is over any closed loop $\mathcal{L}$, and I is the current enclosed by the loop. Ampère's law plays a similar role for magnetic fields as Gauss' law does for electric fields, and it is more general than the Biot-Savart law. It is not always true, however, as it turned out that a current is not the only thing that can create a magnetic field. We will return to this point in Sec. 2.3.

2.2.3. Gauss' law for the magnetic field

For a while, it was thought that a piece of magnetic material contained two different kinds of fluid, similar to positive and negative electric charges, which were responsible for the two poles. Eventually, however, it was realised that the magnetic field from a piece of lodestone or other permanent magnetic material could be modelled by a current through a coil of wire, and the theory of two types of "magnetic fluid" was abandoned. This led to the realisation of the curious fact that there are no magnetic monopoles, later summarised by Maxwell in what is today known as Gauss' law for the magnetic field,

$$\oint \mathbf{B} \cdot \mathrm{d}\mathbf{a} = 0. \tag{2.7}$$

Later, Paul Dirac (1902–1984) showed that the existence of magnetic monopoles would explain why electric charge is quantised, i.e., why charge

only exists in multiples of the elementary charge [7]. His paper created a certain interest in the topic, but to this day, magnetic monopoles have never been observed.

2.2.4. Faraday's law

A little later, in 1831, Faraday discovered that a changing magnetic field can induce a current in a wire. Using a metal ring with two pieces of wire wrapped around it, he found that a current would be induced in one wire when he connected the other wire to a battery. Disconnecting the second wire would also produce a current in the first, but in the opposite direction. He also discovered that he could induce a current in a loop of wire by moving a magnet in and out of the loop.

Faraday's law describes the electric field along a closed loop, due to a changing magnetic field through the loop

$$\oint_{\mathcal{L}} \mathbf{E} \cdot \mathrm{d}\mathbf{l} = -\oint_{\mathcal{S}} \frac{\partial \mathbf{B}}{\partial t} \mathrm{d}\mathbf{a}. \tag{2.8}$$

Here, the first integral is to be taken over the closed loop $\mathcal{L}$, and the second over any continuous surface $\mathcal{S}$ bounded by the loop $\mathcal{L}$.

In the middle of the 1830s, this was the status of electromagnetic theory: it had been discovered that electric and magnetic phenomena were intimately connected, and several laws describing the behaviour of electric and magnetic fields were known, including how a changing magnetic field would induce an electric field. Then, in 1841, came the first hint that *light* might in fact be an electromagnetic effect, when Faraday discovered what is today known as Faraday rotation. This effect consists of a rotation of the plane of polarisation when linearly polarised light travels through a dielectric medium in the presence of a magnetic field. Polarised light had been known at least since Rasmus Bartholin (1625–1689) described birefringence in calcite, but was not well understood at the time. With the work of Maxwell, however, that was about to change.

2.3. Maxwell's equations

Almost 25 years after the discovery of Faraday rotation, electromagnetic theory was summed up by James Clerk Maxwell. In his 1865 paper "A

Dynamical Theory of the Electromagnetic Field" [8], he published 20 equations, working with the components of the vector potentials and the scalar potentials. Later, Oliver Heaviside (1850–1925) used modern vector calculus and the concepts of electric and magnetic fields to reformulate 12 of these equations into the four equations we now know as Maxwell's equations, presented here in differential form:

$$\nabla \cdot \mathbf{E} = \frac{1}{\varepsilon_0}\rho \qquad (2.9a)$$

$$\nabla \cdot \mathbf{B} = 0 \qquad (2.9b)$$

$$\nabla \times \mathbf{E} = -\frac{\partial \mathbf{B}}{\partial t} \qquad (2.9c)$$

$$\nabla \times \mathbf{B} = \mu_0 \mathbf{J} + \mu_0 \varepsilon_0 \frac{\partial \mathbf{E}}{\partial t}. \qquad (2.9d)$$

Beginning at the top, these are known as Gauss' law, with ρ the charge density, Gauss' law for magnetism (sometimes claimed not to have a name), Faraday's law and finally Ampère's law with Maxwell's correction, with $\mathbf{J}$ the current density. Maxwell's correction to Ampère's law reflects what was previously mentioned in Sec. 2.2.2, that not only currents can produce magnetic field. Just as a changing electric field will induce a magnetic field, so a changing magnetic field will also induce an electric field.

These equations completely describe the behaviour of electric and magnetic fields, both in vacuum and in materials. However, when working with materials containing charges which can be displaced or even flow under the influence of electric and magnetic fields, it is more convenient to write Maxwell's equations in terms of "free" charges and currents, i.e., those charges and currents we can apply and control.

We introduce the displacement field, $\mathbf{D}$, in a material, which is written

$$\mathbf{D} = \varepsilon \mathbf{E}, \qquad (2.10)$$

where $\varepsilon = \varepsilon_r \varepsilon_0$ is the permittivity of the material, with ε_r known as the relative permittivity. We also define the field $\mathbf{H}$, often known simply as the magnetic field:

$$\mathbf{H} = \frac{\mathbf{B}}{\mu} \tag{2.11}$$

where $\mu = \mu_r \mu_0$ is the permeability of the material, with μ_r similarly known as the relative permeability. Strictly, Eqs. (2.10) and (2.11) are only approximations, valid for what is known as linear materials. For sufficiently strong fields, no linear materials exist, as the fields will start ripping apart the atoms, and even for relatively weak magnetic fields, some materials (like iron) have a non-linear response. Additionally, for changing electric and magnetic fields, both ε and μ are generally functions of both the rate of change and the direction of the fields. For the study of light and optical phenomena in this thesis, however, we will assume that Eqs. (2.10) and (2.11) are valid, and that ε is a complex function of the frequency of oscillation of the electric field. In all systems considered in the papers in this thesis, μ will be a constant equal to μ_0, i.e., we assume non-magnetic materials.

Using Eqs. (2.10) and (2.11), we can thus rewrite Maxwell's equations in terms of the free charge distribution, ρ_f, and the free current density $\mathbf{J}_f$:

$$\nabla \cdot \mathbf{D} = \rho_f \tag{2.12a}$$

$$\nabla \cdot \mathbf{B} = 0 \tag{2.12b}$$

$$\nabla \times \mathbf{E} = -\frac{\partial \mathbf{B}}{\partial t} \tag{2.12c}$$

$$\nabla \times \mathbf{H} = \mathbf{J}_f + \frac{\partial \mathbf{D}}{\partial t}. \tag{2.12d}$$

In these equations, the effect of the electric and magnetic fields on the properties of the material is accounted for by the fields $\mathbf{D}$ and $\mathbf{H}$, given the above assumptions, i.e., that the material is linear and isotropic.

2.4. Electromagnetic waves

In addition to formulating these equations, Maxwell also demonstrated that there are solutions to Maxwell's equations which are at the same time solutions to the wave equation, describing fluctuations of the electric and magnetic fields that travel in straight lines like waves. Assuming we are in vacuum, with no charges and currents present, i.e., $\rho = 0$ and $\mathbf{J} = 0$, we apply the curl operator to Eq. (2.9c), and we find

$$\nabla \times \nabla \times \mathbf{E} = -\nabla \times \frac{\partial \mathbf{B}}{\partial t}, \tag{2.13}$$

which we can rewrite using the vector identity

$$\nabla \times \nabla \times \mathbf{A} = \nabla(\nabla \cdot \mathbf{A}) - \nabla^2 \mathbf{A}. \tag{2.14}$$

We obtain

$$\nabla(\nabla \cdot \mathbf{E}) - \nabla^2 \mathbf{E} = -\nabla \times \frac{\partial \mathbf{B}}{\partial t}. \tag{2.15}$$

Since $\nabla \cdot \mathbf{E} = 0$ in vacuum with no charges present, we can ignore the first term, and finally, applying Eq. (2.9d) with $\mathbf{J} = 0$ to the right hand side of Eq. (2.15), we obtain the wave equation for the electric field

$$\nabla^2 \mathbf{E} = \mu_0 \varepsilon_0 \frac{\partial^2 \mathbf{E}}{\partial t^2}. \tag{2.16}$$

Similarly, we can obtain the wave equation for the magnetic field:

$$\nabla^2 \mathbf{B} = \mu \varepsilon \frac{\partial^2 \mathbf{B}}{\partial t^2}. \tag{2.17}$$

This demonstrates that in vacuum, the electric and magnetic fields obey the wave equation,

$$\nabla^2 f = \frac{1}{c^2} \frac{\partial^2 f}{\partial t^2}. \tag{2.18}$$

with their speed given by

$$c = \frac{1}{\sqrt{\mu_0 \varepsilon_0}}. \tag{2.19}$$

We also note that giving Eq. (2.12) the same treatment, we find that light can propagate in materials with a speed slower than c, given by

$$v = \frac{1}{\sqrt{\mu\varepsilon}}. \tag{2.20}$$

The ratio of the speed of light in vacuum, c, to the speed of light in a material, v,

$$n = \frac{c}{v}, \tag{2.21}$$

is called the refractive index of the material.

The fact that fields obeying Maxwell's equations in vacuum are also solutions of the wave equation was what Maxwell referred to in the opening quote of this chapter:

> " *We can scarcely avoid the inference that light consists in the transverse undulations of the same medium which is the cause of electric and magnetic phenomena.*

Today, we know that Maxwell was right, and that visible light is merely electromagnetic radiation with wavelengths in the range 380 to 740 nanometres, fundamentally no different from for example X-rays or radio waves.

2.4.1. Reflection and refraction

In the previous section, we saw that electric and magnetic fields, obeying Maxwell's equations in vacuum, are also solutions to the wave equation. However, the opposite is not necessarily true. We consider a plane wave, propagating in the x_3-direction, i.e., an electric field whose amplitude is constant along the x_1- and x_2-directions, but changing with x_3 and t. We write this field as

$$\mathbf{E}(x_3, t) = \mathbf{E}_0 e^{i(kx_3 - \omega t)}, \tag{2.22}$$

where $k = 2\pi/\lambda$ is the wavenumber and $\omega = 2\pi c/\lambda$ is the angular frequency, with c the speed of light in vacuum. Similarly, we consider a magnetic field written on the form

$$\mathbf{B}(x_3, t) = \mathbf{B}_0 e^{i(kx_3 - \omega t)}. \tag{2.23}$$

2. Basic theory

While Eqs. (2.22) and (2.23) satisfy the wave equation as they are, Maxwell's equations impose additional constraints. Beginning with Gauss' law in vacuum, we find that

$$\nabla \cdot \mathbf{E}(x_3, t) = \mathrm{i}k E_3 \mathrm{e}^{\mathrm{i}(kx_3 - \omega t)} = 0, \tag{2.24}$$

which requires that $E_3 = 0$. Similarly, Gauss' law for the magnetic field requires $B_3 = 0$. Hence, the directions of the electric and magnetic fields are always perpendicular to the direction of propagation.

Furthermore, Maxwell's equations couple the behaviour of changing electric and magnetic fields. From Faraday's law, we find

$$\nabla \times \mathbf{E}(x_3, t) = \hat{\mathbf{x}}_2 \partial_3 E_1(x_3, t) - \hat{\mathbf{x}}_1 \partial_3 E_2(x_3, t) = -\partial_t \mathbf{B}. \tag{2.25}$$

This can be rewritten into the relations

$$\omega B_1 = -k E_2 \tag{2.26}$$
$$\omega B_2 = k E_1, \tag{2.27}$$

which can be further rewritten into

$$\mathbf{B} = \frac{k}{\omega} \left(\hat{\mathbf{x}}_3 \times \mathbf{E} \right). \tag{2.28}$$

From this, we see that the oscillating electric field is accompanied by an oscillating magnetic field. The electric and magnetic fields are perpendicular to each other, as well as the direction of propagation. We also find that the amplitudes of the electric and magnetic fields are related by

$$B_0 = \frac{1}{c} E_0, \tag{2.29}$$

where we have used that $k = \omega/c$.

Finally, we can use Maxwell's equations, along with the boundary conditions on the electric and magnetic fields, to calculate what happens when an electromagnetic wave passes from one medium to another. We consider a plane interface at $x_3 = 0$, separating two regions, which we will call regions 1 and 2. Region 1 is filled with a medium whose permittivity is a complex number ε_1, and region 2 with a medium with complex

permittivity ε_2. A plane wave, with the electric and magnetic fields given by

$$\mathbf{E}^i(\mathbf{x}, t) = \mathbf{E}_0^i e^{i(\mathbf{k}^i \cdot \mathbf{x} - \omega t)}, \quad \mathbf{B}^i(\mathbf{x}, t) = \mathbf{B}_0^i e^{i(\mathbf{k}^i \cdot \mathbf{x} - \omega t)}, \tag{2.30}$$

propagates towards the interface from region 1. We previously found that the electric and magnetic fields in a propagating plane wave are always perpendicular to each other as well as the direction of propagation, with the relative amplitudes of the fields given by Eq. (2.29). We thus have

$$\mathbf{B}_0^i = \frac{1}{v_1} \hat{\mathbf{k}}^i \times \mathbf{E}_0^i, \tag{2.31}$$

where v_1 is the speed of light in medium 1.

When the plane wave hits the interface between regions 1 and 2, it will in general be partially reflected and partially transmitted. The reflected plane wave, we write

$$\mathbf{E}^r(\mathbf{x}, t) = \mathbf{E}_0^r e^{i(\mathbf{k}^r \cdot \mathbf{x} - \omega t)}, \quad \mathbf{B}^r(\mathbf{x}, t) = \mathbf{B}_0^r e^{i(\mathbf{k}^r \cdot \mathbf{x} - \omega t)}, \tag{2.32}$$

where

$$\mathbf{B}_0^r = \frac{1}{v_1} \hat{\mathbf{k}}^r \times \mathbf{E}_0^r. \tag{2.33}$$

Similarly, the transmitted plane wave can be written

$$\mathbf{E}^t(\mathbf{x}, t) = \mathbf{E}_0^t e^{i(\mathbf{k}^t \cdot \mathbf{x} - \omega t)}, \quad \mathbf{B}^t(\mathbf{x}, t) = \mathbf{B}_0^t e^{i(\mathbf{k}^t \cdot \mathbf{x} - \omega t)}, \tag{2.34}$$

where

$$\mathbf{B}_0^t = \frac{1}{v_2} \hat{\mathbf{k}}^t \times \mathbf{E}_0^t. \tag{2.35}$$

Here, v_2 is the speed of light in medium 2. When we know the general form of the incident, scattered and transmitted field, what remains is to match them up at the boundary. The boundary conditions on the electric and magnetic fields are [9]:

$$\varepsilon_1 E_1^\perp - \varepsilon_2 E_2^\perp = 0, \tag{2.36a}$$

$$B_1^{\perp} - B_2^{\perp} = 0, \tag{2.36b}$$

$$\mathbf{E}_1^{\parallel} - \mathbf{E}_2^{\parallel} = 0, \tag{2.36c}$$

$$\frac{1}{\mu_1}\mathbf{B}_1^{\parallel} - \frac{1}{\mu_2}\mathbf{B}_2^{\parallel} = 0. \tag{2.36d}$$

Assuming $\mu_1 = \mu_2 = 1$, as we will do throughout this thesis, we can combine Eqs. (2.36b) and (2.36d) into

$$\mathbf{B}_1 - \mathbf{B}_2 = 0. \tag{2.36e}$$

It follows that

$$\mathbf{B}_0^i e^{i(\mathbf{k}^i \cdot \mathbf{x} - \omega t)} + \mathbf{B}_0^r e^{i(\mathbf{k}^r \cdot \mathbf{x} - \omega t)} = \mathbf{B}_0^t e^{i(\mathbf{k}^t \cdot \mathbf{x} - \omega t)}, \tag{2.37}$$

when $x_3 = 0$. From this, it is possible to prove that

$$\mathbf{B}_0^i + \mathbf{B}_0^r = \mathbf{B}_0^t, \tag{2.38}$$

and

$$e^{i(\mathbf{k}^i \cdot \mathbf{x} - \omega t)} = e^{i(\mathbf{k}^r \cdot \mathbf{x} - \omega t)} = e^{i(\mathbf{k}^t \cdot \mathbf{x} - \omega t)}$$
$$\Rightarrow \mathbf{k}^i \cdot \mathbf{x} = \mathbf{k}^r \cdot \mathbf{x} = \mathbf{k}^t \cdot \mathbf{x}, \tag{2.39}$$

again when $x_3 = 0$. This leads to

$$k_1^i = k_1^r = k_1^t, \quad k_2^i = k_2^r = k_2^t, \tag{2.40}$$

which is really nothing other than conservation of momentum. A flat interface cannot change the components of the wave vector parallel to the surface, and thus the incident and reflected wave vectors lie in the same plane, called the plane of incidence. We also see that the transmitted wave vector will lie in the same plane. Without loss of generality, we will therefore orient our coordinate system such that the plane of incidence is the $x_1 x_3$ plane, or in other words,

$$k_2^i = k_2^r = k_2^t = 0. \tag{2.41}$$

Furthermore, we find from Eq. (2.40) that

$$k^i \sin \theta_i = k^r \sin \theta_r = k^t \sin \theta_t, \tag{2.42}$$

where $k^i = |\mathbf{k}^i|$ is the magnitude of the wave vector of the incident light (with similar definitions for the reflected and transmitted light). The angle of incidence, θ_i, is measured from the surface normal pointing into region 1, the angle of reflection, θ_r, is measured in the same way, and θ_t is the angle of refraction, measured from the surface normal pointing into region 2.

Since the angular frequency, ω, is the same for all waves, we have

$$k^i v_1 = k^r v_1 = k^t v_2 = \omega. \tag{2.43}$$

This leads immediately to $k^i = k^r$, which combined with Eq. (2.42) gives

$$\theta_i = \theta_r. \tag{2.44}$$

Equation (2.44), the law of reflection, has been known since ancient times, when it was discovered by careful experimentation. Two millennia later, we can derive it from Maxwell's equations and the boundary conditions on the back of an envelope.

From Eqs. (2.42) and (2.43) we also find

$$\frac{\sin \theta_i}{\sin \theta_t} = \frac{n_2}{n_1}, \tag{2.45}$$

where we have used Eq. (2.21) to obtain n_1 and n_2, the refractive indices of media 1 and 2 respectively. Equation (2.45) is known as Snell's law of refraction, though as mentioned in the introduction it was discovered more than 500 years before the birth of Willebrord Snellius. It tells us how a beam of light changes its direction when moving from one material to another.

2.4.2. Fresnel's equations

Having established what happens to the direction of propagation of electromagnetic waves passing from one medium to another, we move on to

their amplitudes. From Eq. (2.38), and still assuming $\mu_1 = \mu_2 = 1$, we can rewrite the boundary conditions given in Eq. (2.36) into

$$\varepsilon_1 \left(E^i_{0\perp} + E^r_{0\perp} \right) = \varepsilon_2 E^t_{0\perp} \tag{2.46a}$$

$$\mathbf{E}^i_{0\parallel} + \mathbf{E}^r_{0\parallel} = \mathbf{E}^i_{0\parallel} \tag{2.46b}$$

$$\mathbf{B}^i_0 + \mathbf{B}^r_0 = \mathbf{B}^t_0. \tag{2.46c}$$

We will now consider separately the two cases where either $\mathbf{E}^i_0$ points along $\hat{\mathbf{x}}_1$, or it points along $\hat{\mathbf{x}}_2$. In the first case, i.e., $\mathbf{E}^i_0 = \hat{\mathbf{x}}_1 E^i_0$, the electric field is parallel to the plane of incidence. This is called p-polarised light, where p is for parallel. In the second case, $\mathbf{E}^i_0 = \hat{\mathbf{x}}_2 E^i_0$, the electric field is perpendicular to the plane of incidence. This is called s-polarised light, where s is for *senkrecht*, which is German for perpendicular. As all other polarisation states can be written as a combination of p- and s-polarised light, we will only deal with these two cases.

We begin by considering p-polarised light. From Eq. (2.46b), we get the condition

$$E^i_0 \cos\theta_i + E^r_0 \cos\theta_r = E^t_0 \cos\theta_t, \tag{2.47}$$

and from Eq. (2.46c), and using the relationship between the electric and magnetic fields given in Eq. (2.28), we obtain

$$\frac{1}{v_1} \left(E^i_0 - E^r_0 \right) = \frac{1}{v_2} E^t_0. \tag{2.48}$$

Using Eq. (2.44), Eqs. (2.47) and (2.48) can be trivially rewritten into

$$E^i_0 + E^r_0 = \frac{\cos\theta_t}{\cos\theta_i} E^t_0. \tag{2.49}$$

$$E^i_0 - E^r_0 = \frac{v_1}{v_2} E^t_0, \tag{2.50}$$

Solving Eqs. (2.49) and (2.50), we can eliminate either E^r_0 or E^t_0, and we get the following expressions for the transmitted and scattered field

amplitudes:

$$E_0^r = \frac{n_1\sqrt{1 - \sin^2\theta_i\frac{n_1^2}{n_2^2}} - n_2\cos\theta_i}{n_1\sqrt{1 - \sin^2\theta_i\frac{n_1^2}{n_2^2}} + n_2\cos\theta_i}E_0^i, \tag{2.51}$$

$$E_0^t = \frac{2n_1\cos\theta_i}{n_1\sqrt{1 - \sin^2\theta_i\frac{n_1^2}{n_2^2}} + n_2\cos\theta_i}E_0^i. \tag{2.52}$$

In arriving at Eqs. (2.51) and (2.52), we have made use of Eq. (2.45) to eliminate the angle of refraction from the expressions.

We then turn to the case of s-polarised light, i.e., $\mathbf{E}_0^i = \hat{\mathbf{x}}_2 E_0^i$, still with the $x_1 x_3$ plane as the plane of incidence. We use Eq. (2.46b), and get

$$E_0^i + E_0^r = E_0^t, \tag{2.53}$$

and from Eq. (2.46c), we get

$$B_0^i\cos\theta_i + B_0^r\cos\theta_r = B_0^t\cos\theta_t. \tag{2.54}$$

Using the relationship between the amplitudes of the electric and magnetic fields, given by Eq. (2.28), as well as the law of reflection, Eq. (2.44), we can rewrite Eq. (2.54) into

$$E_0^i - E_0^r = \frac{v_1\cos\theta_t}{v_2\cos\theta_i}E_0^t. \tag{2.55}$$

And finally, just as in the case of p-polarised light, we can solve Eqs. (2.53) and (2.55) to eliminate either E_0^r or E_0^t, and we find

$$E_0^r = \frac{n_1\cos\theta_1 - n_2\sqrt{1 - \sin^2\theta_i\frac{n_1^2}{n_2^2}}}{n_1\cos\theta_1 + n_2\sqrt{1 - \sin^2\theta_i\frac{n_1^2}{n_2^2}}}E_0^i, \tag{2.56}$$

$$E_0^t = \frac{2n_1\cos\theta_i}{n_1\cos\theta_1 + n_2\sqrt{1 - \sin^2\theta_i\frac{n_1^2}{n_2^2}}}E_0^i. \tag{2.57}$$

Equations (2.51), (2.52), (2.56) and (2.57) are known as Fresnel's equations.

3. The reduced Rayleigh equation

> "The history of science teaches only too plainly the lesson that no single method is absolutely to be relied upon, that sources of error lurk where they are least expected, and that they may escape the notice of the most experienced and conscientious worker.
>
> — Lord Rayleigh

3.1. Introduction

In the previous chapter, we introduced Maxwell's equations, and saw how they could be solved to obtain the reflection and transmission amplitudes for a flat interface between two different media. In this chapter, we will introduce the topic of this thesis, the scattering of light from rough surfaces. While clearly much more interesting and useful for practical applications, this is also considerably more difficult. It is mathematically more challenging, in that it is rather more complicated to obtain an equation that can be solved to find the reflection amplitudes, and it is numerically relatively heavy to solve said equations.

Scattering from rough surfaces was first studied systematically by Lord Rayleigh [10], who considered both acoustic and optical scattering from sinusoidal gratings. He also considered scattering from liquid surfaces, and thus became the first to consider *randomly rough surfaces*. While scattering from liquid surfaces turned out to be an important problem, with applications in for example marine radar, randomly rough surfaces on solids are also abundant both in nature and industrial processes, and scattering from randomly rough surfaces is thus a topic of great interest.
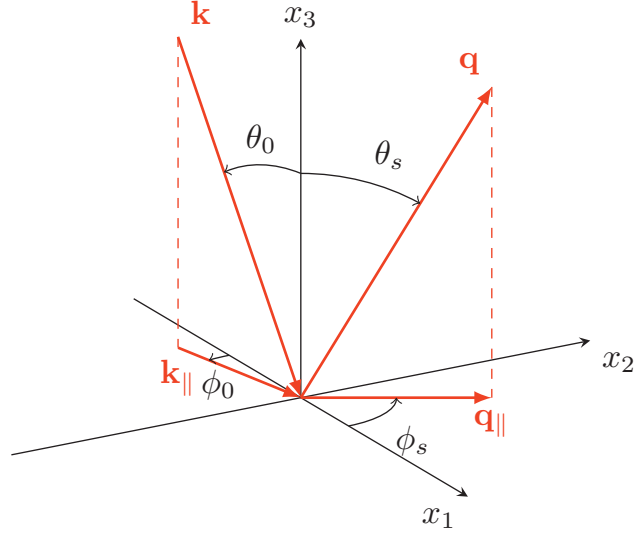
Figure 3.1.: A sketch of the scattering geometry assumed in this work. The figure also shows the coordinate system used, angles of incidence (θ_0, ϕ_0) and scattering (θ_s, ϕ_s), and the corresponding lateral wavevectors $\mathbf{k}_\parallel$ and $\mathbf{q}_\parallel$, respectively.

3.2. Scattering geometry

Throughout the papers included in this thesis, we will consider scattering from either a substrate with a rough surface in vacuum, or from a flat substrate with a film in vacuum, where the film–vacuum interface is rough. In both cases, we divide space into regions, where region 1 $[x_3 > \zeta(\mathbf{x}_\parallel)]$ is assumed to be vacuum ($\varepsilon_1 = 1$). The height of the surface separating regions 1 and 2, measured in the positive x_3 direction from the $x_1 x_2$-plane, is given by the single-valued function $x_3 = \zeta(\mathbf{x}_\parallel)$, where $\mathbf{x}_\parallel = (x_1, x_2, 0)$. The surface profile function, $\zeta(\mathbf{x}_\parallel)$, is assumed to be at least once differentiable with respect to x_1 and x_2.

In the case of the bare substrate in vacuum, the substrate will be called region 2 $[x_3 < \zeta(\mathbf{x}_\parallel)]$, with a complex dielectric function $\varepsilon_2(\omega)$, where the angular frequency is $\omega = 2\pi c/\lambda$. Here, λ is the wavelength of the incident light in vacuum and c is the speed of light in vacuum.

In the case of film on substrate, we divide space into three regions. Again region 1 $[x_3 > \zeta(\mathbf{x}_\parallel)]$ is vacuum ($\varepsilon_1 = 1$). Region 2 $[-d < x_3 < \zeta(\mathbf{x}_\parallel)]$ is the film, with complex dielectric function $\varepsilon_2(\omega)$ and average thickness d, and region 3 ($x_3 < -d$) is the substrate, with complex dielectric function $\varepsilon_3(\omega)$. The interface between the film and the substrate is flat, and parallell to the x_1x_2-plane, while the height of the surface separating the film and the vacuum, measured in the positive x_3 direction from the x_1x_2-plane, is given by the single-valued function $x_3 = \zeta(\mathbf{x}_\parallel)$. As before, $\mathbf{x}_\parallel = (x_1, x_2, 0)$, and $\zeta(\mathbf{x}_\parallel)$ is assumed to be at least once differentiable with respect to x_1 and x_2.

In both the case of the bare substrate and the substrate with film, the angles of incidence (θ_0, ϕ_0) and scattering (θ_s, ϕ_s) are defined positive according to the convention given in Fig. 3.1.

3.3. Surface profiles

In principle, the reduced Rayleigh equation and the scattering theory presented in Sec. 3.4 can be used to calculate the scattering of light from any surface, as long as the Rayleigh hypothesis is satisfied. It could for example be used to simulate the scattering from surface profiles obtained by measurements on real surfaces, to provide a comparison for experimental results. (Note, though, that this is not necessarily straightforward, due to the effort involved in sampling a large surface area with sufficient resolution.) Throughout this thesis, however, we will consider numerically generated randomly rough surface profiles with particular statistical properties. A brief outline of how to numerically generate surface realisations is given here.

The surface profile function, $\zeta(\mathbf{x}_\parallel)$, constitutes a stationary random process defined by

$$
\begin{aligned}
\langle \zeta(\mathbf{x}_\parallel) \rangle &= 0, \\
\langle \zeta(\mathbf{x}_\parallel)\zeta(\mathbf{x}_\parallel') \rangle &= \delta^2 W(\mathbf{x}_\parallel - \mathbf{x}_\parallel'),
\end{aligned}
\tag{3.1}
$$

where the angle brackets denote an average over an ensemble of surface realisations. Here, $W(\mathbf{x}_\parallel - \mathbf{x}_\parallel')$ denotes the height-height auto-correlation function of the surface, normalised so that $W(\mathbf{0}) = 1$ [11], and we have

3. The reduced Rayleigh equation

defined the root-mean-square height of the surface, $\delta = \left\langle \zeta^2(\mathbf{x}_\parallel) \right\rangle^{1/2}$. According to the Wiener-Khinchin theorem [12], the power spectrum of the surface profile function is given by

$$g(\mathbf{k}_\parallel) = \int \mathrm{d}^2 x_\parallel \, W(\mathbf{x}_\parallel) \exp\left(-\mathrm{i}\mathbf{k}_\parallel \cdot \mathbf{x}_\parallel\right). \qquad (3.2)$$

The power spectra which will be considered in the papers included in this thesis are of one of two types: the first is the Gaussian form [13]

$$g(\mathbf{k}_\parallel) = \pi a_1 a_2 \exp\left(-\frac{k_1^2 a_1^2}{4} - \frac{k_2^2 a_2^2}{4}\right), \qquad (3.3)$$

where a_1 and a_2 denote the lateral correlation length along x_1 and x_2 respectively. If $a_1 = a_2$, the surface is isotropic, if $a_1 \neq a_2$ it is anisotropic.

The second type is the cylindrical form [14]

$$g(k_\parallel) = \frac{4\pi}{k_+^2 - k_-^2} \left[\theta(k_\parallel - k_-)\theta(k_+ - k_\parallel)\right], \qquad (3.4)$$

where $k_\parallel = |\mathbf{k}_\parallel|$, θ denotes the Heaviside unit step function, and $k_\pm$ are wavenumber cutoff parameters, with $k_- < k_+$. The cylindrical form in Eq. (3.4) is a two-dimensional generalisation of the power spectrum used in experiments by West and O'Donnell where they confirmed the existence of the enhanced backscattering phenomenon for weakly rough surfaces [15]. We will also use a variation of the cylindrical form where the power spectrum is non-zero in two separate regions. See Ref. [6] (included in this thesis) for a more thorough discussion of both power spectra in general and the double cylindrical power spectrum in particular.

To numerically generate a realisation of a surface profile with a given power spectrum, an array of uncorrelated random numbers with a Gaussian distribution of standard deviation unity and zero mean is created. Then the discrete Fourier transform of this array is taken, which results in an array of random complex numbers which are symmetric about the zero frequency under complex conjugation. Each element of this array, which represents components of the Fourier spectrum, is then multiplied by the value of the power spectrum at the corresponding wave number. Thus, the power spectrum acts as weights on the random numbers, suppressing some frequencies and amplifying others. Finally, the inverse discrete

Fourier transform of the array is taken. Since both the complex random numbers and the power spectrum are symmetric about the zero frequency, the inverse fourier transform results in an array of purely real values, which make up a realisation of the surface profile function with an RMS-height of unity. Multiplying the array by the desired RMS-height yields a realisation of the surface profile with the same number of elements as the original array of random numbers. See also Refs.[16, 13] for more details.

3.4. Scattering theory

In this section, we will introduce the reduced Rayleigh equation for reflection from a substrate with a rough surface in vacuum. We consider a linearly p or s polarised plane wave which is incident on the surface from region 1, with the electric field given by $\mathbf{E}^{(0)}(\mathbf{x};t) = \mathbf{E}^{(0)}(\mathbf{x}|\omega)\exp(-\mathrm{i}\omega t)$ where

$$\mathbf{E}^{(0)}(\mathbf{x}|\omega) = \boldsymbol{\mathcal{E}}^{(0)}(\mathbf{k}_\parallel)\exp\left[\mathrm{i}\mathbf{k}_\parallel \cdot \mathbf{x}_\parallel - \mathrm{i}\alpha_1(k_\parallel)x_3\right], \tag{3.5a}$$

with

$$
\begin{aligned}
\boldsymbol{\mathcal{E}}^{(0)}(\mathbf{k}_\parallel) = {} & -\frac{c}{\omega}\left[\hat{\mathbf{k}}_\parallel \alpha_1(k_\parallel) + \hat{\mathbf{x}}_3 k_\parallel\right]\mathcal{E}_\mathrm{p}^{(0)}(\mathbf{k}_\parallel) \\
& + \left(\hat{\mathbf{x}}_3 \times \hat{\mathbf{k}}_\parallel\right)\mathcal{E}_\mathrm{s}^{(0)}(\mathbf{k}_\parallel),
\end{aligned}
\tag{3.5b}
$$

and

$$\alpha_1(k_\parallel) = \left(\frac{\omega^2}{c^2} - k_\parallel^2\right)^{1/2}, \quad \operatorname{Re}\alpha_1 \geq 0, \ \operatorname{Im}\alpha_1 \geq 0. \tag{3.5c}$$

Throughout this thesis, as well as in the included papers, a caret over a vector indicates a unit vector. The expressions in front of the amplitudes $\mathcal{E}_\mathrm{p}^{(0)}(\mathbf{k}_\parallel)$ and $\mathcal{E}_\mathrm{s}^{(0)}(\mathbf{k}_\parallel)$ in Eq. (3.5b) are the unit polarisation vectors for incident light of p- and s-polarisation respectively. Furthermore, $\mathbf{k}_\parallel = (k_1, k_2, 0)$ denotes the lateral component of the wave vector $\mathbf{k} = \mathbf{k}_\parallel - \alpha(k_\parallel)\hat{\mathbf{x}}_3$ of the incident light, with $\mathbf{k}_\parallel$ related to the angles of incidence indicated in Fig. 3.1 by

$$\mathbf{k}_\parallel = \frac{\omega}{c}\sin\theta_0\left(\cos\phi_0, \sin\phi_0, 0\right), \tag{3.6}$$

3. The reduced Rayleigh equation

where θ_0 and ϕ_0 are the polar and azimuthal angles of incidence, respectively (Fig. 3.1). In the expression for the incident field, $\mathbf{E}^{(0)}(\mathbf{x};t)$, a time harmonic dependence of the form $\exp(-\mathrm{i}\omega t)$ was included. A similar time dependence will be assumed in all field expressions, but will for convenience not be written explicitly.

Above the surface roughness region, i.e., for $x_3 > \max\zeta(\mathbf{x}_\parallel)$, the scattered field can be written in the form of a superposition of *upwards* propagating reflected plane waves, i.e., with a positive sign on the third component of the wave vector:

$$\mathbf{E}^{(\mathrm{s})}(\mathbf{x}|\omega) = \int \frac{\mathrm{d}^2 q_\parallel}{(2\pi)^2} \boldsymbol{\mathcal{E}}^{(\mathrm{s})}(\mathbf{q}_\parallel) \exp\left[\mathrm{i}\mathbf{q}_\parallel \cdot \mathbf{x}_\parallel + \mathrm{i}\alpha_1(q_\parallel)x_3\right], \qquad (3.7\mathrm{a})$$

where

$$\boldsymbol{\mathcal{E}}^{(\mathrm{s})}(\mathbf{q}_\parallel) = \frac{c}{\omega}\left[\hat{\mathbf{q}}_\parallel \alpha_1(q_\parallel) - \hat{\mathbf{x}}_3 q_\parallel\right]\mathcal{E}^{(\mathrm{s})}_{\mathrm{p}}(\mathbf{q}_\parallel) + \left(\hat{\mathbf{x}}_3 \times \hat{\mathbf{q}}_\parallel\right)\mathcal{E}^{(\mathrm{s})}_{\mathrm{s}}(\mathbf{q}_\parallel). \qquad (3.7\mathrm{b})$$

Here, $\mathbf{q} = \mathbf{q}_\parallel + \alpha_1(\mathbf{q}_\parallel)\hat{\mathbf{x}}_3$ is the wave vector of the scattered light, with $\alpha_1(\mathbf{q}_\parallel)$ given by Eq. (3.5c). The integral in Eq. (3.7a) is to be taken over the entire $q_1 q_2$-plane, including the region $q_\parallel > \omega/c$. Note that this means that even though we said we would write the scattered field in the form of a sum of upwards propagating modes, we also include mode which are not propagating in the vacuum at all. In particular, a mode with $q_\parallel \leq \omega/c$ will propagate away from the surface in the vacuum. For a mode with $q_\parallel > \omega/c$, on the other hand, the third component of $\mathbf{q}$, given by $\alpha_1(q_\parallel)$, will be purely imaginary. These are so-called evanescent modes, which decay exponentially to either direction away from the surface, but which under certain circumstances can propagate quite far along the surface. Both propagating modes in the vacuum and evanescent modes on the surface are thus included in $\mathbf{E}^{(\mathrm{s})}(\mathbf{x}|\omega)$.

We will furthermore assume that a linear relationship between the amplitudes of the incident and the scattered fields exists, which we write

$$\mathcal{E}^{(\mathrm{s})}_\alpha(\mathbf{q}_\parallel) = \sum_{\beta=\mathrm{p},\mathrm{s}} R_{\alpha\beta}(\mathbf{q}_\parallel|\mathbf{k}_\parallel)\mathcal{E}^{(0)}_\beta(\mathbf{k}_\parallel), \qquad (3.8)$$

where $\alpha = \mathrm{p},\mathrm{s}$. Here we have introduced the so-called *scattering amplitude*, $R_{\alpha\beta}(\mathbf{q}_\parallel|\mathbf{k}_\parallel)$, which describes how incident light of polarisation β,

28

characterised by a lateral wave vector $\mathbf{k}_\parallel$, is scattered into light of polarisation α, with lateral wave vector $\mathbf{q}_\parallel$. When $q_\parallel \leq \omega/c$, i.e., for vacuum propagating modes, the wave vector $\mathbf{q}_\parallel$ is related to the angles of scattering (θ_s, ϕ_s) by

$$\mathbf{q}_\parallel = \frac{\omega}{c} \sin \theta_s \left(\cos \phi_s, \sin \phi_s, 0 \right). \tag{3.9}$$

Below the surface region, i.e., for $x_3 < \min \zeta(\mathbf{x}_\parallel)$, the transmitted electric field can similarly be written as a sum of *downward* propagating modes:

$$\mathbf{E}^{(t)}(\mathbf{x}_\parallel | \omega) = \int \frac{\mathrm{d}^2 p_\parallel}{(2\pi)^2} \boldsymbol{\mathcal{E}}^{(t)}(\mathbf{p}_\parallel) \exp\left[i\mathbf{p}_\parallel \cdot \mathbf{x}_\parallel - i\alpha_2(p_\parallel) x_3 \right] \tag{3.10a}$$

with

$$\begin{aligned}
\boldsymbol{\mathcal{E}}^{(t)}(\mathbf{p}_\parallel) = &- \frac{1}{\sqrt{\varepsilon_2(\omega)}} \frac{c}{\omega} \left[\hat{\mathbf{p}}_\parallel \alpha_2(p_\parallel) + \hat{\mathbf{x}}_3 p_\parallel \right] \mathcal{E}_{\mathrm{p}}^{(t)}(\mathbf{p}_\parallel) \\
&+ \left(\hat{\mathbf{x}}_3 \times \hat{\mathbf{p}}_\parallel \right) \mathcal{E}_{\mathrm{s}}^{(t)}(\mathbf{p}_\parallel).
\end{aligned} \tag{3.10b}$$

In writing Eq. (3.10) we have introduced the wave vector of the transmitted field $\mathbf{p} = \mathbf{p}_\parallel - \alpha_2(p_\parallel)\hat{\mathbf{x}}_3$, where

$$\alpha_2(p_\parallel) = \left[\varepsilon_2(\omega) \frac{\omega^2}{c^2} - p_\parallel^2 \right]^{1/2}, \quad \mathrm{Re}\,\alpha_2 \geq 0,\ \mathrm{Im}\,\alpha_2 \geq 0. \tag{3.11}$$

Again, the integral in Eq. (3.10) is over the entire $p_1 p_2$-plane.

In complete analogy to what was done for reflection, we assume a linear relation between the amplitudes of the incident and transmitted fields:

$$\mathcal{E}_\alpha^{(t)}(\mathbf{p}_\parallel) = \sum_{\beta=\mathrm{p,s}} T_{\alpha\beta}(\mathbf{p}_\parallel | \mathbf{k}_\parallel) \mathcal{E}_\beta^{(0)}(\mathbf{k}_\parallel), \tag{3.12}$$

where $T_{\alpha\beta}(\mathbf{p}_\parallel | \mathbf{k}_\parallel)$ is the *transmission amplitude*.

The expressions Eqs. (3.5), (3.7), and (3.10) for the electric fields are correct far away from the surface region, and are referred to as the *asymptotic forms*. These equations automatically satisfy the boundary conditions at infinity.

3. The reduced Rayleigh equation

3.4.1. The Rayleigh hypothesis

Above the surface, i.e., in the region $x_3 > \max \zeta(\mathbf{x}_\parallel)$, the total electric field is equal to the sum of the incident and the scattered field, $\mathbf{E}^{(0)}(\mathbf{x}|\omega) + \mathbf{E}^{(\mathrm{s})}(\mathbf{x}|\omega)$. Below the surface, in the region $x_3 < \min \zeta(\mathbf{x}_\parallel)$, it equals the transmitted field, $\mathbf{E}^{(\mathrm{t})}(\mathbf{x}|\omega)$. In the surface roughness region, $\min \zeta(\mathbf{x}_\parallel) \leq x_3 \leq \max \zeta(\mathbf{x}_\parallel)$, these forms of the total field will not generally be valid. In particular, when we are above the surface but still below its maximum point, i.e., $\zeta(\mathbf{x}_\parallel) \leq x_3 < \max \zeta(\mathbf{x}_\parallel)$, the expression for the scattered field may also have terms containing $\exp \left[i\mathbf{q}_\parallel \cdot \mathbf{x}_\parallel - i\alpha_1(q_\parallel)x_3 \right]$. Similarly, the transmitted field in the surface region may contain additional terms similar to Eq. (3.10a) but with the exponential function replaced by $\exp \left[i\mathbf{p}_\parallel \cdot \mathbf{x}_\parallel + i\alpha_2(p_\parallel)x_3 \right]$.

If the surface roughness is sufficiently weak, however, the asymptotic forms of the fields, Eqs. (3.5), (3.7), and (3.10), can be assumed to be a good approximation to the total electric field in the surface roughness region. This assumption is known as the *Rayleigh hypothesis* [17, 10, 18], named after Lord Rayleigh, who used it in his seminal studies of wave scattering from sinusoidal surfaces [17, 10]. For a (one-dimensional) sinusoidal surface, i.e., a surface whose height measured from $x_3 = 0$ can be written $x_3 = \zeta_0 \sin(\Lambda x_1)$, the criterion for the validity of the Rayleigh hypothesis is known to be $\zeta_0 \Lambda < 0.448$, independently of the wavelength of the incident light [19, 20]. For a randomly rough surface, however, the absolute limit of validity of this hypothesis is not generally known. Some numerical studies have been devoted to finding the region of validity for random surfaces, though, including Ref. [21] and [5] (included in this thesis).

Even if no absolute criterion for the validity of the Rayleigh hypothesis for randomly rough surfaces is known, it remains true that it is a small-slope hypothesis. In particular, if the randomly rough surface is characterised by an root-mean-square (RMS) height δ, and a correlation length a (see Sec. 3.2 and Ref. [11] for details), there seems to be a consensus in the literature on the Rayleigh hypothesis being valid if $\delta/a \ll 1$ [21, 18]. We stress that the validity of the Rayleigh hypothesis does not require the amplitude of the surface roughness to be small, only its slope.

3.5. The reduced Rayleigh equations

Assuming that the Rayleigh hypothesis is valid, the total electric field in the surface region, $\min \zeta(\mathbf{x}_\parallel) < x_3 < \max \zeta(\mathbf{x}_\parallel)$, can be written in the asymptotic form given by Eqs. (3.5), (3.7) and (3.10), and these expressions can be used to satisfy the boundary conditions on the electric and magnetic fields at the rough surface $x_3 = \zeta(\mathbf{x}_\parallel)$. If there are no free currents or charges at the boundary, the boundary conditions are given by Eq. (2.36).

Inserting the field expressions from Eqs. (3.5), (3.7) and (3.10), with the amplitudes for the scattered and transmitted fields written in terms of the incident field and the scattering and transmission amplitudes, $R_{\alpha\beta}(\mathbf{q}_\parallel|\mathbf{k}_\parallel)$ and $T_{\alpha\beta}(\mathbf{q}_\parallel|\mathbf{k}_\parallel)$, into Eq. (2.36), one obtains the so-called Rayleigh equations. These are a set of coupled inhomogeneous integral equations, which the reflection and transmission amplitudes should satisfy.

In the mid-1980s, Brown *et al.* [22] showed that either the reflection or transmission amplitude could be eliminated from the Rayleigh equations, resulting in an integral equation for the remaining amplitude only. This equation was later re-derived by Soubret *et al.* in a somewhat more accessible manner [23]. Since this simplified integral equation contains only one of the unknown amplitudes, it is known as the *reduced Rayleigh equation* for reflection or transmission.

3.5.1. Reduced Rayleigh equation for reflection from a single rough interface

If the scattering amplitudes are organised as the 2×2 matrix

$$\mathbf{R}(\mathbf{q}_\parallel|\mathbf{k}_\parallel) = \begin{pmatrix} R_{\mathrm{pp}}(\mathbf{q}_\parallel|\mathbf{k}_\parallel) & R_{\mathrm{ps}}(\mathbf{q}_\parallel|\mathbf{k}_\parallel) \\ R_{\mathrm{sp}}(\mathbf{q}_\parallel|\mathbf{k}_\parallel) & R_{\mathrm{ss}}(\mathbf{q}_\parallel|\mathbf{k}_\parallel) \end{pmatrix}, \tag{3.13}$$

the reduced Rayleigh equation for reflection from a rough surface on a substrate in vacuum can be written in the form [14, 23, 24]

$$\int \frac{\mathrm{d}^2 q_\parallel}{(2\pi)^2} \frac{I\left(\alpha_2(p_\parallel) - \alpha_1(q_\parallel)|\mathbf{p}_\parallel - \mathbf{q}_\parallel\right)}{\alpha_2(p_\parallel) - \alpha_1(q_\parallel)} \mathbf{M}^+(\mathbf{p}_\parallel|\mathbf{q}_\parallel) \mathbf{R}(\mathbf{q}_\parallel|\mathbf{k}_\parallel)$$
$$= -\frac{I\left(\alpha_2(p_\parallel) + \alpha_1(k_\parallel)|\mathbf{p}_\parallel - \mathbf{k}_\parallel\right)}{\alpha_2(p_\parallel) + \alpha_1(k_\parallel)} \mathbf{M}^-(\mathbf{p}_\parallel|\mathbf{k}_\parallel), \tag{3.14a}$$

3. The reduced Rayleigh equation

where

$$I(\gamma|\mathbf{Q}_\parallel) = \int d^2x_\parallel \exp\left[-i\gamma\zeta(\mathbf{x}_\parallel)\right] \exp\left(-i\mathbf{Q}_\parallel \cdot \mathbf{x}_\parallel\right), \qquad (3.14b)$$

and

$$\mathbf{M}^\pm(\mathbf{p}_\parallel|\mathbf{q}_\parallel) = \begin{pmatrix} p_\parallel q_\parallel \pm \alpha_2(p_\parallel)\hat{\mathbf{p}}_\parallel \cdot \hat{\mathbf{q}}_\parallel \alpha_1(q_\parallel) & -\frac{\omega}{c}\alpha_2(p_\parallel)\left[\hat{\mathbf{p}}_\parallel \times \hat{\mathbf{q}}_\parallel\right]_3 \\ \pm\frac{\omega}{c}\left[\hat{\mathbf{p}}_\parallel \times \hat{\mathbf{q}}_\parallel\right]_3 \alpha_1(q_\parallel) & \frac{\omega^2}{c^2}\hat{\mathbf{p}}_\parallel \cdot \hat{\mathbf{q}}_\parallel \end{pmatrix},$$
$$(3.14c)$$

where the integrals in Eq. (3.14a) and (3.14b) are over the entire $\mathbf{q}_\parallel$-plane and $\mathbf{x}_\parallel$-plane, respectively.

As an illustrative exercise, we will now show that the reduced Rayleigh equation for reflection from a flat surface reproduces the Fresnel equations for reflection, Eqs. (2.51) and (2.56), which we derived in the previous chapter.

When $\zeta(\mathbf{x}_\parallel) = 0$, it follows that the integrals $I(\gamma|\mathbf{Q}_\parallel)$ are proportional to delta functions:

$$I(\gamma|\mathbf{Q}_\parallel) = \int d^2x_\parallel \exp\left(-i\mathbf{Q}_\parallel \cdot \mathbf{x}_\parallel\right) = (2\pi)^2\delta^2(\mathbf{Q}_\parallel). \qquad (3.15)$$

Equation (3.14a) thus becomes

$$\int \frac{d^2q_\parallel}{(2\pi)^2} \frac{(2\pi)^2\delta^2(\mathbf{p}_\parallel - \mathbf{q}_\parallel)}{\alpha_2(p_\parallel) - \alpha_1(q_\parallel)} \mathbf{M}^+(\mathbf{p}_\parallel|\mathbf{q}_\parallel)\mathbf{R}(\mathbf{q}_\parallel|\mathbf{k}_\parallel)$$
$$= -\frac{(2\pi)^2\delta^2(\mathbf{p}_\parallel - \mathbf{k}_\parallel)}{\alpha_2(p_\parallel) + \alpha_1(k_\parallel)} \mathbf{M}^-(\mathbf{p}_\parallel|\mathbf{k}_\parallel), \qquad (3.16)$$

Performing the integral on the left hand side, which is now trivial due to the delta function, we obtain

$$\frac{1}{\alpha_2(p_\parallel) - \alpha_1(p_\parallel)} \mathbf{M}^+(\mathbf{p}_\parallel|\mathbf{p}_\parallel)\mathbf{R}(\mathbf{p}_\parallel|\mathbf{k}_\parallel)$$
$$= -\frac{(2\pi)^2\delta^2(\mathbf{p}_\parallel - \mathbf{k}_\parallel)}{\alpha_2(p_\parallel) + \alpha_1(k_\parallel)} \mathbf{M}^-(\mathbf{p}_\parallel|\mathbf{k}_\parallel), \qquad (3.17)$$

Using the fact that the off-diagonal elements of $\mathbf{M}^{\pm}(\mathbf{p}_{\parallel}|\mathbf{q}_{\parallel})$ are 0 when $\mathbf{p}_{\parallel} = \mathbf{q}_{\parallel}$, we easily see that $R_{\mathrm{ps}}(\mathbf{q}_{\parallel}|\mathbf{k}_{\parallel}) = 0$ and $R_{\mathrm{sp}}(\mathbf{q}_{\parallel}|\mathbf{k}_{\parallel}) = 0$. We then obtain the following equations for the two remaining reflection amplitudes:

$$R_{\mathrm{pp}}(\mathbf{p}_{\parallel}|\mathbf{k}_{\parallel}) = (2\pi)^2 \delta^2(\mathbf{p}_{\parallel} - \mathbf{k}_{\parallel}) \frac{\alpha_1(\mathbf{p}_{\parallel}) - \alpha_2(\mathbf{p}_{\parallel})}{\alpha_1(\mathbf{k}_{\parallel}) + \alpha_2(\mathbf{p}_{\parallel})} \frac{M_{11}^{-}(\mathbf{p}_{\parallel}|\mathbf{k}_{\parallel})}{M_{11}^{+}(\mathbf{p}_{\parallel}|\mathbf{p}_{\parallel})} \tag{3.18}$$

$$R_{\mathrm{ss}}(\mathbf{p}_{\parallel}|\mathbf{k}_{\parallel}) = (2\pi)^2 \delta^2(\mathbf{p}_{\parallel} - \mathbf{k}_{\parallel}) \frac{\alpha_1(\mathbf{p}_{\parallel}) - \alpha_2(\mathbf{p}_{\parallel})}{\alpha_1(\mathbf{k}_{\parallel}) + \alpha_2(\mathbf{p}_{\parallel})} \frac{M_{22}^{-}(\mathbf{p}_{\parallel}|\mathbf{k}_{\parallel})}{M_{22}^{+}(\mathbf{p}_{\parallel}|\mathbf{p}_{\parallel})}. \tag{3.19}$$

We immediately note that the remaining delta function ensures that $R_{\mathrm{pp}}(\mathbf{p}_{\parallel}|\mathbf{k}_{\parallel}) = 0$ when $\mathbf{p}_{\parallel} \neq \mathbf{k}_{\parallel}$, and the same for R_{ss}. This is as we expect from Eq. (2.40), the law of reflection. We then insert the M_{11} and M_{22} matrix elements from Eq. (3.14c), and use the fact that $\mathbf{p}_{\parallel}^2 + \alpha_1^2(\mathbf{p}_{\parallel}) = p^2 = \omega^2/c^2$, as well as $\mathbf{p}_{\parallel}^2 + \alpha_2^2(\mathbf{p}_{\parallel}) = \omega^2/v_2^2$, where v_2 is the speed of light in medium 2. Considering for the moment only the fractions in the right hand sides of Eqs. (3.18) and (3.19), and setting $\mathbf{k}_{\parallel} = \mathbf{p}_{\parallel}$, as enforced by the delta function, we can write these as

$$\frac{c^2 \alpha_1(\mathbf{p}_{\parallel}) - v_2^2 \alpha_2(\mathbf{p}_{\parallel})}{c^2 \alpha_1(\mathbf{p}_{\parallel}) + v_2^2 \alpha_2(\mathbf{p}_{\parallel})} = \frac{n_2 \cos\theta_i - \sqrt{1 - \frac{\sin^2\theta_i}{n_2^2}}}{n_2 \cos\theta_i + \sqrt{1 - \frac{\sin^2\theta_i}{n_2^2}}} \tag{3.20}$$

$$\frac{\alpha_1(\mathbf{p}_{\parallel}) - \alpha_2(\mathbf{p}_{\parallel})}{\alpha_1(\mathbf{p}_{\parallel}) + \alpha_2(\mathbf{p}_{\parallel})} = \frac{\cos\theta_i - n_2\sqrt{1 - \frac{\sin^2\theta_i}{n_2^2}}}{\cos\theta_i + n_2\sqrt{1 - \frac{\sin^2\theta_i}{n_2^2}}} \tag{3.21}$$

Here, we have made use of the expression for the refractive index of material 2, $n_2 = c/v_2$, as well as the fact that $n_2 = \sqrt{\varepsilon_2}$ when $\mu_2 = 1$. Inserting these fractions back into Eqs. (3.18) and (3.19), we obtain

$$R_{\mathrm{pp}}(\mathbf{p}_{\parallel}|\mathbf{k}_{\parallel}) = (2\pi)^2 \delta^2(\mathbf{p}_{\parallel} - \mathbf{k}_{\parallel}) \frac{n_2 \cos\theta_i - \sqrt{1 - \frac{\sin^2\theta_i}{n_2^2}}}{n_2 \cos\theta_i + \sqrt{1 - \frac{\sin^2\theta_i}{n_2^2}}}. \tag{3.22}$$

$$R_{\mathrm{ss}}(\mathbf{p}_{\parallel}|\mathbf{k}_{\parallel}) = (2\pi)^2 \delta^2(\mathbf{p}_{\parallel} - \mathbf{k}_{\parallel}) \frac{\cos\theta_i - n_2\sqrt{1 - \frac{\sin^2\theta_i}{n_2^2}}}{\cos\theta_i + n_2\sqrt{1 - \frac{\sin^2\theta_i}{n_2^2}}}. \tag{3.23}$$

3. The reduced Rayleigh equation

Inspection reveals that the prefactor in front of the fraction will cancel when we insert Eqs. (3.22) and (3.23) into Eq. (3.7), using Eq. (3.8) to relate the scattered and incident fields. The delta function is removed by the integral over $\mathbf{q}_\parallel$, ensuring the law of reflection is obeyed. Comparing Eqs. (3.22) and (3.23) to the Fresnel equations for reflection, Eqs. (2.51) and (2.56), with $n_1 = 1$, we see that the reduced Rayleigh equation reduces to the Fresnel equations in the case of a flat interface.

3.5.2. Reduced Rayleigh equation for reflection from a perfectly conducting substrate

The reduced Rayleigh equation for reflection from clean, perfectly conducting, two-dimensional randomly rough surfaces [25] has also been been derived. This system is equivalent to the one discussed in the previous section, in the limit $\varepsilon_2 \to -\infty$. With the same conventions as in the previous section, $\mathbf{R}(\mathbf{q}_\parallel | \mathbf{k}_\parallel)$ will satisfy the equation

$$\int \frac{\mathrm{d}^2 q_\parallel}{(2\pi)^2} \mathbf{M}^+(\mathbf{p}_\parallel | \mathbf{q}_\parallel) \mathbf{R}(\mathbf{q}_\parallel | \mathbf{k}_\parallel) = -\mathbf{M}^-(\mathbf{p}_\parallel | \mathbf{k}_\parallel), \qquad (3.24)$$

where

$$
\begin{aligned}
\mathbf{M}^\pm(\mathbf{p}_\parallel | \mathbf{q}_\parallel) = {}& I(\pm\alpha_1(q_\parallel) | \mathbf{p}_\parallel - \mathbf{q}_\parallel) \\
& \times \begin{pmatrix} \pm\frac{c}{\omega} \frac{p_\parallel q_\parallel - (\omega/c)^2\, \hat{\mathbf{p}}_\parallel \cdot \hat{\mathbf{q}}_\parallel}{\alpha_1(q_\parallel)} & [\hat{\mathbf{p}}_\parallel \times \hat{\mathbf{q}}_\parallel]_3 \\ \pm\frac{\omega}{c} \frac{[\hat{\mathbf{p}}_\parallel \times \hat{\mathbf{q}}_\parallel]_3}{\alpha_1(q_\parallel)} & \hat{\mathbf{p}}_\parallel \cdot \hat{\mathbf{q}}_\parallel \end{pmatrix},
\end{aligned}
\qquad (3.25)
$$

and

$$I\left(\gamma | \mathbf{Q}_\parallel\right) = \int \mathrm{d}^2 x_\parallel \, \exp\left(-\mathrm{i}\mathbf{Q}_\parallel \cdot \mathbf{x}_\parallel\right) \exp\left[-\mathrm{i}\gamma\zeta\left(\mathbf{x}_\parallel\right)\right]. \qquad (3.26)$$

3.5.3. Reduced Rayleigh equation for reflection from a rough film on a flat substrate

The reduced Rayleigh equation for reflection from a film of finite thickness on top of an infinitely thick substrate, where only one interface is rough, has been derived by Soubret *et al.* [23, 24] and Leskova [2, 26]. The

scattering amplitudes, $R_{\alpha\beta}(\mathbf{q}_\parallel|\mathbf{k}_\parallel)$, for reflection from a rough film on a flat substrate satisfy the matrix integral equation

$$\int \frac{\mathrm{d}^2 q_\parallel}{(2\pi)^2} \mathbf{M}^+(\mathbf{p}_\parallel|\mathbf{q}_\parallel)\mathbf{R}(\mathbf{q}_\parallel|\mathbf{k}_\parallel) = -\mathbf{M}^-(\mathbf{p}_\parallel|\mathbf{k}_\parallel), \qquad (3.27)$$

where as before, we use the convention

$$\mathbf{R}(\mathbf{q}_\parallel|\mathbf{k}_\parallel) = \begin{pmatrix} R_{\mathrm{pp}}(\mathbf{q}_\parallel|\mathbf{k}_\parallel) & R_{\mathrm{ps}}(\mathbf{q}_\parallel|\mathbf{k}_\parallel) \\ R_{\mathrm{sp}}(\mathbf{q}_\parallel|\mathbf{k}_\parallel) & R_{\mathrm{ss}}(\mathbf{q}_\parallel|\mathbf{k}_\parallel) \end{pmatrix}, \qquad (3.28)$$

as well as

$$\mathbf{M}^\pm(\mathbf{q}_\parallel|\mathbf{k}_\parallel) = \begin{pmatrix} M_{11}^\pm(\mathbf{q}_\parallel|\mathbf{k}_\parallel) & M_{12}^\pm(\mathbf{q}_\parallel|\mathbf{k}_\parallel) \\ M_{21}^\pm(\mathbf{q}_\parallel|\mathbf{k}_\parallel) & M_{22}^\pm(\mathbf{q}_\parallel|\mathbf{k}_\parallel) \end{pmatrix}, \qquad (3.29)$$

and the matrix elements of $\mathbf{M}^\pm$ are given by:

$$\begin{aligned}
M_{11}^\pm(\mathbf{q}_\parallel|\mathbf{k}_\parallel) = &\pm \left[p_\parallel q_\parallel \pm \alpha_2(p_\parallel)(\hat{\mathbf{p}}_\parallel \cdot \hat{\mathbf{q}}_\parallel)\alpha_1(q_\parallel) \right] \\
&\times \Gamma_{\mathrm{p}}(p_\parallel) \exp\left(-\mathrm{i}\left[\alpha_2(p_\parallel) \mp \alpha_1(q_\parallel)\right] d\right) \frac{I\left(\alpha_2(p_\parallel) \mp \alpha_1(q_\parallel)|\mathbf{q}_\parallel - \mathbf{k}_\parallel\right)}{\alpha_2(p_\parallel) \mp \alpha_1(q_\parallel)} \\
&\pm \left[p_\parallel q_\parallel \mp \alpha_2(p_\parallel)(\hat{\mathbf{p}}_\parallel \cdot \hat{\mathbf{q}}_\parallel)\alpha_1(q_\parallel) \right] \\
&\times \Delta_{\mathrm{p}}(p_\parallel) \exp\left(\mathrm{i}\left[\alpha_2(p_\parallel) \pm \alpha_1(q_\parallel)\right] d\right) \frac{I\left(-\left[\alpha_2(p_\parallel) \pm \alpha_1(q_\parallel)\right]|\mathbf{q}_\parallel - \mathbf{k}_\parallel\right)}{\alpha_2(p_\parallel) \pm \alpha_1(q_\parallel)}
\end{aligned}$$
$$(3.30\mathrm{a})$$

$$\begin{aligned}
M_{12}^\pm(\mathbf{q}_\parallel|\mathbf{k}_\parallel) = &-\frac{\omega}{c}\alpha_2(p_\parallel)\left(\hat{\mathbf{p}}_\parallel \times \hat{\mathbf{q}}_\parallel\right)_3 \\
&\left(\Gamma_{\mathrm{p}}(p_\parallel) \exp\left(-\mathrm{i}\left[\alpha_2(p_\parallel) \mp \alpha_1(q_\parallel)\right] d\right) \frac{I\left(\alpha_2(p_\parallel) \mp \alpha_1(q_\parallel)|\mathbf{q}_\parallel - \mathbf{k}_\parallel\right)}{\alpha_2(p_\parallel) \mp \alpha_1(q_\parallel)} \right. \\
&\left. - \Delta_{\mathrm{p}}(p_\parallel) \exp\left(\mathrm{i}\left[\alpha_2(p_\parallel) \pm \alpha_1(q_\parallel)\right] d\right) \frac{I\left(-\left[\alpha_2(p_\parallel) \pm \alpha_1(q_\parallel)\right]|\mathbf{q}_\parallel - \mathbf{k}_\parallel\right)}{\alpha_2(p_\parallel) \pm \alpha_1(q_\parallel)} \right)
\end{aligned}$$
$$(3.30\mathrm{b})$$

3. The reduced Rayleigh equation

$$M_{21}(\mathbf{q}_\| | \mathbf{k}_\|) = \frac{\omega}{c} \left(\hat{\mathbf{p}}_\| \times \hat{\mathbf{q}}_\| \right)_3 \alpha_1(q_\|)$$

$$\left(\Gamma_{\mathrm{s}}(p_\|) \exp\left(-\mathrm{i}\left[\alpha_2(p_\|) \mp \alpha_1(q_\|)\right] d\right) \frac{I\left(\alpha_2(p_\|) \mp \alpha_1(q_\|) | \mathbf{q}_\| - \mathbf{k}_\|\right)}{\alpha_2(p_\|) \mp \alpha_1(q_\|)} \right.$$

$$\left. + \Delta_{\mathrm{s}}(p_\|) \exp\left(\mathrm{i}\left[\alpha_2(p_\|) \pm \alpha_1(q_\|)\right] d\right) \frac{I\left(-\left[\alpha_2(p_\|) \pm \alpha_1(q_\|)\right] | \mathbf{q}_\| - \mathbf{k}_\|\right)}{\alpha_2(p_\|) \pm \alpha_1(q_\|)} \right)$$

$$\text{(3.30c)}$$

$$M_{22}(\mathbf{q}_\| | \mathbf{k}_\|) = \frac{\omega^2}{c^2} \left(\hat{\mathbf{p}}_\| \cdot \hat{\mathbf{q}}_\| \right)$$

$$\left(\Gamma_{\mathrm{s}}(p_\|) \exp\left(-\mathrm{i}\left[\alpha_2(p_\|) \mp \alpha_1(q_\|)\right] d\right) \frac{I\left(\alpha_2(p_\|) \mp \alpha_1(q_\|) | \mathbf{q}_\| - \mathbf{k}_\|\right)}{\alpha_2(p_\|) \mp \alpha_1(q_\|)} \right.$$

$$\left. + \Delta_{\mathrm{s}}(p_\|) \exp\left(\mathrm{i}\left[\alpha_2(p_\|) \pm \alpha_1(q_\|)\right] d\right) \frac{I\left(-\left[\alpha_2(p_\|) \pm \alpha_1(q_\|)\right] | \mathbf{q}_\| - \mathbf{k}_\|\right)}{\alpha_2(p_\|) \pm \alpha_1(q_\|)} \right).$$

$$\text{(3.30d)}$$

In writing Eq. (3.30), we have introduced the functions

$$\Gamma_{\mathrm{p}}(p_\|) = \varepsilon_2 \alpha_3(p_\|) + \varepsilon_3 \alpha_2(p_\|) \tag{3.31a}$$
$$\Delta_{\mathrm{p}}(p_\|) = \varepsilon_2 \alpha_3(p_\|) - \varepsilon_3 \alpha_2(p_\|) \tag{3.31b}$$

and

$$\Gamma_{\mathrm{s}}(p_\|) = \alpha_3(p_\|) + \alpha_2(p_\|) \tag{3.32a}$$
$$\Delta_{\mathrm{s}}(p_\|) = \alpha_3(p_\|) - \alpha_2(p_\|). \tag{3.32b}$$

Just as was the case previously, the integral $I(\gamma|\mathbf{Q}_\|)$ is given by

$$I\left(\gamma|\mathbf{Q}_\|\right) = \int \mathrm{d}^2 x_\| \, \exp\left(-\mathrm{i}\mathbf{Q}_\| \cdot \mathbf{x}_\|\right) \exp\left[-\mathrm{i}\gamma\zeta\left(\mathbf{x}_\|\right)\right]. \tag{3.33}$$

All these variations of the reduced Rayleigh equations for reflection have a similar structure, and once a framework for numerically solving Eq. (3.14) has been implemented, it is mostly straightforward to extend this to other geometries. For a detailed description of how we solve the reduced Rayleigh equations, the reader is referred to Ref. [4] (included in this thesis).

3.6. Mean differential reflection coefficient

The solution of the reduced Rayleigh equation determines the scattering amplitudes $R_{\alpha\beta}(\mathbf{q}_\parallel|\mathbf{k}_\parallel)$ for a given surface profile, $\zeta(\mathbf{x}_\parallel)$. When the incident field is known, the scattering amplitude completely specifies the total field in the region above the surface. However, it is not directly measurable in experiments. A more useful quantity for comparison with experimental data is the mean differential reflection coefficient (DRC), which is defined as the time-averaged fraction of the incident power scattered into the solid angle $d\Omega_s$ about the scattering direction $\mathbf{q}$. The mean DRC is given by [14]

$$\left\langle \frac{\partial R_{\alpha\beta}}{\partial \Omega_s} \right\rangle = \frac{1}{L^2} \frac{\omega^2}{4\pi^2 c^2} \frac{\cos^2 \theta_s}{\cos \theta_0} \left\langle \left| R_{\alpha\beta}(\mathbf{q}_\parallel|\mathbf{k}_\parallel) \right|^2 \right\rangle, \qquad (3.34)$$

where L^2 is the area of the $x_1 x_2$ plane covered by the rough surface.

The reduced Rayleigh equation, due to the limitations introduced when assuming the Rayleigh hypothesis, can only be used to calculate the scattering from weakly rough surfaces. For this reason, specular (coherent) scattering will dominate the results. When plotting the mean DRC, and derived quantities like the Mueller matrix, it will be convenient to separate the mean DRC into its coherent and incoherent parts. By coherent scattering, we mean the part of the scattered light which does not cancel when the ensemble average of $R_{\alpha\beta}$ is taken, i.e., the part where the scattered field is in phase between surface realisations. Conversely, the incoherent part is the part which cancels in the ensemble average. The component of the mean DRC from incoherent scattering is [14]

$$\begin{aligned}
\left\langle \frac{\partial R_{\alpha\beta}}{\partial \Omega_s} \right\rangle_{\text{incoh}} &= \frac{1}{L^2} \frac{\omega^2}{4\pi^2 c^2} \frac{\cos^2 \theta_s}{\cos \theta_0} \\
&\times \left[\left\langle \left| R_{\alpha\beta}(\mathbf{q}_\parallel|\mathbf{k}_\parallel) \right|^2 \right\rangle - \left| \left\langle R_{\alpha\beta}(\mathbf{q}_\parallel|\mathbf{k}_\parallel) \right\rangle \right|^2 \right].
\end{aligned} \qquad (3.35)$$

The contribution to the mean DRC from the coherently scattered light is given by the difference between Eqs. (3.34) and (3.35). An example plot of the incoherent part of the mean DRC for reflection from a silver surface is presented in Fig. 3.2.
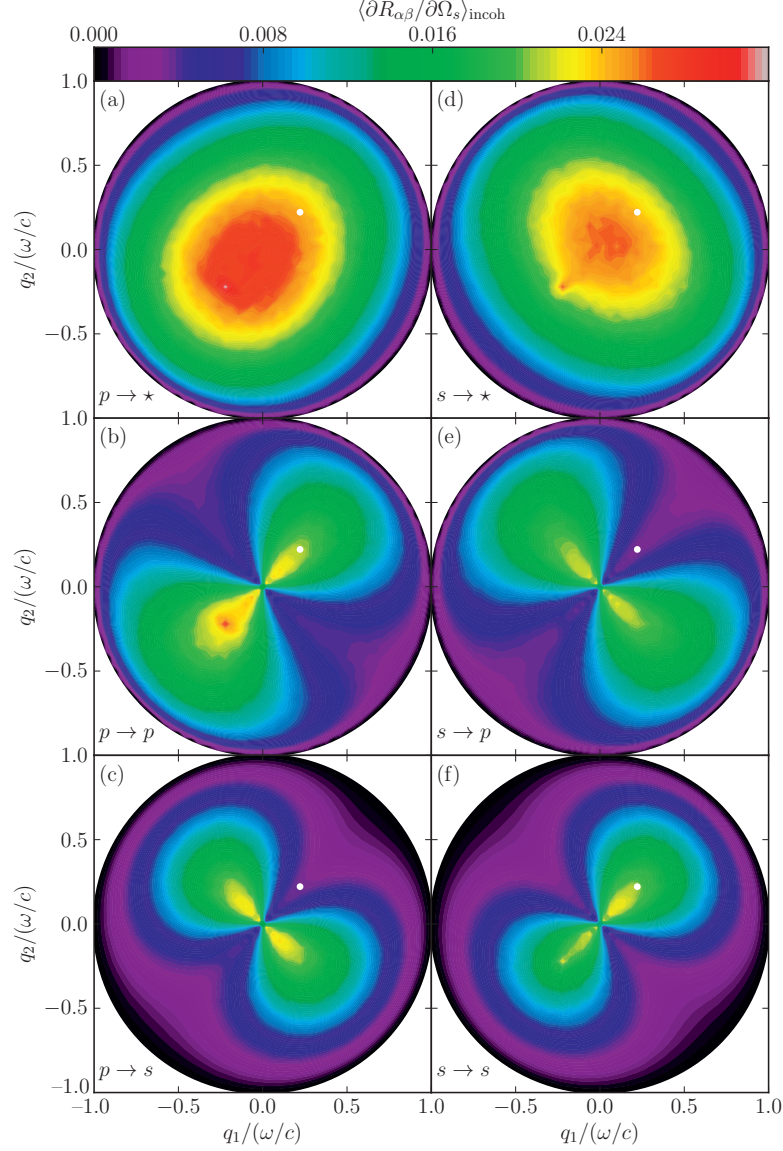
Figure 3.2.: Incoherent part of the mean differential reflection coefficient [Eq. (3.35)], as a function of outgoing lateral wave vector, averaged over 14,200 randomly rough surface realisations on a silver substrate. The wavelength (in vacuum) of the incident light was $\lambda = 457.9$ nm, and the surface power spectrum was Gaussian [Eq. (3.3)], with correlation lengths $a_1 = a_2 = 0.25\lambda$ and RMS height $\delta = 0.025\lambda$. The angle of incidence was $\theta_0 = 18.24°$, and the specular direction is indicated by the white dots.

3.7. Conservation of energy

Energy conservation can be a useful guide to the accuracy of our results. When considering reflection from a metallic substrate, we know that the fraction of reflected power over incident power should be less than one, and in the special case of a non-absorbing metallic sustrate, it should be equal to one. The fraction of incident power, in the form of light of polarisation β, which is scattered into light of polarisation α, is given by the integral of the corresponding mean DRC over the upper hemisphere:

$$\mathcal{U}_{\alpha\beta} = \int d\Omega_s \left\langle \frac{\partial R_{\alpha\beta}}{\partial \Omega_s} \right\rangle. \tag{3.36}$$

Thus, for a non-absorbing metal, if we send in light of polarisation β, we should have

$$\sum_\alpha \mathcal{U}_{\alpha\beta} = 1, \tag{3.37}$$

if energy is conserved in our simulations. While the conservation of energy is useful as a relatively simple test, it is important to note that it is a necessary, but not sufficient, condition for correct results. The use of conservation of energy as a test is discussed in more detail in Ref. [5] (included in this thesis).

Bibliography

[1] T. A. Leskova, P. A. Letnes, A. A. Maradudin, T. Nordam, and I. Simonsen, "The scattering of light from two-dimensional randomly rough surfaces," *Proc. SPIE*, vol. 8172, p. 817209, 2011.

[2] T. Nordam, P. Letnes, I. Simonsen, and A. Maradudin, "Satellite peaks in the scattering of light from the two-dimensional randomly rough surface of a dielectric film on a planar metal surface," *Opt. Express*, vol. 20, no. 10, p. 11336, 2012.

[3] P. A. Letnes, A. A. Maradudin, T. Nordam, and I. Simonsen, "Calculation of the Mueller matrix for scattering of light from two-dimensional rough surfaces," *Phys. Rev. A*, vol. 86, p. 031803, 2012.

[4] T. Nordam, P. A. Letnes, and I. Simonsen, "Numerical simulations of scattering of light from two-dimensional surfaces using the reduced Rayleigh equation," *arXiv:1204.4984 (submitted to Optics Express)*, 2013.

[5] T. Nordam, P. A. Letnes, and I. Simonsen, "Validity of the Rayleigh hypothesis for two-dimensional randomly rough metal surfaces," *Accepted for publication in Proceedings of CCP2012*, 2012.

[6] P. A. Letnes, T. Nordam, and I. Simonsen, "Coherent effects in the scattering of light from two-dimensional rough metal surfaces," *Submitted to Journal of the Optical Society of America A*, 2013.

[7] P. Dirac, "Quantised singularities in the electromagnetic field," *Proc. Roy. Soc. A*, vol. 133, p. 60, 1931.

[8] J. C. Maxwell, "A dynamical theory of the electromagnetic field," *Phil. Trans. R. Soc. Lond.*, vol. 155, p. 459, 1865.

Bibliography

[9] D. J. Griffiths, *Introduction to Electrodynamics.* Prentice-Hall International, 1999.

[10] Lord Rayleigh, "On the dynamical theory of gratings," *Proc. R. Soc. Lond. A*, vol. 79, no. 532, p. 399, 1907.

[11] I. Simonsen, "Optics of surface disordered systems: A random walk through rough surface scattering phenomena," *Eur. Phys. J.-Spec. Top.*, vol. 181, p. 1, 2010.

[12] N. G. V. Kampen, *Stochastic Processes in Physics and Chemistry.* North Holland, 3rd ed., 2007.

[13] I. Simonsen, J. B. Kryvi, A. A. Maradudin, and T. A. Leskova, "Light scattering from anisotropic, randomly rough, perfectly conducting surfaces," *Comp. Phys. Commun.*, vol. 182, p. 1904, 2011.

[14] A. R. Mcgurn and A. A. Maradudin, "Perturbation theory results for the diffuse scattering of light from two-dimensional randomly rough metal surfaces," *Wave Random Media*, vol. 6, no. 3, p. 251, 1996.

[15] S. West and K. A. O'Donnell, "Observations of backscattering enhancement from polaritons on a rough metal surface," *J. Opt. Soc. Am. A*, vol. 12, p. 390, 1995.

[16] A. A. Maradudin, T. Michel, A. R. McGurn, and E. R. Méndez, "Enhanced backscattering of light from a random grating," *Ann. Phys. (NY)*, vol. 203, no. 2, p. 255, 1990.

[17] Lord Rayleigh, *The Theory of Sound*, vol. II. MacMillan, 2nd ed., 1896.

[18] A. A. Maradudin, ed., *Light Scattering and Nanoscale Surface Roughness.* New York: Springer-Verlag, 2007.

[19] R. F. Millar, "On the Rayleigh assumption in scattering by a periodic surface," *Math. Proc. Cambridge*, vol. 65, p. 773, 1969.

[20] R. F. Millar, "On the Rayleigh assumption in scattering by a periodic surface. ii.," *Math. Proc. Cambridge*, vol. 69, p. 217, 1971.

[21] A. V. Tishchenko, "Numerical demonstration of the validity of the Rayleigh hypothesis," *Opt. Express*, vol. 17, p. 17102, 2009.

[22] G. C. Brown, V. Celli, M. Haller, and A. Marvin, "Vector theory of light scattering from a rough surface: Unitary and reciprocal expansions," *Surf. Sci.*, vol. 136, no. 2-3, p. 381, 1984.

[23] A. Soubret, G. Berginc, and C. Bourrely, "Application of reduced Rayleigh equations to electromagnetic wave scattering by two-dimensional randomly rough surfaces," *Phys. Rev. B*, vol. 63, p. 245411, Jun 2001.

[24] A. Soubret, G. Berginc, and C. Bourrely, "Backscattering enhancement of an electromagnetic wave scattered by two-dimensional rough layers," *J. Opt. Soc. Am. A*, vol. 18, p. 2778, Nov 2001.

[25] T. Nordam, P. A. Letnes, I. Simonsen, and A. A. Maradudin, "Numerical solutions of the Rayleigh equations for the scattering of light from a two-dimensional randomly rough perfectly conducting surface." (unpublished), 2012.

[26] T. A. Leskova, "The reduced Rayleigh equation for reflection of light from two-dimensional randomly rough films deposited on flat substrates." unpublished, 2010.

A. Papers

T. A. Leskova, P. A. Letnes, A. A. Maradudin, T. Nordam, and I. Simonsen, "The scattering of light from two-dimensional randomly rough surfaces," *Proc. SPIE*, vol. 8172, p. 817209, 2011

Paper 1

The scattering of light from two-dimensional randomly rough surfaces

T.A. Leskova[a], P.A. Letnes[b], A.A. Maradudin[a], T. Nordam[b] and I. Simonsen[b]

[a]Department of Physics and Astronomy and Institute for Surface and Interface Science
University of California, Irvine CA 92697, U.S.A.
[b]Department of Physics, Norwegian University of Science and Technology (NTNU)
NO-7491 Trondheim, Norway

ABSTRACT

We present results, obtained by rigorous computational approaches, for light of p- and s-polarization scattered from two-dimensional, randomly rough, perfectly conducting, lossy metallic, and dielectric surfaces. The perfectly conducting surfaces we study are characterized by an isotropic power spectrum of the surface roughness and by an anisotropic power spectrum. The mean differential reflection coefficient and the full angular distribution of the intensity of the scattered light are calculated for the perfectly conducting and metal surfaces. From the latter calculations it is found that the computational approach used in these calculations conserves energy in the scattering from a perfectly conducting and from a lossless metal surface with an error that is smaller than 0.5%. Finally, we presents results obtained by a numerical, nonperturbative, solution of the reduced Rayleigh equation for the scattering of p- and s-polarized light from two-dimensional randomly rough, metallic and dielectric surfaces. We show that the results for the metallic surface are in good agreement with results for the same metallic surface obtained by the rigorous computational approach.

Keywords: randomly rough surfaces; mean differential reflection coefficient; impedance boundary condition; reduced Rayleigh equation; Müller integral equations; Franz formulas; Stratton–Chu equation; scattering

1. INTRODUCTION

Despite the significant advances that have been made in the last 15 years or so in approaches to the calculation of the scattering of light from two-dimensional randomly rough perfectly conducting[1–8] and penetrable[6, 9–14] surfaces, such calculations remain computationally intensive, and need further improvements in the methods used in carrying them out. In this paper we review some of our recent work devoted to this problem, and present some new results. The emphasis will be on the results obtained and their significance, but the methods by which the results were obtained will be sketched out.

The physical system we consider in this paper consists of vacuum in the region $x_3 > \zeta(\mathbf{x}_\parallel)$, where $\mathbf{x}_\parallel = (x_1, x_2, 0)$, and the scattering medium in the region $x_3 < \zeta(\mathbf{x}_\parallel)$ (Fig. 1). The latter will be a perfect conductor, a metal, or a dielectric. The surface profile function $\zeta(\mathbf{x}_\parallel)$ is assumed to be a single-valued function of $\mathbf{x}_\parallel$ that is at least twice differentiable with respect to x_1 and x_2, and constitutes a stationary, zero-mean, Gaussian random process defined by $\left\langle \zeta(\mathbf{x}_\parallel)\zeta(\mathbf{x}'_\parallel) \right\rangle = \delta^2 W(\mathbf{x}_\parallel - \mathbf{x}'_\parallel)$. The angle brackets here denote an average over the ensemble of realizations of the surface profile function, and $\delta = \left\langle \zeta^2(\mathbf{x}_\parallel) \right\rangle^{\frac{1}{2}}$ is the rms height of the surface. The power spectrum of the surface roughness is defined by

$$g(\mathbf{k}_\parallel) \quad = \quad \int \mathrm{d}^2 x_\parallel \, W(\mathbf{x}_\parallel) \exp\left(-i\mathbf{k}_\parallel \cdot \mathbf{x}_\parallel\right), \tag{1}$$

where $\mathbf{k}_\parallel = (k_1, k_2, 0)$. Each realization of the surface profile function is generated numerically by a two-dimensional version of the filtering method used in [15], which is based on the power spectrum (1).

This paper is organized as follows. Scattering from two-dimensional randomly rough perfectly conducting surfaces will be discussed in Section 2, both when the surface roughness is characterized by an an isotropic power spectrum and when it is characterized by an anisotropic power spectrum. In Section 3 scattering from a
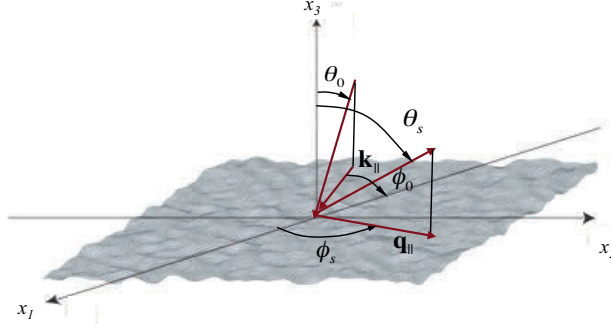
Figure 1. A sketch of the studied scattering geometry. The figure also shows the coordinate system used, angles of incidence (θ_0, ϕ_0) and scattering (θ_s, ϕ_s), and the corresponding transverse wavevectors $\mathbf{k}_\parallel$ and $\mathbf{q}_\parallel$, respectively.

two-dimensional randomly rough penetrable surface is considered, specifically scattering from a metallic surface and from a dielectric surface. Section 4 is devoted to a presentation of results obtained from a purely numerical, nonperturbative, solution of the reduced Rayleigh equation for the scattering of polarized light from a two-dimensional, randomly rough, penetrable surface. A discussion of the results obtained, and conclusions drawn from them, in Section 5, concludes this paper.

2. A PERFECTLY CONDUCTING SURFACE

2.1 Mathematical Formulation

The starting point for the calculation of the electromagnetic field scattered from a two-dimensional rough perfectly conducting surface is the Stratton–Chu formula[16] for the magnetic field in the vacuum

$$\theta(x_3 - \zeta(\mathbf{x}_\parallel))\, \mathbf{H}^>(\mathbf{x}|\omega) = \mathbf{H}(\mathbf{x}|\omega)_{\mathrm{inc}} + \frac{1}{4\pi} \int \mathrm{d}^2 x'_\parallel \ \left. [\boldsymbol{\nabla} g_0(\mathbf{x}|\mathbf{x}')]\right|_{x'_3 = \zeta(\mathbf{x}'_\parallel)} \times \mathbf{J}_H(\mathbf{x}'_\parallel|\omega), \qquad (2)$$

where $\theta(z)$ is the Heaviside unit step function, and $\mathbf{H}(\mathbf{x}|\omega)_{\mathrm{inc}}$ is the magnetic component of the incident field. In writing Eq. (2) we have assumed the time dependence $\exp(-\mathrm{i}\omega t)$ for the field, but have not indicated this explicitly.

The function $g_0(\mathbf{x}|\mathbf{x}')$ is the scalar free-space Green's function,

$$g_0(\mathbf{x}|\mathbf{x}') \quad = \quad \frac{\exp\left[\mathrm{i}\frac{\omega}{c}\,|\mathbf{x} - \mathbf{x}'|\right]}{|\mathbf{x} - \mathbf{x}'|} \tag{3a}$$

$$= \quad \int \frac{\mathrm{d}^2 q_\parallel}{(2\pi)^2} \frac{2\pi\mathrm{i}}{\alpha_0(q_\parallel)} \exp\left[\mathrm{i}\mathbf{q}_\parallel \cdot (\mathbf{x}_\parallel - \mathbf{x}'_\parallel)\right] \exp\left[\mathrm{i}\alpha_0(q_\parallel)|x_3 - x'_3|\right], \tag{3b}$$

where ω and c are the angular frequency and speed of light in vacuum, respectively, while $\alpha_0(q_\parallel) = [(\omega/c)^2 - q_\parallel^2]^{\frac{1}{2}}$, with $\mathrm{Re}\,\alpha_0(q_\parallel) > 0$, $\mathrm{Im}\,\alpha_0(q_\parallel) > 0$. The electric surface current $\mathbf{J}_H(\mathbf{x}_\parallel|\omega)$ is defined by $\mathbf{J}_H(\mathbf{x}_\parallel|\omega) = [\mathbf{n} \times \mathbf{H}^>(\mathbf{x}|\omega)]_{x_3 = \zeta(\mathbf{x}_\parallel)}$, where $\mathbf{n} = (-\zeta_1(\mathbf{x}_\parallel), -\zeta_2(\mathbf{x}_\parallel), 1)$ and $\zeta_j(\mathbf{x}_\parallel) \equiv \partial\zeta(\mathbf{x}_\parallel)/\partial x_j$ $(j = 1, 2)$. On evaluating Eq. (2) at $x_3 = \zeta(\mathbf{x}_\parallel) + \eta$ and at $x_3 = \zeta(\mathbf{x}_\parallel) - \eta$, where η is a positive infinitesimal, adding the resulting two equations, and taking the vector cross product of the sum with $\mathbf{n}$, we obtain the integral equation satisfied by $\mathbf{J}_H(\mathbf{x}_\parallel|\omega)$,

$$\mathbf{J}_H(\mathbf{x}_\parallel|\omega) \quad = \quad 2\mathbf{J}_H^{(i)}(\mathbf{x}_\parallel|\omega) + \frac{1}{2\pi} P \int \mathrm{d}^2 x'_\parallel \ \mathbf{n} \times \left\{ [\![\boldsymbol{\nabla} g_0(\mathbf{x}|\mathbf{x}')]\!] \times \mathbf{J}_H(\mathbf{x}'_\parallel|\omega) \right\}, \tag{4}$$

where $\mathbf{J}_H^{(i)}(\mathbf{x}_\parallel|\omega)_{\mathrm{inc}} = \mathbf{n} \times \mathbf{H}(\mathbf{x}|\omega)_{\mathrm{inc}}|_{x_3=\zeta(\mathbf{x}_\parallel)}$, P denotes the Cauchy principal value, and we have introduced the definition

$$\left[\!\left[f(\mathbf{x}|\mathbf{x}') \right]\!\right] \quad = \quad f(\mathbf{x}|\mathbf{x}')\bigg|_{\substack{x_3=\zeta(\mathbf{x}_\parallel) \\ x_3'=\zeta(\mathbf{x}_\parallel')}} . \tag{5}$$

Because $\mathbf{n} \cdot \mathbf{J}_H(\mathbf{x}_\parallel|\omega) = 0$, only two components of $\mathbf{J}_H(\mathbf{x}_\parallel|\omega)$ are independent. We choose them to be $J_H(\mathbf{x}_\parallel|\omega)_1$ and $J_H(\mathbf{x}_\parallel|\omega)_2$, and obtain $J_H(\mathbf{x}_\parallel|\omega)_3$ from

$$J_H(\mathbf{x}_\parallel|\omega)_3 = \zeta_1(\mathbf{x}_\parallel)J_H(\mathbf{x}_\parallel|\omega)_1 + \zeta_2(\mathbf{x}_\parallel)J_H(\mathbf{x}_\parallel|\omega)_2. \tag{6}$$

The two coupled, inhomogeneous, two-dimensional integral equations satisfied by $J_H(\mathbf{x}_\parallel|\omega)_{1,2}$ are solved by converting them into matrix equations. This is done by generating a realization of the surface profile function on a grid of N^2 points within a square region of the $x_1 x_2$ plane of edge L, where the discretization intervals for both directions are $\Delta x = L/N$. The integrals over this region are carried out by means of a two-dimensional version of the extended midpoint method,[17] and the values of $J_H(\mathbf{x}_\parallel|\omega)_1$ and $J_H(\mathbf{x}_\parallel|\omega)_2$ are calculated at the points of this grid. The resulting matrix equations are solved by means of the biconjugate gradient stabilized method.[18] The values of $J_H(\mathbf{x}_\parallel|\omega)_3$ are then obtained by the use of Eq. (6).

In these calculations the incident electric field has the form of a p- or s-polarized Gaussian beam, propagating in the direction of $\mathbf{k} = (\omega/c)(\sin\theta_0\cos\phi_0, \sin\theta_0\sin\phi_0, -\cos\theta_0)$. In the case that $\mathbf{k}_\parallel = k_\parallel\hat{\mathbf{x}}_1$, it is given by

$$\mathbf{E}_\nu(\mathbf{x}|\omega)_{\mathrm{inc}} \quad = \quad \int_{q_\parallel < \frac{\omega}{c}} \mathrm{d}^2q_\parallel\, \hat{\boldsymbol{\mathcal{E}}}_\nu^{(i)}(\mathbf{q}_-|\omega)\exp\left[i\mathbf{q}_- \cdot \mathbf{x}\right] W(\mathbf{q}_\parallel|\mathbf{k}_\parallel), \tag{7}$$

where $\nu = p$ or s, $\mathbf{q}_\pm(\mathbf{q}_\parallel,\omega) = \mathbf{q}_\parallel \pm \alpha_0(q_\parallel)\hat{\mathbf{x}}_3$, and $W(\mathbf{q}_\parallel|\mathbf{k}_\parallel)$ is

$$W(\mathbf{q}_\parallel|\mathbf{k}_\parallel) = \frac{w^2}{2\pi}\exp\left[-\frac{w^2}{2}(\mathbf{q}_\parallel - \mathbf{k}_\parallel)^2\right]. \tag{8}$$

For an incident field that is p polarized

$$\hat{\boldsymbol{\mathcal{E}}}_p^{(i)}(\mathbf{q}_-|\omega) \quad = \quad \frac{\alpha_0(q_\parallel)\hat{\mathbf{x}}_1 + q_1\hat{\mathbf{x}}_3}{[q_1^2 + \alpha_0^2(q_\parallel)]^{\frac{1}{2}}}, \tag{9a}$$

while for an incident field that is s polarized

$$\hat{\boldsymbol{\mathcal{E}}}_s^{(i)}(\mathbf{q}_-|\omega) \quad = \quad \frac{q_1 q_2\hat{\mathbf{x}}_1 - [q_1^2 + \alpha_0^2(q_\parallel)]\hat{\mathbf{x}}_2 - q_2\alpha_0(q_\parallel)\hat{\mathbf{x}}_3}{\frac{\omega}{c}[q_1^2 + \alpha_0^2(q_\parallel)]^{\frac{1}{2}}}. \tag{9b}$$

The scattered electric field, written in terms of $\mathbf{J}_H(\mathbf{x}_\parallel|\omega)$, is

$$\mathbf{E}(\mathbf{x}|\omega)_{\mathrm{sc}} \quad = \quad \int \frac{\mathrm{d}^2q_\parallel}{(2\pi)^2}\left[\mathcal{E}_p(\mathbf{q}_+|\omega)\hat{\boldsymbol{\gamma}}_p(\mathbf{q}_+|\omega) + \mathcal{E}_s(\mathbf{q}_+|\omega)\hat{\boldsymbol{\gamma}}_s(\mathbf{q}_+|\omega)\right]\exp\left[i\mathbf{q}_+ \cdot \mathbf{x}\right], \tag{10}$$

where

$$\hat{\boldsymbol{\gamma}}_p(\mathbf{q}_+|\omega) \quad = \quad \frac{-\alpha_0(q_\parallel)\hat{\mathbf{q}}_\parallel + q_\parallel\hat{\mathbf{x}}_3}{\omega/c} \tag{11a}$$

$$\hat{\boldsymbol{\gamma}}_s(\mathbf{q}_+|\omega) \quad = \quad \hat{\mathbf{q}}_\parallel \times \hat{\mathbf{x}}_3, \tag{11b}$$

and ($\nu = p, s$)

$$\mathcal{E}_\nu(\mathbf{q}_+|\omega) \quad = \quad -\frac{(\omega/c)}{2\alpha_0(q_\parallel)}\int \mathrm{d}^2x_\parallel\, \hat{\boldsymbol{\gamma}}_\nu(\mathbf{q}_+|\omega) \cdot \mathbf{J}_H(\mathbf{x}_\parallel|\omega)\exp\left[-i\mathbf{q}_\parallel \cdot \mathbf{x}_\parallel - i\alpha_0(q_\parallel)\zeta(\mathbf{x}_\parallel)\right]. \tag{12}$$

The differential reflection coefficient $(\partial R/\partial \Omega_s)$ is defined such that $(\partial R/\partial \Omega_s)\mathrm{d}\Omega_s$ is the fraction of the total time-averaged flux incident on the surface that is scattered into the element of solid angle $\mathrm{d}\Omega_s$ about the scattering direction (θ_s, ϕ_s). Since we are studying the scattering of light from a randomly rough surface, it is the average of this quantity over the ensemble of realizations of the surface profile function that we need to calculate. The mean differential reflection coefficient for the scattering of light of polarization β, the projection of whose wave vector on the mean scattering surface is $\mathbf{k}_{\parallel}$, into light of polarization α, the projection of whose wave vector on the mean scattering surface is $\mathbf{q}_{\parallel}$, is given by

$$\left\langle \frac{\partial R_{\alpha\beta}}{\partial \Omega_s} \right\rangle = \frac{1}{4\pi^2} \left(\frac{\omega}{c} \right)^3 \cos^2 \theta_s \frac{\left\langle |\mathcal{E}_\alpha(\mathbf{q}_+|\omega)|^2 \right\rangle}{p_{\mathrm{inc}}}, \tag{13}$$

where for both polarizations of the incident light,

$$p_{\mathrm{inc}} = w^4 \int_{q_{\parallel} < \frac{\omega}{c}} \mathrm{d}^2 q_{\parallel} \, \alpha_0(q_{\parallel}) \exp\left[-w^2(\mathbf{q}_{\parallel} - \mathbf{k}_{\parallel})^2 \right]. \tag{14}$$

The dependence of the right-hand side of this equation on the polarization index β is through the dependence of the amplitude $\mathcal{E}_\alpha(\mathbf{q}_+|\omega)$ on the surface current $\mathbf{J}_H(\mathbf{x}_{\parallel}|\omega)$ in Eq. (12). The surface current satisfies Eq. (4) in which the inhomogeneous term depends on the incident field and hence on its polarization $\beta = p, s$. Therefore $\mathcal{E}_\alpha(\mathbf{q}_+|\omega)$ depends implicitly on the polarization β of the incident field and consequently so does the mean differential reflection coefficient.

If one is interested in nonspecular effects, it is the contribution to the mean differential reflection coefficient from the light that has been scattered incoherently (diffusely) that is of interest. It is given by

$$\left\langle \frac{\partial R_{\alpha\beta}}{\partial \Omega_s} \right\rangle_{\mathrm{incoh}} = \frac{1}{4\pi^2} \left(\frac{\omega}{c} \right)^3 \cos^2 \theta_s \frac{\left\langle |\mathcal{E}_\alpha(\mathbf{q}_+|\omega)|^2 \right\rangle - \left| \left\langle \mathcal{E}_\alpha(\mathbf{q}_+|\omega) \right\rangle \right|^2}{p_{\mathrm{inc}}}. \tag{15}$$

We now turn to some results obtained on the basis of this method.

2.2 Results for a Perfectly Conducting Surface

2.2.1 An Isotropic Roughness Power Spectrum

The first set of calculations were carried out for a two-dimensional randomly rough perfectly conducting surface defined by an isotropic surface height autocorrelation function, *i.e.* one that depends on the vector $\mathbf{x}_{\parallel}$ only through its magnitude. We have chosen for it the Gaussian form $W(\mathbf{x}_{\parallel}) = \exp(-x_{\parallel}^2/a^2)$. The characteristic length a is called the transverse correlation length of the surface roughness. The power spectrum of the surface, given by Eq. (1), in this case has the form

$$g(\mathbf{k}_{\parallel}) = \pi a^2 \exp\left(-\frac{k_{\parallel}^2 a^2}{4} \right). \tag{16}$$

We have carried out calculations of the scattering of p-polarized light from such a surface with an rms height $\delta = \lambda$ and a transverse correlation length $a = 2\lambda$, where λ is the wavelength of the incident field in vacuum. The incident field had the form of a Gaussian beam, Eq. (7), with $w = 4\lambda$. The surface, covering an area $L^2 = 16\lambda \times 16\lambda$ in the mean surface plane, was generated at the points of a 112×112 grid of mesh size $\Delta x = \lambda/7$ for both directions.

In Fig. 2 we plot the mean differential reflection coefficients as functions of the polar scattering angle θ_s for the in-plane ($\phi_s = 0°, 180°$) and out-of-plane ($\phi_s = \pm 90°$) co-($p \to p$) and cross-($p \to s$) polarized scattering when a p-polarized Gaussian beam is incident on the surface at angles of incidence (θ_0, ϕ_0) given by $(0°, 0°)$ and $(20°, 0°)$. Results obtained for $12\,000$ realizations of the surface profile function were averaged to obtain these figures. The calculations for each realization of the surface profile function required 76 CPU seconds on an Intel Core 2 CPU (Q9550) operating at 2.83 GHz and running the Linux operating system. For the roughness
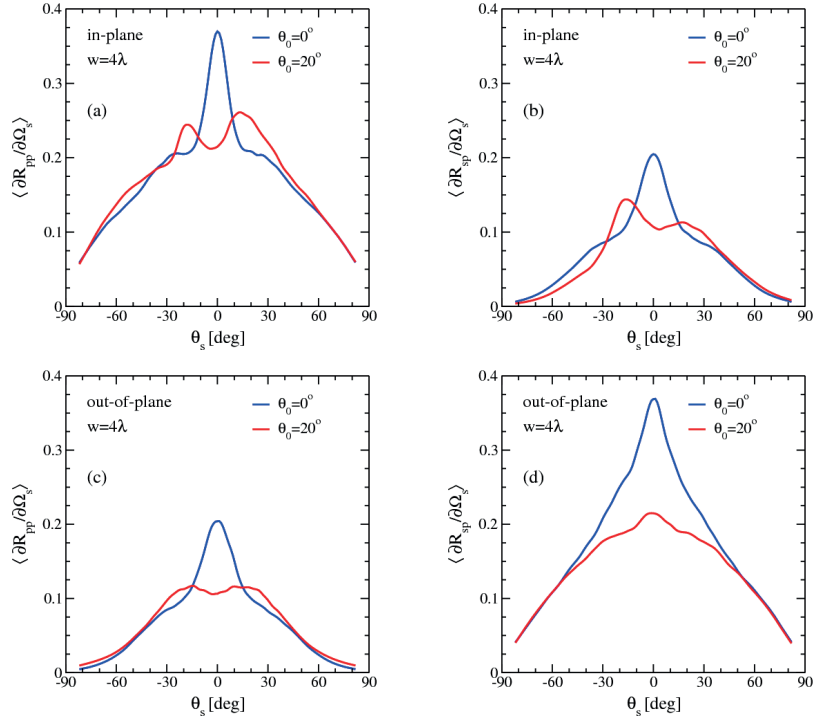
Figure 2. The mean differential reflection coefficients, $\langle \partial R_{\alpha\beta}/\partial\Omega_s \rangle$ $(\beta \to \alpha)$, as functions of the polar scattering angle θ_s for the in-plane ($\phi_s = \phi_0$ or $\phi_s = \phi_0 + 180°$) (a) co-polarized ($p \to p$) and (b) cross-polarized scattering ($p \to s$), and the out-of-plane ($\phi_s = \phi_0 \pm 90°$) (c) co-polarized ($p \to p$) and (d) cross-polarized scattering ($p \to s$) of a p-polarized incident beam ($\beta = p$) of width $w = 4\lambda$ ($\theta_0 = 0°$ and $\theta_0 = 20°$; $\phi_0 = 0°$) scattered from a Gaussian randomly rough perfectly conducting surface. The Gaussian correlated surface had a correlation length $a = 2\lambda$ and an rms height $\delta = \lambda$. To facilitate comparison between the various configurations presented in this figure, notice that we have used similar scales for all ordinate axes. Moreover, to simplify the presentation of the figures, a convention was adopted where negative (positive) values of θ_s correspond to $\phi_s = \phi_0 + 180°$ ($\phi_s = \phi_0$). (After Ref. 7).

parameters assumed in these calculations the contribution to the mean differential reflection coefficient from the light scattered coherently is smaller than the contribution from the light scattered incoherently by a factor of approximately 10^{-4}.

There is no single scattering contribution to the mean differential reflection coefficient in the cases of in-plane cross-polarized [Fig. 2(b)] and out-of-plane co-polarized [Fig. 2(c)] scattering.[1] What is plotted in these figures therefore is due to multiple scattering only. The results plotted in Figs. 2(a) and 2(d) contain a contribution from single-scattering processes.

The peaks in the retroreflection directions in the results for in-plane co-polarized scattering [Fig. 2(a)] are enhanced backscattering peaks.[19–22] However, as we will see from the full angular distribution of the intensity of the scattered light, the structures seen as peaks in the results for in-plane cross-polarized scattering [Fig. 2(b)] are not real peaks. The results that the out-of-plane co- and cross-polarized scattering [Figs. 2(c) and 2(d)] are even functions of θ_s are consequences of the scattering geometry, namely that $\phi_0 = 0°$, $\phi_s = \pm 90°$, and the isotropy of the power spectrum of the surface roughness.

The full angular distribution of the intensity of the scattered light is presented as contour plots in Fig. 3,
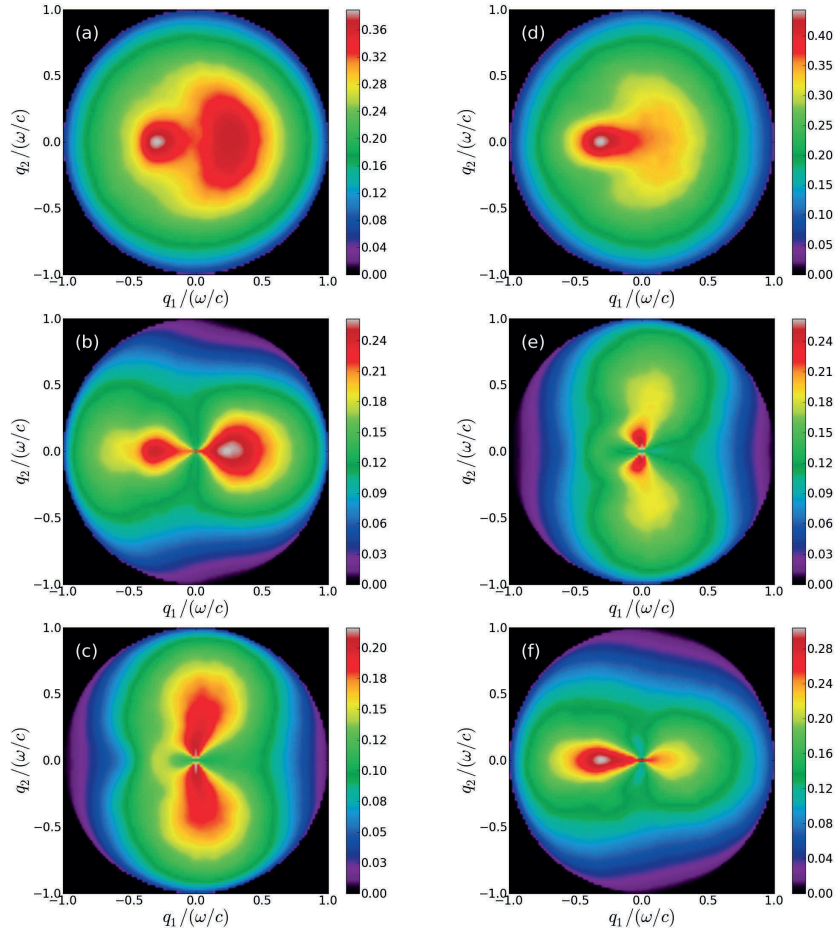
Figure 3. The complete angular distributions of the mean differential reflection coefficient, $\langle \partial R_{\alpha\beta}/\partial\Omega_s \rangle$, for the scattering of an β-polarized Gaussian beam incident on the surface at polar angle $\theta_0 = 20°$ and azimuthal angle $\phi_0 = 0°$. The perfectly conducting rough surface was characterized by a Gaussian height distribution of rms-value $\delta = \lambda$ and a Gaussian correlation function of transverse correlation length $a = 2\lambda$. The incident beam was p polarized in Figs. 3(a)–(c) [left column], and s polarized in Figs. 3(d)–(f) [right column]. Moreover, in the top two figures [Figs. 3(a) and (d)] the polarization of the scattered light was not recorded; in Figs. 3(b) and (e) [central row] only p-polarized scattered light was recorded; while the bottom two figures correspond to recording only s-polarized scattered light [Figs. 3(c) and (f)]. The rough surface, covering an area $16\lambda \times 16\lambda$, was discretized at a grid of 112×112 points corresponding to a discretization interval $\lambda/7$ for both directions. The presented figures were obtained by averaging results for the differential reflection coefficient obtained for $12\,000$ surface realizations. (After Ref. 7).

which correspond to polar and azimuthal angles of incidence $(\theta_0, \phi_s) = (20°, 0°)$, when the incident beam is p polarized and the scattered light is p and s polarized. In Fig. 3(a) we present a contour plot of the mean differential reflection coefficient for the scattering of p-polarized light into both p- and s-polarized scattered light, $i.e.$ the polarization state of the scattered light was not recorded. It is seen that there is a pronounced enhanced backscattering peak in the retroreflection direction at $\theta_s = 20°$ and $\phi_s = 180°$. From Figs. 3(b) and 3(c),

where only p-polarized light or s-polarized scattered light is recorded, respectively, we see that the co-polarized scattering displays a structure that is elongated along the plane of incidence, while the cross-polarized scattering has a scattering pattern that is elongated perpendicular to this plane. In principle an enhanced backscattering peak should be present in the retroreflection direction in both co- and cross-polarized scattering.[20–22] However, for the roughness parameters assumed in this work, instead of a well-defined peak in the retroreflection direction we see a ridge of constant enhanced intensity in parts of the region $q_1 < 0$, forming a semicircle of constant polar scattering angle $\theta_s \approx \theta_0 = 20°$, with $90° < \phi_s < 270°$ [Fig. 3(c)]. In precisely the retroreflection direction, $\theta_s = 20°$ and $\phi_s = 180°$, there is little, if any, additional enhancement in the cross-polarized scattering compared to the intensities at other values of ϕ_s in the interval $[90°, 270°]$. We speculate that the enhancement ridge seen in Fig. 3(c) is a constructive interference effect similar to the effect underlying enhanced backscattering.

We note that if we had examined only the in-plane and out-of-plane results for the same angle of incidence, the peak observed in Fig. 2(b) for $\theta_0 = 20°$ could easily have been interpreted as the well-localized feature in the retroreflection direction similar to the one present for co-polarized scattering in Fig. 3(b). Thus the angular distributions of the intensities of the scattered light, such as those presented in Fig. 3, can provide information that helps in better understanding multiple scattering phenomena.

When the incident beam was s polarized, we obtain the results presented in Figs. 3(d)–(f). Also here an enhanced backscattering peak is observed, and the intensity distributions of the co- and cross-polarized scattered light are oriented along and perpendicular to the plane of incidence, respectively.

A necessary, but not sufficient, criterion for the accuracy of a scattering calculation is that energy be conserved in the scattering process. In scattering from a perfectly conducting surface this requires that the total time-averaged scattered flux must equal the total time-averaged incident flux. This requirement can be stated as

$$U_\beta(\theta_0, \phi_0) = \sum_{\alpha=p,s} \int d\Omega_s \left\langle \frac{\partial R_{\alpha\beta}}{\partial \Omega_s} \right\rangle = 1 \qquad \beta = p, s. \tag{17}$$

Under the conditions assumed in obtaining the results presented in Figs. 2 and 3, the value of $U_p(\theta_0, \phi_0)$ and $U_s(\theta_0, \phi_0)$ were calculated to be 0.9962 and 0.9966, respectively. Consequently, the computational approach outlined in Section 2 conserves energy in the scattering process with an error that is smaller than 0.5%. This error is expected to be reduced further by decreasing the sampling interval Δx and/or by increasing the area (L^2) of the the mean surface.

2.2.2 An Anisotropic Roughness Power Spectrum

The existing computational studies of the scattering of light from two-dimension randomly rough perfectly conducting surfaces[1–7] have been based on the assumption that the surface profile function $\zeta(\mathbf{x}_\parallel)$ is a stationary, zero-mean, *isotropic*, Gaussian random process. Very little work has been devoted to the case where $\zeta(\mathbf{x}_\parallel)$ is an *anisotropic* random process. In this section we present results obtained by the rigorous computational approach described in Section 2.1 for the light scattered from a two-dimensional, randomly rough, perfectly conducting surface defined by a surface profile function that is a stationary, zero-mean, anisotropic, Gaussian random process.

The surface we assume in these calculations is defined by a surface height autocorrelation function that has an anisotropic Gaussian form, $W(\mathbf{x}_\parallel) = \exp[-(x_1/a_1)^2 - (x_2/a_2)^2]$ where, for specificity, we assume that $a_1 < a_2$. Thus, we will refer to the x_1 and x_2 axes as the minor and major axes of the anisotropy, respectively. The power spectrum of the surface roughness, defined by Eq. (1), in the present case has the form

$$g(\mathbf{k}_\parallel) = \pi a_1 a_2 \exp\left[-\frac{k_1^2 a_1^2}{4} - \frac{k_2^2 a_2^2}{4} \right], \tag{18}$$

and is elongated along the minor anisotropy axis.

To provide a reference against which results for the angular distribution of the fields scattered from an anisotropic random surface can be compared, we first present, in Fig. 4, contour plots of the angular distributions of the fields scattered from an *isotropic* random surface. The incident field is a p-polarized beam with the width
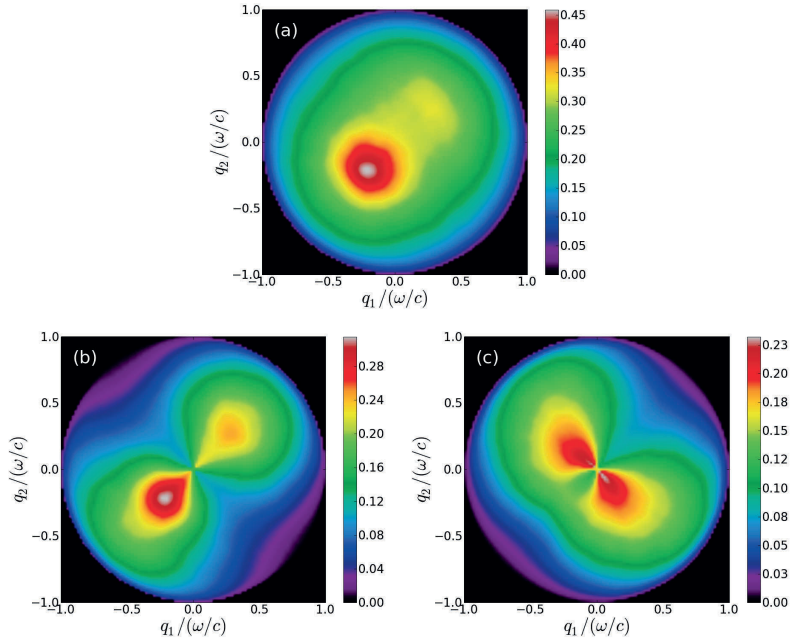
Figure 4. A p-polarized beam of wavelength λ and width $w = 4\lambda$ is scattered from an *isotropic* perfectly conducing rough surface characterized by a Gaussian height distribution of rms-value $\delta = \lambda/2$ and a Gaussian correlation function of correlation lengths $a_1 = a_2 = \lambda$. The panels show contour plots of the full angular distributions of the mean differential reflection coefficient, $\langle \partial R_{\alpha p}/\partial \Omega_s \rangle$, obtained by a rigorous computer simulation approach for the scattering of the beam incident on the rough surface at a polar angle $\theta_0 = 20°$ and an azimuthal angle $\phi_0 = 45°$. The three panels correspond to various configurations for the polarization of the scattered light. They are: (a) the polarization of the scattered light is not recorded $[\alpha = p, s]$; (b) only p-polarized scattered light is measured $[\alpha = p]$; and (c) only s-polarized scattered light is recorded $[\alpha = s]$. The rough surface, covering an area $16\lambda \times 16\lambda$, was discretized on a grid of 112×112 points corresponding to a discretization interval $\lambda/7$ for both directions. The presented figures were obtained by averaging results for the differential reflection coefficient obtained for 6 000 surface realizations. (After Ref. 8).

parameter $w = 4\lambda$, where λ is the wavelength of the field. The polar and azimuthal angles of incidence are $(\theta_0, \phi_0) = (20°, 45°)$. The surface is characterized by the Gaussian power spectrum (16), with a correlation length $a = \lambda$. The rms height of the surface is $\delta = \lambda/2$. The surface was generated on the same grid as the surface studied in Section 2.2.1. The mean differential reflection coefficient was obtained as the arithmetic average of results obtained for 6000 realizations of the surface profile function. The three panels in this figure correspond to different choices for the polarization of the scattered light. Thus, in obtaining Fig. 4(a) the polarization of the scattered light was not recorded; in obtaining Fig. 4(b) only the p-polarized component of the scattered light was recorded; while in obtaining Fig. 4(c) only the s-polarized component of the scattered light was recorded.

We see from these results that the co-polarized $(p \to p)$ scattering has a dipole-like angular distribution with the main intensity oriented parallel to the plane of incidence [Fig. 4(b)]. In contrast the cross-polarized $(p \to s)$ scattering has its main intensity distribution oriented perpendicular to the plane of incidence [Fig. 4(c)]. In both cases the intensity distributions are symmetric with respect to the plane of incidence, and the scattered intensity patterns simply rotate as the azimuthal angle of incidence ϕ_0 is changed. When the polarization of the scattered light is not recorded [Fig. 4(a)], the pronounced peak in the retroreflection direction $(\theta_s = \theta_0, \phi_s = \phi_0 + 180°)$ is the enhanced backscattering peak.
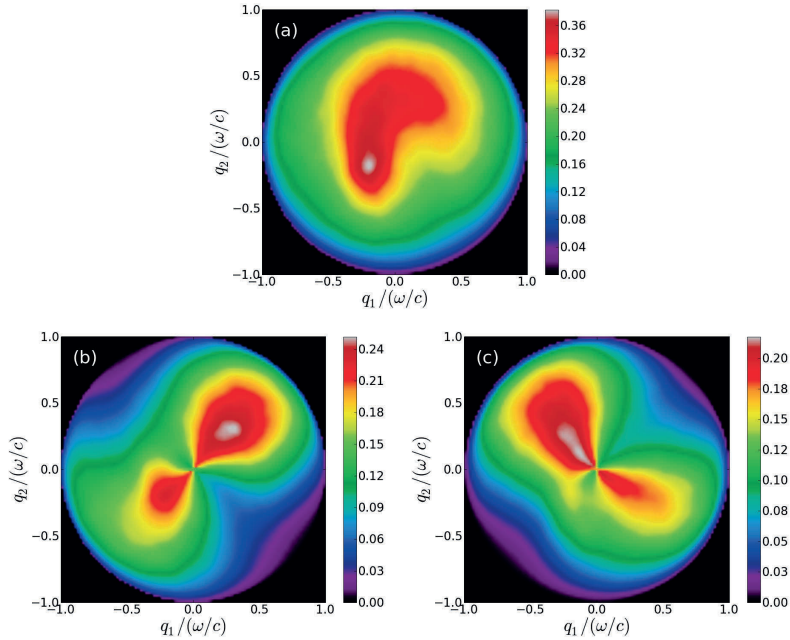
Figure 5. Same as Fig. 4 with the only difference that now the rough surface is *weakly anisotropic* and characterized by the correlation lengths $a_1 = \lambda$ and $a_2 = 1.5\lambda$. (After Ref. 8).

Turning now to the scattering from an anisotropic surface, in Fig. 5 we present contour plots of the full angular distributions of the mean differential reflection coefficients when the randomly rough surface is defined by the power spectrum (18) with $a_1 = \lambda$ and $a_2 = 1.5\lambda$. The remaining experimental and computational parameters have the values used in obtaining the results presented in Fig. 4. The three panels correspond to different choices for the polarization of the scattered light. In obtaining Fig. 5(a) the polarization of the scattered light was not recorded; in obtaining Fig. 5(b) only the p-polarized component of the scattered light was recorded; while in obtaining Fig. 5(c) only the s-polarized component of the scattered light was recorded. Unlike in the scattering of light from an isotropic surface, the intensity distribution of light scattered from an anisotropic surface in general is not symmetric with respect to the plane of incidence. It is only when the plane of incidence is parallel to either the minor or the major axis of the anisotropy that this type of symmetry obtains.

The dipole-like angular intensity patterns in Figs. 5(b) and 5(c) are no longer symmetric with respect to the plane of incidence, as their isotropic equivalents are. This asymmetry is particularly pronounced in the cross-polarized scattering [Fig. 5(c)]. It is explained by the fact that the cross-polarized component of the mean differential reflection coefficient to the lowest (second) order in the surface profile function is proportional to $g(\mathbf{q}_\parallel - \mathbf{k}_\parallel) \, [(\hat{\mathbf{q}}_\parallel \times \hat{\mathbf{k}}_\parallel)_3]^2$, where $\mathbf{q}_\parallel = (\omega/c)\sin\theta_s(\cos\phi_s \sin\phi_s, 0)$.[23] When the power spectrum $g(\mathbf{k}_\parallel)$ is given by Eq. (18), this function is not symmetric with respect to the plane of incidence.

The co-polarized scattering pattern [Fig. 5(b)] is explained in a similar fashion. In this case the contribution to the mean differential reflection coefficient of the lowest order in the surface profile function contains terms proportional to $g(\mathbf{q}_\parallel - \mathbf{k}_\parallel)(\hat{\mathbf{q}}_\parallel - \hat{\mathbf{k}}_\parallel)^m$ with $m = 1, 2$.[23] The maxima of these functions are in the forward scattering direction and, for an anisotropic surface, move away from the plane of incidence toward the minor axis of the anisotropy.

3. A PENETRABLE SURFACE

3.1 Mathematical Formulation

In calculating the electromagnetic field scattered from a two-dimensional randomly rough surface a convenient starting point are the Franz formulas of electromagnetic scattering theory.[24, 25] These formulas for the magnetic and electric fields in the vacuum region $x_3 > \zeta(\mathbf{x}_\parallel)$ can be written as

$$
\mathbf{H}^>(\mathbf{x}|\omega) = \mathbf{H}(\mathbf{x}|\omega)_{\text{inc}} + \frac{1}{4\pi}\boldsymbol{\nabla} \times \int \mathrm{d}^2x'_\parallel \ g_0(\mathbf{x}|\mathbf{x}')|_{x'_3=\zeta(\mathbf{x}'_\parallel)}\mathbf{J}_H(\mathbf{x}'_\parallel|\omega)
$$
$$
-\frac{\mathrm{i}c}{4\pi\omega}\boldsymbol{\nabla} \times \boldsymbol{\nabla} \times \int \mathrm{d}^2x'_\parallel \ g_0(\mathbf{x}|\mathbf{x}')|_{x'_3=\zeta(\mathbf{x}'_\parallel)}\mathbf{J}_E(\mathbf{x}'_\parallel|\omega) \tag{19a}
$$

$$
\mathbf{E}^>(\mathbf{x}|\omega) = \mathbf{E}(\mathbf{x}|\omega)_{\text{inc}} + \frac{1}{4\pi}\boldsymbol{\nabla} \times \int \mathrm{d}^2x'_\parallel \ g_0(\mathbf{x}|\mathbf{x}')|_{x'_3=\zeta(\mathbf{x}'_\parallel)}\mathbf{J}_E(\mathbf{x}'_\parallel|\omega)
$$
$$
+\frac{\mathrm{i}c}{4\pi\omega}\boldsymbol{\nabla} \times \boldsymbol{\nabla} \times \int \mathrm{d}^2x'_\parallel \ g_0(\mathbf{x}|\mathbf{x}')|_{x'_3=\zeta(\mathbf{x}'_\parallel)}\mathbf{J}_H(\mathbf{x}'_\parallel|\omega). \tag{19b}
$$

The Franz formulas for the magnetic and electric fields in the scattering medium $x_3 < \zeta(\mathbf{x}_\parallel)$ can be written as

$$
\mathbf{H}^<(\mathbf{x}|\omega) = -\frac{1}{4\pi}\boldsymbol{\nabla} \times \int \mathrm{d}^2x'_\parallel \ g_\varepsilon(\mathbf{x}|\mathbf{x}')|_{x'_3=\zeta(\mathbf{x}'_\parallel)}\mathbf{J}_H(\mathbf{x}'_\parallel|\omega)
$$
$$
+\frac{\mathrm{i}c}{4\pi\omega}\boldsymbol{\nabla} \times \boldsymbol{\nabla} \times \int \mathrm{d}^2x'_\parallel \ g_\varepsilon(\mathbf{x}|\mathbf{x}')|_{x'_3=\zeta(\mathbf{x}'_\parallel)}\mathbf{J}_E(\mathbf{x}'_\parallel|\omega) \tag{20a}
$$

$$
\mathbf{E}^<(\mathbf{x}|\omega) = -\frac{1}{4\pi}\boldsymbol{\nabla} \times \int \mathrm{d}^2x'_\parallel \ g_\varepsilon(\mathbf{x}|\mathbf{x}')|_{x'_3=\zeta(\mathbf{x}'_\parallel)}\mathbf{J}_E(\mathbf{x}'_\parallel|\omega)
$$
$$
-\frac{\mathrm{i}c}{4\pi\omega\varepsilon(\omega)}\boldsymbol{\nabla} \times \boldsymbol{\nabla} \times \int \mathrm{d}^2x_\parallel \ g_\varepsilon(\mathbf{x}|\mathbf{x}')|_{x'_3=\zeta(\mathbf{x}'_\parallel)}\mathbf{J}_H(\mathbf{x}'_\parallel|\omega). \tag{20b}
$$

In writing these equations we have introduced the vectors

$$
\mathbf{J}_H(\mathbf{x}_\parallel|\omega) = \left[\mathbf{n} \times \mathbf{H}^>(\mathbf{x}|\omega)\right]\big|_{x_3=\zeta(\mathbf{x}_\parallel)}, \tag{21a}
$$
$$
= \left[\mathbf{n} \times \mathbf{H}^<(\mathbf{x}|\omega)\right]\big|_{x_3=\zeta(\mathbf{x}_\parallel)}, \tag{21b}
$$

and

$$
\mathbf{J}_E(\mathbf{x}_\parallel|\omega) = \left[\mathbf{n} \times \mathbf{E}^>(\mathbf{x}|\omega)\right]\big|_{x_3=\zeta(\mathbf{x}_\parallel)}, \tag{22a}
$$
$$
= \left[\mathbf{n} \times \mathbf{E}^<(\mathbf{x}|\omega)\right]\big|_{x_3=\zeta(\mathbf{x}_\parallel)}. \tag{22b}
$$

The vector $\mathbf{n}$ has been defined in Section 2.1. The scalar free-space Green's function for an infinite scattering medium is defined by

$$
g_\varepsilon(\mathbf{x}|\mathbf{x}') = \frac{\exp\left[-\left|\mathbf{x} - \mathbf{x}'\right|/d(\omega)\right]}{\left|\mathbf{x} - \mathbf{x}'\right|} \tag{23a}
$$
$$
= \int \frac{\mathrm{d}^2k_\parallel}{(2\pi)^2} \frac{2\pi}{\beta(k_\parallel)} \exp\left[\mathrm{i}\mathbf{k}_\parallel \cdot (\mathbf{x}_\parallel - \mathbf{x}'_\parallel)\right]\exp\left[-\beta(k_\parallel)|x_3 - x'_3|\right], \tag{23b}
$$

where

$$
\beta(k_\parallel) = \left[k_\parallel^2 + \frac{1}{d^2(\omega)}\right]^{\frac{1}{2}}, \qquad \operatorname{Re}\beta(k_\parallel) > 0, \operatorname{Im}\beta(k_\parallel) < 0, \tag{24}
$$

and $d(\omega) = (c/\omega)[-\varepsilon(\omega)]^{-\frac{1}{2}}$, $\mathrm{Re}\, d(\omega) > 0$, $\mathrm{Im}\, d(\omega) > 0$, while $\varepsilon(\omega)$ is the dielectric function of the scattering medium.

To obtain the equations satisfied by $\mathbf{J}_H(\mathbf{x}_\parallel|\omega)$ and $\mathbf{J}_E(\mathbf{x}_\parallel|\omega)$ we proceed as follows. We take the vector cross product of Eqs. (19a) and (20a) with the vector $\mathbf{n}$, evaluate each product at $x_3 = \zeta(\mathbf{x}_\parallel) + \eta$, and $x_3 = \zeta(\mathbf{x}_\parallel) - \eta$, respectively, where η is a positive infinitesimal, and add the resulting equations. In this way we obtain the equation

$$
\begin{aligned}
\mathbf{J}_H(\mathbf{x}_\parallel|\omega) \;=\; & \mathbf{J}_H(\mathbf{x}_\parallel|\omega)_{\mathrm{inc}} + \frac{1}{4\pi} P \int \mathrm{d}^2 x'_\parallel \; [\![\mathbf{n} \times \{ \boldsymbol{\nabla} \times [g_0(\mathbf{x}|\mathbf{x}') - g_\varepsilon(\mathbf{x}|\mathbf{x}')] \mathbf{J}_H(\mathbf{x}'_\parallel|\omega) \}]\!] \\
& - \frac{\mathrm{i}c}{4\pi\omega} \int \mathrm{d}^2 x'_\parallel \; [\![\mathbf{n} \times \{ \boldsymbol{\nabla} \times \boldsymbol{\nabla} \times [g_0(\mathbf{x}|\mathbf{x}') - g_\varepsilon(\mathbf{x}|\mathbf{x}')] \mathbf{J}_E(\mathbf{x}'_\parallel|\omega) \}]\!],
\end{aligned} \tag{25a}
$$

where $\mathbf{J}_H(\mathbf{x}_\parallel|\omega)_{\mathrm{inc}} = \mathbf{n} \times \mathbf{H}(\mathbf{x}|\omega)_{\mathrm{inc}}|_{x_3=\zeta(\mathbf{x}_\parallel)}$, and P denotes the Cauchy principal value.

If we next take the vector cross product of Eq. (19b) and of $\varepsilon(\omega)$ times Eq. (20b) with the vector $\mathbf{n}$, evaluate each product at $x_3 = \zeta(\mathbf{x}_\parallel) + \eta$, and at $x_3 = \zeta(\mathbf{x}_\parallel) - \eta$, respectively, and add the resulting equations, we obtain

$$
\begin{aligned}
\mathbf{J}_E(\mathbf{x}_\parallel|\omega) \;=\; & 2\frac{\mathbf{J}_E(\mathbf{x}_\parallel|\omega)_{\mathrm{inc}}}{1 + \varepsilon(\omega)} + \frac{2}{4\pi[1 + \varepsilon(\omega)]} P \int \mathrm{d}^2 x'_\parallel \; [\![\mathbf{n} \times \{ \boldsymbol{\nabla} \times [g_0(\mathbf{x}|\mathbf{x}') - \varepsilon(\omega)g_\varepsilon(\mathbf{x}|\mathbf{x}')] \mathbf{J}_E(\mathbf{x}'_\parallel|\omega) \}]\!] \\
& + \frac{2\mathrm{i}c}{4\pi\omega[1 + \varepsilon(\omega)]} \int \mathrm{d}^2 x'_\parallel \; [\![\mathbf{n} \times \{ \boldsymbol{\nabla} \times \boldsymbol{\nabla} \times [g_0(\mathbf{x}|\mathbf{x}') - g_\varepsilon(\mathbf{x}|\mathbf{x}')] \mathbf{J}_H(\mathbf{x}'_\parallel|\omega) \}]\!],
\end{aligned} \tag{25b}
$$

where $\mathbf{J}_E(\mathbf{x}_\parallel|\omega)_{\mathrm{inc}} = \mathbf{n} \times \mathbf{E}(\mathbf{x}|\omega)_{\mathrm{inc}}|_{x_3=\zeta(\mathbf{x}_\parallel)}$.

In obtaining Eq. (25) we have used the results

$$
\begin{aligned}
\lim_{\eta \to 0^+} \int \mathrm{d}^2 x'_\parallel \; \mathbf{n}(\mathbf{x}_\parallel) \times & \left\{ \boldsymbol{\nabla} \times \left[g(\mathbf{x}|\mathbf{x}')\Big|_{\substack{x_3=\zeta(\mathbf{x}_\parallel) \\ x'_3=\zeta(\mathbf{x}'_\parallel)\pm\eta}} \mathbf{J}(\mathbf{x}'_\parallel|\omega) \right] \right\} \\
& = \pm 2\pi \mathbf{J}(\mathbf{x}_\parallel|\omega) + P \int \mathrm{d}^2 x'_\parallel \; \mathbf{n}(\mathbf{x}_\parallel) \times \left\{ [\![\boldsymbol{\nabla} \times [g(\mathbf{x}|\mathbf{x}')] \, \mathbf{J}(\mathbf{x}'_\parallel|\omega)]\!] \right\},
\end{aligned} \tag{26}
$$

where $g(\mathbf{x}|\mathbf{x}')$ is either $g_0(\mathbf{x}|\mathbf{x}')$ or $g_\varepsilon(\mathbf{x}|\mathbf{x}')$, $\mathbf{J}(\mathbf{x}_\parallel|\omega)$ is either $\mathbf{J}_H(\mathbf{x}_\parallel|\omega)$ or $\mathbf{J}_E(\mathbf{x}_\parallel|\omega)$, and P denotes the Cauchy principal value. Equations of the type of Eq. (25) are called Müller integral equations.[26,27] These equations are convenient for numerical calculations. Because $g_0(\mathbf{x}|\mathbf{x}')$ and $g_\varepsilon(\mathbf{x}|\mathbf{x}')$ have the same limiting behavior as $\mathbf{x}' \to \mathbf{x}$, the most divergent terms in the integrands, associated with the second derivatives of these Green's functions, cancel, rendering the resulting integrals integrable. The terms containing the first derivatives of the Green's functions possess integrable singularities.

From the definitions of $\mathbf{J}_{H,E}(\mathbf{x}_\parallel|\omega)$ it follows that $\mathbf{n} \cdot \mathbf{J}_{H,E}(\mathbf{x}_\parallel|\omega) = 0$. Therefore $\mathbf{J}_{H,E}(\mathbf{x}_\parallel|\omega)$ have only two independent elements, which we choose to be $J_{H,E}(\mathbf{x}_\parallel|\omega)_1$ and $J_{H,E}(\mathbf{x}_\parallel|\omega)_2$. The elements $J_{H,E}(\mathbf{x}_\parallel|\omega)_3$ are then obtained from the analogues of Eq. (6). Equations (25) thus provide a system of four coupled, inhomogeneous two-dimensional integral equations for $J_{H,E}(\mathbf{x}_\parallel|\omega)_{1,2}$.

By the use of a local impedance boundary condition,[28]

$$
J_E(\mathbf{x}_\parallel|\omega)_i \;=\; K_{ij}(\mathbf{x}_\parallel|\omega) J_H(\mathbf{x}_\parallel|\omega)_j \qquad (i = 1, 2), \tag{27}
$$

the dependence on $J_E(\mathbf{x}_\parallel|\omega)_{1,2}$ can be removed from Eq. (25a), yielding a pair of coupled, inhomogeneous, two-dimensional, integral equations for $J_H(\mathbf{x}_\parallel|\omega)_{1,2}$. These equations are converted into matrix equations in the manner described in Section 2, which are then solved by the biconjugate gradient stabilized method. The solutions are used to calculate the contribution to the mean differential reflection coefficient from the light scattered incoherently, by the use of the expressions obtained in Section 2.
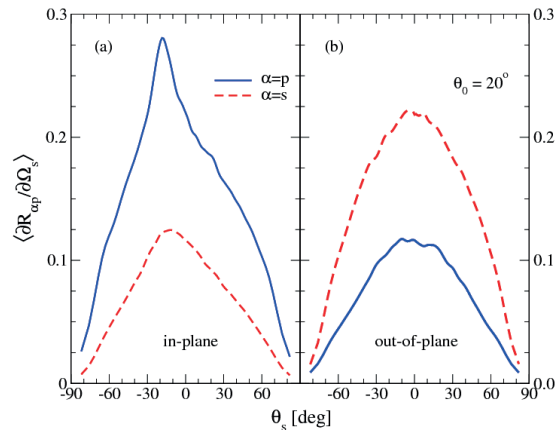
Figure 6. The mean differential reflection coefficients, $\langle \partial R_{\alpha p} / \partial \Omega_s \rangle$ $(p \to \alpha)$ for a p-polarized incident beam of wavelength $\lambda = 632.8$nm and width $w = 4\lambda$, whose polar angle of incidence is $\theta_0 = 20°$, as functions of the polar scattering angle θ_s for the (a) in-plane and (b) out-of-plane scattering. Negative values for θ_s are interpreted as in the caption to Fig. 2. The scattering system assumed in obtaining these results consisted of a silver substrate $(\varepsilon(\omega) = -16 + i1.088)$ separated from vacuum by a Gaussian-correlated randomly rough surface of rms-height $\delta = \lambda/4$ and correlation length $a = \lambda/2$. The randomly rough surface covered an area of $16\lambda \times 16\lambda$ and the discretization length used in the numerical calculations was $\Delta x = \lambda/7$ thus resulting in a 112×112 grid of $\mathbf{x}_\parallel$ values. A total of 5 000 surface realizations were used to calculate $\langle \partial R_{\alpha p} / \partial \Omega_s \rangle$. (After Ref. 14).

3.2 Results for a Penetrable Surface

3.2.1 A Metallic Surface

We first present results for scattering from a metallic surface. We have carried out numerical simulations for the scattering of a p-polarized beam of light of wavelength $\lambda = 632.8$ nm and width parameter $w = 4\lambda$, incident on a randomly rough silver surface. The dielectric function of silver at this wavelength is $\varepsilon(\omega) = -16.00 + i1.088$.[29] The surface roughness is characterized by the Gaussian power spectrum (16) with a correlation length $a = \lambda/2$, and an rms height $\delta = \lambda/4$. The rough surface was assumed to cover an area $16\lambda \times 16\lambda$ on the mean scattering surface, and the discretization length Δx was $\lambda/7$ on a 112×112 grid of $\mathbf{x}_\parallel$ values.

In Fig. 6 we present the mean differential reflection coefficients as functions of the polar scattering angle θ_s for the in-plane [Fig. 6(a)] and out-of-plane $(\phi_s = \pm 90°)$ [Fig. 6(b)], co-$(p \to p)$ and cross-$(p \to s)$ scattering of the beam when the polar and azimuthal angles of incidence (θ_0, ϕ_0) are $(20°, 0°)$. The results obtained from $N_p = 5\,000$ realizations of the surface profile function were averaged to obtain these results. The calculations required 96 CPU seconds on a 2.67 GHz Intel i7 CPU for each realization of the surface profile function. The peak at $\theta_s = -20°$ in the mean differential reflection coefficient for in-plane co-polarized scattering plotted in Fig. 6(a) is the enhanced backscattering peak.

For the same parameters we present in Figs. 7(a)–(c) the full angular distribution of the mean differential reflection coefficient when the polarization state of the scattered light is not recorded [Fig. 7(a)], when only the p-polarized component of the scattered light is recorded [Fig. 7(b)], and when only the s-polarized component of the scattered light is recorded [Fig. 7(c)]. Similar results, but for an s-polarized incident beam, are presented in Figs. 7(d)–(f). The peaks observed in Figs. 7(a), 7(b), 7(d), and 7(f) in the retroreflection direction $(\theta_s = \theta_0, \phi_s = \phi_0 + 180°)$ are the enhanced backscattering peaks.

From a knowledge of the full angular distribution of the mean differential reflection coefficient, the conservation of energy in the scattering process can be checked by means of Eq. (17). For this purpose the full angular distribution of the mean differential reflection coefficient was calculated for "nonabsorbing" silver, *i.e.* for the
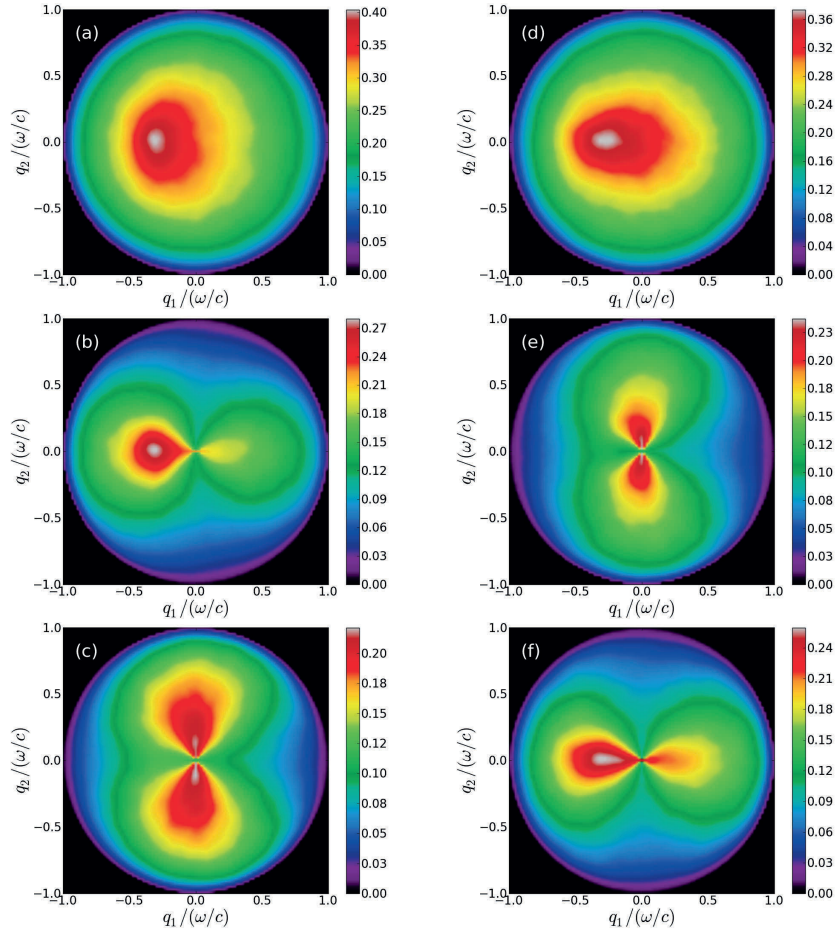
Figure 7. Similar to Fig. 3, but now the scattering medium is silver, and therefore penetrable. The roughness and numerical parameters assumed in obtaining these results are identical to those used to obtain the results of Fig. 6.

case in which the imaginary part of its dielectric function was set equal to zero, so that $\varepsilon(\omega) = -16.00$. For the parameters used in obtaining the results presented in Figs. 6 and 7 it was found that $U_{p,s}(20°, 0°) > 0.995$, a result that demonstrates the accuracy of our computational approach.

In order to obtain such a good unitarity value it was necessary to treat not only the diagonal elements of the matrix versions of Eq. (25) accurately, but also close-to-diagonal elements, because of the singular behavior of the Green's functions for small arguments. The need to treat close-to-diagonal matrix elements more accurately than matrix elements between more widely separated points in the solution of the volume integral equation arising in scattering from finite-sized objects has also been noted.[30] If the extended midpoint method was used in calculating the off-diagonal matrix elements, while the diagonal elements were treated exactly, as in [6] and [9], a value of $U_p(20°, 0°) = 0.834$ was obtained. The ability to calculate unitarity values, and the need to treat close-to-diagonal matrix elements accurately to obtain good unitarity values, are some of the main results of this work.

4. SOLUTION OF THE REDUCED RAYLEIGH EQUATIONS

4.1 Mathematical Formulation

The calculation of the electromagnetic field scattered from a randomly rough surface of a penetrable medium is greatly simplified if the field in the scattering medium does not need to be taken into account. The use of an impedance boundary condition at the interface between the medium of incidence and the scattering medium accomplishes this, so that only the field in the medium of incidence needs to be determined.

The same result can also be achieved by the use of the reduced Rayleigh equation for calculating the scattered field. In this section we present this equation and describe its numerical solution.

We begin by writing the electric field in the vacuum region $x_3 > \zeta(\mathbf{x}_\parallel)$ as the sum of an incident and a scattered field, $\mathbf{E}(\mathbf{x}; t) = \left[\mathbf{E}^{(i)}(\mathbf{x}|\omega) + \mathbf{E}^{(s)}(\mathbf{x}|\omega) \right] \exp(-i\omega t)$, where

$$\mathbf{E}^{(i)}(\mathbf{x}|\omega) = \left\{ \frac{c}{\omega} \left[\alpha_0(k_\parallel) \hat{\mathbf{k}}_\parallel + k_\parallel \hat{\mathbf{x}}_3 \right] \mathcal{E}_p^{(i)}(\mathbf{k}_\parallel) + [\hat{\mathbf{k}}_\parallel \times \hat{\mathbf{x}}_3] \, \mathcal{E}_s^{(i)}(\mathbf{k}_\parallel) \right\} \exp\left[i\mathbf{k}_\parallel \cdot \mathbf{x}_\parallel - i\alpha_0(k_\parallel) x_3 \right] , \tag{28a}$$

$$\mathbf{E}^{(s)}(\mathbf{x}|\omega) = \int \frac{d^2 q_\parallel}{(2\pi)^2} \left\{ \frac{c}{\omega} \left[-\alpha_0(q_\parallel) \hat{\mathbf{q}}_\parallel + q_\parallel \hat{\mathbf{x}}_3 \right] \mathcal{E}_p^{(s)}(\mathbf{q}_\parallel) + [\hat{\mathbf{q}}_\parallel \times \hat{\mathbf{x}}_3] \, \mathcal{E}_s^{(s)}(\mathbf{q}_\parallel) \right\} \exp\left[i\mathbf{q}_\parallel \cdot \mathbf{x}_\parallel + i\alpha_0(q_\parallel) x_3 \right] . \tag{28b}$$

Note that the factors appearing in Eq. (28) in front of $\mathcal{E}_\alpha^{(i)}(\mathbf{k}_\parallel)$ and $\mathcal{E}_\alpha^{(s)}(\mathbf{q}_\parallel)$ ($\alpha = p, s$) are the polarization vectors as defined previously in Section 2.1, but now written out explicitly. Maxwell's equations imply a linear relation between the amplitudes $\mathcal{E}_\alpha^{(s)}(\mathbf{q}_\parallel)$ and $\mathcal{E}_\beta^{(i)}(\mathbf{k}_\parallel)$ of the form ($\alpha = p, s$, $\beta = p, s$)

$$\mathcal{E}_\alpha^{(s)}(\mathbf{q}_\parallel) = \sum_\beta R_{\alpha\beta}(\mathbf{q}_\parallel | \mathbf{k}_\parallel) \mathcal{E}_\beta^{(i)}(\mathbf{k}_\parallel). \tag{29}$$

The contribution to the mean differential reflection coefficient from the incoherent (diffuse) component of the scattered light, when incident light of β polarization (whose wave vector has the projection $\mathbf{k}_\parallel$ on the mean scattering surface) into light of α polarization (whose wave vector has the projection $\mathbf{q}_\parallel$ on the mean scattering surface), is given by

$$\left\langle \frac{\partial R_{\alpha\beta}}{\partial \Omega_s} \right\rangle_{\text{incoh}} = \frac{1}{S} \left(\frac{\omega}{2\pi c} \right)^2 \frac{\cos^2 \theta_s}{\cos \theta_0} \left[\left\langle \left| R_{\alpha\beta}(\mathbf{q}_\parallel | \mathbf{k}_\parallel) \right|^2 \right\rangle - \left| \left\langle R_{\alpha\beta}(\mathbf{q}_\parallel | \mathbf{k}_\parallel) \right\rangle \right|^2 \right] , \tag{30}$$

where S is the area of the plane $x_3 = 0$ covered by the rough surface.

It was shown by Celli and his colleagues[32] by the use of the Rayleigh hypothesis,[33] the extinction theorem,[34] and the vectorial equivalent of the Kirchhoff integral,[35] that the scattering amplitudes $R_{\alpha\beta}(\mathbf{q}_\parallel | \mathbf{k}_\parallel)$ satisfy the matrix integral equation

$$\int \frac{d^2 q_\parallel}{(2\pi)^2} \frac{I(\alpha(p_\parallel) - \alpha_0(q_\parallel) | \mathbf{p}_\parallel - \mathbf{q}_\parallel)}{\alpha(p_\parallel) - \alpha_0(q_\parallel)} \, \mathbf{M}(\mathbf{p}_\parallel | \mathbf{q}_\parallel) \mathbf{R}(\mathbf{q}_\parallel | \mathbf{k}_\parallel) = -\frac{I(\alpha(p_\parallel) + \alpha_0(k_\parallel) | \mathbf{p}_\parallel - \mathbf{k}_\parallel)}{\alpha(p_\parallel) + \alpha_0(k_\parallel)} \mathbf{N}(\mathbf{p}_\parallel | \mathbf{k}_\parallel), \tag{31}$$

with R_{pp} and R_{ps} forming the first row of the matrix $\mathbf{R}$, where

$$I(\gamma | \mathbf{Q}_\parallel) = \int d^2 x_\parallel \exp\left[-i\gamma \zeta(\mathbf{x}_\parallel) \right] \exp\left[-i\mathbf{Q}_\parallel \cdot \mathbf{x}_\parallel \right] , \tag{32}$$

and $\alpha(p_\parallel) = [\varepsilon(\omega)(\omega/c)^2 - p_\parallel^2]^{\frac{1}{2}}$, with $\operatorname{Re} \alpha(p_\parallel) > 0$, $\operatorname{Im} \alpha(p_\parallel) > 0$. The matrices $\mathbf{M}(\mathbf{p}_\parallel | \mathbf{q}_\parallel)$ and $\mathbf{N}(\mathbf{p}_\parallel | \mathbf{k}_\parallel)$ are given by

$$\mathbf{M}(\mathbf{p}_\parallel | \mathbf{q}_\parallel) = \begin{pmatrix} [p_\parallel q_\parallel + \alpha(p_\parallel) \hat{\mathbf{p}}_\parallel \cdot \hat{\mathbf{q}}_\parallel \alpha_0(q_\parallel)] & -\frac{\omega}{c} \alpha(p_\parallel) [\hat{\mathbf{p}}_\parallel \times \hat{\mathbf{q}}_\parallel]_3 \\ \frac{\omega}{c} [\hat{\mathbf{p}}_\parallel \times \hat{\mathbf{q}}_\parallel]_3 \, \alpha_0(q_\parallel) & \frac{\omega^2}{c^2} \hat{\mathbf{p}}_\parallel \cdot \hat{\mathbf{q}}_\parallel \end{pmatrix} \tag{33a}$$

and

$$\mathbf{N}(\mathbf{p}_\parallel | \mathbf{k}_\parallel) = \begin{pmatrix} [p_\parallel k_\parallel - \alpha(p_\parallel) \hat{\mathbf{p}}_\parallel \cdot \hat{\mathbf{k}}_\parallel \alpha_0(k_\parallel)] & -\frac{\omega}{c} \alpha(p_\parallel) [\hat{\mathbf{p}}_\parallel \times \hat{\mathbf{k}}_\parallel]_3 \\ -\frac{\omega}{c} [\hat{\mathbf{p}}_\parallel \times \hat{\mathbf{k}}_\parallel]_3 \, \alpha_0(k_\parallel) & \frac{\omega^2}{c^2} \hat{\mathbf{p}}_\parallel \cdot \hat{\mathbf{k}}_\parallel \end{pmatrix} . \tag{33b}$$
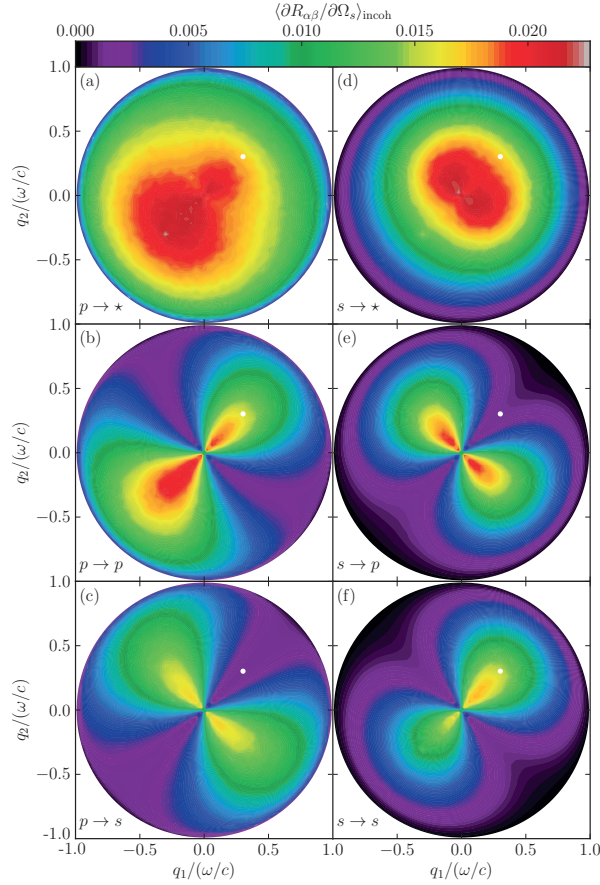
Figure 8. Full angular intensity distribution of the light scattered incoherently from a two-dimensional randomly rough silver surface calculated by solving the reduced Rayleigh equations. Light of either p (left column) or s polarization (right column) is incident on the surface at angles of incidence $(\theta_0, \phi_0) = (25°, 45°)$. The wavelength (in vacuum) of the incident light is $\lambda = 632.8$ nm for which frequency $\omega = 2\pi/\lambda$ the dielectric function of silver is $\varepsilon(\omega) = -16.0 + 1.088$i. The white dots indicate the position of the specular direction. The surface parameters assumed in these calculations are $L = 25\lambda$; $\delta = \lambda/40$; and $a = \lambda/4$. The surface was discretized so that $Q = 6.4\omega/c$ or equivalently $\Delta x = \pi/Q \approx 0.0781\lambda$. Figures 8(a)–(c) correspond to a p-polarized plane incident wave, while in Figs. 8(d)–(f) the incident plane wave is s polarized. In Figs. 8(a) and (d) all scattered light is recorded, *i.e.* no distinction is made between scattered p- and s-polarized light. However, in Figs. 8(b) and (e) only the scattered p-polarized light is recorded, while Figs. 8(c) and (f) include only s-polarized scattered light. The presented figures were obtained by averaging the results for the differential reflection coefficient obtained for $N_p = 10\,000$ surface realizations.

Although purely numerical, nonperturbative solutions of the reduced Rayleigh equations for the scattering of light from one-dimensional randomly rough clean metal surfaces[36,37] and coated perfectly conducting surfaces[38,39] have been carried out, up to now Eq. (31) has been solved only by small-amplitude perturbation theory through terms of third order in the surface profile fuction.[23,40,41] Here we present some preliminary results for the mean differential reflection coefficient obtained by a purely numerical, nonperturbative solution of Eqs. (31)–(33). This was done by generating a realization of the surface profile as this was done in the preceding two sections, and evaluating the function $I(\gamma|\mathbf{Q}_\parallel)$ by expanding the integrand in Eq. (32) in powers of $\zeta(\mathbf{x}_\parallel)$, and

calculating the Fourier transform of $\zeta^n(\mathbf{x}_\parallel)$ by the Fast Fourier Transform. As in previous sections, the random surface covered a square region of the $x_1 x_2$ plane of edge L, and a grid of N^2 points was created within this square so that the (linear) sampling interval is $\Delta x = L/N$. The infinite limits of integration in Eq. (31) were replaced by finite ones: $|q_1| < Q/2$, $|q_2| < Q/2$ where $Q = \pi/\Delta x$. A quadratic grid within the square region of the $q_1 q_2$ plane of edge Q was constructed with a grid constant $\Delta q = 2\pi/L$. The integral over this region in Eq. (31) was carried out by a two-dimensional version of the extended midpoint method, and the values of $R_{\alpha\beta}(\mathbf{q}_\parallel|\mathbf{k}_\parallel)$ were calculated for values of $\mathbf{q}_\parallel$ at the points of this grid for a given value of $\mathbf{k}_\parallel$, which was a point on the same grid. The resulting matrix equations were solved by LU factorization. This is a slower solution method than the biconjugate gradient stabilized method, but has the advantage of being able to handle multiple right-hand sides, *i.e.* different angles of incidence, more-or-less with no extra addition to the computational time. With the reflection amplitudes, $R_{\alpha\beta}(\mathbf{q}_\parallel|\mathbf{k}_\parallel)$, available, the differential reflection coefficient was then calculated by the use of Eq. (30).

4.2 Results Obtained by the Solution of the Reduced Rayleigh Equations

4.2.1 A Metallic Surface

As the first example of the application of this approach to the scattering of light from a penetrable surface we apply it to the scattering of a p- or s-polarized plane wave of wavelength $\lambda = 632.8$ nm incident on a silver surface. The dielectric function of silver at this wavelength is $\varepsilon(\omega) = -16 + \mathrm{i}1.088$.[29] The roughness of the surface was characterized by the Gaussian power spectrum, Eq. (16), where the transverse correlation length was given the value $a = \lambda/4$, while the rms height of the surface was $\delta = \lambda/40$. In the calculations the rough surface was assumed to cover an area of $25\lambda \times 25\lambda$ of the plane $x_3 = 0$, while for the wavenumber cut-off we assumed $Q = 6.4\omega/c$, which corresponds to a spatial discretization interval of $\Delta x = \pi/Q \approx 0.0781\lambda$ (for both directions).

In Fig. 8 we present contributions to the mean differential reflection coefficients from the light scattered incoherently as functions of q_1 and q_2 when a plane wave is incident on the surface at angles $(\theta_0, \phi_0) = (25°, 45°)$. Figure 8(a) corresponds to a p-polarized incident plane wave being scattered by the rough surface into both p- and s-polarized light, *i.e.* the polarization state of the scattered light was not recorded. However, in Figs. 8(b) and 8(c) contour plots of the same quantity are presented for the cases where only p-polarized or s-polarized scattered light, respectively, are recorded. Similar results are presented in Figs. 8(d)–(f) for the case when the incident light is s-polarized. An arithmetic average of results obtained for $N_p = 10\,000$ realizations of the surface profile function was carried out to produce Fig. 8.

By artificially putting the imaginary part of the dielectric constant of the metal to zero, $\mathrm{Im}\,\varepsilon(\omega) \equiv 0$, so that there is no absorption in the scattering system, it has been found that the numerical method used to solve the reduced Rayleigh equation, Eq. (31), conserves energy with an error smaller than 0.5% for the parameters assumed here.

The numerical calculations used to obtain the results of Fig. 8 required for each realization of the surface profile function approximately 8.8 cpu hours on a single 12-core 2.4 GHz AMD Opteron computer node and using approximately 20 GB of memory.

The calculations whose results are presented in Fig. 8 and which were performed by solving numerically the reduced Rayleigh equations (31), could also have been done by solving the Müller equations, as was discussed in Section 3. In order to compare the two approaches, we present in Fig. 9 the results obtained by these two methods for the contributions to the mean differential reflection coefficients from the light scattered incoherently as functions of the polar scattering angle θ_s for the in-plane ($\phi_s = 0°, 180°$) and out-of-plane ($\phi_s = \pm90°$) co-($s \to s$) and cross-($s \to p$) polarized scattering when an s-polarized wave is incident on the surface at angles of incidence $(\theta_0, \phi_0) = (25°, 0°)$. The roughness parameters assumed in obtaining these results are identical to those assumed in obtaining Fig. 8. The numerical parameters used to obtain these results were those of Fig. 8 when using the reduced Rayleigh equation. However, when solving the Müller equations, a Gaussian beam of width ($w = 4\lambda$) was assumed to be incident on the surface, which was discretized with an interval $\Delta x = \lambda/7$ (in both directions). It is observed from Fig. 9 that the two approaches produce quantitatively similar results. The minor differences between the results of the two approaches we believe are due to the differences in the areas covered by the rough surfaces, and to the differences in the discretization intervals, assumed in the two sets of calculations, which have not been optimized as yet.

From the results presented in Figs. 8 and 9, we can draw the conclusions that a purely numerical, nonperturbative solution of the reduced Rayleigh equation yields accurate results for the mean differential reflection coefficient that are in good agreement with those obtained by the use of the Müller equations.

4.2.2 A Dielectric Surface

The reduced Rayleigh equation (31) can also be used for calculating the field scattered from a dielectric surface. We apply it here to calculate the contribution to the mean differential reflection coefficient from the incoherent component of the scattered light when a p- or s-polarized plane wave whose wavelength in vacuum is $\lambda = 632.8$ nm is incident at $(\theta_0, \phi_0) = (27.5°, 45°)$ on the surface of a dielectric medium whose dielectric constant is assumed to be $\varepsilon_d = 2.64$ (photoresist). The results are presented in Fig. 10. The randomly rough surface had an rms roughness of $\delta = 3\lambda/200 = 0.015\lambda$ and it covered a $20\lambda \times 20\lambda$ area in the $x_3 = 0$ plane. Moreover, the wavenumber cut-off assumed in these calculations was $Q = 8\omega/c$, corresponding to a discretization interval of $\Delta x = \pi/Q = 0.0625\lambda$. Except for these differences, the remaining roughness and computational parameters were the same as the ones assumed in the calculations that produced Fig 8.

By comparing Figs. 8 and 10 it is observed that the overall structure of the angular distributions of the intensity of the light scattered from a metal and dielectric is rather similar, and that, as expected, the scattered intensity for the metallic surface is stronger (by a factor of about 70) than that for the dielectric surface.

5. DISCUSSION AND CONCLUSIONS

We have shown that the use of the method of moments and the biconjugate gradient stabilized method provides a formally exact solution to the scattering of p- and s-polarized light from a two-dimensional randomly rough perfectly conducting surface, with a modest expenditure of computational time. The addition of an impedance boundary condition on a two-dimensional rough surface to these two methods has been shown to provide a formally exact solution to the scattering of polarized light from two-dimensional randomly rough metallic surfaces, also with a modest expenditure of computational time.
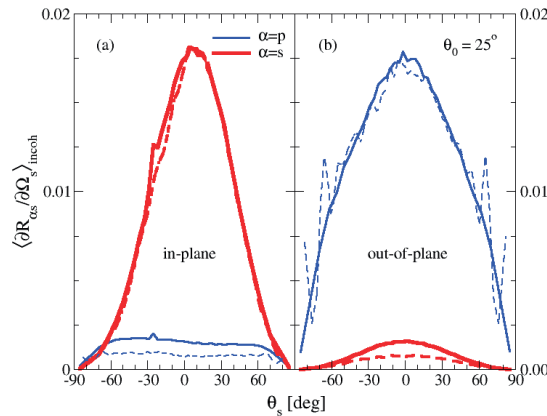
Figure 9. Comparison of the mean differential reflection coefficients for the scattering of s polarized waves from a rough silver surface with the roughness parameters given in the caption of Fig. 8. The results were obtained by two different numerical approaches: the solution of the reduced Rayleigh equation (solid lines), and by the use of the rigorous approach (dashed lines). The numerical parameters and number of surface realizations assumed when using the former approach were those used to obtain the results presented in Fig. 8. However, when using the rigorous approach, the parameters given in the caption to Fig. 6 were assumed with the exception that now $\theta_0 = 25°$, $L = 20\lambda$, and only a small number of surface realizations were used ($N_p = 750$) to obtain these results.

Figure 10. Full angular intensity distribution of the light scattered incoherently from a two-dimensional randomly rough dielectric surface calculated by solving the reduced Rayleig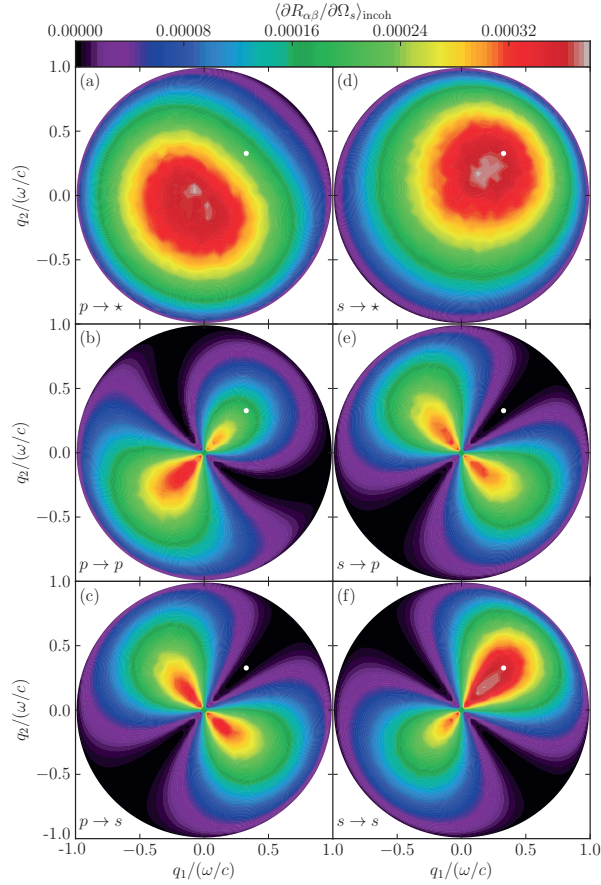h equations. The dielectric substrate was taken to be photoresist which at the frequency of the incident light $\lambda = 632.8\,\text{nm}$ is characterized by a dielectric constant $\varepsilon(\omega) = 2.64$. The angles of incidence assumed are $(\theta_0, \phi_0) = (27.5°, 45°)$, and the white dots indicate the position of the specular direction. These figures were obtained by averaging results for the scattered intensity obtained for $N_p = 6\,000$ surface realizations. The surface parameters assumed in these calculations were $L = 20\lambda$; $\delta = 3\lambda/200 = 0.015\lambda$; and $a = \lambda/4$. The surface discretization was done so that $Q = 8\omega/c$, or equivalently, $\Delta x = \pi/Q = 0.0625\lambda$. The remaining parameters and the organization of the sub-figures are identical to those of Fig. 8.

The computational methods employed in these calculations have made it possible to obtain a formally exact full angular distribution of the intensity of the light scattered from a strongly rough random surface. In the case of scattering from a perfectly conducting surface, and from a metallic surface when the imaginary part of its dielectric function is set equal to zero, knowledge of the full angular distribution of the intensity of the scattered light enables the conservation of energy in the scattering process to be checked. It was found to be satisfied with an error smaller than 0.5%, a result that testifies to the accuracy of the methods used in our calculations and the adequacy of the discretization of the mean scattering surface employed in them.

We have also presented results obtained from a rigorous numerical solution of the reduced Rayleigh equation for the scattering of p- and s-polarized light from a penetrable surface. These results demonstrate the feasibility

of using this equation in studies of the scattering of light from weakly rough surfaces. The good agreement between the results obtained by the solution of the reduced Rayleigh equation and those obtained by the use of the rigorous computational method indicates that the simpler approach yields accurate results for scattering from surfaces that are not very rough. The limits of validity of this equation have yet to be determined.

The success of the methods used in carrying out the calculations described here opens the door to rigorous computational studies of other properties of electromagnetic waves scattered from two-dimensional randomly rough surfaces. These include calculations of the ellipsometric parameters of metallic and dielectric surfaces, transmission through dielectric surfaces, and all of the elements of the Mueller matrix for scattering from and transmission through such surfaces. This work will be reported elsewhere.

REFERENCES

1. P. Tran, V. Celli, and A.A. Maradudin, "Electromagnetic scattering from a two-dimensional, randomly rough, perfectly conducting surface: Iterative methods," J. Opt. Soc. Am. A **11**, 1685–1689 (1994).
2. R.L. Wagner, J. Song, and W.C. Chew, "Monte Carlo simulation of electromagnetic scattering from two-dimensional random rough surfaces," IEEE Trans. Antennas Propag. **45**, 235–245 (1997).
3. K. Pak, L. Tsang, C.H. Chan, and J.T. Johnson, "Backscattering enhancement of electromagnetic waves from two-dimensional perfectly conducting random rough surfaces based on Monte Carlo simulations," J. Opt. Soc. Am. A **12**, 2491–2499 (1995).
4. J.T. Johnson, L. Tsang, R.T. Shin, K. Pak, C.H. Chan, A. Ishimaru, and Y. Kuga, "Backscattering enhancement of electromagnetic waves from two-dimensional perfectly conducting random rough surfaces: a comparison of Monte Carlo simulations with experimental data," IEEE Trans. Antennas Propag. **44**, 748–756 (1996).
5. D. Torrungrueng, H.-T. Chou, and J.T. Johnson, "A novel acceleration algorithm for the computation of scattering from two-dimensional large-scale perfectly conducting random rough surfaces with the forward-backward method," IEEE Trans. Geosci. Remote Sensing **38**, 1656–1668 (2000).
6. G. Soriano and M. Saillard, "Scattering of electromagnetic waves from two-dimensional rough surfaces with an impedance approximation," J. Opt. Soc. Am. A **18**, 124–133 (2001).
7. I. Simonsen, A.A. Maradudin, and T.A. Leskova, "Scattering of electromagnetic waves from two-dimensional randomly rough perfectly conducting surfaces: The full angular intensity disribution," Phys. Rev. A **81**, 013806 (1–13) (2010).
8. I. Simonsen, J.B. Kryvi, A.A. Maradudin, and T.A. Leskova, "Light scattering from anisotropic, randomly rough, perfectly conducting surfaces," Comp. Phys. Commun. **182**, 1904–1908 (2011).
9. P. Tran and A.A. Maradudin, "Scattering of electromagnetic waves from a randomly rough 2D metallic surface," Opt. Commun. **110**, 269–273 (1994).
10. L. Tsang, C.H. Chan, and K. Pak, "Backscattering enhancement of a two-dimensional random rough surface (three-dimensional scattering) based on Monte Carlo simulations," J. Opt. Soc. Am. A **11**, 711–715 (1994).
11. K. Pak, L. Tsang, and J.T. Johnson, "Numerical simulations and backscattering enhancement of electromagnetic waves from two-dimensional dielectric random rough surfaces with the sparse-matrix canonical grid method," J. Opt. Soc. Am. A **14**, 1515–1529 (1997).
12. N. Engheta, W.D. Murphy, V. Rokhlin, and M.S. Vassiliou, "The fast multipole method (FMM) for electromagnetic scattering problems," IEEE Trans. Antennas Propag. **40**, 634–641 (1992).
13. V. Jandhyala, B. Shanker, E. Michielssen and W.C. Chew, "Fast algorithm for the analysis of scattering by dielectric rough surfaces," J. Opt. Soc. Am. A **15**, 1877–1885 (1998).
14. I. Simonsen, A.A. Maradudin, and T.A. Leskova, "Scattering of electromagnetic waves from two-dimensional randomly rough penetrable surfaces," Phys. Rev. Lett. **104**, 223904 (1–4) (2010).

15. A.A. Maradudin, T. Michel, A.R. McGurn, and E.R. Méndez, "Enhanced backscattering of light from a random grating," Ann. Phys. (N.Y.) **203**, 255–307 (1990).

16. J.A. Kong, *Electromagnetic Theory*, 3rd ed. (EMW Publishing, Cambridge, MA, 2005), p. 674.

17. W.H. Press, S.A. Teukolsky, W.T. Vetterling, and B. P. Flannery, *Numerical Recipes in Fortran*, 2nd ed. (Cambridge, University Press, New York, 1992), p. 129.

18. H. Van der Vorst, "Bi-CGSTAB: A fast and smoothly converging variant of Bi-CG for the solution of nonsymmetric linear systems," SIAM J. Sci. Stat. Comp. **13**, 631–644 (1992).

19. A.R. McGurn, A.A. Maradudin and V. Celli, "Localization effects in the scattering of light from a randomly rough grating," Phys. Rev. B**31**, 4866–4871 (1985).

20. E.R. Méndez and K.A. O'Donnell, "Observation of depolarization and backscattering enhancement in light scattering from Gaussian random surfaces," Opt. Commun. **61**, 91–95 (1987).

21. D. Torrungrueng and J.T. Johnson, "Numerical studies of backscattering enhancement of electromagnetic waves from two-dimensional random rough surfaces with the forward-backward/novel spectral acceleration method," J. Opt. Soc. Am. A **18**, 2518–2526 (2001).

22. E.I. Chaikina, P. Negrete-Regagnon, V. Ruiz-Cortés, and E.R. Méndez, "Measurements of the hemispherical scattering distribution function of rough dielectric surfaces," Opt. Commun. **205** 215–221 (2002).

23. A.R. McGurn and A.A. Maradudin, "Perturbation theory results for the diffuse scattering of light from two-dimensional randomly rough surfaces," Waves in Random Media **6**, 251–267 (1996).

24. W. Franz, "Zur Formulierung des Huygenschen Prinzips," Z. Naturforsch. **3a**, 500–506 (1948).

25. Ref. 16, pp. 674–675.

26. C. Müller, *Foundations of the Mathematical Theory of Electromagnetic Waves* (Springer-Verlag, Berlin, 1969), Secs. 21 and 23.

27. N. Morita, N. Kumagai, and J.R. Mautz, *Integral Equation Methods for Electromagnetics* (Artech House, Boston, 1990), Sec. 3.5.2.

28. A.A. Maradudin, "The impedance boundary condition at a two-dimensional rough metal surface," Opt. Commun. **116**, 452–467 (1995).

29. P.B. Johnson and R.W. Christy, "Optical Constants of the Noble Metals," Phys. Rev. B **6**, 4370–4379 (1972).

30. J.P. Kotthaus and O.J.F. Martin, "Accurate solution of the volume integral equation for high-permittivity scatterers," IEEE Trans. Antennas Propag. **48**, 1719-1726 (2000).

31. A.A. Maradudin and E.R. Méndez, "The utility of an impedance boundary condition in the scattering of light from one-dimensional randomly rough dielectric surfaces," Opt. Spectrosc. **80**, 409–420 (1996).

32. G.C. Brown, V. Celli, M. Haller, and A. Marvin, "Vector theory of light scattering from a rough surface: unitary and reciprocal expansions," Surf. Sci. **136**, 381–397 (1984).

33. Lord Rayleigh, *The Theory of Sound*, 2nd ed. (Dover, New York, 1945), vol. II, pp. 89-96, pp. 297–311.

34. E. Wolf, "A generalized extinction theorem and its role in scattering theory," in *Coherence and Quantum Optics*, eds. L. Mandel and E. Wolf (Plenum, New York, 1973), pp. 339-357.

35. J.D. Jackson, *Classical Electrodynamics*, 2nd ed. (Wiley, New York, 1962), Section 9.9.

36. T.R. Michel, "Resonant light scattering from weakly rough random surfaces and imperfect gratings," J. Opt. Soc. Am. A **11**, 1874–1885 (1994).

37. T.R. Michel, M.E. Knotts and K.A. O'Donnell, "Scattering by plasmon polaritons on a rough surface with a periodic component," J. Opt. Soc. Am. A **12**, 548–559 (1995).

38. A. Madrazo and A.A. Maradudin, "Numerical solution of the reduced Rayleigh equation for the scattering of electromagnetic waves from a rough dielectric film on perfectly conducting substrates," Opt. Commun. **134**, 251–263 (1997).

39. I. Simonsen and A.A. Maradudin, "Numerical solution of of electromagnetic waves scattered from planar dielectric films deposited on rough perfectly conducting substrates," Opt. Commun. **162**, 99–111 (1999).

40. J.T. Johnson, "Third order small perturbation method for scattering from dielectric rough surfaces," J. Opt. Soc. Am. A **16**, 2720–2736 (1999).

41. A. Soubret, G. Berginc, and C. Bourrely, "Application of reduced Rayleigh equations to electromagnetic wave scattering by two-dimensional randomly rough surfaces," Phys. Rev. B **63**, 245411 (1–20) (2003).

T. Nordam, P. Letnes, I. Simonsen, and A. Maradudin, "Satellite peaks in the scattering of light from the two-dimensional randomly rough surface of a dielectric film on a planar metal surface," *Opt. Express*, vol. 20, no. 10, p. 11336, 2012

Paper 2

Satellite peaks in the scattering of light from the two-dimensional randomly rough surface of a dielectric film on a planar metal surface

T. Nordam,[1] **P.A. Letnes,**[1] **I. Simonsen,**[1,*] **and A.A. Maradudin**[2]

[1]*Department of Physics, Norwegian University of Science and Technology (NTNU)
NO-7491 Trondheim, Norway*
[2]*Department of Physics and Astronomy, University of California,
Irvine CA 92697, USA*

*Ingve.Simonsen@phys.ntnu.no

Abstract: A nonperturbative, purely numerical, solution of the reduced Rayleigh equation for the scattering of p- and s-polarized light from a dielectric film with a two-dimensional randomly rough surface deposited on a planar metallic substrate, has been carried out. It is found that satellite peaks are present in the angular dependence of the elements of the mean differential reflection coefficient in addition to an enhanced backscattering peak. This result resolves a conflict between the results of earlier approximate theoretical studies of scattering from this system.

© 2012 Optical Society of America

OCIS codes: (290.1483) BSDF, BRDF, and BTDF; (290.4210) Multiple scattering; (290.5825) Scattering theory; (290.5880) Scattering, rough surfaces.

References and links

1. A. R. McGurn, A. A. Maradudin, and V. Celli, "Localization effects in the scattering of light from a randomly rough grating," Phys. Rev. B **31**, 4866–4871 (1985).
2. M. Nieto-Vesperinas and J. M. Soto-Crespo, "Monte Carlo simulations for scattering of electromagnetic waves from perfectly conductive random rough surfaces," Opt. Lett. **12**, 979–981 (1987).
3. A. A. Maradudin, E. R. Méndez, and T. Michel, "Backscattering effects in the elastic scattering of p-polarized light from a large-amplitude random metallic grating," Opt. Lett. **14**, 151–153 (1989).
4. I. Simonsen, "Optics of surface disordered systems," Eur. Phys. J.–Spec. Top. **181**, 1–103 (2010).
5. A. McGurn and A. Maradudin, "An analogue of enhanced backscattering in the transmission of light through a thin film with a randomly rough surface," Opt. Commun. **72**, 279–285 (1989).
6. V. Freilikher, E. Kanzieper, and A. Maradudin, "Coherent scattering enhancement in systems bounded by rough surfaces," Phys. Rep. **288**, 127–204 (1997).
7. V. Freilikher, M. Pustilnik, and I. Yurkevich, "Wave scattering from a bounded medium with disorder," Phys. Lett. A **193**, 467–470 (1994).
8. A. McGurn and A. Maradudin, "Perturbation theory results for the diffuse scattering of light from two-dimensional randomly rough metal surfaces," Wave. Random Media **6**, 251–267 (1996).
9. J. T. Johnson, "Third-order small-perturbation method for scattering from dielectric rough surfaces," J. Opt. Soc. Am. A **16**, 2720–2736 (1999).
10. A. Soubret, G. Berginc, and C. Bourrely, "Application of reduced Rayleigh equations to electromagnetic wave scattering by two-dimensional randomly rough surfaces," Phys. Rev. B **63**, 245411 (2001).
11. I. Simonsen, A. A. Maradudin, and T. A. Leskova, "Scattering of electromagnetic waves from two-dimensional randomly rough perfectly conducting surfaces: The full angular intensity distribution," Phys. Rev. A **81**, 013806 (2010).
12. I. Simonsen, A. A. Maradudin, and T. A. Leskova, "Scattering of electromagnetic waves from two-dimensional randomly rough penetrable surfaces," Phys. Rev. Lett. **104**, 223904 (2010).

13. I. Simonsen, J. B. Kryvi, A. A. Maradudin, and T. A. Leskova, "Light scattering from anisotropic, randomly rough, perfectly conducting surfaces," Comput. Phys. Commun. **182**, 1904–1908 (2011).
14. T. Kawanishi, H. Ogura, and Z. L. Wang, "Scattering of an electromagnetic wave from a slightly random dielectric surface: Yoneda peak and Brewster angle in incoherent scattering," Wave. Random Media **7**, 351–384 (1997).
15. A. Soubret, G. Berginc, and C. Bourrely, "Backscattering enhancement of an electromagnetic wave scattered by two-dimensional rough layers," J. Opt. Soc. Am. A **18**, 2778–2788 (2001).
16. E. R. Méndez, E. I. Chaikina, and H. M. Escamilla, "Observation of satellite peaks and dips in the scattering of light in a double-pass geometry," Opt. Lett. **24**, 705–707 (1999).
17. T. Nordam, P. A. Letnes, and I. Simonsen, "Numerical simulations of scattering of light from two-dimensional surfaces using the reduced Rayleigh equation," http://arxiv.org/abs/1204.4984.
18. T. A. Leskova, P. A. Letnes, A. A. Maradudin, T. Nordam, and I. Simonsen, "The scattering of light from two-dimensional randomly rough surfaces," Proc. SPIE **8172**, 817209 (2011).
19. T. A. Leskova, Department of Physics and Astronomy, University of California, Irvine CA 92697, U.S.A. (personal communication, 2010).
20. J. T. Johnson, "Third-order small-perturbation method for scattering from dielectric rough surfaces," J. Opt. Soc. Am. A **16**, 2720–2736 (1999).
21. A. Maradudin, T. Michel, A. McGurn, and E. Méndez, "Enhanced backscattering of light from a random grating," Ann. Phys. **203**, 255–307 (1990).
22. W. Press, B. Flannery, S. Teukolsky, and W. Vetterling, *Numerical recipes*, 3rd ed. (Cambridge Univ Press, 2007).
23. P. B. Johnson, "Optical constants of the noble metals," Phys. Rev. **6**, 4370–4379 (1972).
24. C. S. West and K. A. O'Donnell, "Observations of backscattering enhancement from polaritons on a rough metal surface," J. Opt. Soc. Am. A **12**, 390–397 (1995).
25. A. Madrazo and A. Maradudin, "Numerical solutions of the reduced Rayleigh equation for the scattering of electromagnetic waves from rough dielectric films on perfectly conducting substrates," Opt. Commun. **134**, 251–263 (1997).
26. I. Simonsen and A. Maradudin, "Numerical simulation of electromagnetic wave scattering from planar dielectric films deposited on rough perfectly conducting substrates," Opt. Commun. **162**, 99–111 (1999).

In the earliest analytic [1] and computer simulation [2,3] studies of the multiple scattering of light from clean one-dimensional randomly rough surfaces of perfect conductors or of penetrable media, the focus was on the phenomenon of enhanced backscattering. This is the presence of a well-defined peak in the retroreflection direction in the angular dependence of the intensity of the light that has been scattered incoherently (diffusely).

In subsequent work on the multiple scattering of light from free-standing or supported films with a one-dimensional randomly rough surface that support two or more guided waves, new effects were discovered [4]. These include enhanced transmission, which is the presence of a well-defined peak in the anti-specular direction in the angular dependence of the intensity of the light transmitted through the film [5]. Perhaps more interesting was the discovery of satellite peaks in the angular dependence of the intensity of the light scattered from or transmitted through the film. These are well-defined peaks present on both sides of the enhanced backscattering and enhanced transmission peaks, respectively, that arise from the coherent interference of guided waves with the frequency of the incident light, but with different wavenumbers [6].

It should be noted, however, that the prediction of these satellite peaks was first made in the context of the scattering of electromagnetic waves from a dielectric film containing a random distribution of volume scatterers [7], rather than from a randomly rough surface, when the thickness of the film is small compared to the mean free path of the electromagnetic wave in the random medium.

In analytic [8–10] and computer simulation calculations [11–13] of the multiple scattering of light from clean two-dimensional randomly rough surfaces of perfect conductors and penetrable media, enhanced backscattering was observed in the results. However, when attention turned to the scattering of light from a perfectly conducting surface coated with a dielectric film, conflicting results were obtained. In these studies the dielectric-perfect conductor interface was assumed to be planar, while the vacuum-dielectric interface was assumed to be a two-dimensional randomly rough interface. In the first of these studies Kawanishi *et al.* [14]

applied the stochastic functional approach to this problem and found no evidence for satellite peaks in their results. They suggested that the ensemble averaging of the intensity of the scattered field restores isotropy in the mean scattering plane, and thereby eliminates the occurrence of special scattering angles at which satellite peaks could occur. In subsequent work in which the reduced Rayleigh equation for scattering from this structure [10, 15] was solved in the form of expansions of the amplitudes of the p- and s-polarized components of the scattered field in powers of the surface profile function through terms of third order, satellite peaks were found. However, the contribution to the scattering amplitudes associated with the third-order term was larger than that from the first-order term for the roughness and experimental parameters assumed in that work. It is therefore possible that these values fell outside the ranges for which a perturbative solution of the reduced Rayleigh equation is reliable.

Although satellite peaks were observed in experiments carried out by Méndez *et al.* [16] that utilized the double passage of polarized light through a random phase screen, the experimental conditions were sufficiently different from those studied theoretically in Refs. [10, 14], that these results could not be used to support the predictions of either of these studies.

In an effort to resolve the issue of whether satellite peaks do or do not exist in the scattering of light from a rough dielectric film deposited on the planar surface of a metal, in this paper we carry out a nonperturbative, purely numerical, solution of the reduced Rayleigh equation [17] for the scattering of p- and s-polarized light from a structure consisting of a dielectric film deposited on a metal substrate when the dielectric-metal interface is planar, while the vacuum-dielectric interface is a two-dimensional randomly rough interface. This is an approach that was used successfully in recent calculations of the scattering of p- and s-polarized light from a two-dimensional randomly rough interface between a dielectric and a metal [17, 18], which prompts its application to the present problem.

The system we study consists of vacuum (ε_1) in the region $x_3 > d + \zeta\left(\mathbf{x}_\parallel\right)$, where $\mathbf{x}_\parallel = (x_1, x_2, 0)$; a dielectric film (ε_2) in the region $0 < x_3 < d + \zeta\left(\mathbf{x}_\parallel\right)$; and a lossy metal (ε_3) in the region $x_3 < 0$. The surface profile function $\zeta\left(\mathbf{x}_\parallel\right)$ is assumed to be a single-valued function of $\mathbf{x}_\parallel$ that is differentiable with respect to x_1 and x_2, and constitutes a zero-mean, stationary, isotropic, Gaussian random process defined by

$$\left\langle \zeta(\mathbf{x}_\parallel)\zeta(\mathbf{x}'_\parallel) \right\rangle = \delta^2 W\left(\left|\mathbf{x}_\parallel - \mathbf{x}'_\parallel\right|\right). \tag{1}$$

The angle brackets here denote an average over the ensemble of realizations of the surface profile function, and $\delta = \left\langle \zeta^2\left(\mathbf{x}_\parallel\right) \right\rangle^{1/2}$ is the rms height of the surface roughness.

The electric field in the vacuum $\left[x_3 > d + \zeta\left(\mathbf{x}_\parallel\right)\right]$ is the sum of an incident field and a scattered field, $\mathbf{E}(\mathbf{x};t) = \left[\mathbf{E}(\mathbf{x}|\omega)_{\mathrm{inc}} + \mathbf{E}(\mathbf{x}|\omega)_{\mathrm{sc}}\right]\exp\left(-\mathrm{i}\omega t\right)$, where

$$
\begin{aligned}
\mathbf{E}(\mathbf{x}|\omega)_{\mathrm{inc}} = &\left\{ \frac{c}{\omega}\left[\hat{\mathbf{k}}_\parallel \alpha_1(k_\parallel) + \hat{\mathbf{x}}_3 k_\parallel\right] B_{\mathrm{p}}(\mathbf{k}_\parallel) + \left(\hat{\mathbf{x}}_3 \times \hat{\mathbf{k}}_\parallel\right) B_{\mathrm{s}}(\mathbf{k}_\parallel) \right\} \\
&\times \exp\left(\mathrm{i}\mathbf{k}_\parallel \cdot \mathbf{x}_\parallel - \mathrm{i}\alpha_1(k_\parallel)x_3\right)
\end{aligned}
\tag{2a}
$$

$$
\begin{aligned}
\mathbf{E}(\mathbf{x}|\omega)_{\mathrm{sc}} = &\int \frac{\mathrm{d}^2 q_\parallel}{(2\pi)^2}\left\{ \frac{c}{\omega}\left[\hat{\mathbf{q}}_\parallel \alpha_1(q_\parallel) - \hat{\mathbf{x}}_3 q_\parallel\right] A_{\mathrm{p}}(\mathbf{q}_\parallel) + \left(\hat{\mathbf{x}}_3 \times \hat{\mathbf{q}}_\parallel\right) A_{\mathrm{s}}(\mathbf{q}_\parallel) \right\} \\
&\times \exp\left(\mathrm{i}\mathbf{q}_\parallel \cdot \mathbf{x}_\parallel + \mathrm{i}\alpha_1(q_\parallel)x_3\right),
\end{aligned}
\tag{2b}
$$

while the subscripts p and s denote the p-polarized and s-polarized components of these fields with respect to the local planes of incidence and scattering. A caret over a vector indicates that it is a unit vector, and the vector $\mathbf{k}_\parallel$ is defined as $\mathbf{k}_\parallel = (k_1, k_2, 0)$ (with similar definitions for $\mathbf{q}_\parallel$

and $\mathbf{p}_\parallel$). The functions $\alpha_i(q_\parallel)$ $(i = 1, 2, 3)$ are defined by

$$\alpha_i(q_\parallel) = \left[\varepsilon_i \left(\frac{\omega}{c} \right)^2 - q_\parallel^2 \right]^{1/2}, \qquad \operatorname{Re} \alpha_i(q_\parallel) > 0, \operatorname{Im} \alpha_i(q_\parallel) > 0. \tag{3}$$

A linear relation exists between the amplitudes $A_\alpha(\mathbf{q}_\parallel)$ and $B_\beta(\mathbf{k}_\parallel)$ $(\alpha, \beta = \mathrm{p}, \mathrm{s})$, which we write as

$$A_\alpha(\mathbf{q}_\parallel) = \sum_\beta R_{\alpha\beta}(\mathbf{q}_\parallel | \mathbf{k}_\parallel) B_\beta(\mathbf{k}_\parallel) \tag{4}$$

where $R_{\alpha\beta}$ is the scattering amplitude for incident β-polarized light scattered into α-polarized light. The convention we use with respect to the polarization subscripts is

$$\mathbf{R}(\mathbf{q}_\parallel | \mathbf{k}_\parallel) = \begin{pmatrix} R_{\mathrm{pp}}(\mathbf{q}_\parallel | \mathbf{k}_\parallel) & R_{\mathrm{ps}}(\mathbf{q}_\parallel | \mathbf{k}_\parallel) \\ R_{\mathrm{sp}}(\mathbf{q}_\parallel | \mathbf{k}_\parallel) & R_{\mathrm{ss}}(\mathbf{q}_\parallel | \mathbf{k}_\parallel) \end{pmatrix}. \tag{5}$$

It has been shown by Soubret *et al.* [10] and Leskova [19] that the scattering amplitudes $\left[R_{\alpha\beta}(\mathbf{q}_\parallel | \mathbf{k}_\parallel) \right]$ satisfy the matrix integral equation

$$\int \frac{\mathrm{d}^2 q_\parallel}{(2\pi)^2} \mathbf{M}(\mathbf{p}_\parallel | \mathbf{q}_\parallel) \mathbf{R}(\mathbf{q}_\parallel | \mathbf{k}_\parallel) = -\mathbf{N}(\mathbf{p}_\parallel | \mathbf{k}_\parallel), \tag{6}$$

called a *reduced Rayleigh equation* because it is an equation for only the scattered field in the medium of incidence, and not for the fields in the film and in the substrate. The effects of the latter two fields are contained in the elements of the matrices $\mathbf{M}(\mathbf{p}_\parallel | \mathbf{q}_\parallel)$ and $\mathbf{N}(\mathbf{p}_\parallel | \mathbf{k}_\parallel)$. With the shorthand notation $\alpha(q_\parallel, \omega) \equiv \alpha(q_\parallel)$, the elements of these matrices in the forms obtained by

Leskova [19] are

$$M_{pp}(\mathbf{p}_\parallel|\mathbf{q}_\parallel) = \left[p_\parallel q_\parallel + \alpha_2(p_\parallel)(\hat{\mathbf{p}}_\parallel \cdot \hat{\mathbf{q}}_\parallel)\alpha_1(q_\parallel) \right]$$
$$\times \Gamma_p(p_\parallel) \exp\left(-i\left[\alpha_2(p_\parallel) - \alpha_1(q_\parallel)\right]d\right) \frac{I\left(\alpha_2(p_\parallel) - \alpha_1(q_\parallel)|\mathbf{p}_\parallel - \mathbf{q}_\parallel\right)}{\alpha_2(p_\parallel) - \alpha_1(q_\parallel)}$$
$$+ \left[p_\parallel q_\parallel - \alpha_2(p_\parallel)(\hat{\mathbf{p}}_\parallel \cdot \hat{\mathbf{q}}_\parallel)\alpha_1(q_\parallel) \right]$$
$$\times \Delta_p(p_\parallel) \exp\left(i\left[\alpha_2(p_\parallel) + \alpha_1(q_\parallel)\right]d\right) \frac{I\left(-\left[\alpha_2(p_\parallel) + \alpha_1(q_\parallel)\right]|\mathbf{p}_\parallel - \mathbf{q}_\parallel\right)}{\alpha_2(p_\parallel) + \alpha_1(q_\parallel)} \tag{7a}$$

$$M_{ps}(\mathbf{p}_\parallel|\mathbf{q}_\parallel) = -\frac{\omega}{c}\alpha_2(p_\parallel)\left(\hat{\mathbf{p}}_\parallel \times \hat{\mathbf{q}}_\parallel\right)_3$$
$$\left(\Gamma_p(p_\parallel) \exp\left(-i\left[\alpha_2(p_\parallel) - \alpha_1(q_\parallel)\right]d\right) \frac{I\left(\alpha_2(p_\parallel) - \alpha_1(q_\parallel)|\mathbf{p}_\parallel - \mathbf{q}_\parallel\right)}{\alpha_2(p_\parallel) - \alpha_1(q_\parallel)} \right.$$
$$\left. - \Delta_p(p_\parallel) \exp\left(i\left[\alpha_2(p_\parallel) + \alpha_1(q_\parallel)\right]d\right) \frac{I\left(-\left[\alpha_2(p_\parallel) + \alpha_1(q_\parallel)\right]|\mathbf{p}_\parallel - \mathbf{q}_\parallel\right)}{\alpha_2(p_\parallel) + \alpha_1(q_\parallel)} \right) \tag{7b}$$

$$M_{sp}(\mathbf{p}_\parallel|\mathbf{q}_\parallel) = \frac{\omega}{c}\left(\hat{\mathbf{p}}_\parallel \times \hat{\mathbf{q}}_\parallel\right)_3 \alpha_1(q_\parallel)$$
$$\left(\Gamma_s(p_\parallel) \exp\left(-i\left[\alpha_2(p_\parallel) - \alpha_1(q_\parallel)\right]d\right) \frac{I\left(\alpha_2(p_\parallel) - \alpha_1(q_\parallel)|\mathbf{p}_\parallel - \mathbf{q}_\parallel\right)}{\alpha_2(p_\parallel) - \alpha_1(q_\parallel)} \right.$$
$$\left. + \Delta_s(p_\parallel) \exp\left(i\left[\alpha_2(p_\parallel) + \alpha_1(q_\parallel)\right]d\right) \frac{I\left(-\left[\alpha_2(p_\parallel) + \alpha_1(q_\parallel)\right]|\mathbf{p}_\parallel - \mathbf{q}_\parallel\right)}{\alpha_2(p_\parallel) + \alpha_1(q_\parallel)} \right) \tag{7c}$$

$$M_{ss}(\mathbf{p}_\parallel|\mathbf{q}_\parallel) = \frac{\omega^2}{c^2}\left(\hat{\mathbf{p}}_\parallel \cdot \hat{\mathbf{q}}_\parallel\right)$$
$$\left(\Gamma_s(p_\parallel) \exp\left(-i\left[\alpha_2(p_\parallel) - \alpha_1(q_\parallel)\right]d\right) \frac{I\left(\alpha_2(p_\parallel) - \alpha_1(q_\parallel)|\mathbf{p}_\parallel - \mathbf{q}_\parallel\right)}{\alpha_2(p_\parallel) - \alpha_1(q_\parallel)} \right.$$
$$\left. + \Delta_s(p_\parallel) \exp\left(i\left[\alpha_2(p_\parallel) + \alpha_1(q_\parallel)\right]d\right) \frac{I\left(-\left[\alpha_2(p_\parallel) + \alpha_1(q_\parallel)\right]|\mathbf{p}_\parallel - \mathbf{q}_\parallel\right)}{\alpha_2(p_\parallel) + \alpha_1(q_\parallel)} \right), \tag{7d}$$

and

$$
\begin{aligned}
N_{\mathrm{pp}}(\mathbf{p}_\parallel|\mathbf{k}_\parallel) = & - \left[p_\parallel k_\parallel - \alpha_2(p_\parallel)(\hat{\mathbf{p}}_\parallel \cdot \hat{\mathbf{k}}_\parallel)\alpha_1(k_\parallel) \right] \\
& \times \Gamma_{\mathrm{p}}(p_\parallel) \exp\left(-\mathrm{i}\left[\alpha_2(p_\parallel)+\alpha_1(k_\parallel)\right]d\right) \frac{I\left(\alpha_2(p_\parallel)+\alpha_1(k_\parallel)|\mathbf{p}_\parallel - \mathbf{k}_\parallel\right)}{\alpha_2(p_\parallel)+\alpha_1(k_\parallel)} \\
& - \left[p_\parallel k_\parallel + \alpha_2(p_\parallel)(\hat{\mathbf{p}}_\parallel \cdot \hat{\mathbf{k}}_\parallel)\alpha_1(k_\parallel) \right] \\
& \times \Delta_{\mathrm{p}}(p_\parallel) \exp\left(\mathrm{i}\left[\alpha_2(p_\parallel)-\alpha_1(k_\parallel)\right]d\right) \frac{I\left(-\left[\alpha_2(p_\parallel)-\alpha_1(k_\parallel)\right]|\mathbf{p}_\parallel - \mathbf{k}_\parallel\right)}{\alpha_2(p_\parallel)-\alpha_1(k_\parallel)}
\end{aligned}
\tag{8a}
$$

$$
\begin{aligned}
N_{\mathrm{ps}}(\mathbf{p}_\parallel|\mathbf{k}_\parallel) = & -\frac{\omega}{c}\alpha_2(p_\parallel)\left(\hat{\mathbf{p}}_\parallel \times \hat{\mathbf{k}}_\parallel\right)_3 \\
& \times \left(\Gamma_{\mathrm{p}}(p_\parallel) \exp\left(-\mathrm{i}\left[\alpha_2(p_\parallel)+\alpha_1(k_\parallel)\right]d\right) \frac{I\left(\alpha_2(p_\parallel)+\alpha_1(k_\parallel)|\mathbf{p}_\parallel - \mathbf{k}_\parallel\right)}{\alpha_2(p_\parallel)+\alpha_1(k_\parallel)} \right. \\
& \left. - \Delta_{\mathrm{p}}(p_\parallel) \exp\left(\mathrm{i}\left[\alpha_2(p_\parallel)-\alpha_1(k_\parallel)\right]d\right) \frac{I\left(-\left[\alpha_2(p_\parallel)-\alpha_1(k_\parallel)\right]|\mathbf{p}_\parallel - \mathbf{k}_\parallel\right)}{\alpha_2(p_\parallel)-\alpha_1(k_\parallel)} \right)
\end{aligned}
\tag{8b}
$$

$$
\begin{aligned}
N_{\mathrm{sp}}(\mathbf{p}_\parallel|\mathbf{k}_\parallel) = & \frac{\omega}{c}\left(\hat{\mathbf{p}}_\parallel \times \hat{\mathbf{k}}_\parallel\right)_3 \alpha_1(k_\parallel) \\
& \times \left(\Gamma_{s}(p_\parallel) \exp\left(-\mathrm{i}\left[\alpha_2(p_\parallel)+\alpha_1(k_\parallel)\right]d\right) \frac{I\left(\alpha_2(p_\parallel)+\alpha_1(k_\parallel)|\mathbf{p}_\parallel - \mathbf{k}_\parallel\right)}{\alpha_2(p_\parallel)+\alpha_1(k_\parallel)} \right. \\
& \left. + \Delta_{s}(p_\parallel) \exp\left(\mathrm{i}\left[\alpha_2(p_\parallel)-\alpha_1(k_\parallel)\right]d\right) \frac{I\left(-\left[\alpha_2(p_\parallel)-\alpha_1(k_\parallel)\right]|\mathbf{p}_\parallel - \mathbf{k}_\parallel\right)}{\alpha_2(p_\parallel)-\alpha_1(k_\parallel)} \right)
\end{aligned}
\tag{8c}
$$

$$
\begin{aligned}
N_{\mathrm{ss}}(\mathbf{p}_\parallel|\mathbf{k}_\parallel) = & \frac{\omega^2}{c^2}\left(\hat{\mathbf{p}}_\parallel \cdot \hat{\mathbf{k}}_\parallel\right) \\
& \times \left(\Gamma_{s}(p_\parallel) \exp\left(-\mathrm{i}\left[\alpha_2(p_\parallel)+\alpha_1(k_\parallel)\right]d\right) \frac{I\left(\alpha_2(p_\parallel)+\alpha_1(k_\parallel)|\mathbf{p}_\parallel - \mathbf{k}_\parallel\right)}{\alpha_2(p_\parallel)+\alpha_1(k_\parallel)} \right. \\
& \left. + \Delta_{s}(p_\parallel) \exp\left(\mathrm{i}\left[\alpha_2(p_\parallel)-\alpha_1(k_\parallel)\right]d\right) \frac{I\left(-\left[\alpha_2(p_\parallel)-\alpha_1(k_\parallel)\right]|\mathbf{p}_\parallel - \mathbf{k}_\parallel\right)}{\alpha_2(p_\parallel)-\alpha_1(k_\parallel)} \right).
\end{aligned}
\tag{8d}
$$

In writing Eqs. (7) and (8) we have introduced the functions

$$
\Gamma_{\mathrm{p}}(p_\parallel) = \varepsilon_2 \alpha_3(p_\parallel,\omega) + \varepsilon_3 \alpha_2(p_\parallel,\omega) \tag{9a}
$$
$$
\Delta_{\mathrm{p}}(p_\parallel) = \varepsilon_2 \alpha_3(p_\parallel,\omega) - \varepsilon_3 \alpha_2(p_\parallel,\omega) \tag{9b}
$$

and

$$
\Gamma_{\mathrm{s}}(p_\parallel) = \alpha_3(p_\parallel,\omega) + \alpha_2(p_\parallel,\omega) \tag{10a}
$$
$$
\Delta_{\mathrm{s}}(p_\parallel) = \alpha_3(p_\parallel,\omega) - \alpha_2(p_\parallel,\omega), \tag{10b}
$$

as well as

$$
I\left(\gamma|\mathbf{Q}_\parallel\right) = \int \mathrm{d}^2 x_\parallel \, \exp\left(-\mathrm{i}\mathbf{Q}_\parallel \cdot \mathbf{x}_\parallel\right) \exp\left[-\mathrm{i}\gamma\zeta\left(\mathbf{x}_\parallel\right)\right]. \tag{11}
$$

The scattering amplitudes $\left[R_{\alpha\beta}(\mathbf{q}_\parallel|\mathbf{k}_\parallel)\right]$ play a central role in the present theory because the mean differential reflection coefficient, an experimentally measurable function, can be expressed in terms of these amplitudes. The differential reflection coefficient $(\partial R/\partial\Omega_s)$ is defined

such that $(\partial R/\partial\Omega_s)d\Omega_s$ is the fraction of the total time-averaged flux incident on the surface that is scattered into the element of solid angle $d\Omega_s$ about the scattering direction (θ_s, ϕ_s). Since we are studying the scattering of light from a randomly rough surface, it is the average of this function over the ensemble of realizations of the surface profile function that we need to calculate. The contribution to the mean differential reflection coefficient from the incoherent (diffuse) component of the scattered light, when incident light of β polarization whose wave vector has the projection $\mathbf{k}_\parallel$ on the mean scattering surface is scattered into light of α polarization whose wave vector has the projection $\mathbf{q}_\parallel$ on the mean scattering surface, denoted $\langle \partial R_{\alpha\beta}/\partial\Omega_s \rangle_{\text{incoh}}$, is given by

$$\left\langle \frac{\partial R_{\text{pp}}}{\partial\Omega_s} \right\rangle_{\text{incoh}} = \frac{1}{S}\frac{\sqrt{\varepsilon_1}}{4\pi^2}\frac{\omega}{c}\frac{\alpha_1^2(q_\parallel)}{\alpha_1(k_\parallel)} \left[\left\langle |R_{\text{pp}}(\mathbf{q}_\parallel|\mathbf{k}_\parallel)|^2 \right\rangle - |\langle R_{\text{pp}}(\mathbf{q}_\parallel|\mathbf{k}_\parallel) \rangle|^2 \right] \tag{12a}$$

$$\left\langle \frac{\partial R_{\text{ps}}}{\partial\Omega_s} \right\rangle_{\text{incoh}} = \frac{1}{S}\frac{\varepsilon_1^{3/2}}{4\pi^2}\frac{\omega}{c}\frac{\alpha_1^2(q_\parallel)}{\alpha_1(k_\parallel)} \left[\left\langle |R_{\text{ps}}(\mathbf{q}_\parallel|\mathbf{k}_\parallel)|^2 \right\rangle - |\langle R_{\text{ps}}(\mathbf{q}_\parallel|\mathbf{k}_\parallel) \rangle|^2 \right] \tag{12b}$$

$$\left\langle \frac{\partial R_{\text{sp}}}{\partial\Omega_s} \right\rangle_{\text{incoh}} = \frac{1}{S}\frac{1}{4\pi^2\sqrt{\varepsilon_1}}\frac{\omega}{c}\frac{\alpha_1^2(q_\parallel)}{\alpha_1(k_\parallel)} \left[\left\langle |R_{\text{sp}}(\mathbf{q}_\parallel|\mathbf{k}_\parallel)|^2 \right\rangle - |\langle R_{\text{sp}}(\mathbf{q}_\parallel|\mathbf{k}_\parallel) \rangle|^2 \right] \tag{12c}$$

$$\left\langle \frac{\partial R_{\text{ss}}}{\partial\Omega_s} \right\rangle_{\text{incoh}} = \frac{1}{S}\frac{\sqrt{\varepsilon_1}}{4\pi^2}\frac{\omega}{c}\frac{\alpha_1^2(q_\parallel)}{\alpha_1(k_\parallel)} \left[\left\langle |R_{\text{ss}}(\mathbf{q}_\parallel|\mathbf{k}_\parallel)|^2 \right\rangle - |\langle R_{\text{ss}}(\mathbf{q}_\parallel|\mathbf{k}_\parallel) \rangle|^2 \right], \tag{12d}$$

where S is the area of the plane $x_3 = 0$ covered by the rough surface. The two-dimensional wave vectors $\mathbf{k}_\parallel$ and $\mathbf{q}_\parallel$ are defined in terms of the polar and azimuthal angles of incidence (θ_0, ϕ_0) and scattering (θ_s, ϕ_s), respectively, by $\mathbf{k}_\parallel = \sqrt{\varepsilon_1}(\omega/c)\sin\theta_0\ (\cos\phi_0, \sin\phi_0, 0)$ and $\mathbf{q}_\parallel = \sqrt{\varepsilon_1}(\omega/c)\sin\theta_s(\cos\phi_s, \sin\phi_s, 0)$. Thus these wave vectors in Eq. (12) are restricted to the domains $k_\parallel < \sqrt{\varepsilon_1}(\omega/c)$ and $q_\parallel < \sqrt{\varepsilon_1}(\omega/c)$ of the q_1q_2 plane.

Up to now Eq. (6) has been solved by small-amplitude perturbation theory through terms of third order in the surface profile function [10, 20]. Here we present results for the mean differential reflection coefficient and for the full angular distribution of the intensity of the scattered light obtained by a nonperturbative, purely numerical solution of Eqs. (6)–(11), as described in Ref. [17]. This was done by generating a realization of the surface profile function numerically on a grid of N_x^2 points within a square region of the x_1x_2 plane of edge L, so that the (linear) sampling interval was $\Delta x = L/N_x$. A two-dimensional version of the filtering method used in [17, 21] was used to generate the profile function [13]. The function $I(\gamma|\mathbf{Q}_\parallel)$ was then evaluated by expanding the integrand in powers of the surface profile function $\zeta(\mathbf{x}_\parallel)$, and calculating the Fourier transform of $\zeta^n(\mathbf{x}_\parallel)$ by the fast Fourier transform. In evaluating the integral over $\mathbf{q}_\parallel$ in Eq. (6) the infinite limits were replaced by finite ones: $(q_1^2 + q_2^2)^{1/2} \le Q/2$. The Nyquist sampling theorem requires that $|q_1|$ and $|q_2|$ be smaller than $Q_c = \pi/\Delta x$ [22, p. 605]. The components of the vector $\mathbf{p}_\parallel - \mathbf{q}_\parallel$ entering $I(\gamma|\mathbf{p}_\parallel - \mathbf{q}_\parallel)$ lie in the interval $[-Q, Q]$, so we have chosen $Q = Q_c$. A grid with a grid constant $\Delta q_1 = \Delta q_2 = \Delta q = 2\pi/L$ was constructed within the circular region of the q_1q_2 plane where $(q_1^2 + q_2^2) \le Q/2$. The integral over this region in Eq. (6) was carried out by a two-dimensional version of the extended midpoint method [22, p. 161] and the values of $R_{\alpha\beta}(\mathbf{q}_\parallel|\mathbf{k}_\parallel)$ were calculated for values of $\mathbf{q}_\parallel$ at the points of this grid for a given value of $\mathbf{k}_\parallel$, which was also a point on this grid. The resulting matrix equations were solved by LU factorization and backsubstitution. The values of $R_{\alpha\beta}(\mathbf{q}_\parallel|\mathbf{k}_\parallel)$ and $|R_{\alpha\beta}(\mathbf{q}_\parallel|\mathbf{k}_\parallel)|^2$ were then calculated for N_p realizations of the surface profile function. An arithmetic average of the N_p results for each of these functions yielded the averages $\langle R_{\alpha\beta}(\mathbf{q}_\parallel|\mathbf{k}_\parallel) \rangle$ and $\langle |R_{\alpha\beta}(\mathbf{q}_\parallel|\mathbf{k}_\parallel)|^2 \rangle$, from which the incoherent contribution to the mean differential reflection coefficients were calculated according to Eq. (12).

We apply this approach to the scattering of p- and s-polarized plane waves, whose wavelength is $\lambda = 633$ nm, incident from vacuum ($\varepsilon_1 = 1$) on a dielectric film ($\varepsilon_2 = 2.6896 + 0.01i$) coating a silver surface ($\varepsilon_3 = -18.28 + 0.481i$) [23]. The mean thickness of the film is $d = 0.756\lambda = 478.5$ nm. The roughness of the vacuum-dielectric interface is characterized by a two-dimensional version of the West–O'Donnell power spectrum [24] given by [8]

$$g(|\mathbf{k}_{\parallel}|) = \frac{4\pi}{k_+^2 - k_-^2} \theta(|\mathbf{k}_{\parallel}| - k_-)\theta(k_+ - |\mathbf{k}_{\parallel}|), \tag{13}$$

where $\theta(x)$ is the Heaviside unit step function, and $k_- = 0.82(\omega/c)$, $k_+ = 1.97(\omega/c)$. The rms height of the surface roughness was assumed to be $\delta = \lambda/40 = 15.82$ nm, the surface was discretized on a grid of resolution $\Delta x_1 = \Delta x_2 = 0.123\lambda = 77.6$ nm and the edge of the (quadratic) surface was $L = 55\lambda = 34.8$ μm.

The contribution to the mean differential reflection coefficient $\langle \partial R_{\alpha\beta}(\mathbf{q}_{\parallel}|\mathbf{k}_{\parallel})/\partial\Omega_s \rangle_{\text{incoh}}$ from single-scattering processes [second order in $\zeta(\mathbf{x}_{\parallel})$] is proportional to $g(|\mathbf{q}_{\parallel} - \mathbf{k}_{\parallel}|)$ [8]. Since the power spectrum (13) is identically zero for $|\mathbf{k}_{\parallel}| < k_-$, there is no contribution to the mean differential reflection coefficient from the light scattered incoherently by single-scattering processes when the wave vectors $\mathbf{q}_{\parallel}$ and $\mathbf{k}_{\parallel}$ satisfy the inequality $|\mathbf{q}_{\parallel} - \mathbf{k}_{\parallel}| < k_-$. The contribution to $\langle \partial R_{\alpha\beta}(\mathbf{q}_{\parallel}|\mathbf{k}_{\parallel})/\partial\Omega_s \rangle_{\text{incoh}}$ when this condition is satisfied is due only to multiple-scattering processes, including the enhanced backscattering peak and the satellite peaks. These features are more clearly visible in this case because they do not ride on a large background due to single-scattering processes. This is the reason that the calculations whose results are presented here were carried out on the basis of the power spectrum (13).

In Fig. 1(a) we present the contribution to the mean differential reflection coefficient from the light scattered incoherently as functions of the polar scattering angle θ_s for the in-plane ($\phi_s = \phi_0 = 45°$) co-(p→p, s→s) and cross-(p→s, s→p) polarized scattering when a p- or s-polarized plane wave is incident on the dielectric surface at angles of incidence (θ_0, ϕ_0) given by $(0.74°, 45°)$. (In figures showing in-plane or out-of-plane scattering, we depart from the commonly accepted principle of not using negative polar angles, in that we allow for negative θ_s.). An arithmetic average of results obtained for $N_p = 11,165$ realizations of the surface profile function was carried out to produce these figures. In Fig. 1(b) we present the analogous results for out-of-plane ($\phi_s = \phi_0 \pm 90°$) scattering when the roughness and experimental parameters have the values assumed in generating Fig. 1(a).

In the results depicted in Fig. 1(a) [1(b)] single-scattering processes give no contributions to the mean differential reflection coefficient for $-53.8° < \theta_s < 56.4°$ ($-55.08° < \theta_s < 55.08°$). In both figures a well-defined enhanced backscattering peak is seen in the retroreflection direction. In addition, in Fig. 1(a) additional peaks are seen on both sides of the enhanced backscattering peak in the s → s co-polarized scattering contribution to the mean differential reflection coefficient. These peaks are identified as satellite peaks.

We base this identification on the following consideration. It was shown in [6] that in the in-plane co-polarized scattering of light of frequency ω from a one-dimensional randomly rough surface of a film system when the plane of incidence is perpendicular to the generators of the surface, satellite peaks occur at scattering angles given by

$$\sin\theta_s^{(m,n)} = -\sin\theta_0 \pm \frac{c}{\omega\sqrt{\varepsilon_1}}[q_m(\omega) - q_n(\omega)]. \tag{14}$$

The wave numbers $q_1(\omega), q_2(\omega), \ldots, q_N(\omega)$ are the wavenumbers of the guided waves supported by the film structure at the frequency of the incident light. Not all of the peaks predicted by Eq. (14) may be present in the mean differential reflection coefficient. This happens when the absolute value of the right-hand side of Eq. (14) is greater than unity. Then the corresponding
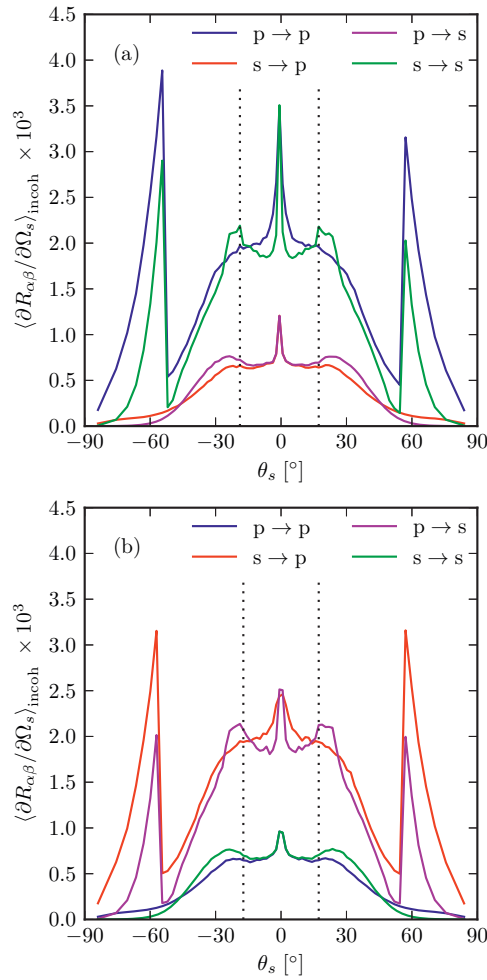
Fig. 1. (a) The contributions to the mean differential reflection coefficient as functions of the polar scattering angle θ_s from the in-plane ($\phi_s = \phi_0$) co-polarized (p→p, s→s) and cross-polarized (p→s, s→p) scattering of light incident on the two-dimensional randomly rough surface of a dielectric film deposited on the planar surface of silver, whose dielectric constant is $\varepsilon_3 = -18.28 + 0.481i$. The wavelength of the incident light is $\lambda = 633$ nm, the angles of incidence are $(\theta_0, \phi_0) = (0.74°, 45°)$. The dielectric constant of the film is $\varepsilon_2 = 2.6896 + 0.01i$, and its mean thickness is $d = 478.5$ nm. The roughness of the surface is characterized by the power spectrum in Eq. (13), with $k_- = 0.82(\omega/c)$, $k_+ = 1.97(\omega/c)$, and its rms height is $\delta = \lambda/40 = 15.82$ nm. (b) The same as (a) for out-of-plane ($\phi_s = \phi_0 + 90°$) scattering.

peak lies in the nonradiative region of the $q_1 q_2$ plane. In addition, among the real satellite peaks that should appear in the radiative region, not all may be sufficiently intense to be observable.

The scattering angles defined by Eq. (14) are expected to give the angles at which satellite peaks occur in the in-plane co-polarized scattering from the two-dimensional randomly rough surface of the film system studied here.

In the absence of absorption and roughness the $\{q_j(\omega)\}$ are the solutions of the dispersion relation

$$
\begin{aligned}
\alpha_2(q_\parallel, \omega) = \frac{1}{2\varepsilon_1\varepsilon_3} \Big(& \varepsilon_2 \left[\varepsilon_1 \beta_3(q_\parallel, \omega) + \varepsilon_3 \beta_1(q_\parallel, \omega) \right] \cot \left[\alpha_2(q_\parallel, \omega)d \right] \\
& \pm \big\{ \varepsilon_2^2 \left[\varepsilon_1 \beta_3(q_\parallel, \omega) + \varepsilon_3 \beta_1(q_\parallel, \omega) \right]^2 \cot^2 \left[\alpha_2(q_\parallel, \omega)d \right] \\
& + 4\varepsilon_1\varepsilon_2^2\varepsilon_3 \beta_1(q_\parallel, \omega)\beta_3(q_\parallel, \omega) \big\}^{1/2} \Big)
\end{aligned}
\tag{15a}
$$

in p polarization, and

$$
\begin{aligned}
\alpha_2(q_\parallel, \omega) = \frac{1}{2} \Big(& \left[\beta_1(q_\parallel, \omega) + \beta_3(q_\parallel, \omega) \right] \cot \left[\alpha_2(q_\parallel, \omega)d \right] \\
& \pm \big\{ \left[\beta_1(q_\parallel, \omega) + \beta_3(q_\parallel, \omega) \right]^2 \cot^2 \left[\alpha_2(q_\parallel, \omega)d \right] \\
& + 4\beta_1(q_\parallel, \omega) + \beta_3(q_\parallel, \omega) \big\}^{1/2} \Big)
\end{aligned}
\tag{15b}
$$

in s polarization. In these equations $\beta_i(q_\parallel, \omega) = \left[q_\parallel^2 - \varepsilon_i(\omega/c)^2 \right]^{1/2}$ for $i = 1, 3$, while $\alpha_2(q_\parallel, \omega)$ is defined in Eq. (3). The film structure studied in this paper is found to support two guided waves in p-polarization, whose wave numbers are

$$
q_1(\omega) = 1.4391(\omega/c), \quad q_2(\omega) = 1.0119(\omega/c),
\tag{16a}
$$

and two guided waves in s polarization, with wave numbers

$$
q_1(\omega) = 1.5467(\omega/c), \quad q_2(\omega) = 1.2432(\omega/c).
\tag{16b}
$$

These results predict satellite peaks at scattering angles $\theta_s = -25.22°$ and $23.74°$ in p polarization and at $\theta_s = -18.13°$ and $16.65°$ in s polarization when we are considering in-plane scattering, assuming the same angles of incidence as in Fig. 1. These scattering angles are indicated by vertical dotted lines in Fig. 1(a). The peaks at $\theta_s = -18.13°$ and $16.65°$ are seen in the s→s co-polarized scattering contribution to the mean differential reflection coefficient. There is no evidence of satellite peaks at $\theta_s^{(1,2)} = -25.22°$ and $23.74°$ in the p→p co-polarized scattering contribution to the mean differential reflection coefficient, presumably because they are too weak to be seen. These results disagree with those of [10], in which no satellite peaks were found in the in-plane s→s scattering contribution to the mean differential reflection coefficient (although they are present in this contribution when the dielectric film is deposited on a planar perfectly conducting surface). However, in [10] the surface roughness was characterized by a Gaussian power spectrum, not the West–O'Donnell power spectrum assumed here. The results of earlier calculations [25] of the scattering of p- and s-polarized light from a film with a one-dimensional randomly rough surface characterized by a Gaussian power spectrum that is deposited on a planar perfectly conducting surface, display satellite peaks more weakly than when the roughness is characterized by a West–O'Donnell power spectrum [26].

Turning now to the results for out-of-plane scattering presented in Fig. 1(b), we see that an enhanced backscattering peak is present in each scattering configuration. It is cut off in each configuration. This is an artifact of the present calculation that results from the line defined by

$\phi_s = \phi_0 \pm 90°$ being exactly one grid point away from the backscattering direction. It is important to note that in out-of-plane scattering the predominant contribution to the differential reflection coefficient is in the cross-polarized part. We see that the satellite peaks are now observed in the p→s scattering configuration, meaning that incident p-polarized light excites both of the s-polarized guided modes with wave vectors in the $\phi = \phi_0 \pm 90°$ directions, which subsequently interfere to cause satellite peaks in out-of-plane scattering. Hence, the well-known "satellite peaks" found in scattering from 1D surfaces turn into a kind of "satellite rings" for scattering from 2D surfaces, where part of the ring is co-polarized (s→s in-plane) and part of the ring is cross-polarized (p→s out-of-plane).

In Fig. 2 we present contour plots of the complete angular distribution of the mean differential reflection coefficient for the light scattered incoherently from the film system studied here. The material and experimental parameters used in producing these results have the same values used in obtaining Fig. 1.

Light of p polarization (left column) or s polarization (right column) is incident on the structure. In Figs. 2(a) and 2(d) all of the scattered light is recorded; in Figs. 2(b) and 2(e) only the p-polarized scattered light is recorded; while in Figs. 2(c) and 2(f) only the s-polarized scattered light is recorded. In Fig. 2(f) we see two regions of high intensity in the in-plane polarized (s→s) intensity distribution, centered at radii of approximately $0.29(\omega/c)$ at $\phi_s = 45°$, and $0.31(\omega/c)$ at $\phi_s = 225°$. These are the satellite peaks seen in the plot of $\langle \partial R_{ss}/\partial \Omega_s \rangle_{incoh}$ presented in Fig. 1(a). No such regions of high intensity are seen in Fig. 2(b) at radii of $0.34(\omega/c)$ at $\phi_s = 45°$ and $0.52(\omega/c)$ at $\phi_s = 225°$, where satellite peaks are predicted by Eq. (14) for in-plane co-polarized scattering of p-polarized incident light. This result is consistent with the absence of satellite peaks in the result for $\langle \partial R_{pp}/\partial \Omega_s \rangle_{incoh}$ presented in Fig. 1(a). The intensity maxima in the out-of-plane cross-polarized (p→s) scattering intensity distribution depicted in Fig. 2(c) correspond to the peaks at $\theta_s \approx 19°$ seen in the plot of $\langle \partial R_{sp}/\partial \Omega_s \rangle_{incoh}$ presented in Fig. 1(b).

The result that satellite peaks are observed in scattering processes in which the scattered light is s polarized, independent of the polarization of the incident light, is an interesting result of the present calculations. It may be connected with the fact that s-polarized light is reflected more strongly from a dielectric surface than is p-polarized light.

In Fig. 3 we present results analogous to those presented in Fig. 1, but for angles of incidence $(\theta_0, \phi_0) = (5.19°, 45°)$. In Fig. 3(a) we present results for the in-plane ($\phi_s = \phi_0$) co-(p→p, s→s) and cross-(p→s, s→p) polarized scattering, while in Fig. 3(b) we present results for out-of-plane ($\phi_s = \phi_0 \pm 90°$) co-(p→p, s→s) and cross-(p→s, s→p) polarized scattering. In the results presented in Fig. 3(a) [3(b)] single-scattering processes give no contribution to the mean differential reflection coefficient for $-46.85° < \theta_s < 65.57°$ ($-54.59° < \theta_s < 54.59°$). The limits of these angular regions are clearly seen in these figures.

A well-defined enhanced backscattering peak is seen in the results plotted in Fig. 3(a). Satellite peaks are predicted by Eq. (14) to occur (in-plane) at $\theta_s^{(1,2)} = -31.18°$ and $19.68°$ for p-polarized incident light, and at $\theta_s^{(1,2)} = -23.20°$ and $12.30°$ for s-polarized incident light, when the angles of incidence were the same as in Fig. 3. These scattering angles are indicated by vertical dotted lines in this figure. Peaks at $\theta_s = -23.20°$ and $\theta_s = 12.30°$ are present in the s→s co-polarized scattering contribution to the mean differential reflection coefficient. There is no suggestion of peaks at $\theta_s = -31.8°$ and $19.68°$ in the p→p co-polarized scattering contribution to the mean differential reflection coefficient, nor any suggestions of peaks in the cross-polarized (p→s, s→p) contribution to it.

The results for out-of-plane scattering presented in Fig. 3(b) show no enhanced backscattering peaks. The reason for this is simply that since the abscissa points along $\phi = \phi_0 \pm 90°$, it does not cut through the backscattering peak, localized at $(\theta_s, \phi_s) = (\theta_0, \phi_0 + 180°)$. We do
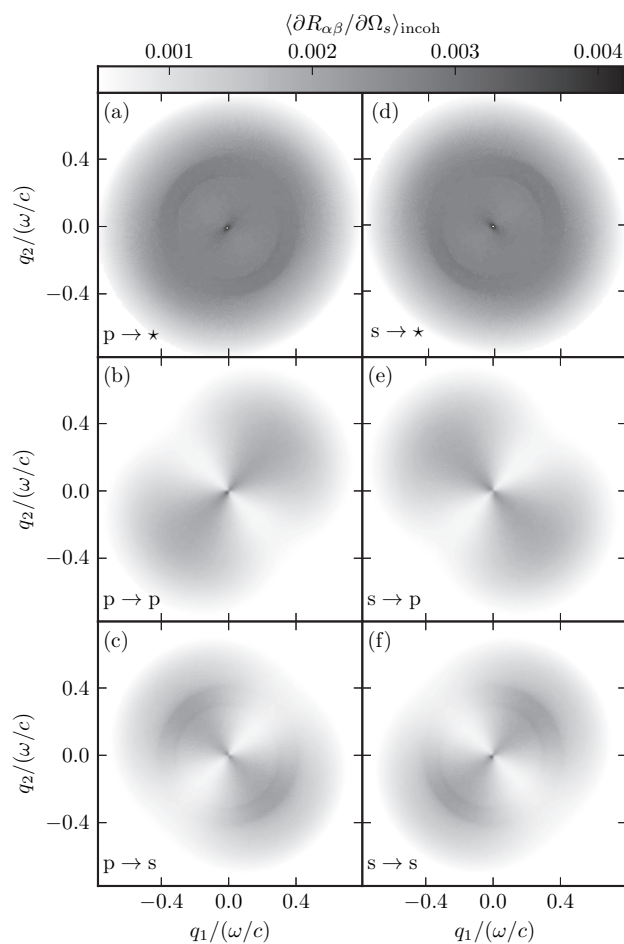
Fig. 2. The complete angular distribution of the mean differential reflection coefficient $\langle \partial R_{\alpha\beta}/\partial\Omega_s \rangle_{\mathrm{incoh}}$ for the light scattered incoherently from the film structure. The material and experimental parameters assumed here are those used in obtaining the plots presented in Fig. 1. Light of either p (left column) or s (right column) polarization is incident on the structure. In (a) and (d) all (diffusely) scattered light is recorded. In (b) and (e) only the p-polarized scattered light is recorded, while in (c) and (f) only the s-polarized scattered light is recorded. The dark dot in each panel indicates the enhanced backscattering peak. Note that the gray scale bar is cut at both ends in order to enhance the satellite rings. Also note that the contribution from single scattering is suppressed, i.e. the differential reflection coefficient is artificially set to 0 for $\left| \mathbf{q}_\parallel - \mathbf{k}_\parallel \right| > k_-$.
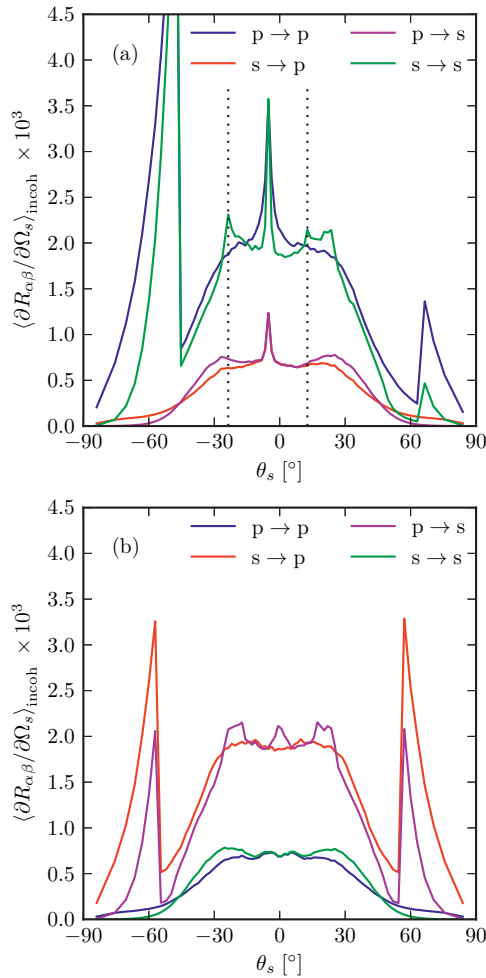
Fig. 3. The same as Fig. 1, but for angles of incidence given by $(\theta_0, \phi_0) = (5.19°, 45°)$.

see some remainders of the satellite ring structure; the low peaks around $\theta_s \approx \pm20°$ are part of the rings to the upper left in Fig. 4. As the rings decay in strength away from the direction $\phi = \phi_0 \pm 90°$, they are weaker than what is seen in-plane.

As a necessary, but not sufficient, condition of the validity of our simulation results is energy conservation. If all materials in the scattering system are lossless, i.e. $\text{Im}(\varepsilon_i) = 0$ ($i = 1, 2, 3$), the power of the scattered light has to be equal to the power of the incident light. Under these conditions, energy was conserved within 0.03% in our simulations.

In conclusion, in this paper we have presented a nonperturbative approach to the solution of
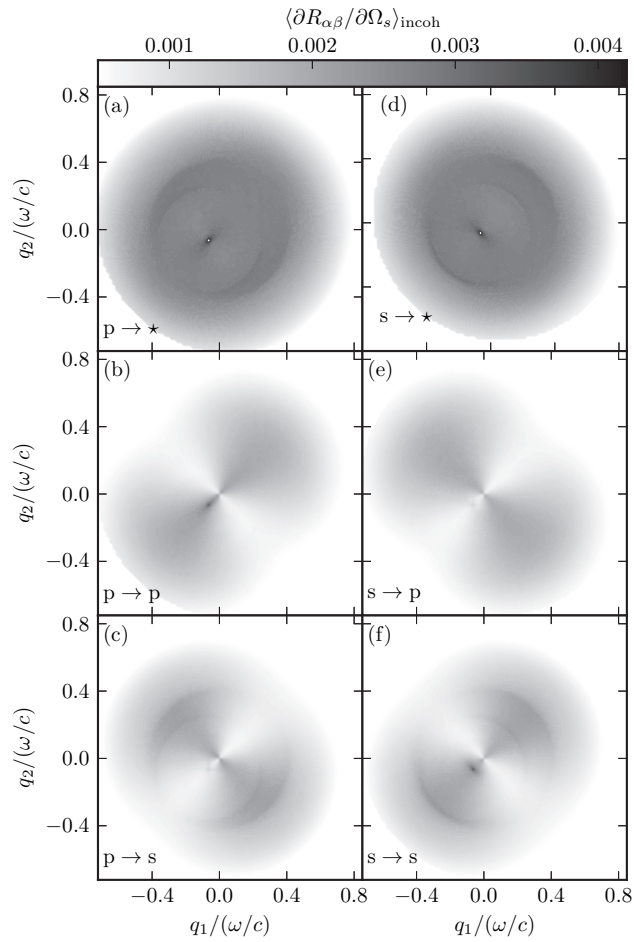
Fig. 4. The same as Fig. 2, but for angles of incidence given by $(\theta_0, \phi_0) = (5.19°, 45°)$. Note that the color bar is cut at both ends in order to enhance the satellite rings. Also note that the contribution from single scattering is suppressed, i.e. the differential reflection coefficient is artificially set to 0 for $\left|\mathbf{q}_\parallel - \mathbf{k}_\parallel\right| > k_-$.

the reduced Rayleigh equation for the scattering of polarized light from a dielectric film with a two-dimensional randomly rough surface deposited on a planar metallic surface. We have applied this result to calculate the contributions to the mean differential reflection coefficient from the in-plane co- and cross-polarized components of the light scattered incoherently, as well as from the out-of-plane co-and cross-polarized components of the light scattered incoherently. The out-of-plane scattering contributions have not been calculated in earlier perturbative studies of this problem [10, 14]. In addition, we have calculated the full angular distribution of the intensity of the scattered light, which has helped to refine the conclusions drawn from the calculations of the mean differential reflection coefficient. The main physical result obtained in this work is the demonstration that satellite peaks (or rings) can arise in scattering from the film structure studied here. This result is in agreement with the results of Soubret *et al.* [10] but not with those of Kawanishi *et al.* [14]. A detailed study of the conditions under which satellite peaks occur is lacking, but perhaps the approach developed here will be used to determine them. The work reported here also opens the door to the possibility of calculating other properties of the light scattered from the film system studied here, such as all the elements of the associated Mueller matrix, and offers the possibility of designing such structures to possess specified scattering properties. These are problems that have to be left to the future.

Acknowledgements

P. A. Letnes, A. A. Maradudin, T. Nordam, and I. Simonsen, "Calculation of the Mueller matrix for scattering of light from two-dimensional rough surfaces," *Phys. Rev. A*, vol. 86, p. 031803, 2012

Paper 3

Calculation of the Mueller matrix for scattering of light from two-dimensional rough surfaces

P. A. Letnes,[1,*] A. A. Maradudin,[2,†] T. Nordam,[1,‡] and I. Simonsen[1,§]

[1]*Department of Physics, Norwegian University of Science and Technology, NO-7491 Trondheim, Norway*
[2]*Department of Physics and Astronomy, and Institute for Surface and Interface Science, University of California,
Irvine, California 92697, USA*

We calculate all the elements of the Mueller matrix for light scattering from a two-dimensional randomly rough lossy metal surface. The calculations are carried out for arbitrary angles of incidence by the use of nonperturbative numerical solutions of the reduced Rayleigh equations. We foresee that the ability to model polarization effects in light scattering from surfaces will enable better interpretation of experimental data and allow for the design of surfaces which possess useful polarization effects.

PACS number(s): 42.25.−p, 41.20.−q

Introduction. When light is scattered from a surface, it carries a great deal of information about the statistical properties of the surface in its polarization. Even when the structures in question are beyond the imaging limit, polarized optical scattering can be employed to distinguish between material inhomogeneities, particles, or even buried defects and the roughness of both interfaces of thin films [1]. However, to extract information from experimental data, one has to be able to model the polarization effects [2]. The ability to calculate the polarization effects found in light scattering also opens the door to the possibility of designing surfaces which produce specified polarization properties in the scattered or transmitted light [3,4].

All the information about the polarization transformations light undergoes when scattered from rough surfaces is contained in the Mueller matrix [5–7]. Still, very few calculations of the Mueller matrix for a two-dimensional randomly rough surface have so far been carried out by numerical methods, largely because calculations of the scattering of light from such surfaces are still computationally demanding [8–11].

An exception [12] is a calculation of the Mueller matrix for perfectly conducting and metallic surfaces characterized by a surface profile function that is a stationary, zero-mean, isotropic, Gaussian random process, defined by a Gaussian surface height autocorrelation function. These calculations were carried out by a ray-tracing approach on the assumption that the surface was illuminated at normal incidence. In this work it was also shown that due to the assumptions of normal incidence and the isotropy of the surface statistics, the elements of the corresponding Mueller matrix possess certain symmetry properties. Experimental Mueller matrices have later been interpreted using the ray-tracing method [13]. Zhang and Bahar [14] carried out an approximate analytic calculation of the elements of the Mueller matrix for the scattering of light from two-dimensional randomly rough dielectric surfaces coated uniformly with a different dielectric material. A related, yet qualitatively different, system is that of a slab of random

scatterers deposited on a substrate. The Mueller matrix of this system was discussed by Lam and Ishimaru [15,16].

In this Rapid Communication we report a step toward realizing the possibilities mentioned above. We present an approach to calculating, for arbitrary angles of incidence, all the elements of the Mueller matrix for the scattering of light from a two-dimensional weakly rough surface. It is based on nonperturbative numerical solutions of the reduced Rayleigh equation for the scattering of p- and s-polarized light from a two-dimensional rough penetrable surface [10,17].

Theory and computational method. The system we study consists of vacuum in the region $x_3 > \zeta(\mathbf{x}_\parallel)$, where $\mathbf{x}_\parallel = (x_1, x_2, 0)$, and a metal whose dielectric function, for angular frequency ω, is $\varepsilon(\omega)$ in the region $x_3 < \zeta(\mathbf{x}_\parallel)$. The surface profile function $\zeta(\mathbf{x}_\parallel)$ is assumed to be a single-valued function of $\mathbf{x}_\parallel$ that is differentiable with respect to x_1 and x_2, and constitutes a stationary, zero-mean, isotropic, Gaussian random process defined by $\langle \zeta(\mathbf{x}_\parallel) \zeta(\mathbf{x}'_\parallel) \rangle = \delta^2 W(|\mathbf{x}_\parallel - \mathbf{x}'_\parallel|)$. The angle brackets here and in all that follows denote an average over the ensemble of realizations of the surface profile function, and $\delta = \langle \zeta^2(\mathbf{x}_\parallel) \rangle^{1/2}$ is the rms height of the surface. Each realization of the surface profile function was generated numerically by the filtering method [11,18].

We begin by writing the electric field in the vacuum region $x_3 > \zeta(\mathbf{x}_\parallel)$ as the sum of an incident and a scattered field, $\mathbf{E}(\mathbf{x},t) = [\mathbf{E}^{(0)}(\mathbf{x}|\omega) + \mathbf{E}^{(s)}(\mathbf{x}|\omega)] \exp(-i\omega t)$, where

$$\mathbf{E}^{(0)}(\mathbf{x}|\omega) = [\mathcal{E}_p^{(0)}(\mathbf{k}_\parallel)\hat{\mathbf{e}}_p^{(0)}(\mathbf{k}_\parallel) + \mathcal{E}_s^{(0)}(\mathbf{k}_\parallel)\hat{\mathbf{e}}_s^{(0)}(\mathbf{k}_\parallel)]$$
$$\times \exp[i\mathbf{k}_\parallel \cdot \mathbf{x}_\parallel - i\alpha_0(k_\parallel)x_3], \quad (1a)$$

$$\mathbf{E}^{(s)}(\mathbf{x}|\omega) = \int \frac{d^2q_\parallel}{(2\pi)^2} [\mathcal{E}_p^{(s)}(\mathbf{q}_\parallel)\hat{\mathbf{e}}_p^{(s)}(\mathbf{q}_\parallel) + \mathcal{E}_s^{(s)}(\mathbf{q}_\parallel)\hat{\mathbf{e}}_s^{(s)}(\mathbf{q}_\parallel)]$$
$$\times \exp[i\mathbf{q}_\parallel \cdot \mathbf{x}_\parallel + i\alpha_0(q_\parallel)x_3]. \quad (1b)$$

Here $\mathbf{k}_\parallel = (k_1, k_2, 0)$, the unit polarization vectors are $\hat{\mathbf{e}}_p^{(0)}(\mathbf{k}_\parallel) = (c/\omega)[\alpha_0(k_\parallel)\hat{\mathbf{k}}_\parallel + k_\parallel\hat{\mathbf{x}}_3]$, $\hat{\mathbf{e}}_s^{(0)}(\mathbf{k}_\parallel) = \hat{\mathbf{k}}_\parallel \times \hat{\mathbf{x}}_3$, $\hat{\mathbf{e}}_p^{(s)}(\mathbf{q}_\parallel) = (c/\omega)[-\alpha_0(q_\parallel)\hat{\mathbf{q}}_\parallel + q_\parallel\hat{\mathbf{x}}_3]$, $\hat{\mathbf{e}}_s^{(s)}(\mathbf{q}_\parallel) = \hat{\mathbf{q}}_\parallel \times \hat{\mathbf{x}}_3$, while $\alpha_0(q_\parallel) = [(\omega/c)^2 - q_\parallel^2]^{1/2}$, with $\mathrm{Re}\,\alpha_0(q_\parallel) > 0$, $\mathrm{Im}\,\alpha_0(q_\parallel) > 0$. Here, c is the speed of light in vacuum, and a caret over a vector indicates that it is a unit vector. In terms of the polar and azimuthal angles of incidence (θ_0, ϕ_0) and scattering (θ_s, ϕ_s), the vectors $\mathbf{k}_\parallel$ and $\mathbf{q}_\parallel$ are given by $\mathbf{k}_\parallel = (\omega/c) \sin\theta_0(\cos\phi_0, \sin\phi_0, 0)$ and $\mathbf{q}_\parallel = (\omega/c) \sin\theta_s(\cos\phi_s, \sin\phi_s, 0)$.

---

*Paul.Anton.Letnes@gmail.com
†aamaradu@uci.edu
‡Tor.Nordam@ntnu.no
§Ingve.Simonsen@ntnu.no

A linear relation exists between the amplitudes $\mathcal{E}_\alpha^{(s)}(\mathbf{q}_\parallel)$ and $\mathcal{E}_\beta^{(0)}(\mathbf{k}_\parallel)$, which we write in the form ($\alpha = p,s$)

$$\mathcal{E}_\alpha^{(s)}(\mathbf{q}_\parallel) = \sum_{\beta=p,s} R_{\alpha\beta}(\mathbf{q}_\parallel|\mathbf{k}_\parallel)\mathcal{E}_\beta^{(0)}(\mathbf{k}_\parallel). \qquad (2)$$

It was shown by Brown *et al.* [17] that the scattering amplitudes $R_{\alpha\beta}(\mathbf{q}_\parallel|\mathbf{k}_\parallel)$ satisfy the matrix integral equation (the reduced Rayleigh equation)

$$\int \frac{d^2 q_\parallel}{(2\pi)^2} \frac{I(\alpha(p_\parallel) - \alpha_0(q_\parallel)|\mathbf{p}_\parallel - \mathbf{q}_\parallel)}{\alpha(p_\parallel) - \alpha_0(q_\parallel)} \mathcal{N}_+(\mathbf{p}_\parallel|\mathbf{q}_\parallel)\mathbf{R}(\mathbf{q}_\parallel|\mathbf{k}_\parallel)$$

$$= -\frac{I(\alpha(p_\parallel) + \alpha_0(k_\parallel)|\mathbf{p}_\parallel - \mathbf{k}_\parallel)}{\alpha(p_\parallel) + \alpha_0(k_\parallel)} \mathcal{N}_-(\mathbf{p}_\parallel|\mathbf{k}_\parallel), \qquad (3)$$

with R_{pp} and R_{ps} forming the first row of the matrix $\mathbf{R}$, where

$$I(\gamma|\mathbf{Q}_\parallel) = \int d^2 x_\parallel \exp[-i\gamma\zeta(\mathbf{x}_\parallel)] \exp(-i\mathbf{Q}_\parallel \cdot \mathbf{x}_\parallel), \quad (4)$$

and $\alpha(p_\parallel) = [\varepsilon(\omega)(\omega/c)^2 - p_\parallel^2]^{1/2}$, with $\operatorname{Re}\alpha(p_\parallel) > 0$, $\operatorname{Im}\alpha(p_\parallel) > 0$. The matrices $\mathcal{N}_\pm(\mathbf{p}_\parallel|\mathbf{q}_\parallel)$ are given by

$$\mathcal{N}_\pm(\mathbf{p}_\parallel|\mathbf{q}_\parallel)$$
$$= \begin{pmatrix} p_\parallel q_\parallel \pm \alpha(p_\parallel)\hat{\mathbf{p}}_\parallel \cdot \hat{\mathbf{q}}_\parallel \alpha_0(q_\parallel) & -\frac{\omega}{c}\alpha(p_\parallel)[\hat{\mathbf{p}}_\parallel \times \hat{\mathbf{q}}_\parallel]_3 \\ \pm\frac{\omega}{c}[\hat{\mathbf{p}}_\parallel \times \hat{\mathbf{q}}_\parallel]_3 \alpha_0(q_\parallel) & \frac{\omega^2}{c^2}\hat{\mathbf{p}}_\parallel \cdot \hat{\mathbf{q}}_\parallel \end{pmatrix}. \qquad (5)$$

These equations were solved by the method described in detail in Ref. [10]. First, a realization of the surface profile function was generated on a grid of $N_x \times N_x$ points within a square

region of the $x_1 x_2$ plane of edge L. In evaluating the $\mathbf{q}_\parallel$ integral in Eq. (3) the infinite limits of integration were replaced by finite ones, $|\mathbf{q}_\parallel| < \mathcal{Q}/2$, and the integral was carried out by a two-dimensional version of the extended midpoint rule [19] using a grid in the $q_1 q_2$ plane that is determined by the Nyquist sampling theorem and the properties of the discrete Fourier transform. The function $I(\gamma|\mathbf{Q}_\parallel)$ was evaluated by expanding the integrand in Eq. (4) in powers of $\zeta(\mathbf{x}_\parallel)$ and calculating the Fourier transform of $\zeta^n(\mathbf{x}_\parallel)$ by the fast Fourier transform. The resulting equations were solved by LU factorization.

The scattering amplitudes $R_{\alpha\beta}(\mathbf{q}_\parallel|\mathbf{k}_\parallel)$ play a central role in the calculation of the elements of the Mueller matrix. In terms of these amplitudes the elements of the Mueller matrix $\mathbf{M}$ are [20]

$$M_{11} = C(|R_{pp}|^2 + |R_{sp}|^2 + |R_{ps}|^2 + |R_{ss}|^2),$$
$$M_{12} = C(|R_{pp}|^2 + |R_{sp}|^2 - |R_{ps}|^2 - |R_{ss}|^2),$$
$$M_{13} = C(R_{pp}R_{ps}^* + R_{sp}R_{ss}^* + R_{ps}R_{pp}^* + R_{ss}R_{sp}^*),$$
$$M_{14} = iC(R_{pp}R_{ps}^* + R_{sp}R_{ss}^* - R_{ps}R_{pp}^* - R_{ss}R_{sp}^*),$$
$$M_{21} = C(|R_{pp}|^2 - |R_{sp}|^2 + |R_{ps}|^2 - |R_{ss}|^2),$$
$$M_{22} = C(|R_{pp}|^2 - |R_{sp}|^2 - |R_{ps}|^2 + |R_{ss}|^2),$$
$$M_{23} = C(R_{pp}R_{ps}^* - R_{sp}R_{ss}^* + R_{ps}R_{pp}^* - R_{ss}R_{sp}^*),$$
$$M_{24} = iC(R_{pp}R_{ps}^* - R_{sp}R_{ss}^* - R_{ps}R_{pp}^* + R_{ss}R_{sp}^*),$$
$$M_{31} = C(R_{pp}R_{sp}^* + R_{sp}R_{pp}^* + R_{ps}R_{ss}^* + R_{ss}R_{ps}^*),$$
$$M_{32} = C(R_{pp}R_{sp}^* + R_{sp}R_{pp}^* - R_{ps}R_{ss}^* - R_{ss}R_{ps}^*),$$
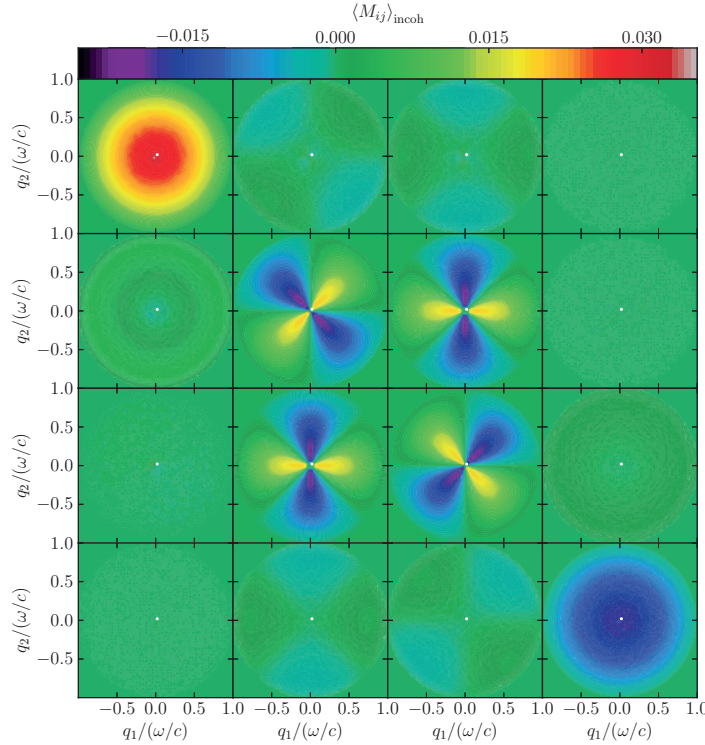
FIG. 1. (Color online) Color-level plots of the contribution to the Mueller matrix elements from the light scattered incoherently as functions of q_1 and q_2 for angles of incidence $(\theta_0,\phi_0) = (2°,45°)$. An ensemble consisting of $N_p = 10\,000$ surface realizations was used in obtaining these results. The elements, $\langle M_{ij}\rangle_{\text{incoh}}$ $(i,j = 1,2,3,4)$, are organized as a matrix with $\langle M_{11}\rangle_{\text{incoh}}$ in the top left corner, $\langle M_{12}\rangle_{\text{incoh}}$ top row and second column, etc. The white spots indicate the specular direction in reflection.

FIG. 2. (Color online) Same as Fig. 1, but now for angles of incidence $(\theta_0, \phi_0) = (25°, 45°)$.

$$M_{33} = C(R_{pp}R_{ss}^* + R_{sp}R_{ps}^* + R_{ps}R_{sp}^* + R_{ss}R_{pp}^*),$$

$$M_{34} = iC(R_{pp}R_{ss}^* + R_{sp}R_{ps}^* - R_{ps}R_{sp}^* - R_{ss}R_{pp}^*),$$

$$M_{41} = -iC(R_{pp}R_{sp}^* - R_{sp}R_{pp}^* + R_{ps}R_{ss}^* - R_{ss}R_{ps}^*),$$

$$M_{42} = -iC(R_{pp}R_{sp}^* - R_{sp}R_{pp}^* - R_{ps}R_{ss}^* + R_{ss}R_{ps}^*),$$

$$M_{43} = -iC(R_{pp}R_{ss}^* - R_{sp}R_{ps}^* + R_{ps}R_{sp}^* - R_{ss}R_{pp}^*),$$

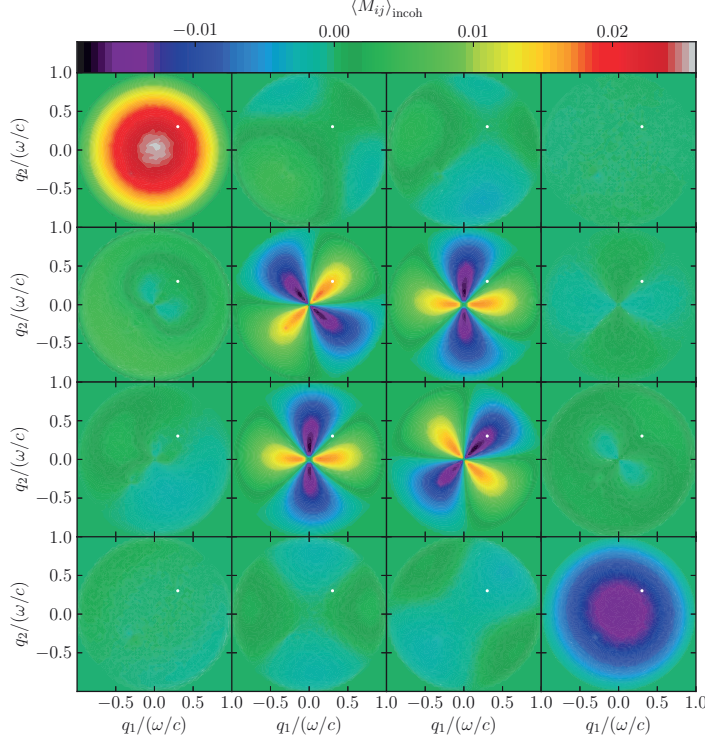$$M_{44} = C(R_{pp}R_{ss}^* - R_{sp}R_{ps}^* - R_{ps}R_{sp}^* + R_{ss}R_{pp}^*), \qquad (6)$$

where

$$C = \frac{1}{2L^2}\left(\frac{\omega}{2\pi c}\right)^2 \frac{\cos^2\theta_s}{\cos\theta_0}, \qquad (7)$$

and L^2 is the area of the plane $x_3 = 0$ covered by the rough surface. For clarity, we note that the conventions used in deriving the above expressions for the elements of the Mueller matrix are as follows. The Stokes parameters are defined as

$$\begin{pmatrix} I \\ Q \\ U \\ V \end{pmatrix} = \begin{pmatrix} |E_p|^2 + |E_s|^2 \\ |E_p|^2 - |E_s|^2 \\ 2\,\mathrm{Re}(E_p E_s^*) \\ 2\,\mathrm{Im}(E_p E_s^*) \end{pmatrix}, \qquad (8)$$

where the superscript * denotes complex conjugation, and E_p and E_s are the amplitudes of the p- and s-polarized components of the electric field, respectively. It is also of importance to note that the definition of the handedness of

circularly polarized light is opposite to that of, e.g., Hauge *et al.* [21].

As we are concerned with scattering from a randomly rough surface, it is the average, $\langle\mathbf{M}\rangle$, of the Mueller matrix over the ensemble of realizations of the surface profile function that we seek. In evaluating an average of the form $\langle R_{\alpha\beta}R_{\gamma\delta}^*\rangle$ we can write $R_{\alpha\beta}$ as the sum of its mean value and its fluctuation about the mean, $R_{\alpha\beta} = \langle R_{\alpha\beta}\rangle + (R_{\alpha\beta} - \langle R_{\alpha\beta}\rangle)$. We then obtain the result $\langle R_{\alpha\beta}R_{\gamma\delta}^*\rangle = \langle R_{\alpha\beta}\rangle\langle R_{\gamma\delta}^*\rangle + (\langle R_{\alpha\beta}R_{\gamma\delta}^*\rangle - \langle R_{\alpha\beta}\rangle\langle R_{\gamma\delta}^*\rangle)$. The first term on the right-hand side of this equation arises in the contribution to an element of the ensemble averaged Mueller matrix from the light scattered coherently (specularly); the second term arises in the contribution to that ensemble averaged matrix element from the light scattered incoherently (diffusely). It is the latter contribution, $\langle\mathbf{M}\rangle_{\text{incoh}}$, that we calculate.

Results. We have calculated in this way the 16 elements of the Mueller matrix when light of wavelength $\lambda = 457.9$ nm is incident on a two-dimensional randomly rough silver surface whose dielectric function at this wavelength is $\varepsilon(\omega) = -7.5 + 0.24i$ [22]. The roughness of the surface is defined by a surface height autocorrelation function $W(|\mathbf{x}_\parallel|) = \exp(-x_\parallel^2/a^2)$, where $a = \lambda/4$ and the rms height $\delta = \lambda/40$. For the numerical parameters we used $L = 25\lambda$ and $N_x = 319$, which implies that $\mathcal{Q}/2 = 3.2(\omega/c)$ is the cutoff in the integral in Eq. (3) [10]. The calculated Mueller matrices were found to be physically realizable and therefore self-consistent by the method of Ref. [23].
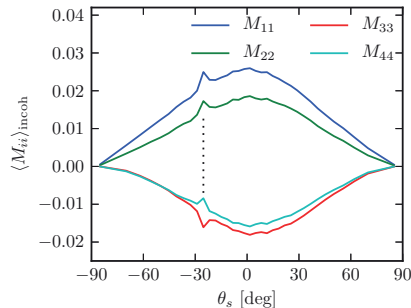
FIG. 3. (Color online) The incoherent contribution to the diagonal Mueller matrix elements, $\langle M_{ii} \rangle_{\mathrm{incoh}}$, in the plane of incidence (parameters as in Fig. 2). The vertical dotted line indicates the backscattering direction. The lines, from top to bottom, correspond to $i = 1,2,4$ and 3.

The results presented in Fig. 1 were obtained for angles of incidence $(\theta_0, \phi_0) = (2°, 45°)$, i.e., for essentially normal incidence. The first thing to notice from Fig. 1 is that the individual matrix elements possess the symmetry properties predicted by Bruce [12,24]. The elements of the first and last column are circularly symmetric; each element of the second and third columns is invariant under a combined 90° rotation about the origin and a change of sign; and the elements of the second column are 45° rotations of the elements of the third column in the same row [25]. Note that the elements $\langle M_{31} \rangle_{\mathrm{incoh}}$, $\langle M_{41} \rangle_{\mathrm{incoh}}$, $\langle M_{14} \rangle_{\mathrm{incoh}}$, and $\langle M_{24} \rangle_{\mathrm{incoh}}$ are zero to the precision used in this calculation. However, simulations indicate that this does not hold for anisotropic surfaces.

The results presented in Fig. 2 were obtained for angles of incidence $(\theta_0, \phi_0) = (25°, 45°)$, and display some interesting features. The elements $\langle M_{11} \rangle_{\mathrm{incoh}}$, $\langle M_{22} \rangle_{\mathrm{incoh}}$, and $\langle M_{33} \rangle_{\mathrm{incoh}}$ contain a (weak) enhanced backscattering peak at $\mathbf{q}_{\parallel} = -\mathbf{k}_{\parallel}$ (Fig. 3). The absolute value of the element $\langle M_{44} \rangle_{\mathrm{incoh}}$ has a dip in the retroreflection direction. This dip is not present in the results of a calculation based on small-amplitude perturbation theory to the lowest (second) order in the surface profile function, and is therefore a multiple-scattering effect, just as the enhanced backscattering peak is. In contrast to what was the case for normal incidence, the elements $\langle M_{31} \rangle_{\mathrm{incoh}}$ and $\langle M_{24} \rangle_{\mathrm{incoh}}$ are no longer zero.

If we denote the ensemble average of the contribution to a *normalized* element of the Mueller matrix from the light that has been scattered incoherently by $m_{ij} = \langle M_{ij} \rangle_{\mathrm{incoh}} / \langle M_{11} \rangle_{\mathrm{incoh}}$, we can estimate the order of magnitude of the Mueller matrix elements by calculating the quantities $s_{ij} = \langle |m_{ij}(\mathbf{q}_{\parallel})| \rangle_{\mathbf{q}_{\parallel}}$, where

$$\langle f(\mathbf{q}_{\parallel}) \rangle_{\mathbf{q}_{\parallel}} = \int d^2 q_{\parallel} \, f(\mathbf{q}_{\parallel}) \frac{c^2}{\pi \omega^2}, \qquad (9)$$

and the integral over $\mathbf{q}_{\parallel}$ is taken over the circular region $0 < q_{\parallel} < \omega/c$. It was found that s_{11}, s_{22}, s_{23}, s_{32}, s_{33}, s_{44} are of $O(1)$, s_{12}, s_{13}, s_{21}, s_{34}, s_{42}, s_{43} are of $O(0.1)$, and s_{14}, s_{24}, s_{31}, s_{41} are of $O(0.01)$. These results are only weakly dependent on the polar angle of incidence θ_0, for the values of θ_0 assumed in this study.

Conclusion. We have presented an approach to the calculation of all 16 elements of the Mueller matrix for light scattered from a two-dimensional, randomly rough, lossy metal surface, for arbitrary values of the polar and azimuthal angles of incidence. It is based on a rigorous numerical solution of the reduced Rayleigh equation for the scattering of p- and s-polarized light from a two-dimensional rough surface of a penetrable medium that captures multiple-scattering processes of all orders. The results display multiple-scattering effects in certain matrix elements, such as an enhanced backscattering peak in the retroreflection direction, and an unexpected dip in the same direction. The matrix elements also display symmetry properties that, for normal incidence, agree with those predicted by Bruce [12].

The approach used and the results presented in this Rapid Communication will lead to a better understanding of the polarimetric properties of random surfaces. Such knowledge may be critical for improved photovoltaic and remote sensing applications. It also has the potential to be used in engineering surface structures which produce well-defined polarization properties in scattered and transmitted light.

[1] T. A. Germer, in *Light Scattering and Nanoscale Surface Roughness*, edited by A. A. Maradudin (Springer, Berlin, 2007), pp. 259–284.

[2] J. Ellis, P. Caillard, and A. Dogariu, J. Opt. Soc. Am. A **19**, 43 (2002).

[3] Z. Ghadyani, I. Vartiainen, I. Harder, W. Iff, A. Berger, N. Lindlein, and M. Kuittinen, Appl. Opt. **50**, 2451 (2011).

[4] A. A. Maradudin, E. R. Méndez, and T. A. Leskova, *Designer Surfaces* (Elsevier Science, Amsterdam, 2008).

[5] H. Mueller, J. Opt. Soc. Am. **38**, 661 (1948).

[6] W. S. Bickel and W. M. Bailey, Am. J. Phys. **53**, 468 (1985).

[7] R. A. Chipman, *Handbook of Optics* (McGraw-Hill, New York, 1994).

[8] I. Simonsen, A. A. Maradudin, and T. A. Leskova, Phys. Rev. A **81**, 013806 (2010).

[9] I. Simonsen, A. A. Maradudin, and T. A. Leskova, Phys. Rev. Lett. **104**, 223904 (2010).

[10] T. Nordam, P. A. Letnes, and I. Simonsen, arXiv:1204.4984.

[11] I. Simonsen, J. B. Kryvi, A. A. Maradudin, and T. A. Leskova, Comput. Phys. Commun. **182**, 1904 (2011).

[12] N. C. Bruce, Waves Random Media **8**, 15 (1998).

[13] R. G. Priest and S. R. Meier, Opt. Eng. **41**, 988 (2002).

[14] Y. Zhang and E. Bahar, IEEE Trans. Antennas Propag. **47**, 949 (1999).

[15] C. M. Lam and A. Ishimaru, IEEE Trans. Antennas Propag. **41**, 851 (1993).

[16] C. M. Lam and A. Ishimaru, IEEE Trans. Antennas Propag. **42**, 145 (1994).

[17] G. C. Brown, V. Celli, M. Haller, and A. Marvin, Surf. Sci. **136**, 381 (1984).

[18] A. A. Maradudin, T. Michel, A. R. McGurn, and E. R. Mendez, Ann. Phys. **203**, 255 (1990).

[19] W. H. Press, S. A. Teukolsky, W. T. Vetterling, and B. P. Flannery, *Numerical Recipes in C*, 2nd ed. (Cambridge University Press, Cambridge, UK, 1992).

[20] D. S. Flynn and C. Alexander, Opt. Eng. **34**, 1646 (1995).

[21] P. S. Hauge, R. H. Muller, and C. G. Smith, Surf. Sci. **96**, 81 (1980).

[22] P. B. Johnson and R. W. Christy, Phys. Rev. B **6**, 4370 (1972).

[23] S. R. Cloude, Proc. SPIE **1166**, 177 (1989).

[24] Note that whereas Bruce assumes $\phi_0 = 0°$, we assume $\phi_0 = 45°$. This leads to the confusing situation where our results appear to be rotated with respect to those found in Ref. [12], when in fact they are not.

[25] It should be noted that the scattering amplitudes f_{sp} and f_{ps} in Bruce's Eq. (1) correspond to our R_{ps} and R_{sp}, respectively.

T. Nordam, P. A. Letnes, and I. Simonsen, "Numerical simulations of scattering of light from two-dimensional surfaces using the reduced Rayleigh equation," *arXiv:1204.4984 (submitted to Optics Express)*, 2013

Paper 4

Numerical Simulations of Scattering of Light from Two-Dimensional Surfaces Using the Reduced Rayleigh Equation

T. Nordam, P.A. Letnes, I. Simonsen

Department of Physics, The Norwegian University of Science and Technology (NTNU),
NO-7491 Trondheim, Norway

tor.nordam@gmail.com

paul.anton.letnes@gmail.com

Ingve.Simonsen@ntnu.no

OCIS codes: (290.1483) BSDF, BRDF, and BTDF; (290.4210) Multiple scattering; (290.5825) Scattering theory; (290.5880) Scattering, rough surfaces.

Abstract: A formalism is introduced for the non-perturbative, purely numerical, solution of the reduced Rayleigh equation for the scattering of light from two-dimensional penetrable rough surfaces. As an example, we apply this formalism to study the scattering of p- or s-polarized light from two-dimensional dielectric or metallic randomly rough surfaces by calculating the full angular distribution of the co- and cross-polarized intensity of the scattered light. In particular, we present calculations of the mean differential reflection coefficient for glass and silver surfaces characterized by (isotropic or anisotropic) Gaussian and cylindrical power spectra. The proposed method is found, within the validity of the Rayleigh hypothesis, to give reliable results. For a non-absorbing metal surface the conservation of energy was explicitly checked, and found to be satisfied to within 0.03%, or better, for the parameters assumed. This testifies to the accuracy of the approach and a satisfactory discretization.

References and links

1. A. A. Maradudin, ed., *Structured Surfaces as Optical Metamaterials* (Cambridge University Press, New York, 2011).
2. V. M. Agranovich and Y. N. Gartstein, "Spatial dispersion and negative refraction of light," Phys.-Usp. **49**, 1029–1944 (2006).
3. J. D. Joannopoulos, S. G. Johnson, J. N. Winn, and R. D. Meade, *Photonic Crystals: Molding the Flow of Light* (Princeton University Press, NJ, 2008), 2nd ed.
4. J. B. Pendry, L. Martín-Moreno, and F. J. Garcia-Vidal, "Mimicking surface plasmons with structured surfaces," Science **305**, 847–848 (2004).
5. J. B. Pendry, D. Schurig, and D. R. Smith, "Controlling electromagnetic fields," Science **312**, 1780–1782 (2006).
6. D. Schurig, J. J. Mock, B. J. Justice, S. A. Cummer, J. B. Pendry, A. F. Starr, and D. R. Smith, "Metamaterial electromagnetic cloak at microwave frequencies," Science **314**, 977–980 (2006).
7. B. Baumeier, T. A. Leskova, and A. A. Maradudin, "Cloaking from surface plasmon polaritons by a circular array of point scatterers," Phys. Rev. Lett. **103**, 246803 (2009).
8. A. A. Maradudin, E. R. Méndez, and T. A. Leskova, *Designer Surfaces* (Elsevier Science, New York, 2008).
9. E. R. Méndez, E. E. García-Guerrero, T. A. Leskova, A. A. Maradudin, J. Muñoz-López, and I. Simonsen, "Design of one-dimensional random surfaces with specified scattering properties," Appl. Phys. Lett. **81**, 798 (2002).

10. Lord Rayleigh, "On the dynamical theory of gratings," Proceedings of the Royal Society of London. Series A **79**, 399–416 (1907).
11. Lord Rayleigh, *The Theory of Sound*, vol. II (MacMillan, London, 1896), 2nd ed. Pp. 89, 297–311.
12. L. Mandelstam, "Über die rauhigkeit freier flüssigkeitsoberflächen," Ann. Phys. (Leipzig) **346**, 609–624 (1913).
13. F. G. Bass and I. M. Fuks, *Wave Scattering from Statistically Rough Surfaces* (Pergamon, Oxford, UK, 1979).
14. J. A. Ogilvy, *Theory of wave scattering from random rough surfaces* (IOP Publishing, Bristol, UK, 1991).
15. A. G. Voronovich, *Wave scattering from Rough Surfaces* (Springer Verlag, Berlin, 1999), 2nd ed.
16. M. Nieto-Vesperinas, *Scattering and Diffraction in Physical Optics* (World Scientific Publishing Company, Singapore, 2006), 2nd ed.
17. A. A. Maradudin, ed., *Light Scattering and Nanoscale Surface Roughness* (Springer-Verlag, New York, 2007).
18. A. V. Zayats, I. I. Smolyaninov, and A. A. Maradudin, Phys. Rep. **408**, 131 (2005).
19. I. Simonsen, "Optics of surface disordered systems: A random walk through rough surface scattering phenomena," Eur. Phys. J.-Spec. Top. **181**, 1 (2010).
20. A. R. McGurn, A. A. Maradudin, and V. Celli, Phys. Rev. B **31**, 4866 (1985).
21. S. West and K. A. O'Donnell, J. Opt. Soc. Am. A **12**, 390 (1995).
22. E. R. Méndez and K. A. O'Donnell, Opt. Commun. **61**, 91 (1987).
23. Z.-H. Gu, R. S. Dummer, A. A. Maradudin, A. R. McGurn, and E. R. Méndez, Appl. Opt. **30**, 4094 (1991).
24. V. Freilikher, M. Pustilnik, and I. Yurkevich, Phys. Lett. A **193**, 467 (1994).
25. A. A. Maradudin, T. Michel, A. R. McGurn, and E. R. Méndez, "Enhanced backscattering of light from a random grating," Ann. Phys. (NY) **203**, 255 – 307 (1990).
26. A. Taflove and S. C. Hagness, *Computational Electrodynamics: The Finite-Difference Time-Domain Method* (Artech House, Norwood, MA, 2005), 3rd ed.
27. J. L. Volakis, A. Chatterjee, and L. C. Kempel, *Finite Element Method Electromagnetics: Antennas, Microwave Circuits, and Scattering Applications* (IEEE Press, New York, 2001).
28. J. Jin, *The Finite Element Method in Electromagnetics* (Wiley-IEEE Press, New York, 2002), 2nd ed.
29. M. Bonnet, *Boundary Integral Equation Methods for Solids and Fluids* (Wiley, Chichester, England, 1999).
30. W. Hackbush, *Integral Equations: Theory and Numerical Treatment* (Birkhauser Verlag, Basel, Switzerland, 1995).
31. R. F. Harrington, *Field Computation by Moment Methods*, IEEE Press Series on Electromagnetic Wave Theory (Wiley-IEEE Press, New York, 1993).
32. J. P. Boyd, *Chebychev and Fourier Spectral Methods* (Dover, New York, 2001), 2nd ed.
33. I. Simonsen, J. B. Kryvi, A. A. Maradudin, and T. A. Leskova, "Light scattering from anisotropic, randomly rough, perfectly conducting surfaces," Comp. Phys. Commun. **182**, 1904 (2011).
34. G. C. Brown, V. Celli, M. Haller, and A. Marvin, "Vector theory of light scattering from a rough surface: Unitary and reciprocal expansions," Surf. Sci. **136**, 381 – 397 (1984).
35. A. Madrazo and A. A. Maradudin, "Numerical solutions of the reduced rayleigh equation for the scattering of electromagnetic waves from rough dielectric films on perfectly conducting substrates," Opt. Commun. **134** (1997).
36. I. Simonsen and A. A. Maradudin, "Numerical simulation of electromagnetic wave scattering from planar dielectric films deposited on rough perfectly conducting substrates," Opt. Commun. **162**, 99 (1999).
37. I. Simonsen, "Enhanced back and forward scattering in the reflection of light from weakly rough random metal surfaces," Phys. Status Solidi B **247**, 2075 (2010).
38. A. R. Mcgurn and A. A. Maradudin, "Perturbation theory results for the diffuse scattering of light from two-dimensional randomly rough metal surfaces," Wave Random Media **6**, 251 – 267 (1996).
39. A. Soubret, G. Berginc, and C. Bourrely, "Application of reduced rayleigh equations to electromagnetic wave scattering by two-dimensional randomly rough surfaces," Phys. Rev. B **63**, 245411 (2001).
40. A. Soubret, G. Berginc, and C. Bourrely, "Backscattering enhancement of an electromagnetic wave scattered by two-dimensional rough layers," J. Opt. Soc. Am. A **18**, 2778–2788 (2001).
41. A. M. Kern and O. J. F. Martin, "Surface integral formulation for 3d simulations of plasmonic and high permittivity nanostructures," J. Opt. Soc. Am. A **26**, 732–740 (2009).
42. A. A. Maradudin, "The reduced Rayleigh equation for transmission of light trough a two-dimensional randomly rough surface," (2012). Unpublished.
43. T. A. Leskova, "The reduced Rayleigh equation for reflection of light from two-dimensional randomly rough films deposited on flat substrates," (2010). Unpublished.
44. T. Nordam, P. A. Letnes, I. Simonsen, and A. A. Maradudin, "Satellite peaks in the scattering of light from the two-dimensional randomly rough surface of a dielectric film on a planar metal surface," Optics Express **20**, 11336–11350 (2012).
45. I. Simonsen, A. A. Maradudin, and T. A. Leskova, "Scattering of electromagnetic waves from two-dimensional randomly rough perfectly conducting surfaces: The full angular intensity distribution," Phys. Rev. A **81**, 013806 (2010).
46. I. Simonsen, A. A. Maradudin, and T. A. Leskova, "The scattering of electromagnetic waves from two-dimensional randomly rough penetrable surfaces," Phys. Rev. Lett. **104**, 223904 (2010).

47. N. G. V. Kampen, *Stochastic Processes in Physics and Chemistry* (North Holland, 2007), 3rd ed.
48. R. F. Millar, Proc. Camb. Phil. Soc. **65**, 773 (1969).
49. R. F. Millar, Proc. Camb. Phil. Soc. **69**, 217 (1971).
50. A. V. Tishchenko, Opt. Express **17**, 17102 (2009).
51. J. D. Jackson, *Classical Electrodynamics* (John Wiley & Sons, New York, 2007), 3rd ed.
52. J. A. Stratton, *Electromagnetic Theory*, IEEE Press Series on Electromagnetic Wave Theory (Wiley-IEEE Press, New York, 2007).
53. T. Nordam, P. A. Letnes, I. Simonsen, and A. A. Maradudin, "Numerical solutions of the rayleigh equations for the scattering of light from a two-dimensional randomly rough perfectly conducting surface," (2012). Unpublished.
54. W. H. Press, S. A. Teukolsky, W. T. Vetterling, and B. P. Flannery, *Numerical Recipes in Fortran. The Art of Scientific Computing* (Cambridge University Press, Cambridge, 1992), 2nd ed.
55. A. G. Navarrete Alcalá, E. I. Chaikina, E. R. Méndez, T. A. Leskova, and A. A. Maradudin, "Specular and diffuse scattering of light from two-dimensional randomly rough metal surfaces: experimental and theoretical results," Wave Random Media **19**, 600–636 (2009).
56. H. A. van der Vorst, "Bi-cgstab: A fast and smoothly converging variant of bi-cg for the solution of nonsymmetric linear systems," SIAM J. Sci. Stat. Comp. **13**, 631–644 (1992).
57. E. Agullo, C. Augonnet, J. Dongarra, M. Faverge, J. Langou, H. Ltaief, and S. Tomov, "Lu factorization for accelerator-based systems," in "Computer Systems and Applications (AICCSA), 2011 9th IEEE/ACS International Conference on," (IEEE, 2011), pp. 217–224.

1. Introduction

Wave scattering from rough surfaces is an old discipline which keeps attracting a great deal of attention from the scientific and technological community. Several important technologies in our society rely on such knowledge, with radar being a prime example. In the past, the interaction of light with rough surfaces was often considered an extra complication that had to be taken into account in order to properly interpret or invert scattering data. However, with the advent of nanotechnology, rough structures can be used to design novel materials with tailored optical properties. Examples include: metamaterials [1, 2], photonic crystals [3], spoof plasmons [4], optical cloaking [5–7], and designer surfaces [8, 9]. These developments have made it even more important to have available efficient and accurate simulation tools to calculate both the far- and near-field behavior of the scattered and transmitted fields for any frequency of the incident radiation, including potential resonance frequencies of the structure.

Lord Rayleigh was the first to perform systematic studies of wave scattering from rough surfaces when, in the late 1800s, he studied the intensity distribution of a wave scattered from a sinusoidal surface [10,11]. More than three decades later, Mandel'shtam studied light scattering from *randomly rough* surfaces [12] thereby initiating the field of wave scattering from surface disordered systems. Since the initial publication of these seminal works, numerous studies on wave scattering from randomly rough surfaces have appeared in the literature [13–19], and several new multiple scattering phenomena have been predicted and confirmed experimentally. These phenomena include the enhanced backscattering and enhanced transmission phenomena, the satellite peak phenomenon, and coherent effects in the intensity-intensity correlation functions [19–24].

These studies, and the methods they use, can be categorized as either perturbative or purely numerical (and non-pertubative). While the former group of methods is mainly limited to weakly rough surfaces, and therefore have limited applicability, the latter group of methods can be applied to a wider class of surface roughnesses. Rigorous numerical methods can in principle be used to study the wave scattering from surfaces of any degree of surface roughness. Such simulations are routinely performed for systems where the interface has a one-dimensional roughness, i.e., where the surface structure is constant along one of the two directions of the mean plane [19, 25]. However, for the practically more relevant situation of a two-dimensional rough surface, the purely numerical and rigorous methods are presently less used due to their computationally intensive nature. The reason for this complexity is the fact that for a randomly

rough surface there is no symmetry or periodicity in the surface structure that can be used to effectively reduce the simulation domain. For a periodic surface, it is sufficient to simulate a single unit cell, while for a random surface the unit cell is in principle infinite.

A wide range of simulation methods are currently available for simulating the interaction of light with matter, including the finite-difference time-domain (FDTD) method [26], the finite-element method (FEM) [27, 28], the related surface integral equation techniques also known as the boundary element method (BEM) or the method of moments (MoM) [29–33], the reduced Rayleigh equation (RRE) technique [18, 34–40], and spectral methods [32].

The FDTD and FEM methods discretize the whole volume of the simulation domain. Due to the complex and irregular shape of a (randomly) rough surface, it is often more convenient, and may give more accurate results (for the same level of numerical complexity) [41], to base numerical simulations on methods where only the surface itself needs to be discretized. This is the case, for example, for the surface integral technique and the reduced Rayleigh equation methods.

The reduced Rayleigh equation is an integral equation where the unknown is either the scattering amplitude or the transmission amplitude. In the former (latter) case, one talks about the reduced Rayleigh equation for reflection (transmission). For reflection this equation was originally derived by Brown *et al.* [34], and subsequently by Soubret *et al.* [39, 40]. Later it has also been derived for transmission [42] and film geometries [39, 43, 44].

In the past, the surface integral technique has been used to study light scattering from two-dimensional randomly rough, perfectly conducting or penetrable surfaces [33, 45, 46]. However, to date, a direct numerical and non-perturbative solution of the two-dimensional reduced Rayleigh equation has not appeared in the literature, even if its one-dimensional analog has been solved numerically and has been used to study the scattering from, and transmission through, one-dimensional rough surfaces [35–37]. The lesson learned from the one-dimensional scattering studies reported in Refs. [35–37] is that simulations based on a direct numerical solution of the reduced Rayleigh equation may give accurate non-perturbative results for systems where alternative methods struggle to give the same level of accuracy. Moreover, the reduced Rayleigh method also requires less memory for the same surface dimensions when compared to, e.g., the rigorous surface integral technique.

The main aim of this paper is to present a numerical method and formalism for the solution of the two-dimensional reduced Rayleigh equation for reflection. While we exclusively consider reflection, the formalism for transmission will be almost identical, and the resulting equation will have a similar form as for reflection. Additionally, the equation for transmission or reflection for a film geometry, i.e., for a film of finite thickness on top of a substrate, where only one interface is rough, will also have a similar form. The method presented will be illustrated by applying it to the study of the scattering of p- or s-polarized light from two-dimensional metallic or dielectric media separated from vacuum by an isotropic or anisotropic randomly rough surface.

This paper is organized as follows: First, in Sec. 2 we present the scattering geometry to be considered. We will then present some relevant scattering theory, including the reduced Rayleigh equation for the geometry under study (Sec. 3), followed by a detailed description of how the equation can be solved numerically (Sec. 4). Next, we will present some simulation results obtained by the introduced method (Sec. 5). We then discuss some of the computational challenges of this method (Sec. 6), and, finally, in Sec. 7 we draw some conclusions.

2. Scattering Geometry

We consider a system where a rough surface separates two regions. Region 1 is assumed to be vacuum ($\varepsilon_1 = 1$), and region 2 is filled with a metal or dielectric characterized by a complex
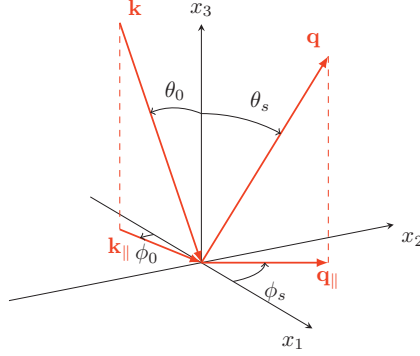
Fig. 1: (Color online) A sketch of the scattering geometry assumed in this work. The figure also shows the coordinate system used, angles of incidence (θ_0, ϕ_0) and scattering (θ_s, ϕ_s), and the corresponding lateral wavevectors $\mathbf{k}_\parallel$ and $\mathbf{q}_\parallel$, respectively.

dielectric function $\varepsilon_2(\omega)$, where the angular frequency is $\omega = 2\pi c/\lambda$, with λ being the wavelength of the incident light in vacuum and c the speed of light in vacuum. The height of the surface measured in the positive x_3 direction from the $x_1 x_2$-plane is given by the single-valued function $x_3 = \zeta(\mathbf{x}_\parallel)$, where $\mathbf{x}_\parallel = (x_1, x_2, 0)$, which is assumed to be at least once differentiable with respect to x_1 and x_2. Angles of incidence (θ_0, ϕ_0) and scattering (θ_s, ϕ_s) are defined positive according to the convention given in Fig. 1.

In principle, the theory to be presented in Sec. 3 can be used to calculate the scattering of light from any surface, provided it is not too rough. However, in this paper, we will consider randomly rough surfaces where $\zeta(\mathbf{x}_\parallel)$ constitutes a stationary random process defined by

$$
\begin{aligned}
\langle \zeta(\mathbf{x}_\parallel) \rangle &= 0, \\
\langle \zeta(\mathbf{x}_\parallel) \zeta(\mathbf{x}_\parallel{}') \rangle &= \delta^2 W(\mathbf{x}_\parallel - \mathbf{x}_\parallel{}'),
\end{aligned}
\tag{1}
$$

where the angle brackets denote an average over an ensemble of surface realizations. In writing Eqs. (1) we have defined the root-mean-square height of the surface, $\delta = \langle \zeta^2(\mathbf{x}_\parallel) \rangle^{1/2}$, and $W(\mathbf{x}_\parallel - \mathbf{x}_\parallel{}')$ denotes the height-height auto-correlation function of the surface, normalized so that $W(\mathbf{0}) = 1$ [19]. According to the Wiener-Khinchin theorem [47], the power spectrum of the surface profile function is given by

$$
g(\mathbf{k}_\parallel) = \int \mathrm{d}^2 x_\parallel \, W(\mathbf{x}_\parallel) \exp\left(-i\mathbf{k}_\parallel \cdot \mathbf{x}_\parallel\right).
\tag{2}
$$

The power spectra that will be considered in this work are of either the Gaussian form [33]

$$
g(\mathbf{k}_\parallel) = \pi a_1 a_2 \exp\left(-\frac{k_1^2 a_1^2}{4} - \frac{k_2^2 a_2^2}{4}\right),
\tag{3}
$$

where a_i $(i = 1, 2)$ denotes the lateral correlation length for direction i, or the cylindrical form [38]

$$
g(k_\parallel) = \frac{4\pi}{k_+^2 - k_-^2} \left[\theta(k_\parallel - k_-)\theta(k_+ - k_\parallel)\right],
\tag{4}
$$

where $k_\parallel = |\mathbf{k}_\parallel|$, θ denotes the Heaviside unit step function, and $k_\pm$ are wavenumber cutoff parameters, with $k_- < k_+$. The cylindrical form in Eq. (4) is a two-dimensional generalization of the power spectrum used in the experiments where West and O'Donnell confirmed the existence of the enhanced backscattering phenomenon for weakly rough surfaces [21].

3. Scattering Theory

We consider a linearly p- or s-polarized plane wave which is incident on the surface from region 1, with the electric field given by $\mathbf{E}^{(0)}(\mathbf{x};t) = \mathbf{E}^{(0)}(\mathbf{x}|\omega)\exp(-i\omega t)$ where

$$\mathbf{E}^{(0)}(\mathbf{x}|\omega) = \mathscr{E}^{(0)}(\mathbf{k}_\parallel)\exp\left[i\mathbf{k}_\parallel \cdot \mathbf{x}_\parallel - i\alpha_1(k_\parallel)x_3\right], \tag{5a}$$

with

$$\mathscr{E}^{(0)}(\mathbf{k}_\parallel) = -\frac{c}{\omega}\left[\hat{\mathbf{k}}_\parallel\alpha_1(k_\parallel) + \hat{\mathbf{x}}_3 k_\parallel\right]\mathscr{E}_p^{(0)}(\mathbf{k}_\parallel) + \left(\hat{\mathbf{x}}_3 \times \hat{\mathbf{k}}_\parallel\right)\mathscr{E}_s^{(0)}(\mathbf{k}_\parallel), \tag{5b}$$

and

$$\alpha_1(k_\parallel) = \left(\frac{\omega^2}{c^2} - k_\parallel^2\right)^{1/2}, \quad \mathrm{Re}\,\alpha_1 \geq 0, \; \mathrm{Im}\,\alpha_1 \geq 0. \tag{5c}$$

Here, and in the rest of the paper, a caret over a vector indicates a unit vector. The expressions in front of the amplitudes $\mathscr{E}_\alpha^{(0)}(\mathbf{k}_\parallel)$ $(\alpha = p,s)$ in Eq. (5b) correspond to unit polarization vectors for incident light of linear polarization α. Moreover, $\mathbf{k}_\parallel = (k_1, k_2, 0)$ denotes the lateral component of the wave vector $\mathbf{k} = \mathbf{k}_\parallel - \alpha(k_\parallel)\hat{\mathbf{x}}_3$. When the lateral wavenumber satisfies $k_\parallel \leq \omega/c$, as will be assumed here, $\mathbf{k}_\parallel$ is related to the angles of incidence according to

$$\mathbf{k}_\parallel = \frac{\omega}{c}\sin\theta_0\left(\cos\phi_0, \sin\phi_0, 0\right), \tag{6}$$

where c denotes the speed of light in vacuum and θ_0 and ϕ_0 are the polar and azimuthal angles of incidence, respectively (Fig. 1). When writing the field of incidence, $\mathbf{E}^{(0)}(\mathbf{x};t)$, a time harmonic dependence of the form $\exp(-i\omega t)$ was assumed. A similar time dependence will be assumed for all field expressions, but not indicted explicitly.

Above the surface roughness region, i.e., for $x_3 > \max \zeta(\mathbf{x}_\parallel)$, the scattered field can be written as a superposition of *upwards* propagating reflected plane waves:

$$\mathbf{E}^{(s)}(\mathbf{x}|\omega) = \int \frac{d^2q_\parallel}{(2\pi)^2}\mathscr{E}^{(s)}(\mathbf{q}_\parallel) \times \exp\left[i\mathbf{q}_\parallel \cdot \mathbf{x}_\parallel + i\alpha_1(q_\parallel)x_3\right], \tag{7a}$$

where

$$\mathscr{E}^{(s)}(\mathbf{q}_\parallel) = \frac{c}{\omega}\left[\hat{\mathbf{q}}_\parallel\alpha_1(q_\parallel) - \hat{\mathbf{x}}_3 q_\parallel\right]\mathscr{E}_p^{(s)}(\mathbf{q}_\parallel) + \left(\hat{\mathbf{x}}_3 \times \hat{\mathbf{q}}_\parallel\right)\mathscr{E}_s^{(s)}(\mathbf{q}_\parallel). \tag{7b}$$

The integration in Eq. (7a) is over the entire plane, including the evanescent region $q_\parallel > \omega/c$. Therefore, both propagating and evanescent modes are included in $\mathbf{E}^{(s)}(\mathbf{x}|\omega)$.

We will assume that a linear relationship exists between the amplitudes of the incident and the scattered fields, and we write (for $\alpha = p,s$)

$$\mathscr{E}_\alpha^{(s)}(\mathbf{q}_\parallel) = \sum_{\beta=p,s} R_{\alpha\beta}(\mathbf{q}_\parallel|\mathbf{k}_\parallel)\mathscr{E}_\beta^{(0)}(\mathbf{k}_\parallel). \tag{8}$$

Here we have introduced the so-called *scattering amplitude* $R_{\alpha\beta}(\mathbf{q}_{\parallel}|\mathbf{k}_{\parallel})$, which describes how incident β-polarized light characterized by a lateral wave vector $\mathbf{k}_{\parallel}$ is converted by the surface roughness into scattered light of polarization α and lateral wave vector $\mathbf{q}_{\parallel}$. When $q_{\parallel} \leq \omega/c$, the wave vector $\mathbf{q}_{\parallel}$ is related to the angles of scattering (θ_s, ϕ_s) by

$$\mathbf{q}_{\parallel} = \frac{\omega}{c} \sin\theta_s \left(\cos\phi_s, \sin\phi_s, 0\right). \tag{9}$$

Below the surface region, i.e., for $x_3 < \min \zeta(\mathbf{x}_{\parallel})$, the transmitted electric field can be written as

$$\mathbf{E}^{(t)}(\mathbf{x}_{\parallel}|\omega) = \int \frac{\mathrm{d}^2 p_{\parallel}}{(2\pi)^2} \mathscr{E}^{(t)}(\mathbf{p}_{\parallel}) \times \exp\left[i\mathbf{p}_{\parallel} \cdot \mathbf{x}_{\parallel} - i\alpha_2(p_{\parallel})x_3\right] \tag{10a}$$

with

$$\mathscr{E}^{(t)}(\mathbf{p}_{\parallel}) = -\frac{1}{\sqrt{\varepsilon_2(\omega)}} \frac{c}{\omega} \left[\hat{\mathbf{p}}_{\parallel}\alpha_2(p_{\parallel}) + \hat{\mathbf{x}}_3 p_{\parallel}\right] \mathscr{E}^{(t)}_{\mathrm{p}}(\mathbf{p}_{\parallel}) + \left(\hat{\mathbf{x}}_3 \times \hat{\mathbf{p}}_{\parallel}\right) \mathscr{E}^{(t)}_{\mathrm{s}}(\mathbf{p}_{\parallel}). \tag{10b}$$

In writing Eqs. (10) we have introduced wave vectors of the transmitted field $\mathbf{p} = \mathbf{p}_{\parallel} - \alpha_2(p_{\parallel})\hat{\mathbf{x}}_3$, where

$$\alpha_2(p_{\parallel}) = \left[\varepsilon_2(\omega)\frac{\omega^2}{c^2} - p_{\parallel}^2\right]^{1/2}, \quad \mathrm{Re}\,\alpha_2 \geq 0, \ \mathrm{Im}\,\alpha_2 \geq 0. \tag{11}$$

In complete analogy to what was done for reflection, a transmission amplitude $T_{\alpha\beta}(\mathbf{p}_{\parallel}|\mathbf{k}_{\parallel})$ may be defined via the following linear relation between the amplitudes of the incident and transmitted fields ($\alpha = \mathrm{p}, \mathrm{s}$)

$$\mathscr{E}^{(t)}_{\alpha}(\mathbf{p}_{\parallel}) = \sum_{\beta=\mathrm{p},\mathrm{s}} T_{\alpha\beta}(\mathbf{p}_{\parallel}|\mathbf{k}_{\parallel})\mathscr{E}^{(0)}_{\beta}(\mathbf{k}_{\parallel}). \tag{12}$$

Since the form of the electric fields given by Eqs. (5), (7), and (10) apply far away from the surface region, they are referred to as the *asymptotic forms* of the electric field. These equations automatically satisfy the boundary conditions at infinity.

In passing we note that once the incident field has been specified, the scattered and transmitted fields are fully specified outside the surface roughness region if the reflection $[R_{\alpha\beta}(\mathbf{q}_{\parallel}|\mathbf{k}_{\parallel})]$ and transmission $[T_{\alpha\beta}(\mathbf{p}_{\parallel}|\mathbf{k}_{\parallel})]$ amplitudes are known. We will now address how the reflection amplitude can be calculated.

3.1. The Rayleigh Hypothesis

Above the surface, i.e., in the region $x_3 > \max \zeta(\mathbf{x}_{\parallel})$, the total electric field is equal to the sum of the incident and the scattered field, $\mathbf{E}^{(0)}(\mathbf{x}|\omega) + \mathbf{E}^{(s)}(\mathbf{x}|\omega)$. Below the surface, in the region $x_3 < \min \zeta(\mathbf{x}_{\parallel})$, it equals the transmitted field, $\mathbf{E}^{(t)}(\mathbf{x}|\omega)$. In the surface roughness region, $\min \zeta(\mathbf{x}_{\parallel}) \leq x_3 \leq \max \zeta(\mathbf{x}_{\parallel})$, these forms of the total field will not generally be valid. In particular, when we are above the surface but still below its maximum point, i.e., $\zeta(\mathbf{x}_{\parallel}) \leq x_3 < \max \zeta(\mathbf{x}_{\parallel})$, the expression for the scattered field will also have terms containing $\exp\left[i\mathbf{q}_{\parallel} \cdot \mathbf{x}_{\parallel} - i\alpha_1(q_{\parallel})x_3\right]$. Similarly, the transmitted field in the surface region has to contain an additional term similar to Eq. (10a) but with the exponential function replaced by $\exp\left[i\mathbf{q}_{\parallel} \cdot \mathbf{x}_{\parallel} + i\alpha_2(q_{\parallel})x_3\right]$ (and a different amplitude).

If the surface roughness is sufficiently weak, however, the asymptotic form of the fields, Eqs. (5), (7), and (10), can be assumed to be a good approximation to the total electric field in

the surface roughness region. This assumption is known as the *Rayleigh hypothesis* [10,11,17], in honor of Lord Rayleigh, who first used it in his seminal studies of wave scattering from sinusoidal surfaces [10, 11]. For a (one-dimensional) sinusoidal surface, $x_3 = \zeta_0 \sin(\Lambda x_1)$, the criterion for the validity of the Rayleigh hypothesis, and thus equations that can be derived from it (like the reduced Rayleigh equation to be introduced below), is known to be $\zeta_0 \Lambda < 0.448$, independent of the wavelength of the incident light [48, 49]. For a randomly rough surface, however, the absolute limit of validity of this hypothesis is not generally known, though some numerical studies have been devoted to finding the region of validity for random surfaces [50]. Even if no absolute criterion for the validity of the Rayleigh hypothesis for randomly rough surfaces is known, it remains true that it is a small-slope hypothesis. In particular, if the randomly rough surface is characterized by an rms height δ, and a correlation length a (see Sec. 2 and Ref. [19] for details), there seems to be a consensus in the literature on the Rayleigh hypothesis being valid if $\delta/a \ll 1$ [17, 50]. We stress that the validity of the Rayleigh hypothesis does not require the amplitude of the surface roughness to be small, only its slope.

3.2. The Reduced Rayleigh Equations

Under the assumption that the Rayleigh hypothesis is valid, the total electric field in the surface region, $\min \zeta(\mathbf{x}_\parallel) < x_3 < \max \zeta(\mathbf{x}_\parallel)$, can be written in the form given by Eqs. (5), (7) and (10) [with Eqs. (8) and (12)]. Hence, these asymptotic fields can be used to satisfy the usual boundary conditions on the electromagnetic field at the rough surface $x_3 = \zeta(\mathbf{x}_\parallel)$ [51, 52]. In this way, one obtains the so-called Rayleigh equations, a set of coupled inhomogeneous integral equations, which the reflection and transmission amplitudes should satisfy.

In the mid-1980s, it was demonstrated by Brown *et al.* [34] that either the reflection or transmission amplitude could be eliminated from the Rayleigh equations, resulting in an integral equation for the remaining amplitude only. Since this latter integral equation contains only the field above (below) the rough surface, it has been termed the *reduced Rayleigh equation* for reflection (transmission). Subsequently, reduced Rayleigh equations for two-dimensional film geometries, i.e., a film of finite thickness on top of an infinitely thick substrate, where only one interface is rough, was derived by Soubret *et al.* [39, 40] and Leskova [43, 44]. Moreover, reduced Rayleigh equations for reflection from clean, perfectly conducting, two-dimensional randomly rough surfaces [53] and reduced Rayleigh equations for transmission through clean, penetrable two-dimensional surfaces [42] have been derived.

For the purposes of the present study, we limit ourselves to a scattering system consisting of a clean, penetrable, two-dimensional rough surface $x_3 = \zeta(\mathbf{x}_\parallel)$ (Sec. 2). If the scattering amplitudes are organized as the 2×2 matrix

$$\mathbf{R}(\mathbf{q}_\parallel | \mathbf{k}_\parallel) = \begin{pmatrix} R_{pp}(\mathbf{q}_\parallel | \mathbf{k}_\parallel) & R_{ps}(\mathbf{q}_\parallel | \mathbf{k}_\parallel) \\ R_{sp}(\mathbf{q}_\parallel | \mathbf{k}_\parallel) & R_{ss}(\mathbf{q}_\parallel | \mathbf{k}_\parallel) \end{pmatrix}, \tag{13}$$

the reduced Rayleigh equation (for reflection) for this geometry can be written in the form [38–40]

$$\int \frac{\mathrm{d}^2 q_\parallel}{(2\pi)^2} \frac{I\left(\alpha_2(p_\parallel) - \alpha_1(q_\parallel)|\mathbf{p}_\parallel - \mathbf{q}_\parallel\right)}{\alpha_2(p_\parallel) - \alpha_1(q_\parallel)} \mathbf{M}^+(\mathbf{p}_\parallel | \mathbf{q}_\parallel) \mathbf{R}(\mathbf{q}_\parallel | \mathbf{k}_\parallel)$$
$$= -\frac{I\left(\alpha_2(p_\parallel) + \alpha_1(k_\parallel)|\mathbf{p}_\parallel - \mathbf{k}_\parallel\right)}{\alpha_2(p_\parallel) + \alpha_1(k_\parallel)} \mathbf{M}^-(\mathbf{p}_\parallel | \mathbf{k}_\parallel), \tag{14a}$$

where

$$I(\gamma | \mathbf{Q}_\parallel) = \int \mathrm{d}^2 x_\parallel \exp\left[-\mathrm{i}\gamma\zeta(\mathbf{x}_\parallel)\right] \exp\left(-\mathrm{i}\mathbf{Q}_\parallel \cdot \mathbf{x}_\parallel\right), \tag{14b}$$

and

$$\mathbf{M}^{\pm}(\mathbf{p}_{\parallel}|\mathbf{q}_{\parallel}) = \begin{pmatrix} p_{\parallel}q_{\parallel} \pm \alpha_2(p_{\parallel})\hat{\mathbf{p}}_{\parallel} \cdot \hat{\mathbf{q}}_{\parallel}\alpha_1(q_{\parallel}) & -\frac{\omega}{c}\alpha_2(p_{\parallel})\left[\hat{\mathbf{p}}_{\parallel} \times \hat{\mathbf{q}}_{\parallel}\right]_3 \\ \pm\frac{\omega}{c}\left[\hat{\mathbf{p}}_{\parallel} \times \hat{\mathbf{q}}_{\parallel}\right]_3\alpha_1(q_{\parallel}) & \frac{\omega^2}{c^2}\hat{\mathbf{p}}_{\parallel} \cdot \hat{\mathbf{q}}_{\parallel} \end{pmatrix}, \tag{14c}$$

where the integrals in Eqs. (14a) and (14b) are over the entire $\mathbf{q}_{\parallel}$-plane and $\mathbf{x}_{\parallel}$-plane, respectively. Reduced Rayleigh equations for transmission, or film geometries with only one rough interface, will have a similar structure to Eq. (14) [39, 40], and can be solved in a completely analogous fashion.

It should be mentioned that the reduced Rayleigh equation can serve as a starting point for most, if not all, perturbation theoretical approaches to the study of scattering from rough surfaces [19]. For example, McGurn and Maradudin studied the scattering of light from two-dimensional rough surfaces based on the reduced Rayleigh equation, going to fourth order in the expansion in the surface profile function, and demonstrating the presence of enhanced backscattering [38].

3.3. Mean Differential Reflection Coefficient

The solution of the reduced Rayleigh equation determines the scattering amplitudes $R_{\alpha\beta}(\mathbf{q}_{\parallel}|\mathbf{k}_{\parallel})$. While this quantity completely specifies the total field in the region above the surface, it is not directly measurable in experiments. A more useful quantity is the mean differential reflection coefficient (DRC), which is defined as the time-averaged fraction of the incident power scattered into the solid angle $d\Omega_s$ about the scattering direction $\mathbf{q}$. The mean DRC is defined as [38]

$$\left\langle \frac{\partial R_{\alpha\beta}}{\partial \Omega_s} \right\rangle = \frac{1}{L^2}\frac{\omega^2}{4\pi^2 c^2}\frac{\cos^2\theta_s}{\cos\theta_0}\left\langle \left|R_{\alpha\beta}(\mathbf{q}_{\parallel}|\mathbf{k}_{\parallel})\right|^2\right\rangle, \tag{15}$$

where L^2 is the area of the plane $x_3 = 0$ covered by the rough surface. In this work, we are mainly interested in diffuse (incoherent) scattering. Since we consider weakly rough surfaces, the specular (coherent) scattering will dominate, and it will be convenient to separate the mean DRC into its coherent and incoherent parts. By coherent scattering, we mean the part of the scattered light which does not cancel when the ensemble average of $R_{\alpha\beta}$ is taken, i.e., the part where the scattered field is in phase between surface realizations. Conversely, the incoherent part is the part which cancels in the ensemble average. The component of the mean DRC from incoherent scattering is [38]

$$\left\langle \frac{\partial R_{\alpha\beta}}{\partial \Omega_s} \right\rangle_{\text{incoh}} = \frac{1}{L^2}\frac{\omega^2}{4\pi^2 c^2}\frac{\cos^2\theta_s}{\cos\theta_0}\left[\left\langle \left|R_{\alpha\beta}(\mathbf{q}_{\parallel}|\mathbf{k}_{\parallel})\right|^2\right\rangle - \left|\left\langle R_{\alpha\beta}(\mathbf{q}_{\parallel}|\mathbf{k}_{\parallel})\right\rangle\right|^2\right]. \tag{16}$$

The contribution to the mean DRC from the coherently scattered light is given by the difference between Eqs. (15) and (16).

3.4. Conservation of Energy

As a way to check the accuracy of our results, it is useful to investigate energy conservation. If we consider a metallic substrate with no absorption, the reflected power should be equal to the incident power. The fraction of the incident light of polarization β which is scattered into polarization α is given by the integral of the corresponding mean DRC over the upper hemisphere:

$$\mathscr{U}_{\alpha\beta} = \int d\Omega_s \left\langle \frac{\partial R_{\alpha\beta}}{\partial \Omega_s} \right\rangle. \tag{17}$$

For a non-absorbing metal, if we send in light of polarization β, we should have $\sum_\alpha \mathscr{U}_{\alpha\beta} = 1$, if energy is conserved. While the conservation of energy is useful as a relatively simple test, it is important to note that it is a necessary, but not sufficient, condition for correct results.

4. Numerical Solution of the Reduced Rayleigh Equation

The starting point for the numerical solution of the reduced Rayleigh equation is a discretely sampled surface, from which we wish to calculate the reflection. We will limit our discussion to quadratic surfaces of size $L \times L$, sampled on a quadratic grid of $N_x \times N_x$ points with a grid constant

$$\Delta x = \frac{L}{N_x}. \tag{18}$$

In this paper, we will present results for numerically generated random surfaces. These are generated by what is known as the Fourier filtering method. Briefly, it consists of generating uncorrelated random numbers with a Gaussian distribution, transforming them to Fourier space, filtering them with the square root of the surface power spectrum $g(\mathbf{k}_\parallel)$, and transforming them back to real space. The interested reader is referred to, e.g., Refs. [25, 33].

The next step towards the numerical solution of the reduced Rayleigh equation is the evaluation of the integrals $I(\gamma|\mathbf{Q}_\parallel)$ defined in Eq. (14b). These integrals are so-called Fourier integrals and care should be taken when evaluating them due to the oscillating integrands [54]. Using direct numerical integration routines for their evaluation will typically result in inaccurate results. Instead, a (fast) Fourier transform technique with end point corrections may be adapted for their evaluation, and the details of the method is outlined in Ref. [54]. However, these calculations are time consuming, since $I(\gamma|\mathbf{Q}_\parallel)$ must be evaluated for all values of the arguments $\gamma = \alpha_1(p_\parallel) - \alpha_2(q_\parallel)$ and $\gamma = \alpha_1(p_\parallel) - \alpha_2(\mathbf{k}_\parallel)$ [1].

Instead, a computationally more efficient way of evaluating $I(\gamma|\mathbf{Q}_\parallel)$ is to assume that the exponential function $\exp\left[-i\gamma\zeta(\mathbf{x}_\parallel)\right]$, present in the definition of $I(\gamma|\mathbf{Q}_\parallel)$, can be expanded in powers of the surface profile function, and then evaluating the resulting expression term-by-term by Fourier transform. This gives

$$I(\gamma|\mathbf{Q}_\parallel) = \sum_{n=0}^{\infty} \frac{(-i\gamma)^n}{n!} \hat{\zeta}^{(n)}(\mathbf{Q}_\parallel), \tag{19a}$$

where $\hat{\zeta}^{(n)}(\mathbf{Q}_\parallel)$ denotes the Fourier transform of the nth power of the profile function, i.e.,

$$\hat{\zeta}^{(n)}(\mathbf{Q}_\parallel) = \int d^2x_\parallel \, \zeta^n(\mathbf{x}_\parallel) \exp\left(-i\mathbf{Q}_\parallel \cdot \mathbf{x}_\parallel\right). \tag{19b}$$

In practice, the sum in Eq. (19a) will be truncated at a finite value $n = J$, and the Fourier transforms are calculated using a fast Fourier transform (FFT) algorithm.

The advantage of using Eqs. (19) for calculating $I(\gamma|\mathbf{Q}_\parallel)$, rather than the method of Ref. [54], is that the Fourier transform of each power of $\zeta(\mathbf{x}_\parallel)$ can be performed once, and changing the argument γ in $I(\gamma|\mathbf{Q}_\parallel)$ will not require additional Fourier transforms to be evaluated. This results in a significant reduction in computational time. The same method has previously been applied successfully to the numerical solution of the one-dimensional reduced Rayleigh equation [35–37].

It should be noted that the Taylor expansion used to arrive at Eq. (19) requires that $\left|\gamma\zeta(\mathbf{x}_\parallel)\right| \ll 1$ to converge reasonably fast, putting additional constraints on the amplitude of

---

[1]For the calculations used to generate the results presented in this paper, this would amount to evaluating $I(\gamma|\mathbf{Q}_\parallel)$ on the order of 10^{10} times.

the surface roughness which may be more restrictive than those introduced by the Rayleigh hypothesis. Hence, surfaces exist for which the Rayleigh hypothesis is satisfied, but the above expansion method will not converge, and the more time-consuming approach of Ref. [54] will have to be applied.

Next, we need to truncate and discretize the integral over $\mathbf{q}_\parallel$ in Eq. (14a). We discretize $\mathbf{q}_\parallel$ on a grid of equidistant points, with spacing Δq, such that

$$\mathbf{q}_{\parallel ij} = \left(-\frac{\mathscr{Q}}{2} + i\Delta q, -\frac{\mathscr{Q}}{2} + j\Delta q, 0 \right), \tag{20}$$

where $i, j = 0, 1, 2, \ldots, N_q - 1$, and $\mathscr{Q} = \Delta q(N_q - 1)$. Here, N_q denotes the number of points along each direction of the grid. The length of the vector $\mathbf{q}_{\parallel ij}$ we denote by $q_{\parallel ij} = |\mathbf{q}_{\parallel ij}|$. Additionally, we limit the integration over $\mathbf{q}_\parallel$ to the region $q_\parallel \leq \mathscr{Q}/2$. The choice of a circular integration domain reduces the computational cost, and will be discussed in more detail in Sec. 6. Converting the integral into a sum by using a two-dimensional version of the standard mid-point quadrature scheme, we get the equation:

$$\left(\frac{\Delta q}{2\pi}\right)^2 \sum_{q_{\parallel ij} \leq \mathscr{Q}/2} \frac{I\left(\alpha_2(p_\parallel) - \alpha_1(q_{\parallel ij})|\mathbf{p}_\parallel - \mathbf{q}_{\parallel ij}\right)}{\alpha_2(p_\parallel) - \alpha_1(q_{\parallel ij})} \mathbf{M}^+(\mathbf{p}_\parallel | \mathbf{q}_{\parallel ij}) \mathbf{R}(\mathbf{q}_{\parallel ij} | \mathbf{k}_\parallel) =$$
$$-\frac{I\left(\alpha_2(p_\parallel) + \alpha_1(k_\parallel)|\mathbf{p}_\parallel - \mathbf{k}_\parallel\right)}{\alpha_2(p_\parallel) + \alpha_1(k_\parallel)} \mathbf{M}^-(\mathbf{p}_\parallel | \mathbf{k}_\parallel). \tag{21}$$

Here, the sum is to be taken over all $\mathbf{q}_{\parallel ij}$ such that $q_{\parallel ij} \leq \mathscr{Q}/2$, where $q_{\parallel ij} = |\mathbf{q}_{\parallel ij}|$. This sum yields a matrix equation where the unknowns are the four components of $\mathbf{R}(\mathbf{q}_{\parallel ij} | \mathbf{k}_\parallel)$. It is evident from Eq. (8) that if we consider incident light of either p or s polarization, we need only calculate two of the components of the scattering amplitude to fully specify the reflected field. Hence, we solve separately for either p-polarized incident light, i.e., R_{pp} and R_{sp}, or s-polarized incident light, i.e., R_{ss} and R_{ps}. In either case, we have twice as many unknowns as the number of values of $\mathbf{q}_{\parallel ij}$ included in the sum in Eq. (21). Note that the left hand side of the equation system is the same for both incident polarizations, and will also remain the same for all angles of incidence, as $\mathbf{k}_\parallel$ only enters at the right hand side of Eq. (21).

In order to solve for all unknowns, we need to discretize $\mathbf{p}_\parallel$ as well, to obtain a closed set of linear equations. Using the same grid for $\mathbf{p}_\parallel$ as for $\mathbf{q}_\parallel$ will give us the necessary number of equations, as Eq.(21) yields two equations for each value of $\mathbf{p}_\parallel$. Since we integrate over a circular $\mathbf{q}_\parallel$ domain, with $\mathbf{q}_\parallel$ discretized on a quadratic grid, the exact number of values of $\mathbf{q}_{\parallel ij}$ will depend on the particular values of $\mathscr{Q}$ and N_q, but will be approximately $(\pi/4)N_q^2$.

In order to take advantage of the method for calculating $I(\gamma|\mathbf{Q}_\parallel)$ described by Eq. (19), it is essential that all possible values of $\mathbf{p}_\parallel - \mathbf{q}_\parallel$ and $\mathbf{p}_\parallel - \mathbf{k}_\parallel$ [see Eq. (21)] fall on the grid of wave vectors $\mathbf{Q}_\parallel$ resolved by the Fourier transform of the surface profile we used in that calculation. First, we note that when $\mathbf{p}_\parallel$ and $\mathbf{q}_\parallel$ are discretized on the same quadratic grid, the number of possible values for each component of $\mathbf{p}_\parallel - \mathbf{q}_\parallel$ will always be an odd number, $2N_q - 1$, where N_q is the number of possible values for each component of $\mathbf{p}_\parallel$ and $\mathbf{q}_\parallel$. Thus, by choosing N_q such that $2N_q - 1$ equals the number of elements along each axis of the FFT of the surface profile we used to calculate the integrals in Eq. (19b), we ensure that the required number of

points is resolved by the FFT [2]. Hence, we choose

$$N_q = \left\lfloor \frac{N_x + 2}{2} \right\rfloor, \tag{22}$$

where $\lfloor x \rfloor$ is the floor function of x, which is equal to the largest integer less than or equal to x.

Next, we let Δq equal the resolution of the FFT [54], i.e.,

$$\Delta q = \frac{2\pi}{L} \tag{23}$$

and we let $\mathcal{Q}$ be equal to the highest wavenumber resolved by the FFT [54],

$$\mathcal{Q} = \Delta q \lfloor N_x/2 \rfloor. \tag{24}$$

In the end, we get the equation

$$\left(\frac{\Delta q}{2\pi}\right)^2 \sum_{\left|\mathbf{q}_{\parallel ij}\right| \leq \mathcal{Q}/2} \frac{I\left(\alpha_2(p_{\parallel kl}) - \alpha_1(q_{\parallel ij}) | \mathbf{p}_{\parallel kl} - \mathbf{q}_{\parallel ij}\right)}{\alpha_2(p_{\parallel kl}) - \alpha_1(q_{\parallel ij})} \mathbf{M}^+(\mathbf{p}_{\parallel kl}|\mathbf{q}_{\parallel ij})\mathbf{R}(\mathbf{q}_{\parallel ij}|\mathbf{k}_{\parallel mn})$$

$$= -\frac{I\left(\alpha_2(p_{\parallel kl}) + \alpha_1(k_{\parallel mn}) | \mathbf{p}_{\parallel kl} - \mathbf{k}_{\parallel mn}\right)}{\alpha_2(p_{\parallel kl}) + \alpha_1(k_{\parallel mn})} \mathbf{M}^-(\mathbf{p}_{\parallel kl}|\mathbf{k}_{\parallel mn}), \tag{25}$$

where $\mathbf{q}_{\parallel ij}$, as well as $\mathbf{p}_{\parallel kl}$ and $\mathbf{k}_{\parallel mn}$, are defined on the grid given by Eq. (20), with $i, j, k, l, m, n = 0, 1, 2, \ldots, N_q - 1$, and where N_q, Δq and $\mathcal{Q}$ are given by Eqs. (22), (23) and (24), respectively.

Evaluating Eq. (25) for all values of $\mathbf{p}_{\parallel kl}$ satisfying $p_{\parallel kl} \leq \mathcal{Q}/2$, and assuming one value of $\mathbf{k}_{\parallel mn}$, such that $k_{\parallel mn} < \omega/c$, and one incident polarization β, results in a *closed* system of linear equations in $R_{\alpha\beta}(\mathbf{q}_{\parallel ij}|\mathbf{k}_{\parallel mn})$ where $\alpha = \mathrm{p}, \mathrm{s}$. Repeating the procedure for both incident polarizations allows us to obtain all four components of $\mathbf{R}(\mathbf{q}_{\parallel ij}|\mathbf{k}_{\parallel mn})$.

With the reflection amplitudes $R_{\alpha\beta}(\mathbf{q}_{\parallel ij}|\mathbf{k}_{\parallel mn})$ available, the contribution to the mean differential reflection coefficient from the light that has been scattered incoherently is obtained from Eq. (16) after averaging over an ensemble of surface realizations.

In passing we note that to avoid loss of numerical precision by operating on numbers with widely different orders of magnitude, we have rescaled all quantities in our problem to dimensionless numbers. When considering an incoming wave of wavelength λ, angular frequency ω, and wave vector $\mathbf{k}$, we have chosen to rescale all lengths in our problem by multiplying with ω/c, and all wavenumbers by multiplying with c/ω, effectively measuring all lengths in units of $\lambda/2\pi$, and the magnitude of wave vectors in units of ω/c.

5. Results

To demonstrate the use of the formalism for solving the reduced Rayleigh equation, the first set of calculations we carried out was for two-dimensional randomly rough silver surfaces. The surface roughness was characterized by an rms height of $\delta = 0.025\lambda$ and an isotropic Gaussian power spectrum [Eq. (3)] of correlation lengths $a_1 = a_2 = 0.25\lambda$. In Figs. 2(a) and 3(a) we present simulation results for the contribution to the mean differential reflection coefficients

---

[2]Note that since the FFT always resolves the zero frequency, and the FFT of a purely real signal is symmetric about the zero frequency under complex conjugation, it is always possible to calculate an odd number of elements along each axis of the FFT
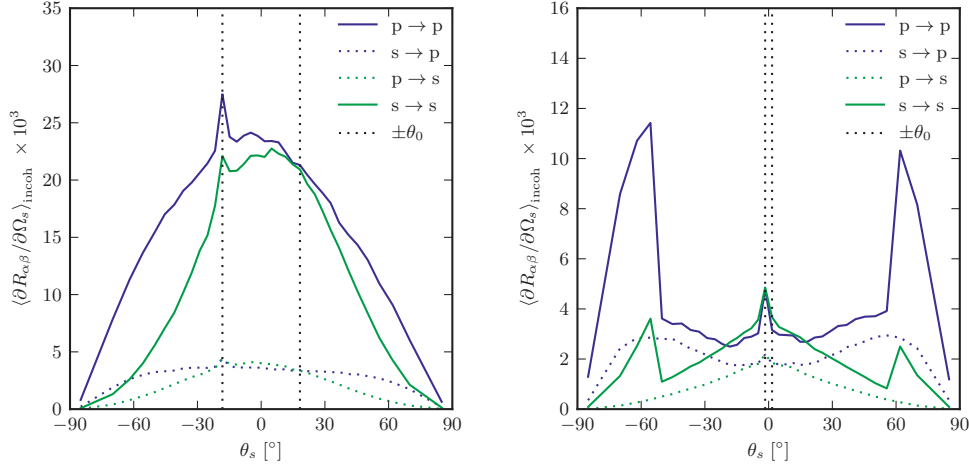
(a) Results averaged over 14,200 randomly rough silver surface realizations. The wavelength (in vacuum) of the incident light was $\lambda = 457.9$ nm, and the dielectric function of silver at this wavelength is $\varepsilon_2 = -7.5 + 0.24i$. The surface power spectrum was Gaussian (Eq. (3)), with correlation lengths $a_1 = a_2 = 0.25\lambda$ and rms height $\delta = 0.025\lambda$. The angle of incidence was $\theta_0 = 18.24°$

(b) Results averaged over 7,000 surface realizations with dielectric constant $\varepsilon_2 = -16 + 1.088i$, which corresponds to silver at $\lambda = 632.8$ nm. The surface power spectrum was of the cylindrical type (Eq. (4))), with $k_- = 0.82\omega/c$, $k_+ = 1.97\omega/c$, and rms roughness $\delta = 0.025\lambda$. The angles of incidence were $\theta_0 = 1.6°$ and $\phi_0 = 45°$.

Fig. 2: Incoherent part of the mean differential reflection coefficient (Eq. (16)), showing only the in-plane scattering as a function of outgoing lateral wave vector. In both cases, the surface realizations covered an area $L \times L$, where $L = 25\lambda$, and the surface was discretized on a grid of 319×319 points. The position of the specular peak (not present in the incoherent part) and the enhanced backscattering peak are indicated by the vertical dashed lines.

from light of wavelength (in vacuum) $\lambda = 457.9$ nm that was scattered incoherently from a rough silver surface of size $25\lambda \times 25\lambda$, discretized into 319×319 points. The dielectric function of silver at this wavelength is $\varepsilon_2 = -7.5 + 0.24i$, and the angles of incidence were $\theta_0 = 18.24°$ and $\phi_0 = 45°$.

Figure 2(a) shows the in-plane scattering for this system. The enhanced backscattering peak, a multiple scattering phenomenon, is clearly visible, and is as expected strongest in $p \rightarrow p$ scattering, since p-polarized light has a stronger coupling to surface plasmon polaritons [19]. Figure 3(a) shows the full angular distribution of the mean DRC for the same system. In Figs. 3(a)(a)–(c) and Figs. 3(a)(d)–(e) the incident light was p- and s-polarized, respectively. Figures 3(a)(c) and 3(a)(f) show scattering into s-polarization, Figs. 3(a)(b) and 3(a)(e) show scattering into p-polarization and in Figs. 3(a)(a) and 3(a)(d) the polarization of the scatted light was not recorded. In particular from Fig. 3(a)(b), we observe that the enhancement features seen in Fig. 2(a) at angular position $\theta_s = -\theta_0$, are indeed enhancements in a well-defined direction corresponding to that of retro-reflection, and not some intensity ridge structure about this direction (as has been seen for other scattering systems [45]). Moreover, the structures of the angular distribution of the intensity of the scattered light depicted in Fig. 3(a) are consistent with what was found by recent studies by using other numerical methods [45,46]. The results presented in Figs. 2(a) and 3(a) were obtained by averaging the DRC over an ensemble consisting of 14,200 surface realizations.

A test of energy conservation was performed by simulating the scattering of light from a non-absorbing silver surface (Im $\varepsilon_2 = 0$) with otherwise the same parameters as those used to obtain
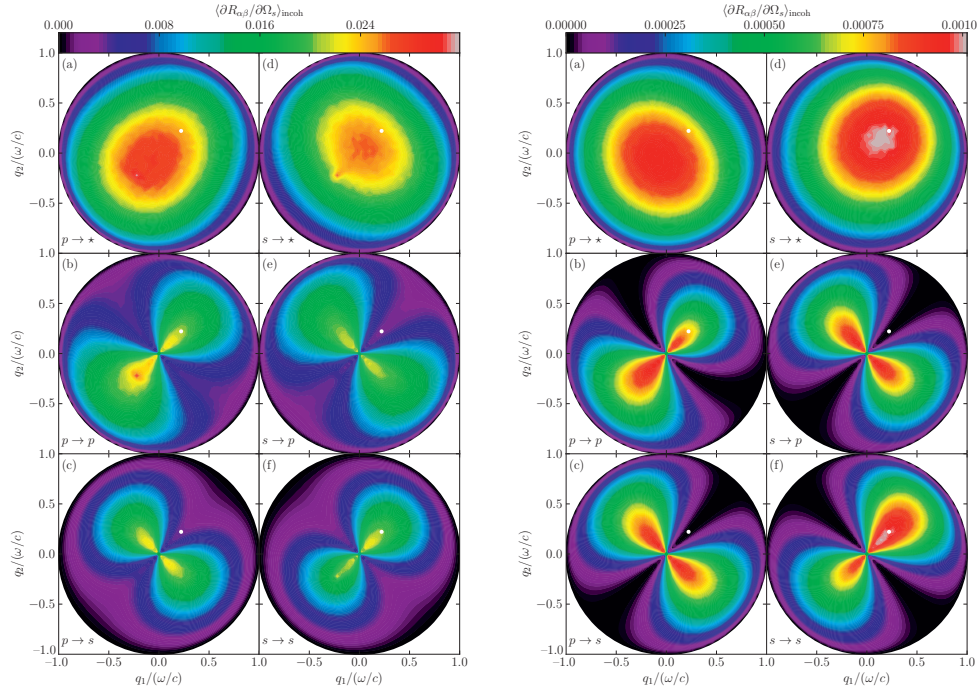
(a) All parameters are the same as in Fig. 2(a).

(b) The same as in Fig. 3(a), except that $\varepsilon_2 = 2.64$, and the results are averaged over 21,800 randomly rough surfaces.

Fig. 3: Incoherent part of the mean differential reflection coefficient (Eq. (16)), showing the full angular distribution as a function of outgoing lateral wave vector. The specular position is indicated by the white dots.

the results of Figs. 2(a) and 3(a). For this scattering system we found $|\mathscr{U} - 1| \le 0.0003$, i.e., energy is conserved to within 0.03%, something that testifies to the accuracy of the approach and a satisfactory discretization.

As a further test, we studied the scattering from a set of (absorbing) silver surfaces with the same parameters used to obtain Figs. 2(a) and 3(a), except that the rms roughness δ was varied between 0 and 0.045λ, while the correlation lengths were held constant at $a_1 = a_2 = 0.25\lambda \equiv a$. For the purpose of comparison, we also performed simulations for a similar set of surfaces but assuming no absorption, i.e., $\varepsilon_2 = -7.5$. The results of these tests are presented in Fig. 4.

The reduced Rayleigh equation is only valid for surfaces of small slopes [17]. We have found that at least for the parameters used in obtaining Fig. 4, our code gives good results for an rms roughness to correlation-length ratio $\delta/a \lesssim 0.12$, as judged by energy conservation. For larger values of δ/a, the results look qualitatively much the same, but the ratio of reflected to incident power starts to become nonphysical (increasing past 1), as seen in Fig. 4. It is noted that decreasing the sampling interval Δq, with $\mathscr{Q}$ unchanged, did not change this conclusion in any significant way, indicating that the observed lack of energy conservation was not caused by poor resolution in discretizing the integral over $\mathbf{q}_\parallel$.

The next set of calculations we performed was for a dielectric substrate characterized by $\varepsilon_2 = 2.64$. Otherwise, all roughness parameters were the same as for the silver surface used to produce Figs. 2(a) and 3(a). The mean differential reflection coefficient for light scattered inco-
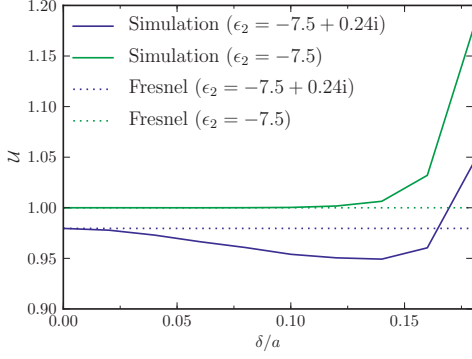
Fig. 4: Ratio of reflected power to incident power, $\mathcal{U}$, as a function of ratio between rms roughness and correlation length, δ/a. Surface size and resolution were the same as for Fig. 2(a), and the surface was randomly rough with a Gaussian power spectrum, correlation length was kept constant at $a = a_1 = a_2 = 0.25\lambda$, while the rms roughness δ was varied from 0.0 to 0.045λ. The Fresnel coefficients have been included for comparison.
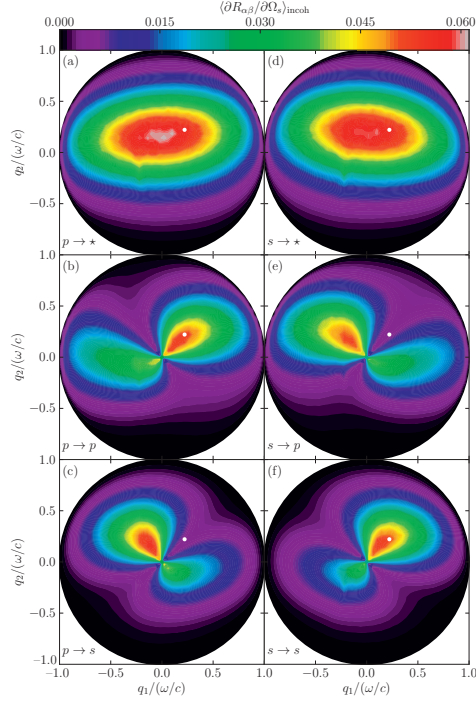

Fig. 5: The same as in Fig. 3(a), except the correlation length of the Gaussian roughness, which is $a_1 = 0.25\lambda$ in the x_1 direction and $a_2 = 0.75\lambda$ in the x_2 direction, and the results are the average of 6,800 surface realizations.

herently by the rough dielectric surface is presented in Fig. 3(b). By comparing these results to those presented in Fig. 3(a), we notice that the dielectric reflects less than the silver (the figures show only the incoherent scattering, but the same holds for the coherent part), which is as expected. The ratio of reflected to incident power for these data was $\mathcal{U} = 0.0467$ for p-polarized light at an angle of incidence of $\theta_0 = 18.24°$. Moreover, from Fig. 3(b) we also notice the absence of the enhanced backscattering peak, which is also to be expected since this phenomenon (for a weakly rough surface) requires the excitation of surface guided modes [19]. Note that for a transparent substrate, it is not possible to verify the conservation of energy without also calculating the transmitted field. Therefore, energy conservation has not been tested for the dielectric substrate geometry.

So far, we have exclusively considered surfaces with statistically isotropic roughness. For the results presented in Fig. 5, we simulated the light scattering from a silver surface of the same parameters as those assumed in producing the results of Figs. 2(a) and 3(a), except that now the surface power spectrum was anisotropic, with correlation lengths $a_1 = 0.25\lambda$ in the x_1 direction and $a_2 = 0.75\lambda$ in the x_2 direction and an rms roughness of $\delta = 0.025\lambda$. Figure 5 shows the incoherent part of the mean DRC averaged over 6,800 surface realizations. In this case, there is more diffuse scattering along the x_1 direction than the x_2 direction, which is to be expected, since a shorter correlation length means the height of the surface changes more rapidly when moving along the surface in this direction. The interested reader is encouraged to

consult Ref. [33] for a more detailed study of light scattering from anisotropic surfaces.

Finally, for the results presented in Fig. 2(b), we have simulated the scattering of light from a surface of size $25\lambda \times 25\lambda$, discretized into 319×319 points, with $\varepsilon_2 = -16 + 1.088i$, corresponding to silver at a wavelength $\lambda = 632.8$ nm. The surface power spectrum was cylindrical [see Eq. (4)], with $k_- = 0.82\omega/c$, $k_+ = 1.97\omega/c$ and rms roughness $\delta = 0.025\lambda$, and the angles of incidence were $(\theta_0, \phi_0) = (1.6°, 45°)$. Figure 2(b) shows the in-plane, incoherent part of the mean differential reflection coefficient averaged over 7,000 surface realizations.

From perturbation theory [17,19], we know that for an incident wave of lateral wave vector $\mathbf{k}_\parallel$ to be scattered *via single scattering* into a reflected wave of lateral wave vector $\mathbf{q}_\parallel$, we must have $g(\mathbf{q}_\parallel - \mathbf{k}_\parallel) > 0$, where $g(\mathbf{k}_\parallel)$ is the surface power spectrum [Eq. (2)]. Since the power spectrum in this case is zero for $|\mathbf{q}_\parallel - \mathbf{k}_\parallel| < 0.82\omega/c$, we have no contribution from single scattering in the angular interval from $\theta_s = -53.5°$ to $\theta_s = 56.7°$ (for the angles of incidence assumed here). The enhanced backscattering peak, which is due to multiple scattering processes, is clearly visible in Fig. 2(b) (at $\theta_s = -\theta_0$) partly because it is not masked by a strong single scattering contribution.

5.1. Comparison with surface integral method

As a way to test our results, we have compared simulation data obtained by the method presented in this paper to results calculated by the surface integral method described in Ref. [33]. In both cases, we considered randomly rough silver surfaces at an incident wavelength of $\lambda = 632.8$ nm, corresponding to a dielectric constant of $\varepsilon_2 = -16 + 1.088i$. The surface roughness was characterized by an isotropic Gaussian powerspectrum, a correlation length of $a = 0.25\lambda$ and rms-roughness $\delta = 0.025\lambda$. In the reduced Rayleigh simulations, we used a quadratic surface of edges $L = 25\lambda$, discretized to 319×319 points. In the surface integral simulations, the quadratic surface had edges $L = 20\lambda$, and was discretized on a grid of 160×160 points. Additionally, for the surface integral method an impedance boundary condition (See Ref. [33] for details) and a finite size beam of full width 8λ was used. The reason for the differences in parameters is the larger memory requirements of the surface integral method.

The results are presented in Figs. 6(a) (p-polarized incident light) and 6(b) (s-polarized incident light), where the data from the reduced Rayleigh simulations are indicated by the solid lines, and the data for the surface integral method by the dashed lines. The results of Figs. 6(a) and 6(b) show that rather consistent results are obtained by the reduced Rayleigh method and the surface integral method at least for the scattering geometries studied here. Moreover, the total reflected energy obtained from the two methods were equal to three significant digits. However, we find that the surface integral method gives slightly less diffuse scattering that what is obtained by the reduced Rayleigh method. We speculate that this is caused by the more limited resolution used in the surface integral simulations.

To increase the resolution in the surface integral simulations to a surface of 319×319 points would have required significantly more memory than the about 12GB required to obtain the reduced Rayleigh simulation results presented here. Performing similar simulations by the surface integral method will require 308GB which is a 25 times increase compared to the requirements of reduced Rayleigh method [33]. Furthermore, if fully rigorous surface integral simulations should be performed, *i.e.* without imposing the impedance boundary conditions, the corresponding memory footprint of the simulations would be 1,234GB. These figures demonstrate some of the significant practical advantages that the reduced Rayleigh equation method has over the more general surface integral method.

(a) Results for p polarized incident light.   (b) Results for s polarized incident light.
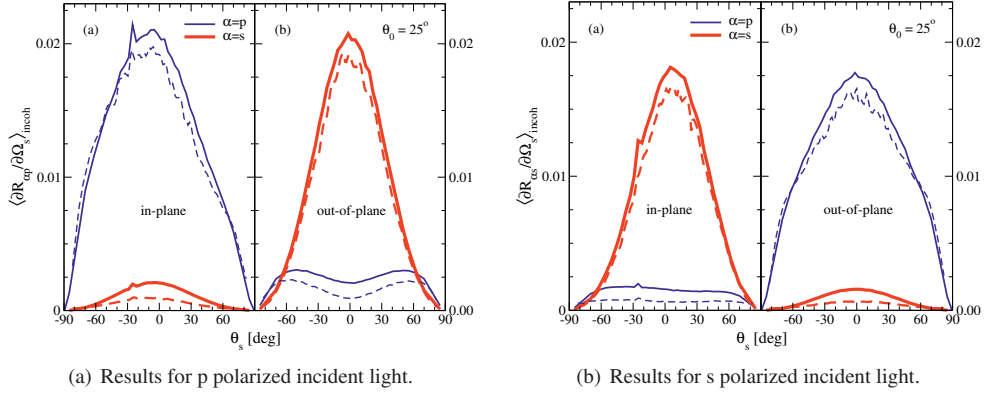
Fig. 6: Comparison of the incoherent part of the mean differential reflection coefficient (Eq. (16)), showing in-plane and out-of-plane scattering as function of scattering angle as calculated by the reduced Rayleigh method (solid lines) and the surface integral method of Ref. [33] (dashed lines). The angle of incidence was $\theta_0 = 25°$. The surface roughness was Gaussian, with a correlation length of $a = 0.25\lambda$ and rms-roughness $\delta = 0.025\lambda$. For the RRE simulations, a quadratic surface of edges $L = 25\lambda$, discretized to 319×319 points was used. In the surface integral simulations, the quadratic surface had edges $L = 20\lambda$, and 160×160 points. In both cases, a dielectric constant of $\varepsilon_2 = -16 + 1.088i$ was used. This corresponds to silver, for an incident wavelength of $\lambda = 632.8$ nm.

5.2. Comparison to experimental data

As a further consistency check of our results, we have compared our simulations to experimental scattering data from well characterized surfaces previously published by Alcalá et al. [55]. The two surfaces in question were prepared on gold substrates. The first surface, sample 0061 in Ref. [55], had roughness characterized by a Gaussian powerspectrum of correlation length $a = 19$ μm and rms-roughness of $\delta = 0.5$ μm. The second surface, sample 7047, was characterized by Gaussian powerspectrum with correlation length $a = 9.5$ μm and rms-roughness of $\delta = 1.6$ μm. The wavelength of the incident light was $\lambda = 10.6$ μm, for which the dielectric constant of gold is $\varepsilon_2 = -2489.77 + 2817.36i$, and the polar angle of incidence was $\theta_0 = 30°$.

In our simulations, we used the same roughness parameters as those used in the experiments by Alcalá et al., and we considered quadratic surface realizations of edges $L = 30\lambda$, discretized to 319×319 points. However, in performing the simulations, we used an approximation where the substrate was treated as a perfect electric conductor. This approximation is expected to be valid as the skin depth of gold at the wavelength of the incident light is about 34 nm [55].

The advantage of assuming that the substrate is a perfect conductor is that the corresponding reduced Rayleigh equations will then not explicitly contain ε_2 [53]. If a large but finite value for ε_2 is used, the series expansion used to calculate the integral $I(\gamma|Q)$ [see Eqs. (14b) and (19a)] will be numerically unstable.

In Figs. 7(a) (sample 0061) and 7(b) (sample 7047) we compare experimental scattering data to the corresponding simulation results obtained by the method just described. We observe from these figures generally good agreement for both polarizations of the incident light. The agreement between the measured and simulated data is best for s polarization. For p polarization, there seems to be a slight shift of the simulated data compared to what was observed experimentally. It is speculated that this may be caused by an alignment problem in the experiment since the specular peak is not located at $\theta_s = \theta_0$ in the measurements of p to p scattering.
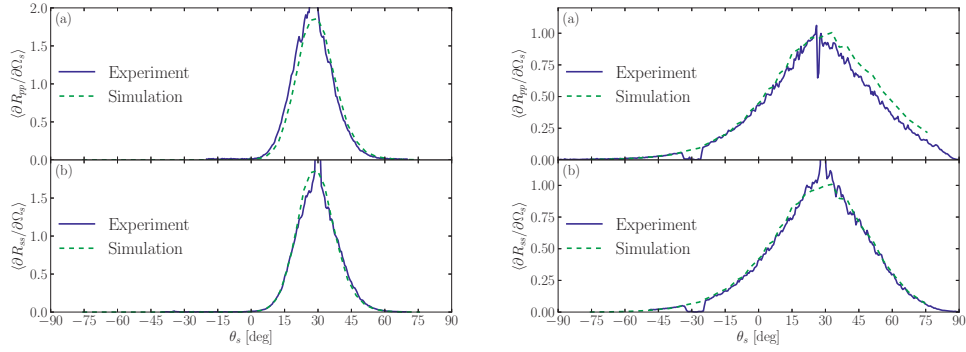
(a) Experimental data obtained by Alcalá et al. [55] (sample 0061). The results shown are for (a) p to p scattering and, (b) s to s scattering.

(b) Experimental data obtained by Alcalá et al. [55] (sample 7047). The results shown are for (a) p to p scattering and, (b) s to s scattering.

Fig. 7: The mean differential reflection coefficient, showing in-plane scattering as function of the scattering angle θ_s. Experimental data obtained by Alcalá et al. [55] for polar angle of incidence $\theta_0 = 30°$, are shown by the blue solid lines, and our simulation results by the green dashed lines. For the simulation results, only the incoherent component of the mean differential reflection coefficients are shown. It is noted that the slight shift of the simulations data relative the measured data for p to p scattering (Fig. 7(b)(a)) is most likely caused by the angle of incidence used in the experiments being somewhat smaller than $\theta_0 = 30°$ which was assumed in the simulations.

6. Discussion

A challenge faced when performing a direct numerical solution of the reduced Rayleigh equation for the scattering of light from two-dimensional rough surfaces is the numerical complexity. In this section, we discuss some of these issues in detail.

6.1. Memory Requirements

Part of the challenge of a purely numerical solution of the reduced Rayleigh equation by the formalism introduced by this study, is that it requires a relatively large amount of memory. With approximately $\mathcal{N} = (\pi/4)N_q^2$ possible values for $\mathbf{q}_\parallel$, the coefficient matrix of the linear equation system will contain approximately $(2\mathcal{N})^2$ elements, where the factor 2 comes from the two outgoing polarizations. Hence, the memory required to hold the left hand side of the equation system will be approximately $4\mathcal{N}^2\eta$, where η is the number of bytes used to store one complex number.

If each element is a single precision complex number, which is what was used to obtain the results presented in this paper, then $\eta = 8$ bytes, and the matrix will require approximately $2\pi^2 N_q^4$ bytes of memory for storage. For instance, with the choice $N_x = 319$, which was used in all the simulations presented in this paper, and that corresponds to $N_q = 160$ [Eq. (22)], the coefficient matrix will take up approximately 12 GB of memory.

Note that if we instead performed the $\mathbf{q}_\parallel$ integration in Eq. (14a) over a square domain of edge $\mathcal{Q}$, the number of elements in the resulting coefficient matrix would be $(2N_q^2)^2 = (16/\pi^2)(2\mathcal{N})^2$. Hence, by restricting the $\mathbf{q}_\parallel$ integration present in the reduced Rayleigh equation to a circular domain of radius $\mathcal{Q}/2$, the memory footprint of the simulation is approximately $\pi^2/16 \approx 0.62$ of what it would have been if a square integration domain of edge $\mathcal{Q}$ was used. For this reason, a circular integration domain has been used in obtaining the results

presented in this paper. However, we have checked and found that using a square $\mathbf{q}_\parallel$ integration domain of a similar size will not affect the results in any noticeable way. Indeed, if this was not the case, it would be a sign that $\mathscr{Q}$ was too small.

When determining the system size, we can freely choose the length of the edge of the square surface, L, and the number of sampling points along each direction, N_x. These parameters will then fix the resolution of the surface, Δx, the resolution in wave vector space, Δq, the number of resolved wave vectors, N_q, and the cutoff in the $\mathbf{q}_\parallel$ integral, $\mathscr{Q}$ [see Eqs. (18), (23), (22), and (24)]. The combination of Δq and $\mathscr{Q}$ then determines the number of resolved wave vectors that actually fall inside the propagating region, $|\mathbf{q}_\parallel| < \omega/c$, which is identical to the number of data points used to produce, e.g., Fig. 3(a).

As we are not free to choose all the parameters of the system, it is clear that some kind of compromise is necessary. The number of sampling points of the surface along each direction, N_x, and how it determines N_q via Eq. (22), determines the amount of memory needed to hold the coefficient matrix, as well as the time required to solve the corresponding linear set of equations. Hence, the parameter N_x is likely limited by practical considerations, typically by available computer hardware or time. For a given value of N_x, it is possible to choose the edge of the square surface, L, to get good surface resolution, at the cost of poor resolution in wave vector space, or vice versa. Note also that changing L will change $\mathscr{Q}$ via Δq [see Eqs. (23) and (24)]. If $\mathscr{Q}$ is not large enough to include evanescent surface modes, like surface plasmon polaritons, multiple scattering will not be correctly included in the simulations, and the results can therefore not be trusted. The optimal compromise between values of N_x and L depends on the system under study.

6.2. Calculation Time

The simulations presented in this paper were performed on shared-memory machines with 24 GB of memory and two six-core 2.4 GHz AMD Opteron processors, running version 2.6.18 of the Linux operating system. The code was parallelized using the MPI library, and the setup of the linear set of equations ran on all 12 cores in the timing examples given. The linear equation solver used was a parallel, dense solver based on LU-decomposition [54] (PCGESV from ScaLAPACK), which runs efficiently on all 12 cores. Setting up the equation system scaled almost perfectly to a large number of cores, while the solver scaled less well, due to the need for communication. Numerically solving the reduced Rayleigh equation for the scattering amplitudes associated with one realization of a rough surface, discretized onto a grid of 319×319 points, took approximately 17 minutes on the architecture described above, and required about 12 GB of memory. Out of this time, approximately 100 seconds was spent setting up the equation system, 950 seconds was spent solving it by LU decomposition, and typically around 1 second was spent on other tasks, including writing data to disk. Table 1 shows timing and memory details of the calculations, including other system sizes.

Based on the discussion in Sec. 6.1, we note that the use of a circular $\mathbf{q}_\parallel$ integration domain also significantly reduces the time required to solve the resulting linear system of equations. When using a dense solver, the time to solve the systems scales as the cube of the number of unknowns. Thus we expect the CPU time to solve the matrix system for a circular integration domain of radius $\mathscr{Q}/2$ to be about half ($\pi^3/2^6$) the time to solve the corresponding system using a square domain of edge $\mathscr{Q}$.

The ratio of the time spent solving one equation system to the total simulation time per surface realization increases with increasing system size, as the time to set up the equation system is $\mathscr{O}(N_x^4)$, while the time to solve the linear system by LU decomposition scales as $\mathscr{O}(N_x^6)$. It is clear from Table 1 that for any surface of useful size the runtime is completely dominated by the time spent in solving the linear set of equations.

Since the time solving the equation system dominates the overall simulation time, we investigated if one could improve the performance of the simulations by using an iterative solver instead of a direct solver based on LU decomposition. For example, Simonsen et al. [45] recently reported good performance using BiCGStab [56] on a dense matrix system of a similar size. In our preliminary investigations into using iterative solvers, we found that convergence with BiCGStab was slow and unreliable for our linear equation systems. However, it should be stressed that we did not use a preconditioning scheme, which could potentially yield significantly improved convergence.

From Eq. (14a) it follows that changing the angles of incidence and/or the polarization of the incident light changes *only* the right hand side of the equation system to be solved. Hence, an advantage of using LU decomposition (over iterative solvers) is that the additional time required to solve the system for several right hand sides is negligible, since the overall majority of time is spent factorizing the matrix. Conversely, the time spent using an iterative solver (like BiCGStab) will scale linearly with the number of right hand sides. For these reasons, we have chosen to use an LU-based solver.

Table 1: Walltime spent to solve the RRE for various values of N_x on a shared-memory machine with two six-core 2.4 GHz AMD Opteron processors. Included are total time (t_{tot}), time to setup the coefficient matrix of the equation system (t_{LHS}) and the time to solve the equation system (t_{solve}). Also included is the memory required to store the coefficient matrix of the linear equation system for each run (M_{LHS}). The time to set up the right hand side of the linear equation system is negligible compared to the left hand side, and have therefore not been included here.

N_x	$t_{LHS}(s)$	$t_{LU}(s)$	$t_{tot}(s)$	$M_{LHS}(GB)$
199	10	58	69	1.8
239	28	171	200	3.8
279	56	429	486	7.0
319	97	946	1,045	12.0
369	154	1,916	2,074	19.2
399	266	3,625	3,895	29.4

6.3. GPU implementation

Currently, performing simulations like those presented in this paper on a single desktop computer is prohibitively time consuming due to inadequate floating point performance. However, the increasing availability of powerful graphics processing units (GPUs) has the potential to provide computing power comparable to that of a powerful parallel machine, but at a fraction of the cost. As the most time-consuming step in our simulations is the LU decomposition of the system matrix (see Table 1), this is where efforts should be made to optimize the code. With this in mind, the simulation code was adapted to (optionally) employ version 1.0 of the MAGMA library [57] for GPU-based LU decomposition. Performance was compared between a regular supercomputing service and a GPGPU (General Purpose GPU) testbed. On the regular service, the code was running on a single compute node containing two AMD 2.3 GHz 16-core processors and 32 GB of main memory. On the GPGPU testbed, the hardware consisted of a single Nvidia Fermi C2050 processor with 3 GB of dedicated memory and 32 GB of main system memory. For these two computer systems, the initial performance tests indicated that the LU decomposition took comparable time on the two architectures for a system of size $N_q = 100$ (the difference was less than 10%). The time using the GPGPU testbed included the transfer

of the system matrix to and from the Fermi card and the decomposition of the matrix. Even though these results are preliminary, it demonstrates that there is a possibility of performing simulations like those reported in this study without having to resort to costly supercomputing resources. Instead, even with limited financial means, they may be performed on single desktop computers with a state-of-the-art GPU.

7. Conclusion

We have introduced a formalism for performing non-perturbative, purely numerical, solutions of the reduced Rayleigh equation for the reflection of light from two-dimensional penetrable rough surfaces, characterized by a complex dielectric function $\varepsilon(\omega)$.

As an example, we have used this formalism to carry out simulations of the scattering of p- or s-polarized light from two-dimensional randomly rough dielectric and metallic surfaces characterized by isotropic or anisotropic Gaussian and cylindrical power spectra. From the scattering amplitudes, obtained by solving the reduced Rayleigh equation, we calculate the mean differential reflection coefficients, and we calculate the full angular distribution of the scattered light, with polarization information. For the scattering of light from weakly rough metal surfaces, the mean differential reflection coefficient shows a well-defined peak in the retro-reflection direction (the enhanced backscattering phenomenon). From previous experimental and theoretical work, this is to be expected for such scattering systems. Moreover, the obtained angular distributions of the intensity of the scattered light show the symmetry properties found for strongly rough surfaces in recent studies using other simulation methods.

For the purpose of evaluating the accuracy of our simulation results, we used the conservation of energy for a corresponding non-absorbing scattering system. This is a required, but not sufficient, condition for the correctness of the numerical simulations. By this method, we found that within the validity of the reduced Rayleigh equation our code produces reliable results, at least for the parameters assumed in this study. In particular, for a rough non-absorbing metal surface of the parameters used in this study, energy was conserved to within 0.03%, or better. This testifies to the accuracy of the approach and a satisfactory discretization. Moreover, we also performed simulations of the scattered intensity for systems where the rms roughness of the surface was systematically increased from zero with the other parameters kept unchanged. It was found that energy conservation was well satisfied (for the parameters assumed) when the ratio of rms roughness (δ) to correlation length (a), satisfied $\delta/a \lesssim 0.12$.

We believe that the results of this paper provide an important addition to the collection of available methods for the numerical simulation of the scattering of light from rough surfaces. The developed approach can be applied to a wide range of scattering systems, including clean and multilayered scattering systems, that are relevant for numerous applications. The memory requirements, while not insignificant, are still smaller than for the surface integral method by about an order of magnitude. Hence, the current method can be applied to systems which were previously outside the reach of numerical simulations.

T. Nordam, P. A. Letnes, and I. Simonsen, "Validity of the Rayleigh hypothesis for two-dimensional randomly rough metal surfaces," *Accepted for publication in Proceedings of CCP2012*, 2012

Paper 5

Validity of the Rayleigh hypothesis for two-dimensional randomly rough metal surfaces

T Nordam, PA Letnes, and I Simonsen

Department of Physics, Norwegian University of Science and Technology (NTNU),
NO-7491 Trondheim, Norway

E-mail: `tor.nordam@gmail.com`

Abstract. The Rayleigh hypothesis is the assumption that the field in the region above (below) a rough surface can be expressed as a weighted sum of upwards (downwards) propagating scattered (transmitted) modes, and that these expressions can be used to satisfy the boundary conditions on the fields at the surface. This hypothesis is expected to be valid for surfaces of sufficiently small slopes. For one-dimensional sinusoidal surfaces, the region of validity is known analytically, while for randomly rough surfaces in one and two dimensions, the limits of validity of the Rayleigh hypothesis are not known. In this paper, we perform a numerical study of the validity of the Rayleigh hypothesis for two-dimensionally rough metal and perfectly conducting surfaces by considering the conservation of energy. It is found for a perfect electric conductor (PEC) that the region of validity is defined by the ratio of the root-mean-square roughness, δ, over the correlation length, a, being less than about 0.2, while for silver we find $\delta/a \lesssim 0.08$ for an incident wavelength $\lambda = 457.9$ nm. Limitations in our simulations made us unable to check the Rayleigh hypothesis for roughness where $\delta \gtrsim 0.13\lambda$.

1. Introduction

Randomly rough surfaces are abundant in nature and such structures may influence surface processes and phenomena in numerous ways. Lord Rayleigh is credited for being the first to study how wave scattering from surfaces is influenced by their roughness. In particular, at the end of the 19th century, he studied how waves are scattered by sinusoidal surfaces [1, 2]. To this end, he assumed that the fields in the *surface region*, defined as the spatial region between the maximum and minimum point of the surface, can be written in a form similar to the asymptotic fields. This means that the reflected (transmitted) fields can be expressed as a weighted sum of upward (downward) propagating plane waves [see Eq. (4) and Ref. 3 for details].

This way of writing the fields in the surface region is an approximation which is expected to be valid if the surface structures have sufficiently small local slopes. Today this approximation is known as the *Rayleigh hypothesis* in honor of its inventor [1–4], and most perturbation theoretical treatments of the scattering problem can be constructed based on the assumption that the Rayleigh hypothesis is valid [3]. Moreover, by applying the Rayleigh hypothesis and imposing the boundary conditions satisfied by the fields at the surface, the so-called *reduced Rayleigh equation* for reflection (transmission) can be derived from the resulting coupled set of integral equations after eliminating the transmission (reflection) amplitudes [3, 5]. The reduced Rayleigh equation, which contains either the unknown reflection or transmission amplitudes, has recently been solved by direct numerical means to produce non-perturbative results [3, 6–8].

To take full advantage of an approximation, it is imperative to know its region of validity. About 75 years after its introduction, it was proven mathematically that the Rayleigh hypothesis for a sinusoidal surface[1], i.e., a surface which deviates from its mean by $x_3 = \zeta_0 \sin(\Lambda x_1)$, is formally valid if $\zeta_0 \Lambda \leq 0.448$ [9, 10]. However, for a randomly rough surface, the precise region of validity is still not formally known. For rough surfaces that are constant along one direction in the mean plane, i.e., their height can be written as $x_3 = \zeta(x_1)$, there have been attempts to use direct numerical solution of the one-dimensional reduced Rayleigh equation to evaluate the validity of the Rayleigh hypothesis [11].

To the best of our knowledge, no attempt at a numerical study of the validity of the Rayleigh hypothesis has been reported in the literature for surfaces that are randomly rough along both directions of the mean plane. The lack of such a study in the literature is probably due to the significant computational cost. The purpose of this paper is to fill this gap in the literature by reporting some preliminary results for the validity of the Rayleigh hypothesis applied to electromagnetic wave scattering from two-dimensional randomly rough metal and perfectly conducting surfaces. Since this problem has no known analytic solution, we approach it by using a purely numerical solution of the reduced Rayleigh equation, which was recently implemented and tested [7].

For scattering from non-absorbing metallic substrates in vacuum, one must require that the power incident upon the rough metal surface equals the power reflected from it, since no energy can be transmitted through the metal. Hence, by numerically studying the conservation of energy in the scattering process over the surface roughness parameter space, one may indirectly get information about the validity of the Rayleigh hypothesis which underlies the simulation approach being used. It should be stressed that the conservation of energy is a necessary, but not sufficient condition for correct results. Hence, the region of validity of the Rayleigh hypothesis for the systems we study here may in fact be even more restricted than what we report.

This paper is organized as follows: In Section 2, we define the geometry and some conventions used throughout the paper. Next, in Section 3, we describe the asymptotic field expansions, and write down the reduced Rayleigh equation for reflection from a perfectly conducting substrate, as well as the expression we will use to evaluate the conservation of energy, and we briefly describe how we proceed to solve the reduced Rayleigh equation. In Section 4, we present our results. We also include a discussion of these results, and what they can tell us about the limits on the validity of the Rayleigh hypothesis, as well as some discussion of other potentially limiting steps in our approach. Finally, we present some concluding remarks and some thoughts about further work in Section 5.

2. Scattering geometry

The system we study consists of vacuum ($\varepsilon_1 = 1$) in the region $x_3 > \zeta\left(\boldsymbol{x}_\parallel\right)$, where $\boldsymbol{x}_\parallel = (x_1, x_2, 0)$ and a perfect electric conductor (PEC) or a metal in the region $x_3 < \zeta\left(\boldsymbol{x}_\parallel\right)$. The surface profile function $\zeta\left(\boldsymbol{x}_\parallel\right)$ is assumed to be a single-valued function of $\boldsymbol{x}_\parallel$ that is differentiable with respect to x_1 and x_2, and constitutes a zero-mean, stationary, isotropic, Gaussian random process defined by

$$\left\langle \zeta(\boldsymbol{x}_\parallel)\zeta(\boldsymbol{x}'_\parallel) \right\rangle = \delta^2 W\left(\left|\boldsymbol{x}_\parallel - \boldsymbol{x}'_\parallel\right|\right). \tag{1}$$

Here the angular brackets denote an average over the ensemble of realizations of the surface profile function. In writing Eq. (1), we have defined the root-mean-square height of the surface, $\delta = \left\langle \zeta^2(\boldsymbol{x}_\parallel) \right\rangle^{1/2}$, and $W(\boldsymbol{x}_\parallel - \boldsymbol{x}'_\parallel)$ is the height-height auto-correlation function of the surface,

---

[1] The coordinate system used is defined in Fig. 1.
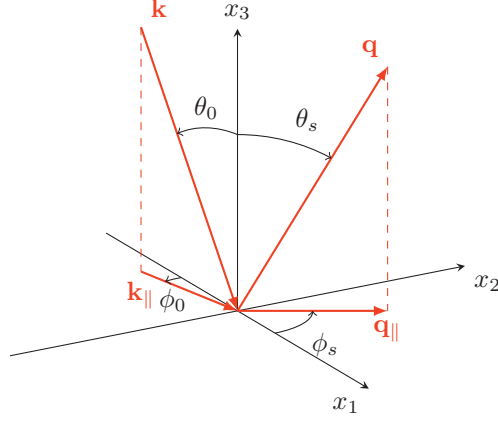
Figure 1. (Color online) A sketch of the scattering geometry assumed in this work. The figure also shows the coordinate system used, angles of incidence (θ_0, ϕ_0) and scattering (θ_s, ϕ_s), and the corresponding lateral wavevectors $\boldsymbol{k}_\parallel$ and $\boldsymbol{q}_\parallel$, respectively.

normalized so that $W(\boldsymbol{0}) = 1$ [3]. The correlation functions that will be considered in this work is isotropic and of the Gaussian form, given by

$$W\left(\left|\boldsymbol{x}_\parallel\right|\right) = \exp\left(-x_\parallel^2/a^2\right), \tag{2}$$

where a denotes the lateral correlation length.

3. Scattering theory

The electric field in the vacuum $\left[x_3 > \zeta\left(\boldsymbol{x}_\parallel\right)\right]$ is the sum of an incident field and a scattered field, $\boldsymbol{E}(\boldsymbol{x};t) = [\boldsymbol{E}(\boldsymbol{x}|\omega)_{\text{inc}} + \boldsymbol{E}(\boldsymbol{x}|\omega)_{\text{sc}}] \exp(-\mathrm{i}\omega t)$, where

$$\boldsymbol{E}(\boldsymbol{x}|\omega)_{\text{inc}} = \left\{\frac{c}{\omega}\left[\hat{\boldsymbol{k}}_\parallel \alpha_1(k_\parallel) + \hat{\boldsymbol{x}}_3 k_\parallel\right] B_{\text{p}}(\boldsymbol{k}_\parallel) + \left(\hat{\boldsymbol{x}}_3 \times \hat{\boldsymbol{k}}_\parallel\right) B_{\text{s}}(\boldsymbol{k}_\parallel)\right\} \exp\left(\mathrm{i}\boldsymbol{k}_\parallel \cdot \boldsymbol{x}_\parallel - \mathrm{i}\alpha_1(k_\parallel)x_3\right)$$

$$\boldsymbol{E}(\boldsymbol{x}|\omega)_{\text{sc}} = \int \frac{\mathrm{d}^2 q_\parallel}{(2\pi)^2}\left\{\frac{c}{\omega}\left[\hat{\boldsymbol{q}}_\parallel \alpha_1(q_\parallel) - \hat{\boldsymbol{x}}_3 q_\parallel\right] A_{\text{p}}(\boldsymbol{q}_\parallel) + \left(\hat{\boldsymbol{x}}_3 \times \hat{\boldsymbol{q}}_\parallel\right) A_{\text{s}}(\boldsymbol{q}_\parallel)\right\} \tag{3}$$

$$\times \exp\left(\mathrm{i}\boldsymbol{q}_\parallel \cdot \boldsymbol{x}_\parallel + \mathrm{i}\alpha_1(q_\parallel)x_3\right).$$

Here the subscripts p and s denote the p-polarized and s-polarized components of these fields with respect to the local planes of incidence and scattering. The expressions in front of the amplitudes A_{p} and B_{p} are the unit polarization vectors for p polarized light, and similarly the expressions in front of the amplitudes A_{s} and B_{s} are the unit polarization vectors for s polarized light. A caret over a vector indicates that it is a unit vector. The third component of the wave vector $\boldsymbol{q}$ in vacuum, $\alpha_1(q_\parallel)$, is given by

$$\alpha_1(q_\parallel) = \left[\left(\frac{\omega}{c}\right)^2 - q_\parallel^2\right]^{1/2}, \qquad \operatorname{Re}\alpha_1(q_\parallel, \omega) > 0,\ \operatorname{Im}\alpha_1(q_\parallel, \omega) > 0. \tag{4}$$

We assume that a linear relation exists between the amplitudes $A_\alpha(\boldsymbol{q}_\parallel)$ and $B_\beta(\boldsymbol{k}_\parallel)$ ($\alpha, \beta = \mathrm{p}, \mathrm{s}$), which we write as

$$A_\alpha(\boldsymbol{q}_\parallel) = \sum_\beta R_{\alpha\beta}(\boldsymbol{q}_\parallel|\boldsymbol{k}_\parallel) B_\beta(\boldsymbol{k}_\parallel).$$

It can be shown that the scattering amplitudes, organized into the following 2×2 matrix

$$\boldsymbol{R}(\boldsymbol{q}_\parallel|\boldsymbol{x}_\parallel) = \left(\begin{array}{cc} R_{\mathrm{pp}}(\boldsymbol{q}_\parallel|\boldsymbol{k}_\parallel) & R_{\mathrm{ps}}(\boldsymbol{q}_\parallel|\boldsymbol{k}_\parallel) \\ R_{\mathrm{sp}}(\boldsymbol{q}_\parallel|\boldsymbol{k}_\parallel) & R_{\mathrm{ss}}(\boldsymbol{q}_\parallel|\boldsymbol{k}_\parallel) \end{array} \right), \tag{5}$$

satisfy the matrix integral equation [12]

$$\int \frac{\mathrm{d}^2 q_\parallel}{(2\pi)^2} \boldsymbol{M}^+(\boldsymbol{p}_\parallel|\boldsymbol{q}_\parallel) \boldsymbol{R}(\boldsymbol{q}_\parallel|\boldsymbol{k}_\parallel) = -\boldsymbol{M}^-(\boldsymbol{p}_\parallel|\boldsymbol{k}_\parallel). \tag{6a}$$

This equation is known as the *reduced* Rayleigh equation since it is an equation for the scattered field in the medium of incidence only. The elements of the matrices $\boldsymbol{M}^\pm$ for a perfect electric conductor take the form

$$\boldsymbol{M}^\pm(\boldsymbol{p}_\parallel|\boldsymbol{q}_\parallel) = I(\pm\alpha_1(q_\parallel)|\boldsymbol{p}_\parallel - \boldsymbol{q}_\parallel) \left(\begin{array}{cc} \pm\frac{c}{\omega}\frac{p_\parallel q_\parallel - (\omega/c)^2\,\hat{\boldsymbol{p}}_\parallel \cdot \hat{\boldsymbol{q}}_\parallel}{\alpha_1(q_\parallel)} & [\hat{\boldsymbol{p}}_\parallel \times \hat{\boldsymbol{q}}_\parallel]_3 \\ \pm\frac{\omega}{c}\frac{[\hat{\boldsymbol{p}}_\parallel \times \hat{\boldsymbol{q}}_\parallel]_3}{\alpha_1(q_\parallel)} & \hat{\boldsymbol{p}}_\parallel \cdot \hat{\boldsymbol{q}}_\parallel \end{array} \right), \tag{6b}$$

where

$$I\left(\gamma|\boldsymbol{Q}_\parallel\right) = \int \mathrm{d}^2 x_\parallel \, \exp\left(-\mathrm{i}\boldsymbol{Q}_\parallel \cdot \boldsymbol{x}_\parallel\right) \exp\left[-\mathrm{i}\gamma\zeta\left(\boldsymbol{x}_\parallel\right)\right]. \tag{6c}$$

For a penetrable metal or dielectric surface, the corresponding matrix elements are given explicitly in Ref. 7, and will not be repeated here.

3.1. Mean Differential Reflection Coefficient

The solution of the reduced Rayleigh equation determines the scattering amplitudes $R_{\alpha\beta}(\boldsymbol{q}_\parallel|\boldsymbol{k}_\parallel)$, where α and β signify the polarization of the reflected and incident light, respectively. When the incident field is known, this quantity completely specifies the scattered field in the region above the maximum point of the surface. However, $R_{\alpha\beta}(\boldsymbol{q}_\parallel|\boldsymbol{k}_\parallel)$ is not directly measurable in experiments. A more useful quantity is the mean differential reflection coefficient (DRC), which is defined as the fraction of the time-averaged incident power which is scattered by the surface into the solid angle $\mathrm{d}\Omega_s$ about the scattering direction $\boldsymbol{q}$ defined by the angles of scattering (θ_s, ϕ_s) (see Fig. 1). The mean DRC is defined as [13]

$$\left\langle \frac{\partial R_{\alpha\beta}}{\partial \Omega_s} \right\rangle = \frac{1}{L^2} \frac{\omega^2}{4\pi^2 c^2} \frac{\cos^2 \theta_s}{\cos \theta_0} \left\langle \left| R_{\alpha\beta}(\boldsymbol{q}_\parallel|\boldsymbol{k}_\parallel) \right|^2 \right\rangle, \tag{7}$$

where L^2 is the area of the plane $x_3 = 0$ covered by the rough surface, and θ_0 is the angle of incidence (see Fig. 1).

3.2. Conservation of Energy

To test whether the Rayleigh hypothesis is fulfilled, we use the conservation of energy as a criterion. Considering a perfectly conducting substrate, all the incident power must be reflected, and we can check whether our calculations conserve energy from the reflected field alone. The fraction of the time-averaged incident power in the form of light of polarization β, scattered by the surface into light of polarization α, is given by the integral of the corresponding mean DRC over the upper hemisphere:

$$\mathcal{U}_{\alpha\beta} = \int \mathrm{d}\Omega_s \left\langle \frac{\partial R_{\alpha\beta}}{\partial \Omega_s} \right\rangle. \tag{8}$$

If the substrate is non-absorbing, and the incident light has polarization β, one should have

$$\mathcal{U}_\beta = \sum_\alpha \mathcal{U}_{\alpha\beta} = 1, \tag{9}$$

since energy is conserved in the scattering process. To improve statistics, we define the quantity

$$\mathcal{U} = \frac{\mathcal{U}_\mathrm{p} + \mathcal{U}_\mathrm{s}}{2}, \tag{10}$$

which we calculate by separately calculating both $\mathcal{U}_\mathrm{p}$ and $\mathcal{U}_\mathrm{s}$ for each surface realisation, and taking their average. This is the quantity we will use when testing the validity of the Rayleigh hypothesis.

While the conservation of energy is a necessary, but not sufficient, condition for correct results, we have previously made successful direct comparisons of results obtained by the numerical solution of the reduced Rayleigh equation for weakly rough surfaces against both experimental data, and simulation results obtained by the rigorous surface integral method [14–16]. We are thus confident that our approach works well for weakly rough surfaces. Furthermore, if we hold the transverse correlation length of the surface roughness fixed, while increasing the rms height of the surface, we typically see that at some point, $\mathcal{U}$ starts increasing past 1. While $\mathcal{U} > 1$ is clearly unphysical, and thus evidence that the technique is not working, $\mathcal{U} = 1$ is not by itself proof that the results are correct (for a non-absorbing substrate). Still, our comparisons with both experimental data and other numerical data indicate that the conservation of energy is a useful guide to the validity of our approach.

Thus, in this paper we use $\mathcal{U} \approx 1$ as a criterion for when our approach is valid when considering a perfect electric conductor, and $\mathcal{U} \lesssim 1$ when considering a penetrable metal. Note that this criterion does not directly test the Rayleigh hypothesis, but rather our complete method for solving the scattering problem, which among other things relies on the Rayleigh hypothesis. There could be other reasons why our approach fails for strongly rough surfaces, and this will be discussed in more detail when considering our results.

3.3. Solving the reduced Rayleigh equation

To solve the reduced Rayleigh equation, we begin by numerically generating a realization of the surface profile function on a grid of N_x^2 points within a square region of the $x_1 x_2$ plane of edge L, so that the in-plane sampling interval is $\Delta x = L/N_x$. A two-dimensional version of the filtering method used in Refs. [7, 16, 17] is used to generate the surface realizations from a given correlation function.

The next step is to evaluate the integrals $I(\gamma|\boldsymbol{Q}_\parallel)$ defined in Eq. (6c). These integrals are so-called Fourier integrals and care should be taken when evaluating them due to the oscillating integrands [18]. Using direct numerical integration routines for their evaluation will typically result in inaccurate results. Instead, a (fast) Fourier transform technique with end

point corrections may be adapted for their evaluation (the details of the method is outlined in Ref. [18]). However, these calculations are time consuming. In solving for $\boldsymbol{R}(\boldsymbol{q}_\parallel|\boldsymbol{k}_\parallel)$, we will discretize both $\boldsymbol{p}_\parallel$, $\boldsymbol{q}_\parallel$ and $\boldsymbol{k}_\parallel$, and $I(\gamma|\boldsymbol{Q}_\parallel)$ must be evaluated for all relevant combinations of the arguments $\gamma = \pm\alpha_1(p_\parallel)$ and $\boldsymbol{Q}_\parallel = \boldsymbol{p}_\parallel - \boldsymbol{q}_\parallel$ and $\boldsymbol{Q}_\parallel = \boldsymbol{p}_\parallel - \boldsymbol{k}_\parallel$. For the calculations used to generate the results presented in this paper, this would amount to evaluating $I(\gamma|\boldsymbol{Q}_\parallel)$ on the order of 10^9 times per surface realization.

A computationally more efficient way of evaluating $I(\gamma|\boldsymbol{Q}_\parallel)$ is to assume that the exponential function $\exp\left[-\mathrm{i}\gamma\zeta(\boldsymbol{x}_\parallel)\right]$, present in the definition of $I(\gamma|\boldsymbol{Q}_\parallel)$, can be expanded in powers of its argument, and then evaluating the resulting expression term-by-term by employing the Fourier transform. This gives

$$I(\gamma|\boldsymbol{Q}_\parallel) = \sum_{n=0}^{\infty} \frac{(-\mathrm{i}\gamma)^n}{n!} \tilde{\zeta}^{(n)}(\boldsymbol{Q}_\parallel), \tag{11a}$$

where $\tilde{\zeta}^{(n)}(\boldsymbol{Q}_\parallel)$ denotes the Fourier transform of the nth power of the surface profile function, i.e.,

$$\tilde{\zeta}^{(n)}(\boldsymbol{Q}_\parallel) = \int \mathrm{d}^2x_\parallel \zeta^n(\boldsymbol{x}_\parallel) \exp\left(-\mathrm{i}\boldsymbol{Q}_\parallel \cdot \boldsymbol{x}_\parallel\right). \tag{11b}$$

In practice, the sum in Eq. (11a) will be truncated at a finite value of n. The Fourier transforms are calculated using a fast Fourier transform (FFT) algorithm.

The primary advantage of using Eqs. (11) for calculating $I(\gamma|\boldsymbol{Q}_\parallel)$ is that the rewrite in Eq. (11a) moves γ outside the integral, and calculating the integral in Eq. (11b) by FFT gives us the value of the integral as a function of $\boldsymbol{Q}_\parallel$. By using the proper discretization, we can make sure that the values of $\boldsymbol{Q}_\parallel$ resolved by the FFT are precisely those we need when setting up a linear equation system to solve for $R_{\alpha\beta}(\boldsymbol{q}_\parallel|\boldsymbol{k}_\parallel)$. This alternative way of evaluating the I-integrals results in a significant reduction in computational time. The same method has previously been applied successfully to the numerical solution of the one-dimensional reduced Rayleigh equation [6, 19, 20].

It should be noted that the Taylor expansion used to arrive at Eq. (11a) requires $\left|\gamma\zeta(\boldsymbol{x}_\parallel)\right| \ll 1$ to converge reasonably fast. Even though the series expansion of the exponential function is always convergent in theory, this procedure might not be numerically stable for large values of $\left|\gamma\zeta(\boldsymbol{x}_\parallel)\right|$, in particular due to the oscillatory nature of the series when $\mathrm{Re}\,\gamma\zeta(\boldsymbol{x}_\parallel) < 0$. Thus, limited numerical precision means that using the expansion presented in Eq. (11a) places additional constraints on the amplitude of the surface roughness which may be more restrictive than those introduced by the Rayleigh hypothesis. In particular, the Rayleigh hypothesis places a constraint on the maximum *slope* of the surface roughness, while the numerical procedure used to evaluate the I-integrals, needed to solve the reduced Rayleigh equation, also limits the *amplitude* of the surface roughness. Hence, surfaces exist for which the Rayleigh hypothesis is satisfied, but the above expansion method will not converge numerically, and the much more time-consuming approach of Ref. 18 will have to be applied.

Finally, in evaluating the integral in Eq. (6a) over $\boldsymbol{q}_\parallel$, the integration limits were truncated to the circular region defined by $\left(q_1^2 + q_2^2\right)^{1/2} \leq Q/2$. The Nyquist sampling theorem requires that $|q_1|$ and $|q_2|$ be smaller than $Q_c = \pi/\Delta x$ [21, p. 605]. The components of the vector $\boldsymbol{p}_\parallel - \boldsymbol{q}_\parallel$ entering $I(\gamma|\boldsymbol{p}_\parallel - \boldsymbol{q}_\parallel)$ lie in the interval $[-Q, Q]$, so we have chosen $Q = Q_c$. A quadratic grid with grid constant $\Delta q = 2\pi/L$ was constructed within the circular region of the q_1q_2 plane where $\left(q_1^2 + q_2^2\right)^{1/2} \leq Q/2$. The integral over this region in Eq. (6a) was carried out by a two-dimensional version of the extended midpoint method [21, p. 161] and the values of $R_{\alpha\beta}(\boldsymbol{q}_\parallel|\boldsymbol{k}_\parallel)$ were calculated for values of $\boldsymbol{q}_\parallel$ on the grid for a given value of $\boldsymbol{k}_\parallel$ (or equivalently, a given angle
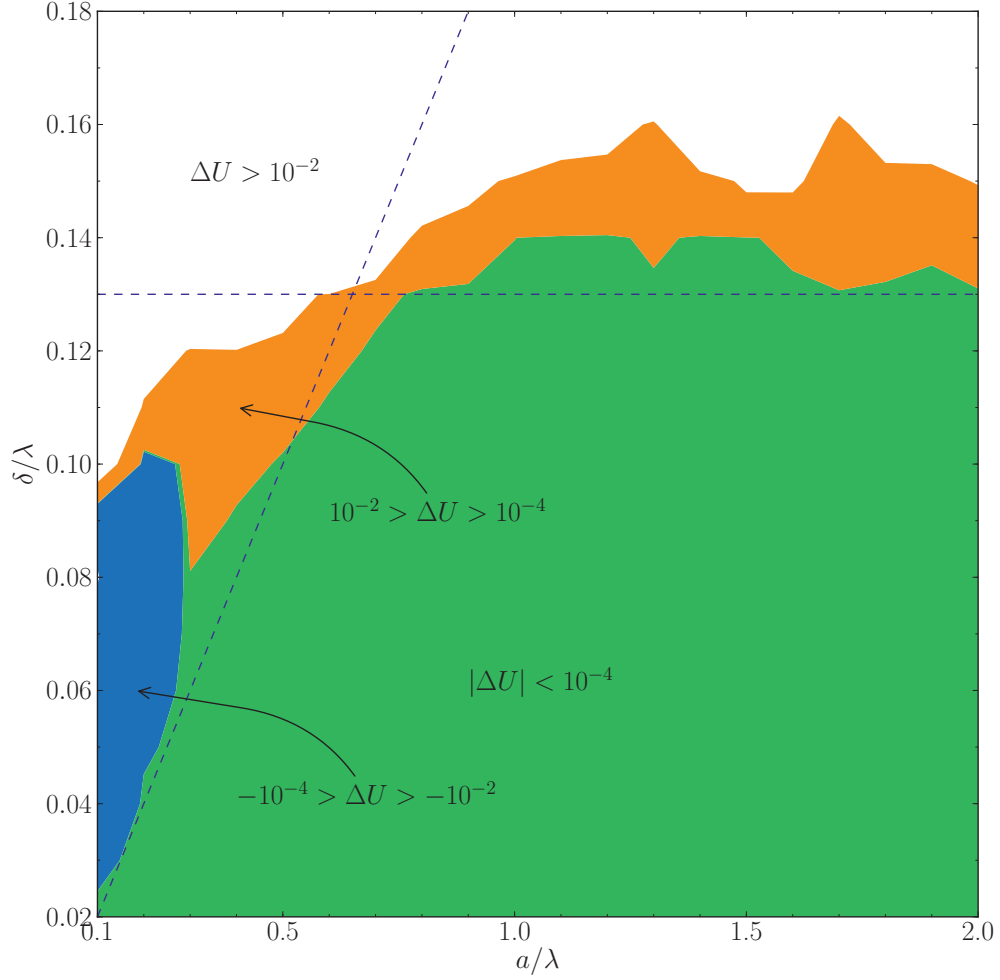
Figure 2. Contour plot of $\Delta \mathcal{U} \equiv \mathcal{U} - 1$, i.e., the deviation from unity of the fraction incident power reflected from randomly rough surfaces on perfectly conducting substrates. The surface roughness is characterized by the correlation function given in Eq. (2), with the correlation length, a, given on the horizontal axis and the rms height of the surface, δ, on the vertical axis. The slope of the diagonal dashed line is given by $\delta/a = 0.2$.

of incidence), which was also a point on the grid. The resulting matrix equations were solved by LU decomposition and back substitution [21, page 48]. In this way we obtain $R_{\alpha\beta}(\boldsymbol{q}_{\parallel}|\boldsymbol{k}_{\parallel})$, from which the mean DRC can be calculated [see Eq. (7)]. For a more detailed description of how we solve the reduced Rayleigh equation, we refer the interested reader to Ref. 7.
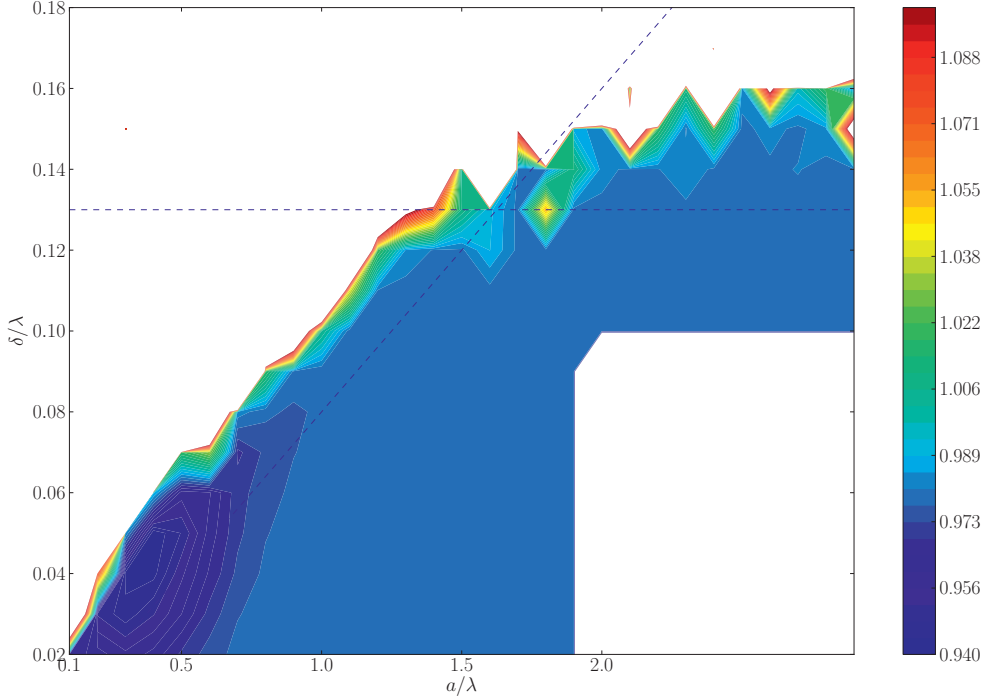
Figure 3. Contour plot of $\mathcal{U}$, the fraction of incident power reflected from randomly rough surfaces on silver substrates. The incident wavelength is 457.9 nm, which corresponds to a dielectric constant of $\epsilon_2 = -7.5 + 0.24i$. The surface roughness is characterized by the correlation function given in Eq. (2), with the correlation length, a, given on the horizontal axis and the rms height, δ, on the vertical axis. The white area in the bottom right corner represents parameters for which we have no data, but where we are confident the value of $\mathcal{U}$ is the same as in the surrounding region. The white area in the upper left represents values of $\mathcal{U}$ greater than 1.1. The slope of the diagonal dashed line is given by $\delta/a = 0.08$.

4. Results

The direct numerical solution method of the reduced Rayleigh equation from Sec. 3 has been used to calculate the scattering amplitudes $R_{\alpha\beta}(\boldsymbol{q}_\parallel | \boldsymbol{k}_\parallel)$ for randomly rough surfaces of edges $L \times L$, where $L = 15\lambda$. The surface profile function $\zeta(\boldsymbol{x}_\parallel)$ was discretized to $N_x \times N_x$ points, with $N_x = 319$, and the roughness was characterized by the height-height autocorrelation function given by Eq. (2). The sum in Eq. (11a) was truncated at $n = 20$. Solving the reduced Rayleigh equation for one surface realization with these parameters takes approximately 17 minutes on a machine with two six-core AMD Opteron 2.1 GHz processors. The majority (around 90%) of this time is spent performing the LU-decomposition of the linear equation system.

The first set of results we present is for a perfectly conducting substrate. For this system, Fig. 2 depicts a contour plot of $\Delta\mathcal{U} \equiv \mathcal{U} - 1$, i.e., the deviation from unity of the fraction of reflected power, as a function of the transverse correlation length, a, and the rms height, δ, of the rough surface. The contours are defined by $-10^{-2} < \Delta\mathcal{U} < -10^{-4}$, $-10^{-4} < \Delta\mathcal{U} < 10^{-4}$, $10^{-4} < \Delta\mathcal{U} < 10^{-2}$, and $10^{-2} < \Delta\mathcal{U}$. The results of Fig. 2 were obtained from calculations

on a grid of points in parameter space defined by $\delta \in [0.02\lambda, 0.18\lambda]$ and $a \in [0.1\lambda, 2.0\lambda]$ with spacing $\Delta\delta = 0.01\lambda$ and $\Delta a = 0.1\lambda$. For each pair of surface parameters (a, δ), we calculated the fraction of reflected power, $\mathcal{U}$, and averaged the solution over 20 surface realizations. This was found to be sufficient to get convergent results, at least for the surface type and parameters considered in this work.

In the wave scattering from a perfectly conducting substrate, one should formally always have $\mathcal{U} \equiv 1$ independent of the level of surface roughness. However, in numerical calculations this condition may, or may not, be satisfied. The latter case may indicate that the numerical method is being applied outside its range of validity, and that the results cannot be trusted. From Fig. 2 we find that for weakly rough surfaces $\mathcal{U}$ deviates from 1 by less than 10^{-4}, and that the boundary between the regions defined by $|\Delta\mathcal{U}| < 10^{-4}$ and $|\Delta\mathcal{U}| > 10^{-4}$ is approximately given by $\delta = 0.2a$ (indicated by the diagonal dashed line in Fig. 2) for sufficiently small δ/λ.

For a Gaussian correlation function, which was used to produce the results of Fig. 2, the rms slope of the surface is given by $\sqrt{2}\delta/a$ [22]. Thus, the limit of the validity of the Rayleigh hypothesis being given by a linear relationship between δ and a is consistent with the local slope of the surface being the critical parameter. Since the Rayleigh hypothesis is a *small slope* approximation, our finding is not unexpected [4]. Hence, for perfectly conducting substrates, we find the Rayleigh hypothesis to be valid for surfaces of rms slope less than about 0.28.

The Rayleigh hypothesis is not expected to introduce any additional restrictions, for example on the amplitude of the rough surface. However, from Fig. 2 we observe that regardless of the correlation length, $\mathcal{U}$ deviates from 1 when $\delta \geq 0.13$. Since this is not an expected consequence of the Rayleigh hypothesis, one may wonder about the cause of this behaviour.

As was discussed in Sec. 3.3, with increasing amplitudes of $\zeta(\boldsymbol{x}_\parallel)$, we no longer expect to be able to accurately calculate the integrals $I(\gamma|\boldsymbol{Q}_\parallel)$. Preliminary tests indicate that this problem can be alleviated somewhat by increasing the order up to which the sum in Eq. (11a) is carried out, but at some point limited numerical precision, leading to numerical cancellations, becomes an issue. Hence, we concluded that the upper finite roughness level for which $\mathcal{U}$ starts deviating significantly from 1 is not a consequence of the Rayleigh hypothesis. Rather, it is a numerical artifact of how the integrals encoding the surface roughness are calculated. We speculate that using an alternative way of calculating $I(\gamma|\boldsymbol{Q}_\parallel)$ which is not based on a series expansion may resolve this issue, but at the cost of significantly increased computational time. A more promising approach might be to employ software libraries which allow calculations to be carried out with arbitrary precision. Tests we have performed, as well as the results of Ref. 11, indicate that higher precision allows the accurate calculation of the integrals $I(\gamma|\boldsymbol{Q}_\parallel)$, though again this comes with a price in terms of computational time.

The second set of results that will be presented is for a silver substrate. Here the wavelength of the incident light was assumed to be 457.9 nm, for which the dielectric function of silver is $\epsilon_2 = -7.5 + 0.24i$. In Fig. 3, we present the dependence over parameter space of $\mathcal{U}$, i.e., the fraction of the incident power reflected from randomly rough silver surfaces. Since the silver substrate is absorbing, $\mathcal{U}$ will now in general be less than 1, but $\mathcal{U} > 1$ still represents an unphysical situation. Again, the values of the rms height, δ, and transverse correlation length, a, were varied, ranging from 0.02 to 0.18λ in 0.01λ increments for δ, and from 0.1λ to 2.9λ in 0.1λ increments for a. For each pair of values, (a, δ), we calculated $\mathcal{U}$, and averaged the solution over 10 surface realizations. The white area in the upper left corner of Fig. 3 represents values where $\mathcal{U} > 1.1$. The large white area in the bottom right corner of Fig. 3 represents surface parameters for which we did not perform any calculations. This was done to reduce computational time, since we are rather confident that for these parameters we will find $\mathcal{U} < 1$.

For a silver substrate, the region of validity of the Rayleigh hypothesis is less pronounced than for the same geometry but with a perfectly conduction substrate. Unlike in a perfect conductor, light can penetrate into the silver and so-called surface modes can be excited.

Changing roughness allows light to couple more or less strongly into intermediate surface modes before being scattered back into the vacuum, and the coupling to surface modes is not only dependent on the amplitude of the surface, but also on the length scale of the surface structures.

Still, with these physical differences between a perfectly conducting and a silver substrate, we observe by comparing Figs. 2 and 3 that the structure of the region of validity of the Rayleigh hypothesis appears roughly similar. For a silver substrate, it follows from an inspection of Fig. 3 that the region of validity is defined by the intersection between the following two regions: (i) $\delta \lesssim 0.08a$ corresponding to a critical rms slope of 0.11; and (ii) $\delta \lesssim 0.13\lambda$. Note that the critical rms slope is less for a silver (0.11) than a PEC substrate (0.28), while the second region is the same for the same two substrates.

5. Conclusions

We have presented preliminary results for the numerical investigation of the validity of the Rayleigh hypothesis obtained by studying the fraction of power reflected from rough surfaces. In this way it is found that the Rayleigh hypothesis is valid for perfectly conducting substrates when $\delta \lesssim 0.2a$ and for silver substrates when $\delta \lesssim 0.08a$, where δ denotes the rms height and a the correlation length of the surfaces roughness. These regions correspond to critical rms slopes of 0.28 (PEC) and 0.11 (silver), respectively. Both regions are bounded upwards by an rms height of approximately $\delta \approx 0.13\lambda$. We argue that this is not an inherent limitation of the Rayleigh hypothesis, which is a small-slope approximation, not a small-amplitude approximation, but rather a consequence of the way we calculate the integrals $I(\gamma|\boldsymbol{Q}_\parallel)$ [see Eq. (11)] present in the reduced Rayleigh equation. It may be possible to get around this limitation by using increased numerical precision, or another algorithm for calculating $I(\gamma|\boldsymbol{Q}_\parallel)$, but at the cost of increased computational time.

Works cited

[1] Lord Rayleigh 1896 *The Theory of Sound* 2nd ed vol II (London: MacMillan) pp. 89, 297–311.
[2] Lord Rayleigh 1907 *Proc. R. Soc. Lon. Ser. A* **79** 399–416
[3] Simonsen I 2010 *Eur. Phys. J.-Spec. Top.* **181** 1
[4] Voronovich A 2007 *Light Scattering and Nanoscale Surface Roughness* (New York: Springer-Verlag) chap 4: Rayleigh Hypothesis, pp 93–107
[5] A Soubret G Berginc C B 2001 *Phys. Rev. B* **63** 245411
[6] Simonsen I and Maradudin A 1999 *Opt. Commun.* **162** 99
[7] Nordam T, Letnes P A and Simonsen I *arXiv:1204.4984*
[8] Nordam T, Letnes P A, Simonsen I and Maradudin A A 2012 *Opt. Express* **20**(10) 11336–11350
[9] Millar R F 1969 *Math. Proc. Cambridge* **65** 773–791
[10] Millar R 1971 *Proc. Camb. Phil. Soc.* **69** 217
[11] Tishchenko A V 2009 *Opt. Express* **17** 17102
[12] Nordam T, Letnes P A, Simonsen I and Maradudin A A 2012 Numerical solutions of the rayleigh equations for the scattering of light from a two-dimensional randomly rough perfectly conducting surface (unpublished)
[13] Mcgurn A R and Maradudin A A 1996 *Wave Random Media* **6** 251 – 267
[14] Simonsen I, Maradudin A A and Leskova T A 2010 *Phys. Rev. A* **81** 013806
[15] Simonsen I, Maradudin A A and Leskova T A 2010 *Phys. Rev. Lett.* **104** 223904
[16] Simonsen I, Kryvi J B, Maradudin A A and Leskova T A 2011 *Comp. Phys. Commun.* **182** 1904
[17] Maradudin A A, Michel T, McGurn A R and Méndez E R 1990 *Ann. Phys. (NY)* **203** 255 – 307
[18] Press W H, Teukolsky S A, Vetterling W T and Flannery B P 1992 *Numerical Recipes in Fortran. The Art of Scientific Computing* 2nd ed (Cambridge: Cambridge University Press)

[19] Madrazo A and Maradudin A A 1997 *Opt. Commun.* **134**
[20] Simonsen I 2010 *Phys. Status Solidi B* **247** 2075
[21] Press W, Flannery B, Teukolsky S and Vetterling W 2007 *Numerical recipes* 3rd ed (Cambridge: Cambridge University Press)
[22] Maradudin A and Michel T 1990 *J. Stat. Phys.* **58**(3-4) 485–501 ISSN 0022-4715 URL http://dx.doi.org/10.1007/BF01112758

P. A. Letnes, T. Nordam, and I. Simonsen, "Coherent effects in the scattering of light from two-dimensional rough metal surfaces," *Submitted to Journal of the Optical Society of America A*, 2013

Paper 6

Coherent effects in the scattering of light from two-dimensional rough metal surfaces

P. A. Letnes,[1, *] T. Nordam,[1, †] and I. Simonsen[1, ‡]

[1]*Department of Physics, The Norwegian University of Science and Technology (NTNU), NO-7491 Trondheim, Norway*

compiled: January 30, 2013

We investigate numerically multiple light scattering phenomena for two-dimensional randomly rough metallic surfaces, where surface plasmon polaritons mediate several surface scattering effects. The scattering problem is solved by numerical solution of the reduced Rayleigh equation for reflection. The multiple scattering phenomena of enhanced backscattering and enhanced forward scattering are observed in the same system, and their presence is due to the excitation of surface plasmon polaritons. The numerical results discussed are qualitatively different from previous results for one-dimensionally rough surfaces, as one-dimensional surfaces have a limited influence on the polarization of light.

OCIS codes: (290.1483) BSDF, BRDF, and BTDF; (290.4210) Multiple scattering; (290.5825) Scattering theory; (290.5880) Scattering, rough surfaces.

1. Introduction

A hot topic in the electronics and photonics community is plasmonics, due to the prediction that surface plasmon polaritons (SPPs) can carry information faster and with less energy loss than electronic circuits [1]. Surface plasmon polaritons can have a penetration depth in metal on the order of 10 nm, i.e., two orders of magnitude smaller than the wavelength of visible light in vacuum. This means that plasmonics allows light to be concentrated and manipulated by structures well below the diffraction limit from classical optics.

Surface plasmon polariton excitation is also being investigated as a way to improve the performance of photovoltaic devices. For thin solar cells, with a thickness on the order of 1 μm, the path length of light travelling through the cell is insufficient to absorb more than a small fraction of the incident energy. By converting light into SPPs which can propagate along the dielectric-metal interface at the back of the photovoltaic cell, it is possible to absorb a larger fraction of the incident energy [2].

Since SPPs propagate along the interface of a metal, they are sensitive to conditions on the surface, making SPPs well suited for sensor applications. Such devices are often called surface plasmon resonance (SPR) sensors, and can be used for, e.g., microarray analysis of proteins [3] or DNA [4].

At a flat interface, incident light cannot couple to SPPs due to momentum mismatch. By manipulating the surface roughness, however, it is possible to control the coupling of incident light into SPPs. In this paper, we consider light reflected from randomly rough surfaces with particular statistical properties, and study the multiple scattering phenomena which arise due to SPPs. Several multiple scattering phenomena have been predicted theoretically and/or confirmed experimentally. For example, enhanced backscattering was predicted by McGurn et al. [5] and later confirmed experimentally by West and O'Donnell [6]. The enhanced backscattering phenomenon is a double scattering phenomenon, caused by constructive interference between a wave scattered (at least) twice by the surface, and its time-reversed partner. The excitation of SPPs is usually involved in this process. For weak (low rms) surface roughness, scattering processes are usually dominated by single scattering, which may mask higher order scattering contributions. Hence, West and O'Donnell designed a surface whose roughness had a power spectrum which suppresses single scattering in a certain angular interval, allowing multiple scattering effects to be seen more clearly [6]. The surface in question had a surface profile function dependent on only one of the axes in the surface plane; colloquially, we refer to such surfaces as "one-dimensional". This power spectrum is now known as the West–O'Donnell spectrum or the rectangular spectrum.

Enhanced forward scattering was first predicted theoretically by O'Donnell [7], who termed it the enhanced specular peak phenomenon[8]. O'Donnell investigated the scattering of light from surfaces with weak, one-dimensional roughness by the use of perturbation theory, and reported an enhancement in the specular direction of the intensity of the light scattered diffusely

———————

[*] paul.anton.letnes@gmail.com
[†] tor.nordam@gmail.com
[‡] Ingve.Simonsen@ntnu.no

by the rough surface. To lowest order in the surface profile function, this phenomenon appears as an eight-order contribution to the intensity within small amplitude perturbation theory, and for one-dimensional surface roughness it is caused by constructive interference between *counterpropagating* SPPs; see Fig. 10 of Ref. 7. To confirm these findings, O'Donnell and Méndez subsequently studied surface scattering from one-dimensional surfaces by direct solution of the one-dimensional reduced Rayleigh equation [9]. Their findings were later confirmed by Simonsen [10] who also performed a detailed numerical study of this phenomenon, focusing on the competition between how light couples into and out from SPPs, and how one SPP can couple to another counterpropagating SPP.

Up till now, the enhanced forward scattering phenomenon has not been studied for two-dimensional randomly rough surfaces neither by perturbation theory nor by computer simulations. Moreover, only a few numerical studies of enhanced backscattering have appeared in the literature for two-dimensional roughness. In this paper, we investigate light scattering from two-dimensionally rough surfaces by means of large scale computer simulations, with a focus on phenomena caused by the excitation and interference of SPPs. In particular, we are interested in the enhanced backscattering phenomenon and the less studied phenomenon of forward scattering enhancement. The understanding of such phenomena could be useful for the understanding and controlling light-plasmon coupling in plasmonic circuits. Furthermore, two-dimensional surface roughness leads to significant polarization effects that cannot be taken into account in a one-dimensional model.

This paper is organized as follows. In Sec. 2, we discuss the relevant theory, including how the statistical properties of the surface roughness decide which scattering processes are allowed. Section 3 presents results from numerical simulations, exhibiting enhanced forward scattering and enhanced backscattering. Finally, concluding remarks are presented in Sec. 4.

2. Theory

The system under study consists of a metallic substrate in vacuum [Fig. 1(a)]. We assume that the vacuum-metal interface has a randomly rough structure, and the metal is characterized by a complex dielectric function $\varepsilon_2(\omega)$. The vacuum dielectric constant is $\varepsilon_1 \equiv 1$. The height of the surface is given by the single-valued function $x_3 = \zeta(\mathbf{x}_\parallel)$, where $\mathbf{x}_\parallel = (x_1, x_2, 0)$ is the lateral component of the position vector, $\mathbf{x}$. We assume that $\zeta(\mathbf{x}_\parallel)$ is at least once differentiable with respect to x_1 and x_2. The angles of incidence (θ_0, ϕ_0) and scattering (θ_s, ϕ_s) are defined positive according to the convention given in Fig. 1(b).

In this paper, we will consider randomly rough surfaces where $\zeta(\mathbf{x}_\parallel)$ constitutes a stationary random pro-

(a) System sketch, seen in the $x_1 x_3$ plane.

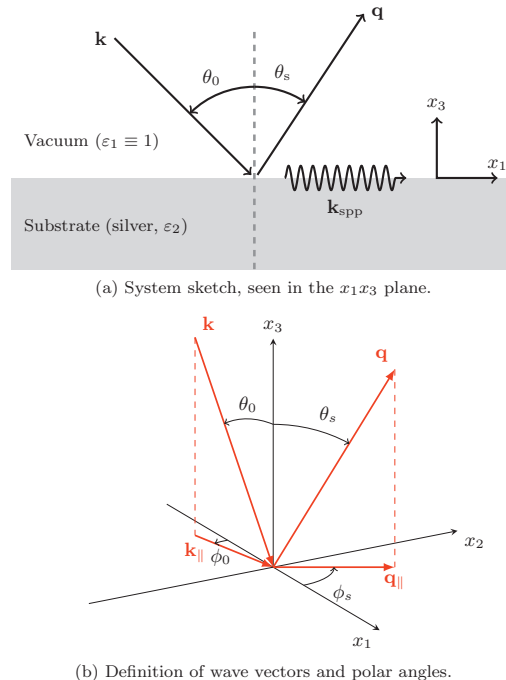(b) Definition of wave vectors and polar angles.

Fig. 1. (Color online) Sketches of the system under study (surface roughness not shown). (a) The light of wave vector $\mathbf{k}$ incident on the surface causes scattering into various propagating modes (of wave vector $\mathbf{q}$) and the excitation of surface plasmon polaritons ($\mathbf{k}_{\mathrm{spp}}$). In this study, we assume $\varepsilon_1(\omega) \equiv 1$, and $\varepsilon_2(\omega)$ is taken from Ref. 11. (b) Definition of the lateral wave vectors ($\mathbf{k}_\parallel$ and $\mathbf{q}_\parallel$) as well as the polar angles of incidence and scattering.

cess defined by

$$\langle \zeta(\mathbf{x}_\parallel) \rangle = 0, \tag{1a}$$

$$\left\langle \zeta(\mathbf{x}_\parallel) \zeta(\mathbf{x}'_\parallel) \right\rangle = \delta^2 W(\mathbf{x}_\parallel - \mathbf{x}'_\parallel), \tag{1b}$$

where the angle brackets denote an average over an ensemble of surface realizations. In writing Eq. (1) we have defined the root-mean-square height of the surface, $\delta = \left\langle \zeta^2(\mathbf{x}_\parallel) \right\rangle^{1/2}$, and $W(\mathbf{x}_\parallel - \mathbf{x}'_\parallel)$ denotes the height-height auto-correlation function of the surface, normalized so that $W(\mathbf{0}) = 1$ [12]. In the discussion below, and when generating realizations of the surface profile function, it is more convenient to work with the power spectrum of the surface, rather than using the auto-correlation function directly. The power spectrum, $g(\mathbf{k}_\parallel)$, of the surface profile function is defined by

$$g(\mathbf{k}_\parallel) = \int \mathrm{d}^2 x_\parallel \, W(\mathbf{x}_\parallel) \exp\left(-\mathrm{i}\mathbf{k}_\parallel \cdot \mathbf{x}_\parallel\right), \tag{2}$$

where $\mathbf{k}_\parallel = (k_1, k_2, 0)$ is the lateral component of the wave vector, $\mathbf{k}$. The power spectra that will be considered in this work are of the cylindrical form, where

$$g(k_\parallel) = \gamma_1 g_1(k_\parallel) + \gamma_2 g_2(k_\parallel) \tag{3a}$$

and g_i ($i = 1, 2$) are given by [13]

$$g_i(k_\parallel) = \frac{4\pi}{k_+^2 - k_-^2} \theta\left(k_\parallel - k_-^{(i)}\right) \theta\left(k_+^{(i)} - k_\parallel\right). \tag{3b}$$

In Eq. (3a), γ_1 and γ_2 are real constants defined such that $\gamma_1, \gamma_2 \geq 0$ and $\gamma_1 + \gamma_2 = 1$. Furthermore, $k_\parallel = |\mathbf{k}_\parallel|$, $\theta(\cdot)$ denotes the Heaviside unit step function, and $k_\pm^{(i)}$ are wavenumber cutoff parameters, with $k_-^{(1)} < k_+^{(1)} < k_-^{(2)} < k_+^{(2)}$. The Heaviside step functions in Eq. (3b) cause each of the g_i's to have a cylindrical shape: g_i is zero for $k_\parallel < k_-^{(i)}$, a positive constant for $k_-^{(i)} \leq k_\parallel < k_+^{(i)}$, and zero for $k_\parallel \geq k_+^{(i)}$. The constants γ_i determine the relative amplitudes of the outer and inner cylindrical parts of the power spectrum. The power spectrum described by Eq. (3) is a two-dimensional generalization of the one used by O'Donnell and Méndez [9] and Simonsen [10] in their previous numerical investigations of enhanced forward scattering from one-dimensional randomly rough surfaces.

We note that the power spectrum used by West and O'Donnell [6] in their experimental confirmation of enhanced backscattering is a one-dimensional special case of Eq. (3), with $\gamma_1 = 1$ and $\gamma_2 = 0$ (or vice versa).

2.A.   The reduced Rayleigh equation

The electric field in the vacuum above the surface $\left[x_3 > \max \zeta\left(\mathbf{x}_\parallel\right)\right]$ can be expressed as the sum of an incident field and a scattered field,

$$\mathbf{E}(\mathbf{x}|t) = \left[\mathbf{E}^{(0)}(\mathbf{x}|\omega) + \mathbf{E}^{(s)}(\mathbf{x}|\omega)\right] \exp\left(-i\omega t\right), \tag{4}$$

where ω is the angular frequency of the incident (and scattered) light. The superscripts (0) and (s) on the electric field vectors indicate the incident and scattered field, respectively. Furthermore,

$$\mathbf{E}^{(0)}(\mathbf{x}|\omega) = \left\{ -\frac{c}{\omega}\left[\hat{\mathbf{k}}_\parallel \alpha_1(k_\parallel) + \hat{\mathbf{x}}_3 k_\parallel\right] \mathcal{E}_{\mathrm{p}}^{(0)}(\mathbf{k}_\parallel) + \left(\hat{\mathbf{x}}_3 \times \hat{\mathbf{k}}_\parallel\right) \mathcal{E}_{\mathrm{s}}^{(0)}(\mathbf{k}_\parallel) \right\} \exp\left[i\mathbf{k}_\parallel \cdot \mathbf{x}_\parallel - i\alpha_1(k_\parallel)x_3\right], \tag{5a}$$

$$\mathbf{E}^{(s)}(\mathbf{x}|\omega) = \int \frac{\mathrm{d}^2 q_\parallel}{(2\pi)^2} \left\{ \frac{c}{\omega}\left[\hat{\mathbf{q}}_\parallel \alpha_1(q_\parallel) - \hat{\mathbf{x}}_3 q_\parallel\right] \mathcal{E}_{\mathrm{p}}^{(s)}(\mathbf{q}_\parallel) + \left(\hat{\mathbf{x}}_3 \times \hat{\mathbf{q}}_\parallel\right) \mathcal{E}_{\mathrm{s}}^{(s)}(\mathbf{q}_\parallel) \right\} \exp\left[i\mathbf{q}_\parallel \cdot \mathbf{x}_\parallel + i\alpha_1(q_\parallel)x_3\right], \tag{5b}$$

where $\mathcal{E}_\alpha^{(0)}(\mathbf{q}_\parallel)$ and $\mathcal{E}_\beta^{(s)}(\mathbf{k}_\parallel)$, with $\alpha, \beta = \mathrm{p, s}$, are the amplitudes of the α-polarized and β-polarized components of these fields with respect to the local planes of incidence and scattering, respectively. The wave vector of the incident light is $\mathbf{k}$, which is of length $|\mathbf{k}| = \omega/c$, where c is the speed of light in vacuum. The expressions in front of the field amplitudes are the unit polarization vectors. The wave vector of the scattered light, $\mathbf{q}$, has lateral component $\mathbf{q}_\parallel = (q_1, q_2, 0)$, and is related to the angles of scattering as indicated by Fig. 1(b). A caret over a vector indicates that it is a unit vector. Finally, the functions $\alpha_i(q_\parallel)$, $i = 1, 2$ are defined by

$$\alpha_i(q_\parallel) = \left[\varepsilon_i \left(\frac{\omega}{c}\right)^2 - q_\parallel^2\right]^{1/2}, \tag{6}$$
$$\mathrm{Re}\, \alpha_i(q_\parallel) > 0, \, \mathrm{Im}\, \alpha_i(q_\parallel) > 0.$$

A linear relation is assumed to exist between the amplitudes $\mathcal{E}_\alpha^{(s)}(\mathbf{q}_\parallel)$ and $\mathcal{E}_\beta^{(0)}(\mathbf{k}_\parallel)$ $(\alpha, \beta = \mathrm{p, s})$, which we express in terms of the scattering amplitudes $R_{\alpha\beta}(\mathbf{q}_\parallel|\mathbf{k}_\parallel)$ [14]:

$$\mathcal{E}_\alpha^{(s)}(\mathbf{q}_\parallel) = \sum_{\beta=p,s} R_{\alpha\beta}(\mathbf{q}_\parallel|\mathbf{k}_\parallel)\mathcal{E}_\beta^{(0)}(\mathbf{k}_\parallel).$$

In order to obtain an equation for the scattering amplitudes, we first write down an expression for the transmitted field, $\mathbf{E}^{(t)}(\mathbf{x}|\omega)$, which is valid in the region $x_3 < \min \zeta(\mathbf{x}_\parallel)$ below the surface. We then assume the Rayleigh hypothesis, which states that for a sufficiently smooth surface, $\left|\nabla\zeta(\mathbf{x}_\parallel)\right| \ll 1$, these asymptotic expressions for the fields are valid also in the surface roughness region $[\min \zeta(\mathbf{x}_\parallel) < x_3 < \max \zeta(\mathbf{x}_\parallel)]$ [15, 16], and can be used to fulfill the boundary conditions satisfied by the electric and magnetic fields at the surface $x_3 = \zeta(\mathbf{x}_\parallel)$. From the resulting set of coupled matrix integral equations, it is possible to eliminate the amplitudes of the transmitted (reflected) field so that a single matrix integral equation results for the amplitudes corresponding to the field above (below) the surface. The resulting equation is known as the reduced Rayleigh equation for reflection (transmission). For details regarding the derivation of the reduced Rayleigh equation, we refer to Refs. 14 and 17.

If the scattering amplitudes are organized as the 2×2 matrix

$$\mathbf{R}(\mathbf{q}_\parallel|\mathbf{k}_\parallel) = \begin{pmatrix} R_{\mathrm{pp}}(\mathbf{q}_\parallel|\mathbf{k}_\parallel) & R_{\mathrm{ps}}(\mathbf{q}_\parallel|\mathbf{k}_\parallel) \\ R_{\mathrm{sp}}(\mathbf{q}_\parallel|\mathbf{k}_\parallel) & R_{\mathrm{ss}}(\mathbf{q}_\parallel|\mathbf{k}_\parallel) \end{pmatrix}, \tag{7}$$

the reduced Rayleigh equation for reflection from a two-dimensional surface can be written in the form [13, 17, 18]

$$\int \frac{d^2 q_{\parallel}}{(2\pi)^2} \frac{I\left(\alpha_2(p_{\parallel}) - \alpha_1(q_{\parallel})|\mathbf{p}_{\parallel} - \mathbf{q}_{\parallel}\right)}{\alpha_2(p_{\parallel}) - \alpha_1(q_{\parallel})} \mathbf{M}^+(\mathbf{p}_{\parallel}|\mathbf{q}_{\parallel}) \mathbf{R}(\mathbf{q}_{\parallel}|\mathbf{k}_{\parallel}) = -\frac{I\left(\alpha_2(p_{\parallel}) + \alpha_1(k_{\parallel})|\mathbf{p}_{\parallel} - \mathbf{k}_{\parallel}\right)}{\alpha_2(p_{\parallel}) + \alpha_1(k_{\parallel})} \mathbf{M}^-(\mathbf{p}_{\parallel}|\mathbf{k}_{\parallel}), \quad (8a)$$

where

$$I(\gamma|\mathbf{Q}_{\parallel}) = \int d^2 x_{\parallel} \exp\left[-i\gamma\zeta(\mathbf{x}_{\parallel})\right] \exp\left(-i\mathbf{Q}_{\parallel} \cdot \mathbf{x}_{\parallel}\right), \quad (8b)$$

and

$$\mathbf{M}^{\pm}(\mathbf{p}_{\parallel}|\mathbf{q}_{\parallel}) = \begin{pmatrix} p_{\parallel}q_{\parallel} \pm \alpha_2(p_{\parallel})\hat{\mathbf{p}}_{\parallel} \cdot \hat{\mathbf{q}}_{\parallel} \alpha_1(q_{\parallel}) & -\frac{\omega}{c}\alpha_2(p_{\parallel})\left[\hat{\mathbf{p}}_{\parallel} \times \hat{\mathbf{q}}_{\parallel}\right]_3 \\ \pm\frac{\omega}{c}\left[\hat{\mathbf{p}}_{\parallel} \times \hat{\mathbf{q}}_{\parallel}\right]_3 \alpha_1(q_{\parallel}) & \frac{\omega^2}{c^2}\hat{\mathbf{p}}_{\parallel} \cdot \hat{\mathbf{q}}_{\parallel} \end{pmatrix}. \quad (8c)$$

The integral in Eq. (8b) is evaluated by expanding the exponential $\exp\left[-i\gamma\zeta(\mathbf{x}_{\parallel})\right]$ in powers of its argument, and integrating the resulting series term-by-term by the fast Fourier transform (FFT). In practice, the sum is truncated at a finite order sufficient to give convergent results ($n = 20$ was used in this work). The integration domain used for the integral in Eq. (8a) is truncated to cover the circular region $q_{\parallel} \leq \mathcal{Q}/2$, and the integration was converted to a finite sum over this domain by a two-dimensional version of the standard mid-point quadrature scheme. From this sum, we can obtain a linear system of equations (one for each value of $\mathbf{p}_{\parallel}$), which can be solved to find $R_{\alpha\beta}(\mathbf{q}_{\parallel}|\mathbf{k}_{\parallel})$.

For the simulations presented in this paper, we have used numerically generated, discrete realizations of the surface profile function. These realizations covered a square area of size $L \times L$ in the $x_1 x_2$ plane, determining the integration limits in Eq. (8b). The surface realizations were discretized onto a quadratic, equidistant grid of $N_x \times N_x$ points. Each realization was generated by a two-dimensional version of the Fourier filtering method presented in, e.g., Refs. 19 and 20. For a detailed discussion of how one can proceed to solve the reduced Rayleigh equation numerically, we refer to Ref. 21.

2.B. Mean differential reflection coefficient

When the incident field is known, the quantity $R_{\alpha\beta}(\mathbf{q}_{\parallel}|\mathbf{k}_{\parallel})$ completely specifies the total electromagnetic field in the region $x_3 > \max \zeta(\mathbf{x}_{\parallel})$. However, $R_{\alpha\beta}(\mathbf{q}_{\parallel}|\mathbf{k}_{\parallel})$ is not directly measurable in experiments. A quantity well suited for experimental studies is the mean differential reflection coefficient (MDRC), $\langle \partial R_{\alpha\beta}/\partial\Omega_s \rangle$, which is defined as the time-averaged fraction of the incident power scattered into the solid angle $d\Omega_s$ about the scattering direction, $\hat{\mathbf{q}}$. The relationship between

$R_{\alpha\beta}(\mathbf{q}_{\parallel}|\mathbf{k}_{\parallel})$ and the MDRC can be written as [13]

$$\left\langle \frac{\partial R_{\alpha\beta}}{\partial\Omega_s} \right\rangle = \frac{1}{L^2} \frac{\omega^2}{4\pi^2 c^2} \frac{\cos^2\theta_s}{\cos\theta_0} \left\langle \left|R_{\alpha\beta}(\mathbf{q}_{\parallel}|\mathbf{k}_{\parallel})\right|^2 \right\rangle. \quad (9)$$

Since we are studying weakly rough surfaces, light scattered coherently (specularly) by the rough surface will dominate. However, some of the light incident on the surface will also be scattered incoherently (diffusely) by the rough surface. In theoretical and numerical studies, it is advantageous to separate these two contributions.

By light scattered coherently by the surface, we mean scattered light that is in phase from one surface realization to the next, so that the intensity of light scattered coherently (from β to α polarization) will be proportional to $\left|\langle R_{\alpha\beta}(\mathbf{q}_{\parallel}|\mathbf{k}_{\parallel})\rangle\right|^2$. The contribution to the MDRC from the light that has been scattered *incoherently* by the rough surface is defined as [13]

$$\left\langle \frac{\partial R_{\alpha\beta}}{\partial\Omega_s} \right\rangle_{\text{incoh}} = \frac{1}{L^2} \frac{\omega^2}{4\pi^2 c^2} \frac{\cos^2\theta_s}{\cos\theta_0}$$
$$\times \left[\left\langle \left|R_{\alpha\beta}(\mathbf{q}_{\parallel}|\mathbf{k}_{\parallel})\right|^2 \right\rangle - \left|\langle R_{\alpha\beta}(\mathbf{q}_{\parallel}|\mathbf{k}_{\parallel})\rangle\right|^2\right]. \quad (10)$$

The contribution to the MDRC from the light scattered *coherently* is therefore given by the difference between Eqs. (9) and (10). We will see below that enhanced backscattering and enhanced forward scattering are both phenomena observed in the *incoherent component* of the MDRC, even if in the case of enhanced forward scattering it is observed in the *specular direction*.

We also note that the quantity $R_{\alpha\beta}(\mathbf{q}_{\parallel}|\mathbf{k}_{\parallel})$ can be used to construct the Mueller matrix for reflection from a rough surface [22]. The Mueller matrix contains all linear transformations of the polarization of light undergoing scattering from a rough surface, including polarization and depolarization.

2.C. Surface plasmon polaritons

Surface plasmon polaritons are electromagnetic modes that are confined to dielectric-metal interfaces, where the dielectric function of the cladding is positive and the (real part of the) dielectric function of the substrate is smaller than the negative of the dielectric function of the cladding [23]. The dispersion relation of SPPs at a flat vacuum-metal interface is [23]

$$k_{\mathrm{spp}}(\omega) = \frac{\omega}{c} \left(\frac{\varepsilon_2(\omega)}{\varepsilon_2(\omega)+1} \right)^{1/2} \qquad (11)$$

where $k_{\mathrm{spp}}(\omega)$ is the length of the wave vector of the SPP mode. For silver at wavelength $\lambda = 457.9$ nm (in vacuum), for which the dielectric function is $\varepsilon_2(\omega) = -7.5 + 0.24i$ [11], it follows that $k_{\mathrm{spp}} = (1.074 + 0.003i)\omega/c$ ($\omega = 2\pi c/\lambda$). The imaginary part of k_{spp} can be interpreted as an inverse decay length of the SPP mode, whereas the real part corresponds to the wave number of the mode.

Multiple scattering phenomena such as the enhanced backscattering and enhanced forward scattering are, for weakly rough surfaces, typically caused by the incident light exciting SPPs that are subsequently scattered zero or more times before coupling into a mode propagating away from the surface [12]. In particular, in one-dimensional small-amplitude perturbation theory, the lowest order contribution to the enhanced forward scattering peak in the mean DRC has its origin in quadruple scattering processes [7, Fig. 10].

2.D. Allowed and forbidden scattering processes

From small amplitude perturbation theory [12, 24], it can be shown that a *single* scattering event from lateral wave vector $\mathbf{k}_\parallel$ to $\mathbf{q}_\parallel$ is allowed only if the power spectrum evaluated at the wave vector transfer $\mathbf{k}_{\mathrm{sc}}$ is non-zero, i.e.,

$$g(\mathbf{k}_{\mathrm{sc}}) > 0, \qquad \mathbf{k}_{\mathrm{sc}} = \mathbf{q}_\parallel - \mathbf{k}_\parallel. \qquad (12)$$

This condition holds for scattering between propagating modes; between evanescent modes; and from propagating to evanescent modes, and vice versa. For isotropic power spectra, such as those studied in this paper [Eq. (3)], the requirement (12) simplifies to

$$g(|\mathbf{k}_{\mathrm{sc}}|) > 0. \qquad (13)$$

To better understand the physical implications of condition (13), and to facilitate our interpretation of the simulation results presented later in this paper, we present a visual model for discussing relevant scattering processes in Fig. 2. Before starting the discussion, we remind the reader that modes for which $k_\parallel \leq \omega/c$ are propagating in the vacuum, whereas for $k_\parallel > \omega/c$, the corresponding fields are evanescent, i.e., the field amplitudes decay exponentially along both directions perpendicular to the surface. Moreover, at the wavelength $\lambda = 457.9$ nm, assumed in the simulations presented below, the vacuum-silver interface supports surface plasmon polaritons of lateral wave vector $k_{\mathrm{spp}} = 1.074\omega/c$ (see Sec. 2.C). For simplicity, we have neglected the imaginary part of the wave number, as it is small compared to its real part.

In passing, we note that the polarization state of light can be modified at each scattering event, subject to the requirement that SPPs are always p-polarized. We will, however, not discuss polarization effects of single scattering events in this section.

We will now discuss Fig. 2, which was produced under the assumption that the surface power spectrum is identical to that in Eq. (3), and characterized by the values for $k_\pm^{(i)}$ used in the later simulations (Sec. 3): $k_-^{(1)} = 0.782\omega/c$, $k_+^{(1)} = 1.366\omega/c$, $k_-^{(2)} = 2.048\omega/c$, and $k_+^{(2)} = 2.248\omega/c$. The annular regions, indicated by blue shaded regions in Fig. 2, represent the nonzero parts of the surface roughness power spectrum.

First, we consider the scattering process $\mathbf{k}_\parallel \to \mathbf{q}_\parallel$ [Fig. 2(a)] that corresponds to the lateral wave vector (or momentum) transfer $\mathbf{k}_{\mathrm{sc}}$. In Fig. 2(a) the incident lateral wave vector, $\mathbf{k}_\parallel$, is placed so that it starts at the origin of wave vector space, O; the same is done for $\mathbf{q}_\parallel$. We superpose blue shaded regions representing the power spectrum so that the center of the power spectrum is located at the end of $\mathbf{k}_\parallel$. Thus, if $\mathbf{k}_{\mathrm{sc}}$ indicates a point inside the blue shaded regions (the power spectrum), the scattering process $\mathbf{k}_\parallel \to \mathbf{q}_\parallel$ is allowed. Moreover, at the same time, if $q_\parallel \leq \omega/c$, the process $\mathbf{k}_\parallel \to \mathbf{q}_\parallel$ results in a scattered mode that can propagate away from the surface. On the assumption that both $\mathbf{k}_\parallel$ and $\mathbf{q}_\parallel$ are propagating in vacuum, one realizes that $\mathbf{k}_\parallel$ [for the value of $\mathbf{k}_\parallel$ used in Fig. 2(a)] can be converted into $\mathbf{q}_\parallel$ through a single interaction with the surface roughness (single scattering) only within a *crescent-like* region. This region is defined by the shaded blue region which resides inside the circle $q_\parallel = \omega/c$, indicated in black in Fig. 2(a). Outside this crescent region, the scattering process is either not allowed or $q_\parallel > \omega/c$, meaning that the mode is evanescent (non-propagating). When later studying the full angular distribution of the scattered light (Fig. 3), we will see that this observation is important.

We now turn to the possibility of exciting SPPs by the incident light, a situation addressed in Fig. 2(b). The excitation $\mathbf{k}_\parallel \to \mathbf{k}_{\mathrm{spp}}$ of SPPs is subject to the constraints in Eq. (13). In particular, we have that the excitation of a surface plasmon polariton by the incident field characterized by $\mathbf{k}_\parallel$ is only allowed if

$$k_-^{(1)} < |\mathbf{k}_{\mathrm{spp}} - \mathbf{k}_\parallel| < k_+^{(1)} \qquad (14)$$

or (less relevant for the parameters used in this study, due to the large θ_0 required)

$$k_-^{(2)} < |\mathbf{k}_{\mathrm{spp}} - \mathbf{k}_\parallel| < k_+^{(2)}. \qquad (15)$$

Consequently, it is only possible (for the power spectrum used in this study) to excite surface plasmon polaritons

(a) Scattering from wave vector $\mathbf{k}_\parallel$ into wave vector $\mathbf{q}_\parallel$. The scattered mode is propagating, since $|\mathbf{q}_\parallel| < \omega/c$, with ω/c indicated by the black ring.

(b) Excitation of a surface plasmon polariton by incident light. The surface plasmon polariton is not propagating in vacuum, as $k_{\mathrm{spp}} > \omega/c$. The parts of the black ring (of radius k_{spp}) which lie in the blue region represent legal SPP excitation processes.

(c) Scattering of a surface plasmon polariton into a bulk propagating mode. Legal propagating modes are those for which $\mathbf{q}_\parallel$ lies inside the blue region and $q_\parallel < \omega/c$.

(d) Scattering of a surface plasmon polariton ($\mathbf{k}_{\mathrm{spp}}^{(1)}$). Two legal scattered modes ($\mathbf{k}_{\mathrm{spp}}^{(2)}$ and $\mathbf{k}_{\mathrm{spp}}^{(3)}$) are shown. The black ring indicates legal wave vectors for SPPs.
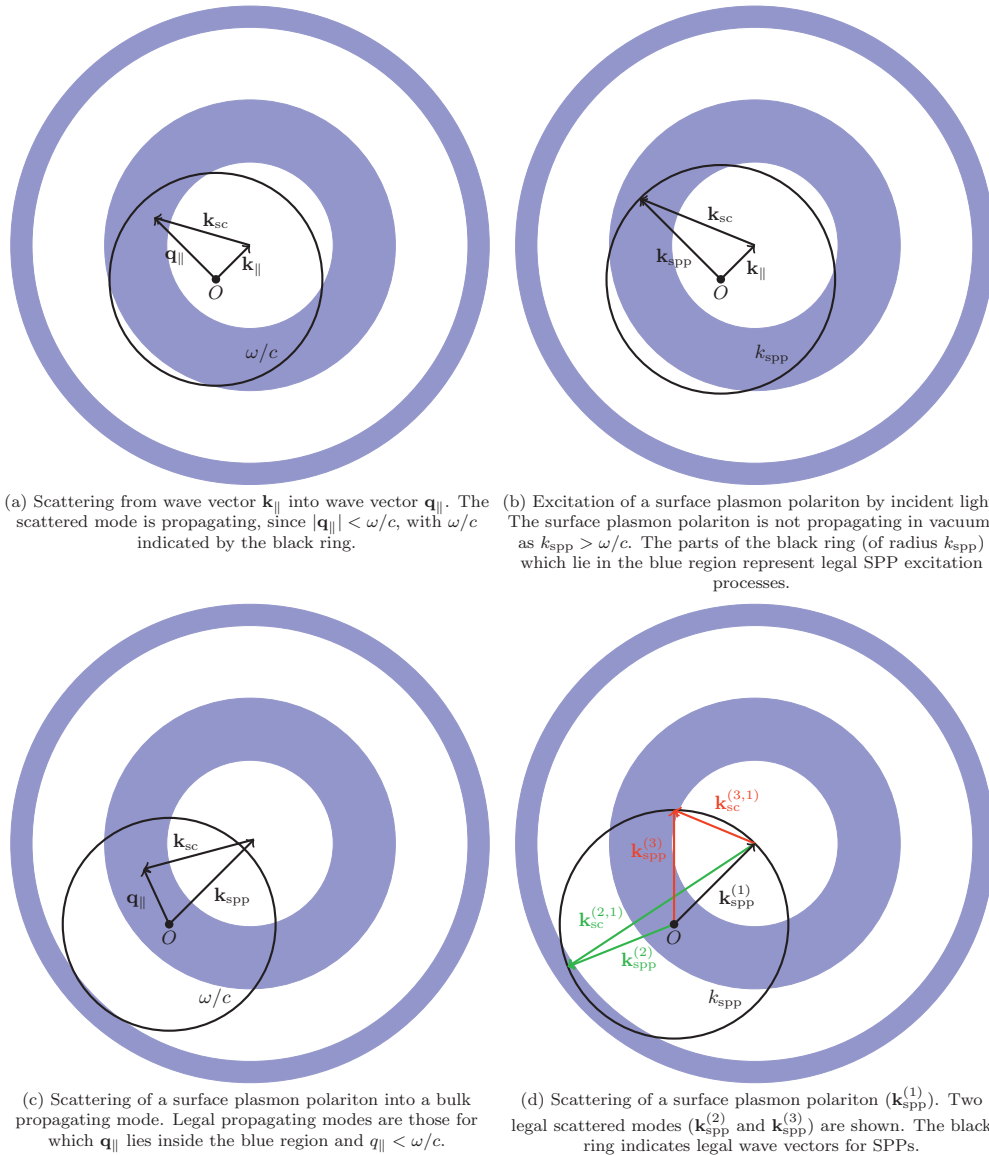
Fig. 2. (Color online) Four scattering processes important for understanding the results of this study. A detailed discussion of the figure is found in the text. All subfigures 2(a)–(d) are drawn to correct and identical scale for the parameters $k_\pm^{(i)}$ and ε_2 used throughout this study. The blue annular regions indicate the non-zero parts of the power spectrum, i.e., the ranges of $\mathbf{k}_{\mathrm{sc}}$ allowed by the power spectrum. The lengths of $\mathbf{k}_\parallel$ in Figs. 2(a) and (b) correspond to $(\theta_0, \phi_0) = (27°, 45°)$.

for small (or very large) angles of incidence. The excitation of a surface plasmon polariton is shown in Fig. 2(b). The black ring indicates the length of the possible SPP wave vectors. In the plane of incidence, surface plasmon polaritons cannot be excited by the incident light for angles of incidence $\theta_0 > 17°$. For out of plane scattering, however, SPP excitation is allowed also for $\theta_0 > 17°$. This is qualitatively different from scattering from a one-

dimensionally rough surface.

2.E. Enhanced backscattering

For weakly rough surfaces, the presence of the enhanced backscattering phenomenon typically requires the excitation of surface plasmon polaritons. For strongly rough surfaces, on the other hand, it can take place through multiple scattering between vacuum propagating modes [25, 26]. For the weakly rough surfaces discussed here, the SPP channel is by far the dominant contribution to the backscattering enhancement. As such, the presence of the enhanced backscattering phenomenon for weakly rough surfaces requires first that incident light can couple to SPPs, i.e., $g\left(\left|\mathbf{k}_{\mathrm{spp}} - \mathbf{k}_{\parallel}\right|\right) > 0$, as discussed in the previous paragraph. Second, the existence of enhanced backscattering requires that SPPs can couple out into the anti-specular direction, i.e., that $g\left(\left|-\mathbf{k}_{\parallel} - \mathbf{k}_{\mathrm{spp}}\right|\right) > 0$. This implies, with the power spectrum used here, that

$$k_{-}^{(1)} < \left|\mathbf{k}_{\mathrm{spp}} + \mathbf{k}_{\parallel}\right| < k_{+}^{(1)}. \tag{16}$$

Coupling from SPPs to vacuum propagating modes is illustrated in Fig. 2(c). For the parameters used in this study, the outer cylindrical part of the power spectrum essentially does not contribute to the scattering process $\mathbf{k}_{\mathrm{spp}} \to \mathbf{k}_{\parallel}$, as $k_{-}^{(2)} \approx \omega/c + k_{\mathrm{spp}}$.

For one-dimensionally randomly rough surfaces [7, 10], the scattered wave vectors are confined to the plane of incidence, and all quantities in Eqs. (12)–(16) can be written as scalars. Thus, there is a sharp and well-defined angular cutoff for the excitation of surface plasmon polaritons in this case. For two-dimensionally rough surfaces, however, incident light can couple to SPPs which do not propagate in the plane of incidence. This can allow scattering processes which would be forbidden in the one-dimensional case, and any limits derived using the one-dimensional model will become "fuzzy" for two-dimensional surfaces.

2.F. Enhanced forward scattering

For SPPs to contribute to enhanced forward scattering, it is required that the power spectrum allows both the excitation and counterpropagation of surface plasmon polaritons, as well as coupling from SPPs to vacuum propagating modes in the specular direction.

For the scattering of an SPP of wavevector $\mathbf{k}_{\mathrm{spp}}^{(1)}$ to an SPP of wavevector $\mathbf{k}_{\mathrm{spp}}^{(2)}$ to be allowed, it is required that $g\left(\left|\mathbf{k}_{\mathrm{spp}}^{(2)} - \mathbf{k}_{\mathrm{spp}}^{(1)}\right|\right) > 0$. For the power spectrum used in this study, this condition is fulfilled if

$$k_{-}^{(1)} < \left|\mathbf{k}_{\mathrm{spp}}^{(2)} - \mathbf{k}_{\mathrm{spp}}^{(1)}\right| < k_{+}^{(1)}, \tag{17}$$

or

$$k_{-}^{(2)} < \left|\mathbf{k}_{\mathrm{spp}}^{(2)} - \mathbf{k}_{\mathrm{spp}}^{(1)}\right| < k_{+}^{(2)}. \tag{18}$$

The counterpropagation requirement is the rationale for adding the outer annulus to the power spectrum (3). This annulus is narrow, and centered at $k_{\parallel} = 2k_{\mathrm{spp}}$, meaning that it facilitates scattering where $|\mathbf{k}_{\mathrm{sc}}| \approx 2k_{\mathrm{spp}}$, i.e., counterpropagation of SPPs. This corresponds to the fulfillment of Eq. (18), and is illustrated by the green vectors in Fig. 2(d) ($\mathbf{k}_{\mathrm{spp}}^{(2)}$ and $\mathbf{k}_{\mathrm{spp}}^{(2,1)}$).

We note that for two-dimensionally rough surfaces it is possible for an SPP to be scattered out-of-plane by the g_1 part of the power spectrum. This can happen when Eq. (17) is fulfilled, as shown in red in Fig. 2(d), where the resulting lateral wave vector is denoted $\mathbf{k}_{\mathrm{spp}}^{(3)}$.

The principles discussed above are also valid for systems consisting of a metallic substrate on which a dielectric thin film has been deposited, with a vacuum or lossless dielectric cladding, where either interface of the film is randomly rough [27]. The generalization to different power spectra should also be obvious. We note that if the power spectrum of the randomly rough surface is, e.g., Gaussian, the single scattering contribution to the MDRC is typically dominant. In such cases, it can be challenging to separate single scattering effects from multiple scattering effects.

3. Results

In this section, we present results for the MDRC when light is scattered from rough silver surfaces. For all the results presented here, the (vacuum) wavelength of the incident light was $\lambda = 457.9\,\mathrm{nm}$, and the dielectric function of the Ag substrate at this wavelength is $\varepsilon_2 = -7.5 + 0.24\mathrm{i}$. The vacuum dielectric function is $\varepsilon_1 = 1$. The rough surfaces were characterized by the power spectrum (3), defined by the wavenumber parameters: $k_{-}^{(1)} = 0.782\omega/c$, $k_{+}^{(1)} = 1.366\omega/c$, $k_{-}^{(2)} = 2.048\omega/c$, and $k_{+}^{(2)} = 2.248\omega/c$. Furthermore, the amplitudes γ_i were chosen such that $\gamma_2/\gamma_1 = 0.75$, which was found in Ref. 10 to give a relatively strong enhanced forward scattering effect. The rms surface roughness was taken to be $\delta = 0.025\lambda$; the edge of the square region covered by the rough surface was $L = 36\lambda$; and this region was discretized at a grid of $N_x = 359$ points along each of the x_1 and x_2 directions.

As the Nyquist theorem [28] relates resolution in position space and wave vector space, the values of N_x and L lead to the following numerical parameters: The wavenumber cutoff in the integral in Eq. (8a) was $\mathcal{Q}/2 = 2.493\omega/c$; the resolution in $\mathbf{q}_{\parallel}$ was $\Delta q = 0.0279\omega/c$; and $N_q = 180$ values of $\mathbf{q}_{\parallel}$ were resolved along each of the q_1 and q_2 axes [21]. The results presented were obtained by averaging the results over an ensemble of 10, 825 surface realizations. Simulating the scattering from one surface realization took approximately 17 minutes on a machine with two six-core AMD Opteron 2.4 GHz processors, and required about 12 GB of memory. For a discussion of the details of how the calculations were performed, we refer to Ref. 21.

In Fig. 3, we present the full angular distribution of the MDRC, including polarization effects. Figure 3(a)–
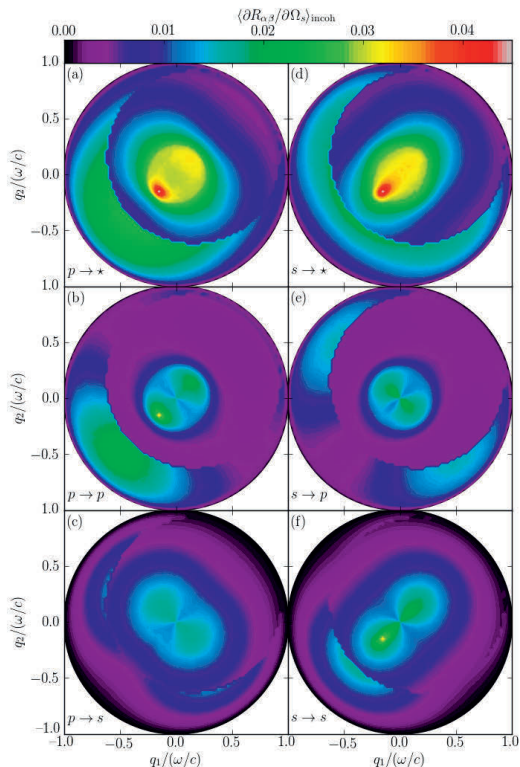
Fig. 3. (Color online) The full angular distribution of the incoherent contribution to the MDRC, assuming the surface properties stated in the text. The angles of incidence were $(\theta_0, \phi_0) = (12.5°, 45°)$. The subplots show scattering (b) from p polarization to p polarization, (e) s → p, (c) p → s, and (f) s → s. In (a), the incident light was p-polarized, but the polarization of the scattered light was not recorded, and in (d) the incident light was s-polarized. The enhanced forward scattering peak is most easily seen in the p → p configuration (b). The sharp circular edge, centered on $\mathbf{k}_\parallel$, is caused by the suppression of single scattering due to the form of the power spectrum; see discussion in Sec. 2.D, Eq. (3) and Fig. 2(a).

(c) shows the MDRC for p-polarized incident light, and in Fig. 3(d)–(f) the incident light was s-polarized. In the upper row, the polarization of the scattered light was not recorded; in the second row, only the p-polarized component of the scattered light was recorded; and in the third row, only the s-polarized component of the scattered light was recorded. The full angular intensity distribution displays important information, hidden from the reader of in-plane or out-of-plane cuts of the MDRC (e.g., Fig. 4). Notably, we observe that the intensity distribution depends on which linear polarization is used to illuminate the surface, as well as which
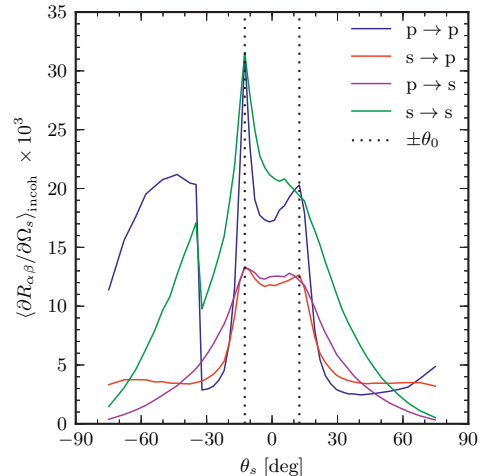

Fig. 4. (Color online) The in-plane (i.e., for $\phi_s = \phi_0$) part of the MDRC for light scattered from a rough silver surface with rms roughness $\delta = 0.025\lambda$. The angles of incidence were $(\theta_0, \phi_0) = (12.5°, 45°)$. The results were obtained by averaging over $10{,}825$ surface realizations. The most prominent enhanced forward scattering peak is in p → p polarization, but a small contribution in s → p polarization can also be seen. Enhanced backscattering is observed in all polarization combinations.
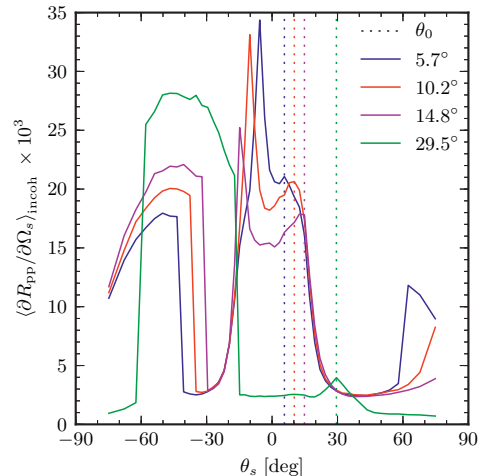

Fig. 5. (Color online) The p → p contribution to the MDRC for the same surface properties as in Fig. 4, for several different angles of incidence. In all cases, we observe the enhanced forward scattering peak. The effect is most powerful in the vicinity of $\theta_0 \approx 12°$. For polar angle of incidence $\theta_0 = 29.5°$, it is not possible to achieve enhanced forward scattering through the in-plane SPP channel; hence, the peak at $\theta_s = 29.5°$ has a different explanation.

linear polarization is recorded in the (simulated) detector. Furthermore, the crescent regions of the MDRC of high intensity show for which angles of scattering single scattering is allowed, as per the theoretical discussion in Sec. 2.D.

One of the significant differences between the light scattering from one-dimensional and two-dimensional rough surfaces is the absence of polarization effects in the former case (assuming the plane of incidence to be perpendicular to the grooves of the surface). Notably, for light scattering from rough two-dimensional surfaces, the light scattered out-of-plane is significantly cross-polarized.

The enhanced forward scattering phenomenon expresses itself as a peak in the specular direction of the intensity of the light scattered incoherently by the rough surface. For this reason, in Figs. 4 and 5 we present the incoherent component of the MDRC in the plane of incidence (i.e., for $\phi_s = \phi_0$).

Figure 4 shows the incoherent component of the MDRC for $\theta_0 = 12.5°$, for all combinations of incident and scattered polarizations. Since SPPs can only be excited in p-polarization, it is reasonable to assume that light scattered through the temporary creation of an SPP will be predominantly p-polarized. When examining Fig. 4, we only observe enhanced forward scattering, i.e., a peak in the forward direction, for p → p and s → p scattering. We also note that the enhanced forward scattering peak is much more well-defined in p → p than in s → p scattering. It is worth noting that for angles $\theta_s > -34.4°$, in-plane single scattering of light is forbidden due to the power spectrum used [Eq. (3) and Fig. 2]. Consequently, the "edge" seen at the left hand side of Fig. 4 is mainly caused by the single scattering of light for angles $\theta_s \leq -34.4°$.

By studying the θ_0 dependence of $\langle \partial R_{\mathrm{pp}} / \partial \Omega_s \rangle$ (Fig. 5), several effects caused by the shape of the power spectrum can be observed. The positions of the "edges" caused by the suppression of single scattering is directly related to the power spectrum: To leading order in the surface profile function, the intensity of single scattering is proportional to the power spectrum of the surface [12, 24]. For the surface parameters assumed here, single scattering is forbidden for $\left| \mathbf{q}_\parallel - \mathbf{k}_\parallel \right| < k_-^{(1)} = 0.782\omega/c$. Thus, the cylindrical shape of the power spectrum leads to a region around $\mathbf{k}_\parallel$ into which less light is scattered, as single scattering is suppressed here.

Also in Fig. 5, a sharp edge is observed for the case of $\theta_0 = 29.5°$, at $\theta_s \approx -60°$. The location of this edge is given by the outer edge of the inner cylinder of the power spectrum, $k_+^{(1)}$. Due to the the power spectrum vanishing between the inner and outer cylinder [Eq. (3)], single scattering is forbidden for $\theta_s < -60°$.

Of greater interest, and one of the main points of this paper, are the peaks observed in the forward and backward directions. The vertical dotted lines in Figs. 4 and 5 show the expected positions of the enhanced forward scattering peaks, and we see that in each case,

these coincide with the observed peaks. The effect is most pronounced for the polar angle of incidence around $\theta_0 \approx 12°$. For angles of incidence above $17°$, it is not possible for surface plasmon polaritons to be excited in the plane of incidence, since the power spectrum (3) is zero for $k_\parallel + k_{\mathrm{spp}} > k_+^{(1)}$ for in-plane scattering [10]. Nevertheless, a peak in the incoherent part of the MDRC and in the specular direction is visible for $\theta_0 = 29.5°$. Our interpretation is that the origin of this peak is the presence of the g_2 part of the power spectrum; see Fig. 7(b) and the corresponding discussion.

In accordance with previous work on light scattering from two-dimensionally randomly rough surfaces [17–19, 21, 22, 27], we observe enhanced backscattering in Figs. 4 and 5. The enhanced backscattering peak is located in the retro-reflection direction, $\theta_s = -\theta_0$. The effect is present in both co-polarized and cross-polarized scattering. This is in contrast to the case of one-dimensional surface roughness, where enhanced backscattering can only be observed in the p → p polarization configuration.

A complete scan of the angles of incidence for which one observes enhanced backscattering and enhanced forward scattering is presented in Fig. 6. In these figures, the enhanced backscattering peak and the enhanced forward scattering peak are shown as "ridges" in the color map. As the ridges follow the $\pm \theta_s$ directions very well, we conclude that they indeed represent the phenomena enhanced backscattering and enhanced forward scattering. For enhanced forward scattering, which is a quadruple scattering effect, the peak is somewhat broader than the enhanced backscattering peak, which is a double (or higher order) scattering effect. Briefly put, the two-dimensional nature of the rough surface allows for more freedom in the choice of scattered wave vectors, leading to a wider peak.

For comparison with the results shown in Fig. 5, we have also performed simulations for the cases where $\gamma_1 = 1, \gamma_2 = 0$ [Fig. 7(a)], or where $\gamma_1 = 0, \gamma_2 = 1$ [Fig. 7(b)]. In the former case, only the inner annulus of the power spectrum is present, and in the latter case, only the outer annulus is present. The other simulation parameters were as follows. The edges of the simulation domain in the $x_1 x_2$ plane was $L = 30\lambda$, and was discretized at $N_x = 319$ points along each of the lateral axes. The dielectric function, the power spectrum parameters $k_\pm^{(i)}$, and the rms surface roughness parameters were the same as before. The parameters N_x and L were reduced for these simulations in order to save computer resources. This also leads to a different discrete set of θ_s being resolved (cf. Fig. 5).

The results for $\gamma_1 = 1, \gamma_2 = 0$ are presented in Fig. 7(a). In this case, incident light can couple to SPPs, but it is not possible to couple from one SPP to another SPP traveling in the opposite direction (counter-propagation). Thus, enhanced backscattering, which to lowest order is a double scattering process, is allowed. Enhanced forward scattering, on the other hand, is a
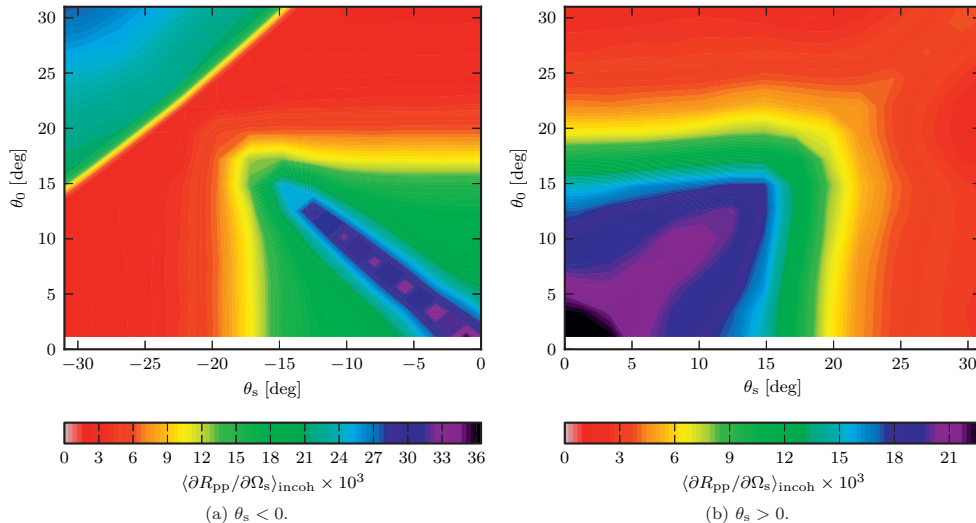
Fig. 6. (Color online) Contour plots of the incoherent, in-plane, and p → p part of the MDRC as a function of angle of incidence (θ_0) and scattering (θ_s). We assume $\phi_s = \phi_0$ in these figures. (a) The enhanced backscattering peak is shown as a purple "ridge" at $\theta_s = -\theta_0$. (b) The enhanced forward scattering peak is shown as a purple "ridge" at $\theta_s = \theta_0$. Note that the color map has been truncated [cf. (a)] to show the peak more clearly.

quadruple scattering process, dependent on scattering from SPPs to counterpropagating SPPs. Hence, there is no enhanced forward scattering peak when $\gamma_2 = 0$. The shoulder visible in Fig. 7(a) does not move as θ_0 increases, meaning that it is not related to the enhanced forward scattering phenomenon, but is a result of the shape of the power spectrum.

In Fig. 7(b), we show the results for $\gamma_1 = 0, \gamma_2 = 1$. In this case, both single scattering and coupling from incident light to SPPs are prohibited. Instead, incident light will excite evanescent modes which are not resonant modes of the surface. These may be scattered several times before coupling out into vacuum propagating modes. The width of the triangular structure seen in the MDRC in Fig. 7(b) is determined by the width of the outer annulus of the power spectrum.

In order to verify the correctness of the numerical results, the total reflected power normalized by the total incident power was calculated. In all cases it was found to be lower than 1, which is expected due to absorption. If one (artificially) assumes the substrate to be lossless, the normalized reflected power should in principle be identical to 1. For the surface parameters used in this study, and with $\mathrm{Im}(\varepsilon_2) = 0$, the normalized total reflected power was 1.000 ± 0.007 for all angles of incidence. We stress that the conservation of energy is a necessary, but not sufficient, criterion for the validity of the simulation results [21].

4. Conclusion

In conclusion, we have studied, by a non-perturbative numerical method, two phenomena observed in rough surface scattering, namely enhanced forward scattering and enhanced backscattering. These are both phenomena observed in the diffuse (incoherent) part of the mean differential reflection coefficient, and are caused by constructive interference between surface plasmon polaritons propagating along a vacuum-metal interface. In particular, the observation of enhanced forward scattering has not previously been reported for systems containing two-dimensionally rough surfaces. The two-dimensional nature of the rough surface studied here gives significantly more freedom in the allowed scattering channels when compared to one-dimensionally rough surfaces, giving less sharp "cutoffs" caused by the power spectrum.

A simple visual model for determining which scattering processes are allowed by two-dimensionally rough surfaces has also been given (Fig. 2). This model can be used to determine for which combinations of angles of incidence and scattering enhanced backscattering and enhanced forward scattering can be observed.

The enhanced forward and backward scattering phenomena are dependent on the presence of surface guided modes. Enhanced backscattering has already been observed in a thin film system in both polarizations [27]. We expect that enhanced forward scattering can also be observed in thin film systems for all polarization combinations, as such structures support surface guided modes
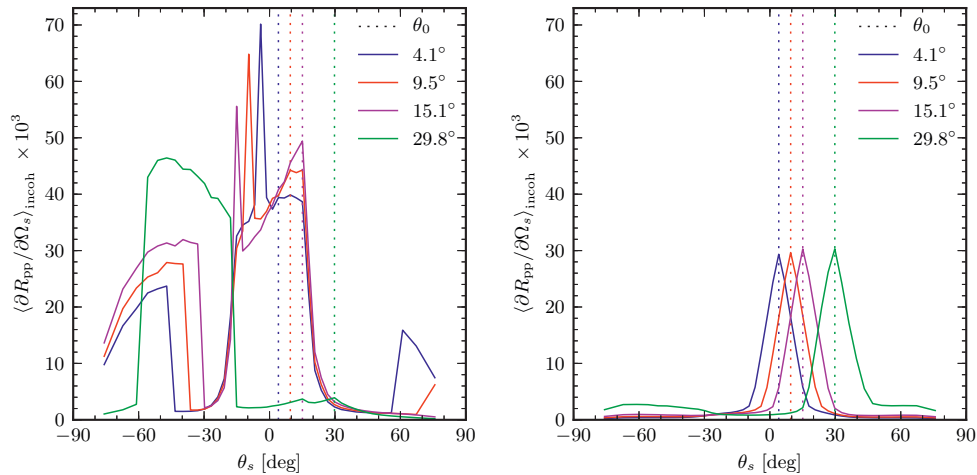
(a) In-plane part of the p → p contribution to the MDRC for a power spectrum with $\gamma_1 = 1$ and $\gamma_2 = 0$.

(b) In-plane part of the p → p contribution to the MDRC for power spectrum with $\gamma_1 = 0$ and $\gamma_2 = 1$.

Fig. 7. (Color online) In plane p → p scattering for power spectra with (a) $\gamma_1 = 1, \gamma_2 = 0$ and (b) $\gamma_1 = 0, \gamma_2 = 1$. With $\gamma_1 = 0, \gamma_2 = 1$, coupling into SPPs is suppressed. With $\gamma_1 = 1, \gamma_2 = 0$, coupling into SPPs is allowed, but not scattering from an SPP to a counterpropagating SPP. This allows enhanced backscattering, but not enhanced forward scattering.

in both p and s polarizations. We leave this investigation to future work, as the required computational effort is significant.

References

[1] E. Ozbay, "Plasmonics: Merging photonics and electronics at nanoscale dimensions," Science **311**, 189–193 (2006).

[2] H. A. Atwater and A. Polman, "Plasmonics for improved photovoltaic devices," Nat. Mater. **9**, 205–213 (2010).

[3] A. Savchenko, E. Kashuba, V. Kashuba, and B. Snopok, "Imaging technique for the screening of proteinprotein interactions using scattered light under surface plasmon resonance conditions," Anal. Chem. **79**, 1349–1355 (2007).

[4] A. Savchenko, E. Kashuba, V. Kashuba, and B. Snopok, "Imaging of plasmid dna microarrays by scattering light under surface plasmon resonance conditions," Sens. Lett. **6**, 705–713 (2008).

[5] A. R. McGurn, A. A. Maradudin, and V. Celli, Phys. Rev. B **31**, 4866 (1985).

[6] C. S. West and K. A. O'Donnell, "Observations of backscattering enhancement from polaritons on a rough metal surface," J. Opt. Soc. Am. A **12**, 390–397 (1995).

[7] K. A. O'Donnell, "High-order perturbation theory for light scattering from a rough metal surface," J. Opt. Soc. Am. A **18**, 1507–1518 (2001).

[8] We have chosen to use the term "enhanced forward scattering", since it is an enhancement in the incoherently scattered light, and since "specular scattering" is often understood to mean "coherent scattering".

[9] K. A. O'Donnell and E. R. Mendéz, "Enhanced specular peaks in diffuse light scattering from weakly rough metal surfaces," J. Opt. Soc. Am. A **20**, 2338–2346 (2003).

[10] I. Simonsen, "Enhanced back and forward scattering in the reflection of light from weakly rough random metal surfaces," phys. status solidi (b) **247**, 2075–2083 (2010).

[11] P. B. Johnson and R. W. Christy, "Optical constants of the noble metals," Phys. Rev. **6**, 4370–4379 (1972).

[12] I. Simonsen, "Optics of surface disordered systems: A random walk through rough surface scattering phenomena," Eur. Phys. J.-Spec. Top. **181**, 1 (2010).

[13] A. R. McGurn and A. A. Maradudin, "Perturbation theory results for the diffuse scattering of light from two-dimensional randomly rough metal surfaces," Wave. Random Media **6**, 251 – 267 (1996).

[14] G. C. Brown, V. Celli, M. Haller, and A. Marvin, "Vector theory of light scattering from a rough surface: Unitary and reciprocal expansions," Surf. Sci. **136**, 381 – 397 (1984).

[15] Lord Rayleigh, "On the dynamical theory of gratings," Proc. R. Soc. Lon. Ser-A **79**, 399–416 (1907).

[16] A. G. Voronovich, *Wave scattering from Rough Surfaces* (Springer Verlag, Berlin, 1999), 2nd ed.

[17] A. Soubret, G. Berginc, and C. Bourrely, "Backscattering enhancement of an electromagnetic wave scattered by two-dimensional rough layers," J. Opt. Soc. Am. A **18**, 2778–2788 (2001).

[18] A. Soubret, G. Berginc, and C. Bourrely, "Application of reduced rayleigh equations to electromagnetic wave scattering by two-dimensional randomly rough surfaces," Phys. Rev. B **63**, 245411 (2001).

[19] A. A. Maradudin, T. Michel, A. R. McGurn, and E. R.

Méndez, "Enhanced backscattering of light from a random grating," Ann. Phys. **203**, 255 – 307 (1990).

[20] I. Simonsen, J. B. Kryvi, A. A. Maradudin, and T. A. Leskova, "Light scattering from anisotropic, randomly rough, perfectly conducting surfaces," Comp. Phys. Commun. **182**, 1904 (2011).

[21] T. Nordam, P. A. Letnes, and I. Simonsen, "Numerical simulations of scattering of light from two-dimensional surfaces using the reduced Rayleigh equation," http://arxiv.org/abs/1204.4984 (2012).

[22] P. A. Letnes, A. A. Maradudin, T. Nordam, and I. Simonsen, "Calculation of all elements of the mueller matrix for scattering of light from a two-dimensional randomly rough metal surface," http://arxiv.org/abs/1108.2599 (accepted, Phys. Rev. A) (2012).

[23] V. Agranovich and D. Mills, eds., *Surface Polaritons: Electromagnetic Waves at Surfaces and Interfaces* (North-Holland Publishing Company, Amsterdam, 1982).

[24] A. A. Maradudin, ed., *Light Scattering and Nanoscale Surface Roughness* (Springer-Verlag, New York, 2007).

[25] I. Simonsen, A. A. Maradudin, and T. A. Leskova, "The scattering of electromagnetic waves from two-dimensional randomly rough penetrable surfaces," Phys. Rev. Lett. **104**, 223904 (2010).

[26] I. Simonsen, A. A. Maradudin, and T. A. Leskova, "The scattering of electromagnetic waves from two-dimensional randomly rough perfectly conducting surfaces: The full angular intensity distribution," Phys. Rev. A **81**, 013806 (2010).

[27] T. Nordam, P. A. Letnes, I. Simonsen, and A. A. Maradudin, "Satellite peaks in the scattering of light from the two-dimensional randomly rough surface of a dielectric film on a planar metal surface," Opt. Express **20**, 11336–11350 (2012).

[28] W. H. Press, S. A. Teukolsky, W. T. Vetterling, and B. P. Flannery, *Numerical Recipes: The Art of Scientific Computing* (Cambridge University Press, Cambridge, New York, 2007), 3rd ed.